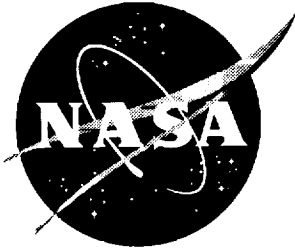


NASA/CP-1999-209699



High-Speed Research: 1994 Sonic Boom Workshop

Configuration Design, Analysis, and Testing

*Edited by
David A. McCurdy
Langley Research Center, Hampton, Virginia*



December 1999

The NASA STI Program Office . . . in Profile

Since its founding, NASA has been dedicated to the advancement of aeronautics and space science. The NASA Scientific and Technical Information (STI) Program Office plays a key part in helping NASA maintain this important role.

The NASA STI Program Office is operated by Langley Research Center, the lead center for NASA's scientific and technical information. The NASA STI Program Office provides access to the NASA STI Database, the largest collection of aeronautical and space science STI in the world. The Program Office is also NASA's institutional mechanism for disseminating the results of its research and development activities. These results are published by NASA in the NASA STI Report Series, which includes the following report types:

- **TECHNICAL PUBLICATION.** Reports of completed research or a major significant phase of research that present the results of NASA programs and include extensive data or theoretical analysis. Includes compilations of significant scientific and technical data and information deemed to be of continuing reference value. NASA counterpart of peer-reviewed formal professional papers, but having less stringent limitations on manuscript length and extent of graphic presentations.
- **TECHNICAL MEMORANDUM.** Scientific and technical findings that are preliminary or of specialized interest, e.g., quick release reports, working papers, and bibliographies that contain minimal annotation. Does not contain extensive analysis.
- **CONTRACTOR REPORT.** Scientific and technical findings by NASA-sponsored contractors and grantees.

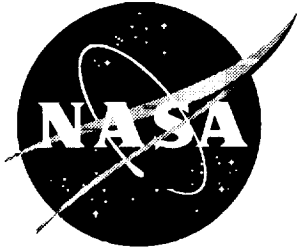
- **CONFERENCE PUBLICATION.** Collected papers from scientific and technical conferences, symposia, seminars, or other meetings sponsored or co-sponsored by NASA.
- **SPECIAL PUBLICATION.** Scientific, technical, or historical information from NASA programs, projects, and missions, often concerned with subjects having substantial public interest.
- **TECHNICAL TRANSLATION.** English-language translations of foreign scientific and technical material pertinent to NASA's mission.

Specialized services that complement the STI Program Office's diverse offerings include creating custom thesauri, building customized databases, organizing and publishing research results . . . even providing videos.

For more information about the NASA STI Program Office, see the following:

- Access the NASA STI Program Home Page at <http://www.sti.nasa.gov>
- Email your question via the Internet to help@sti.nasa.gov
- Fax your question to the NASA STI Help Desk at (301) 621-0134
- Telephone the NASA STI Help Desk at (301) 621-0390
- Write to:
NASA STI Help Desk
NASA Center for AeroSpace Information
7121 Standard Drive
Hanover, MD 21076-1320

NASA/CP-1999-209699



High-Speed Research: 1994 Sonic Boom Workshop

Configuration Design, Analysis, and Testing

Edited by
David A. McCurdy
Langley Research Center, Hampton, Virginia

Proceedings of a workshop sponsored by the
National Aeronautics and Space Administration,
Washington, D.C., and held in
Hampton, Virginia
June 1-3, 1994

National Aeronautics and
Space Administration

Langley Research Center
Hampton, Virginia 23681-2199

December 1999

Available from:

NASA Center for AeroSpace Information (CASI)
7121 Standard Drive
Hanover, MD 21076-1320
(301) 621-0390

National Technical Information Service (NTIS)
5285 Port Royal Road
Springfield, VA 22161-2171
(703) 605-6000

PREFACE

The third High Speed Research Sonic Boom Workshop was held at NASA Langley Research Center on June 1-3, 1994. The purpose of this workshop was to provide a forum for government, industry, and university participants to present and discuss progress in their research. The workshop was organized into sessions dealing with atmospheric propagation; acceptability studies; and configuration design, analysis, and testing. Attendance at the workshop was by invitation only.

The workshop proceedings include papers on design, analysis, and testing of low-boom high speed civil transport configurations and experimental techniques for measuring sonic booms. Significant progress is noted in these areas in the time since the previous workshop a year earlier. The papers include preliminary results of sonic boom wind tunnel tests conducted during 1993 and 1994 on several low-boom designs. Results of a mission performance analysis of all low-boom designs are also included. Two experimental methods for measuring near-field signatures of airplanes in flight are reported.

The use of trade names of manufacturers in this report does not constitute an official endorsement of such products or manufacturers, either expressed or implied, by the National Aeronautics and Space Administration.

David A. McCurdy
Langley Research Center

This page intentionally left blank.

CONTENTS

Preface	iii
Additional F-Functions Useful for Preliminary Design of Shaped-Signature, Low-Boom, Supersonic-Cruise Aircraft Robert J. Mack	1
Sonic Boom Prediction Exercise: Experimental Comparisons Eugene Tu, Samson Cheung, and Thomas Edwards	13
Design and Computational/Experimental Analysis of Low Sonic Boom Configurations Susan E. Cliff, Timothy J. Baker, and Raymond M. Hicks	33
Wind-Tunnel Overpressure Signatures From A Low-Boom HSCT Concept With Aft-Fuselage-Mounted-Engines Robert J. Mack	59
Low Sonic Boom Design Activities at Boeing George T. Haglund	73
Sonic Boom Softening of Reference-H Samson Cheung	89
The Analysis and Design of Low Boom Configurations Using CFD and Numerical Optimization Techniques Michael J. Siclari	107
Mid-Field Sonic Boom Extrapolation Methodology Samson Cheung, Sanford Davis, and Eugene Tu	129
A Performance Assessment of Eight Low-Boom High-Speed Civil Transport Concepts Daniel G. Baize, Marcus O. McElroy, James A. Fenbert, Peter G. Coen Lori P. Ozoroski, Chris S. Domack, Kathy E. Needleman, and Karl A. Geiselhart	149
Measurement of the Basic SR-71 Airplane Near-Field Signature Edward A. Haering, Jr., Stephen A. Whitmore, and L. J. Ehernberger	171

SR-71A Reduced Sonic Boom Modification Design	199
John M. Morgenstern, David B. Bruns, and Peter P. Camacho	
CFD Predictions of Sonic Boom Characteristics for Unmodified and Modified SR-71 Configurations	219
Kamran Fouladi	
Low-Boom SR-71 Modified Signature Demonstration Program	237
David Lux, L. J. Ehernberger, Timothy R. Moes, and Edward A. Haering	
In-Flight Technique for Acquiring Mid- and Far-Field Sonic Boom Signatures	249
Eugene G. Stansbery, Daniel G. Baize, and Domenic Maglieri	
Progress in Sonic-Boom Understanding: Lessons Learned and Next Steps	269
Christine M. Darden	
Participants	293

Additional F-Functions Useful For Preliminary Design Of Shaped-Signature, Low-Boom, Supersonic-Cruise Aircraft

Robert J. Mack

NASA Langley Research Center

Hampton, Virginia

Summary

Two additional low-boom F-functions have been described for use in designing low-boom, shaped-pressure-signature, supersonic-cruise aircraft. Based on the minimization studies of Seebass and George, the drag-nose shock strength trade-off modification of Darden, and the practical modification of Haglund, their use can aid in the design of conceptual low-boom aircraft, provide additional flexibility in the shaping of the low-boom aircraft nose section, and extend the applicability of shaped-pressure-signature methodology.

Introduction

The technology for designing an aircraft to generate a relatively low sonic boom level as experienced by an observer on the ground started with the work of L. B. Jones. His 1961 paper (ref. 1) was applicable to bodies of revolution and supplemented G. B. Whitham's 1952 paper (ref. 2) which described a method for predicting pressure disturbances from projectiles in supersonic flight. When F. Walkden showed (ref. 3) that the lift from a wing-body cruising at supersonic speeds and high altitudes generated ground disturbances which could be replicated by a body of revolution, the theory introduced by Whitham acquired importance as a tool for predicting ground-level sonic-boom pressures from cruising supersonic aircraft, and the minimization method of Jones acquired an importance because it could be applied to a real source of acoustic noise.

Unfortunately, the minimum-boom characteristics of Jones' method imposed a large drag penalty due to the need for a very blunt nose section. Seebass and George applied minimization techniques to the problem and described a method (ref. 4) for obtaining two ground-level pressure signatures and the two corresponding Whitham F-functions which would minimize the sonic-boom through signature shaping. The pressure signatures and F-functions were designed for conditions of minimum overpressure and minimum nose shock, and were characterized as being

“flat-topped” or “ramped.” This advance in sonic-boom minimization was accompanied by some of the same nose bluntness that came with the Jones minimization because the F-functions began with the same Dirac delta function. Darden showed (ref. 5) that vehicle drag could be decreased at the expense of a small increase in sonic boom pressure strength by changing the Dirac delta function to a finite-width “spike” at the front of the Seebass and George low-boom F-functions. However, both signatures still had point-design characteristics such that a “hot day” or a “cold day” atmosphere could cause the disturbance propagation to include “spike” signals or “ramp” signals and generate higher-than minimum pressures. This point-design feature restricted the use of the “ramped” F-function and pressure signature even though the shock strengths were somewhat lower than those achieved when designing with a “flat-top” F-function and pressure signature.

Haglund (ref. 6 and 7) introduced a flat-section between the “spike” and the ramp so that “hot day” and “cold day” variations could be designed into the F-function and the accompanying pressure signature. This removed the point-design limitation, so that the resulting “hybrid” F-function and pressure signature became very attractive for designers employing the shaped-signature approach to low-boom aircraft design.

The triangular “spike” at the front of the F-function reduced the wave drag, but resulted in a vehicle nose with a distinct cusp, if the nose were volume only. This cusp made it difficult, at times, to easily build wind-tunnel models. When the wing and the fuselage nose were coincident, the growth of fuselage area was delayed because the volume and the lift equivalent areas were adequately met with wing-alone volume and lift. This limitation virtually eliminated the “platypus nose” (ref. 8) as a viable, low-boom design feature when the Seebass and George minimization method or the Haglund hybrid method was used in the design process.

The shape of a nose “spike” was given by convenience, not by theory. By changing the shape of the “spike” on the Haglund hybrid F-function, other desirable design features could be introduced while still keeping all the hybrid-shape advantages. Two such modifications will be discussed in this paper. The first modification replaces the forward half of the “spike” with a parabolic-area-growth curve, i.e., a square root function. This modification replaces most of the “cusped spike” with a conical “spike” and makes the aircraft, as well as the wind-tunnel model, much easier to design and build. The second modification replaces the “spike” in the F-function with a linear-area-nose singularity. This re-introduces some of the undesirable drag-producing nose bluntness that was replaced with the cusp, but the bluntness is considerably less than the nose bluntness due to the Dirac delta function, and therefore offers the possibility of using the “platypus nose” design feature or a nose-mounted canard on a low-boom conceptual aircraft.

Equations for the equivalent areas from both F-function modifications are provided, along with a comparison of equivalent areas derived from these F-function equations and the basic F-functions. The four F-functions used in this comparison are the two modified hybrid F-functions introduced in this paper, the linear-spike hybrid F-function, and a hybrid F-function with an approximate Dirac delta function at the nose.

Symbols

A_e aircraft equivalent area, ft^2

- B value of the F-function slope between $y=\xi$ and $y=l_e$ as a fraction, B' , of α
- B' fraction with magnitude greater than, or equal to, 0.0 and less than 1.0
- C value of the F-function between $y=y_f$ and $y=\xi$, $\text{ft}^{1/2}$
- D discontinuity in the F-function at $y=\lambda$, $\text{ft}^{1/2}$
- $F(y)$ the Whitham F-function, $\text{ft}^{1/2}$
- h cruise altitude, ft
- H value of the F-function at $y=y_f/2$, $\text{ft}^{1/2}$
- $I(x)$ unit step function; $I(a)=1.0$ for $x \geq a$ and is zero elsewhere
- l_e effective length of the aircraft, ft
- M cruise Mach number
- p flow-field pressure, psf
- p_a ambient pressure, psf
- Δp $p-p_a$, psf
- t time along pressure signature, sec
- t_0 time of Mach wave arrival on ground, sec
- W beginning cruise weight, lb
- x_e effective length along aircraft longitudinal axis, ft
- y effective length parameter in the Whitham F-function, ft
- y_f effective "nose-bluntness" parameter, ft
- α atmospheric advance which specifies the distance a unit F-function disturbance is ahead of a Mach wave from the same source
- λ effective length that defines the positive part of the F-function, ft
- ξ effective length where "ramp" of slope B starts, ft

Description of F-functions

The F-functions that will be presented and described in this paper were derived from the shaping of the Haglund hybrid F-function (ref. 6 and 7) shown in figure 1. .

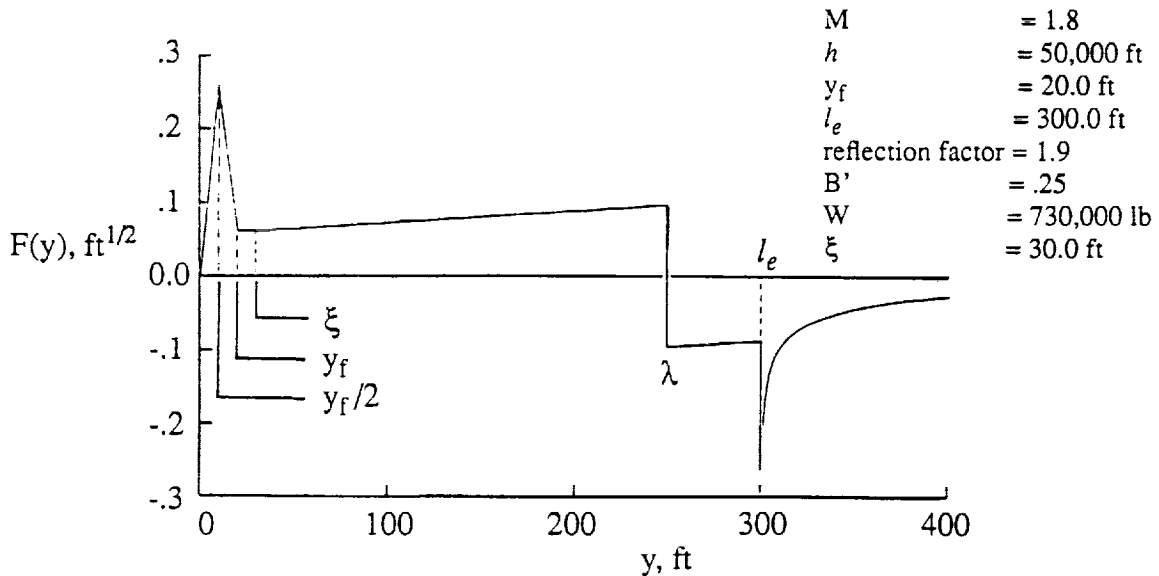


Figure 1. Haglund hybrid F-function with example aircraft design parameters.

In this F-function and in all subsequent F-functions, most of the design parameters used in the derivation are the same as those given in figure 1. The line forming the front of the nose "spike" generates an equivalent area development that is proportional to $x^{5/2}$. A fuselage shape conforming to this initial area growth has a cusp-like nose which can be difficult to build when it is designed for both low sonic boom and low drag. The Dirac delta-function on the original Seebass and George F-functions (ref. 4) provided a more conventional area development, but it also had a sizeable drag penalty. To obtain the benefits of these low-boom design solutions and reduce the potential for drag penalty, two geometrically simple alterations were examined: (1) a conical section on the forward part of the "spike," and (2) a linear-area singularity to replace the entire "spike."

The conical nose "spike." When the linear F-function curve between zero and $y_f/2$ is replaced with a square-root curve, the nose area growth becomes proportional to x^2 instead of $x^{5/2}$, i.e., the nose has a conical instead of a cusped shape. The remainder of the F-function is left unchanged because, like the basic hybrid F-function, it has features that are controlled by all of the input values. This conical-nose hybrid F-function is shown in figure 2.

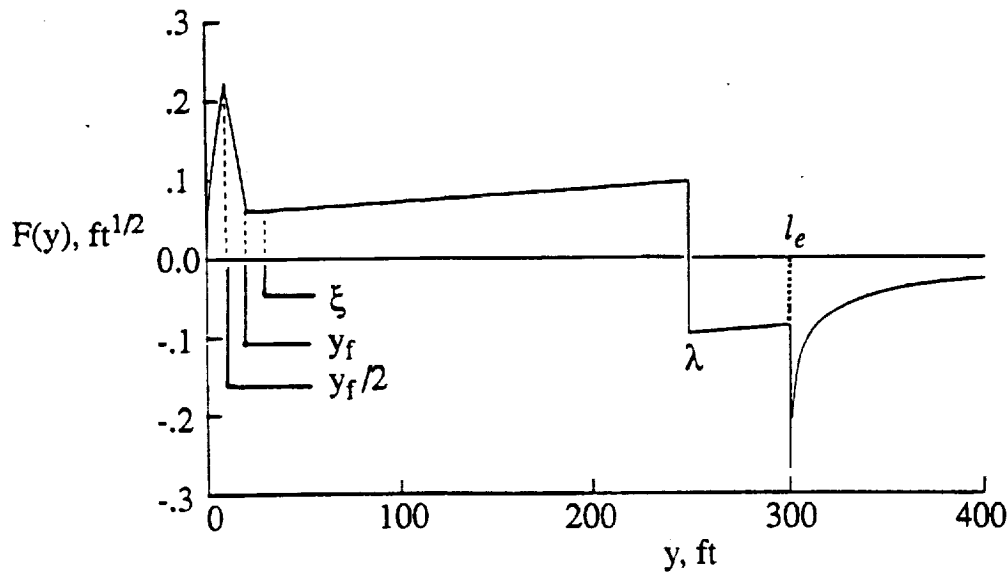


Figure 2. Hybrid F-function modified with a conical-nose "spike."

The equations for the equivalent areas, computed from the Abel integral of this F-function

$$A_e(x) = 4.0 \int_0^x F(y) \sqrt{x-y} dy \quad (1)$$

are given in Appendix A. A comparison of the areas from the basic hybrid F-function and the conical "spike" modified hybrid F-function is shown in figure 3. Since all the input data are the same, the observed differences in the equivalent area distributions are due to the differences in the "spike" of the two F-functions.

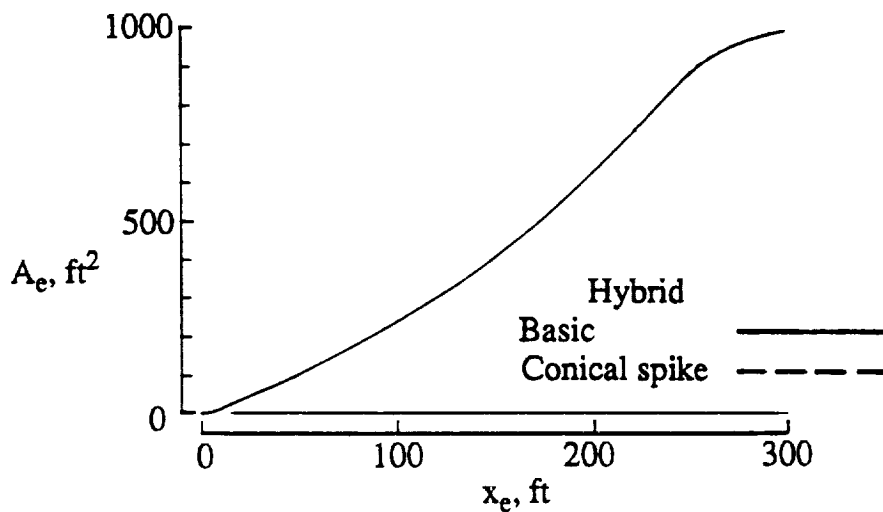


Figure 3. Comparison of equivalent areas from basic and conical-spike hybrid F-function.

The incremental area differences between the two equivalent area distributions are very small and difficult to see in figure 3. In figure 4, the area scale is expanded, and the area comparison is shown for the first 40 feet of effective aircraft length, where the differences are most pronounced.

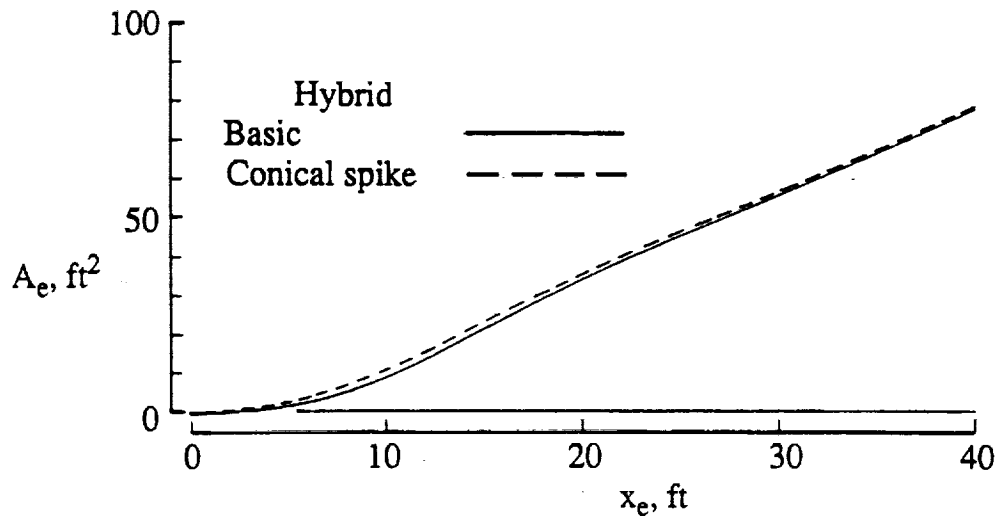


Figure 4. Comparison of the figure 3 area distributions at the nose of an aircraft.

The equivalent areas from the basic and conical-spike hybrid F-functions converge quickly aft of the nose so the overpressure signatures (figure 5) of the conical-spike F-function, low-boom conceptual aircraft are essentially the same as the basic hybrid, low-boom conceptual aircraft.

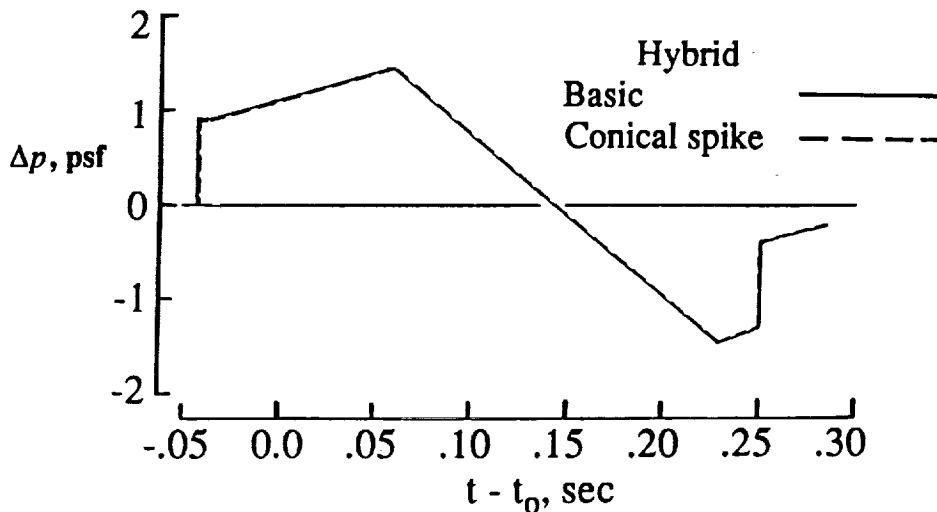


Figure 5. Comparison of hybrid and conical-spike hybrid pressure signatures.

Since the conical-spike F-function generates fuselage-nose equivalent areas with conical normal areas, the nose shape is easily controlled without the need for complex algorithms.

The volumes of the respective conceptual aircraft will also be about the same. Very small, if any, drag penalties should accrue from the use of the conical-spike F-function and its area distribution. If very small values of y_f are used in the conceptual design, then a cusp-like area distribution may still be seen, but the needle-sharp, cusp-like nose of the basic hybrid F-function can be avoided.

Linear-area nose singularity. When the wing apex is placed at the nose of the configuration, the length over which lift extends can be significantly longer than if the wing apex is located in the

conventional position well behind the fuselage nose. This longer lifting length can often be used advantageously to control the flow-field disturbances generated by the aircraft cruising at supersonic speeds. However, if the basic hybrid F-function is used to guide the design of the surfaces of the configuration, an equivalent area situation can easily arise where the usable fuselage volume will not emerge from the wing for a sizeable distance aft of the nose. This feature usually is incompatible with constraints on crew compartment size and location, or passenger compartment volume. An equivalent area growth is required which will permit both the wing and the fuselage to: (1) increase gradually in area and in volume, (2) permit a long lifting length, (3) allow convenient crew and passenger volume in the forward part on the aircraft, (4) meet low drag requirements, and (5) retain low sonic-boom characteristics. Such an equivalent area distribution might be derived from an F-function having a power-law singularity at the nose. An example of this type of F-function is presented in figure 6 where the mathematical singularity is based on an area description which is linearly proportional to the longitudinal variable, x_e .

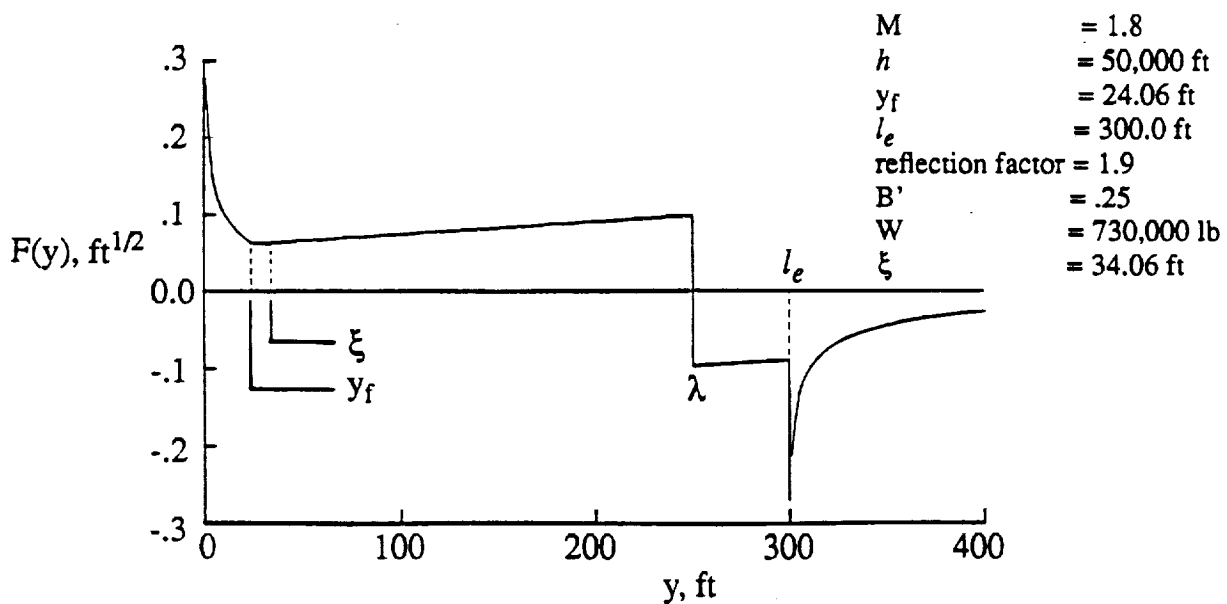


Figure 6. Hybrid F-function with linear-area singularity at the nose.

The equivalent areas obtained by integrating the Abel integral of this F-function are also given in Appendix A. They are shown in figure 7 and are compared with the equivalent areas obtained from a basic hybrid F-function with a linear spike at the nose.

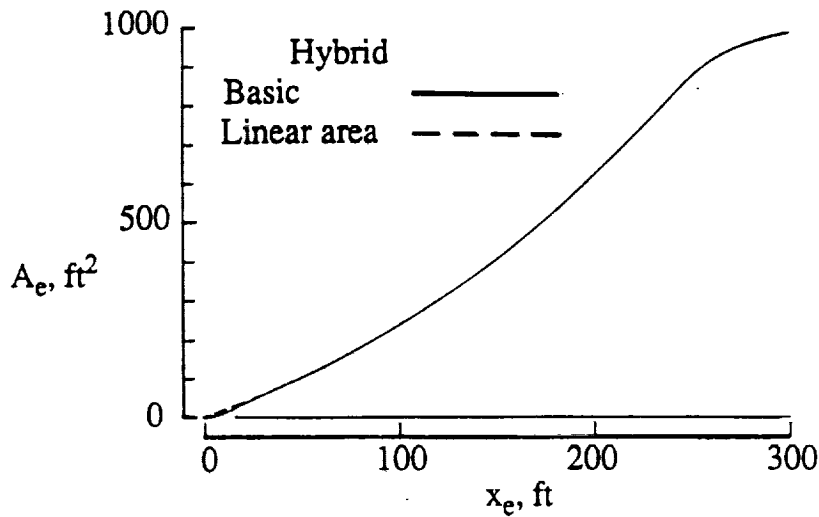


Figure 7. Comparison of equivalent areas from a linear-area hybrid and a basic hybrid F-function.

There is more area and volume under the linear-area hybrid F-function equivalent area curve than under the basic hybrid F-function equivalent area curve. This is seen better if, like the previous area comparison, the areas for the first 40 feet of the nose are compared as shown in figure 8.

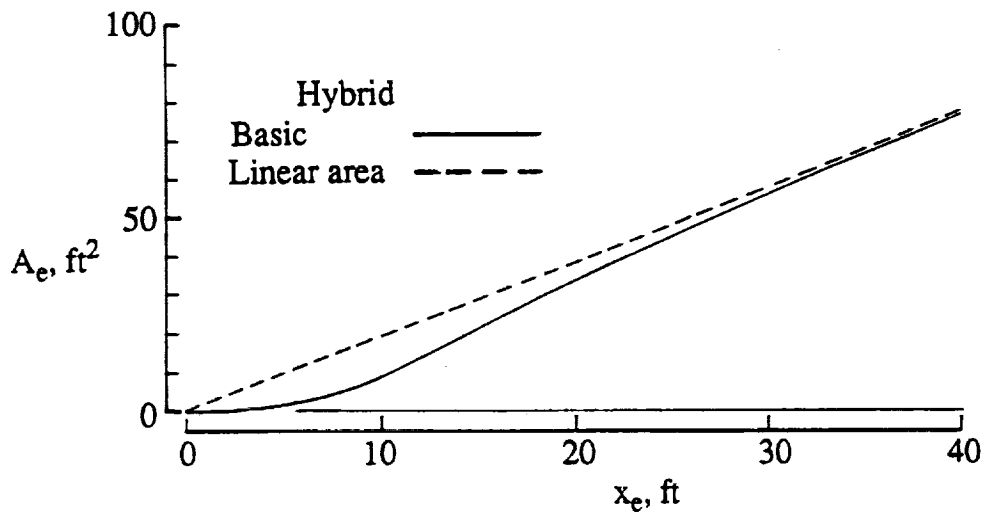


Figure 8. Comparison of the figure 7 area distributions at the nose section of aircraft.

If made into a fuselage nose having volume only, the larger area growth and surface slopes would probably add a sizeable drag increment to the aircraft. However, by starting a "platypus-nose" wing at the front of the aircraft, this extra equivalent area can be distributed into wing volume, wing lift, and fuselage volume contributions. Therefore, surface slopes and forebody drag can be kept under some degree of control because trades between the three flow-field disturbance sources can be made. When this control is exercised, the sonic-boom and the aerodynamic benefits of a longer lifting length can be obtained. The pressure signature obtained from the areas in figure 7 is shown in figure 9 where it is compared with the signature from a basic hybrid F-function.

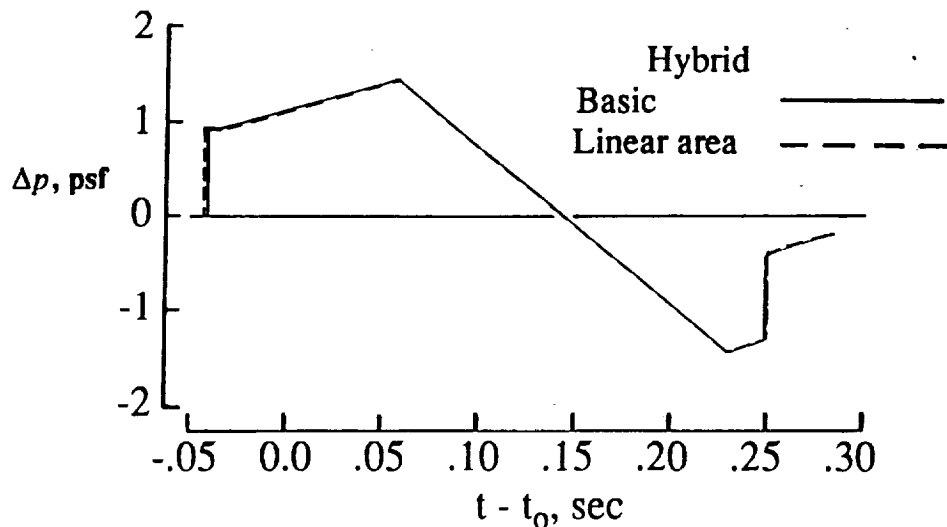


Figure 9. Comparison of pressure signatures from linear-area hybrid and basic hybrid F-functions.

There are only small differences in the two pressure signatures even though there were noticeable differences in the forward area distributions.

One special feature of this F-function must be mentioned. Because the y_f -distance between zero and y_f is described by one curve segment rather than two, there is a degree of design freedom lost. The equation that illustrates this condition is derived from the area balancing relationships required to determine the nose shock strength.

$$C = \text{constant} * \Delta p = 4.0 * y_f / \alpha \quad (2)$$

Mach number and altitude conditions determine the atmospheric advance, α , and the constant used to obtain C from the shock strength. Specifying y_f or the shock strength sets the value of both variables through this equation. Actually, this is a bit oversimplified since the requirement that the tail shock be a specified fraction of the nose shock also enters the F-function iteration process. This situation also exists with the calculation of the other F-function parameters, but in those subsequent iterations, the value of y_f remains fixed. The example used in this paper shows that, in general, the result is a satisfactory solution, even though y_f increased from 20.0 to 24.06 feet and ξ increased from 30.0 to 34.06 feet. With or without these changes, this F-function's practicality and applicability must be judged with the same caution as given the solutions obtained from the other low-boom F-functions.

Another way to appraise the merits of these two additional F-functions, equivalent area distributions, and pressure signatures, is a comparison with a hybrid F-function having a Dirac delta function at its origin. This is the feature that the original optimized and shaped F-functions, introduced by Seebass and George (ref. 4), were given originally and is the asymptotic shape that results by shrinking y_f to zero on these new hybrid F-functions and the "spiked" F-functions. A comparison of equivalent areas derived from these F-functions is shown in figure 10.

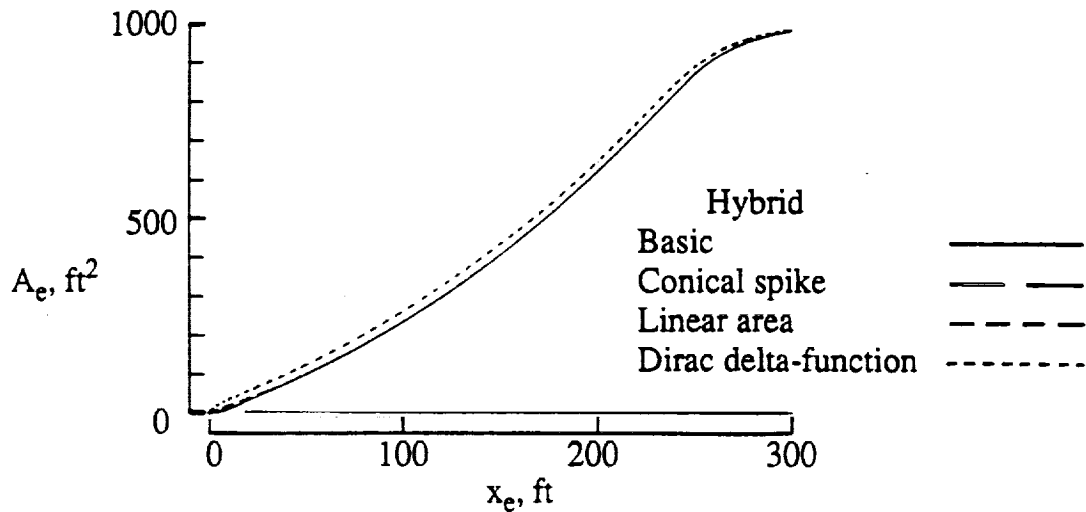


Figure 10. Comparison of Dirac delta function, conical-nose spike, linear-area, and unmodified hybrid F-function equivalent areas.

A plot of the four equivalent areas over the first 40 feet of aircraft length is shown in figure 11 for ease in making the comparisons.

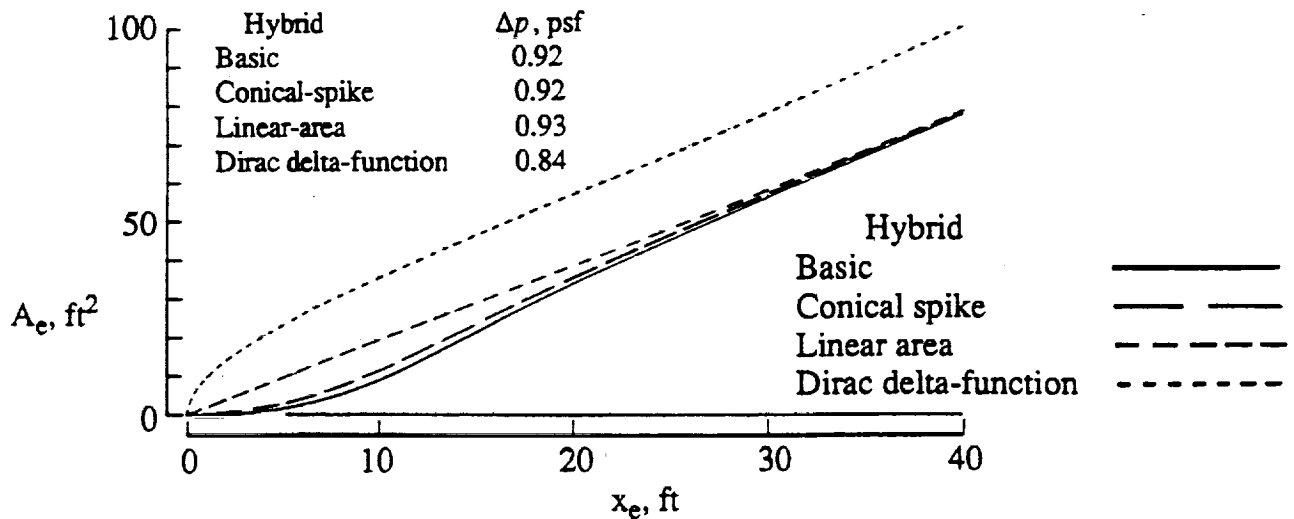


Figure 11. Comparisons of nose-section equivalent areas computed from the four F-functions.

The rapid area growth at the nose due to the Dirac delta function causes most of the drag vs. nose-shock strength problem because the trade-off between wing volume, wing lift, and fuselage volume cannot be accomplished gradually enough to escape a sizeable drag penalty. However, the use of the other hybrid F-functions allows more latitude in making trades, and permits more control over the aircraft design. The success of wind-tunnel models designed and built with the basic hybrid F-function strongly suggests that the modest modification incorporated in the conical-spike hybrid F-function would make it equally useful. If a completely blended wing-body configuration were desired, the linear-area hybrid F-function might be worth trying since it reopens the designer's option of obtaining both the aerodynamic and the sonic-boom benefits

from having a “platypus nose” on a blended wing-fuselage configuration.

Concluding Remarks

Two additional low-boom F-functions have been described for use in designing low-boom, shaped-pressure-signature, supersonic-cruise aircraft. The first, a hybrid F-function with a conical-spike, permits the wind-tunnel or aircraft nose section to be built more easily. A second hybrid F-function with a linear-area spike at the front allows the option of using a “platypus nose” at the front of the model or aircraft and obtaining the aerodynamic and sonic-boom benefits of extra lifting length. Both F-functions supplement the minimum sonic-boom and low sonic-boom design tools already available to the aircraft designer.

References

1. Jones, L. B.: Lower Bounds For Sonic Bangs. *Journal of the Royal Aeronautical Society*, vol. 65, no. 606, June 1961, pp. 433-436.
2. Whitham, G. B.: The Flow Pattern Of A Supersonic Projectile. *Communications on Pure and Applied Mathematics*, vol. V, no. 3, August 1952, pp. 301-348.
3. Walkden, F.: The Shock Pattern of a Wing-Body Combination, Far From The Flight Path, *Aeronautical Quarterly*, vol. IX, pt. 2, May 1958, pp. 164-194.
4. Seebass, R.; and George, A. R.: Sonic-Boom Minimization, *Journal of the Acoustical Society of America*, vol. 51, no. 2, pt. 3, February 1972, pp. 686-694.
5. Darden, Christine M.: Sonic-Boom Minimization With Nose-Bluntness Relaxation, NASA TP-1348, 1979.
6. Haglund, George T.: High Speed Civil Transport Design For Reduced Boom, Boeing Document No. D6-55430, NASA Contract No. NAS1-18377, 1991.
7. Mack, Robert J.; and Haglund, George T.: A Practical Low-Boom Overpressure Signature Based on Minimum Sonic-Boom Theory, *High-Speed Research: Sonic Boom*, vol. II, NASA CP-3173.
8. Robins, A. Warner; Lamb, Milton; and Miller, David S.: Aerodynamic Characteristics at Mach Numbers of 1.5, 1.8, and 2.0 of a Blended Wing-Body Configuration With and Without Integral Canards. NASA TP-1427, 1979.

Appendix A

Equivalent areas obtained from the conical-nose "spike" hybrid F-function:

$$\begin{aligned}
 A_e = & \frac{Hx^2}{\sqrt{2y_f}} \left[\pi - I\left(\frac{y_f}{2}\right) \left(\frac{\pi}{2} - \text{asin} \frac{y_f - x}{x} \right) \right] \\
 & + I\left(\frac{y_f}{2}\right) \left[H \frac{y_f}{2} \sqrt{x - \frac{y_f}{2}} + \frac{5}{3} H \left(x - \frac{y_f}{2}\right)^{3/2} - \frac{32}{15y_f} (H - C) \left(x - \frac{y_f}{2}\right)^{5/2} \right] \\
 & - I(y_f) \frac{32(H - C)}{15y_f} (x - y_f)^{5/2} + I(\xi) \frac{16}{15} B(x - \xi)^{5/2} - I(\lambda) \frac{8}{3} D(x - \lambda)^{3/2} \quad (\text{A.1})
 \end{aligned}$$

Equivalent areas obtained from the linear-area "spike" hybrid F-function:

$$\begin{aligned}
 A_e = & (2.0\pi C \sqrt{y_f}) x + I(y_f) 4.0C \sqrt{y_f} \left[\sqrt{y_f(x - y_f)} - x \left(0.5\pi - \text{atan} \sqrt{\frac{y_f}{x - y_f}} \right) \right] \\
 & + I(y_f) \frac{8}{3} C (x - y_f)^{3/2} + I(\xi) \frac{16}{15} B(x - \xi)^{5/2} - I(\lambda) \frac{8}{3} D(x - \lambda)^{3/2} \quad (\text{A.2})
 \end{aligned}$$

These equations have two common features. First, the last two terms in both equivalent area equations are exactly the same because $F(y)$, for $y > y_f$, has the same description of the same shaping in both hybrid F-functions. The second feature common to both models is the constant-area cylinder that extends from the aircraft effective length, at $y = l_e$, to infinity.

SONIC BOOM PREDICTION EXERCISE: EXPERIMENTAL COMPARISONS

**Eugene Tu
NASA Ames Research Center
Moffett Field, CA**

**Samson Cheung
MCAT Institute
Moffett Field, CA**

**Thomas Edwards
NASA Ames Research Center
Moffett Field, CA**

The success of a future High Speed Civil Transport (HSCT) depends on the ability to accurately assess and, possibly, modify the sonic boom signatures of potential designs. In 1992, the Sonic Boom Steering Committee initiated a prediction exercise to assess the current computational capabilities for the accurate and efficient prediction of sonic boom signatures and loudness levels. A progress report of this effort was given at the Sonic Boom Workshop held at NASA Ames Research Center in 1993 where predictions from CFD and Modified Linear Theory (MLT) methods were given. Comparisons between the methods were made at near-, mid- and far-field locations. However, at that time, experimental data from wind-tunnel tests were not available. The current paper presents a comparison of computational results with the now available experimental data. Further comparisons between the computational methods and analyses of the discrepancies in the results are presented.

The objectives and motivation for the current study are given below. The successful prediction of sonic boom signatures for future HSCT designs depends not only on validated near-field and extrapolation codes, but also on determining the best and consistent use of these computational tools. In essence, it is just as important to evaluate the methodologies used in the prediction of sonic booms.

INTRODUCTION

● OBJECTIVES

- ASSESS CURRENT CAPABILITY TO PREDICT SONIC BOOM SIGNATURES AND LOUDNESS
- CALIBRATE SONIC BOOM PREDICTION METHODS
- CHARACTERIZE REQUIREMENTS FOR ACCURATE SONIC BOOM PREDICTIONS
- GUIDE FURTHER DEVELOPMENT OF PREDICTIVE METHODS

● MOTIVATION

- LOW-BOOM AND BOOM SOFTENED HSCT DESIGNS MAY FEATURE SHAPED SONIC BOOM SIGNATURES
- SUCCESS OF SIGNATURE SHAPING DEPENDS ON RELIABLE PREDICTION OF NEAR-, MID- AND FAR-FIELD

There are two primary types of prediction methods evaluated in this study. Modified Linear Theory (MLT) is a well established method which, due to its high efficiency, is suited for inverse design calculations. More recently, with the aid of high-speed and parallel supercomputers, CFD methods have been consistently maturing towards the potential of becoming powerful design tools. With the lack of major significant physical approximations, CFD methods can handle complex geometries which can have many components contributing to the overall sonic boom characteristics of an aircraft. As the expense decreases, and the limitations are more fully understood, CFD has the potential to provide accurate and efficient predictions of sonic boom characteristics for analysis and design.

BACKGROUND: PREDICTION METHODOLOGIES

- **MODIFIED LINEAR THEORY**
 - WELL-ESTABLISHED PROCEDURE
 - FAST AND EFFICIENT
 - INVERSE DESIGN CAPABILITY
 - HISTORY OF IMPLEMENTATION: EXPERIENCE
 - DIFFICULT TO MODEL COMPLEX GEOMETRIES

- **COMPUTATIONAL FLUID DYNAMICS (CFD)**
 - NO SIGNIFICANT PHYSICAL APPROXIMATIONS
 - COMPLEX GEOMETRY CAPABILITY
 - EXPENSIVE
 - LARGE VARIATION IN PREDICTIONS
 - LIMITATIONS NOT FULLY UNDERSTOOD

A single configuration, Ames Model 3, was selected as the prediction exercise test case. Ames Model 3 is a low-boom design derived from an early Boeing HSCT concept (Boeing-911). The fuselage of Boeing-911 was modified in order to provide a hybrid signature for improved sonic boom characteristics. The original arrow-wing planform and four-engine nacelle placement of Boeing-911 remained unchanged in Ames Model 3. In the current prediction exercise, a horizontal tail is not included in the configuration.

In order to evaluate methodologies as well as codes, no grid, code or extrapolation requirements were specified. Experimental data was obtained from wind tunnel tests of Ames Model 3 in the NASA Ames Unitary Tunnel. Five test conditions were identified for the prediction exercise. Test Cases 1-4 are at a free stream Mach number of 1.68 and various angles of attack. Test Case 2 is the only case where the nacelles were included in the experiment. Test Case 5 was conducted at the higher Mach number of 2.0 and included off-track measurements. The final analysis of the prediction methods was conducted by the Computational Aerosciences Branch at Ames.

APPROACH

- SELECT SINGLE LOW-BOOM CONFIGURATION
 - AMES MODEL 3
- APPLY SONIC BOOM PREDICTION METHODS
 - NO CRITERIA GIVEN FOR GRID, FLOW CODE OR EXTRAPOLATION TECHNIQUE
- OBTAIN EXPERIMENTAL DATA
 - TEST CONDITIONS (MACH, ANGLE OF ATTACK) IDENTIFIED
 - AMES TUNNEL TEST
- PERFORM ANALYSIS OF PERFORMANCE OF METHODS

Five sets of results were submitted for the sonic boom prediction exercise. Of these, four were CFD results and one was from Modified Linear Theory. A brief description of each of the methods follows in the next 2 slides.

The prediction exercise consisted of contributed computations from NASA Ames, NASA Langley/Grumman, and Boeing. Ames provided predictions using three different methods which are outlined below. The CFD code, extrapolation method, rise-time input and loudness code for each method are also given.

The first method from Ames is based on the UPS3D code. UPS3D solves the parabolized Euler/Navier-Stokes equations using a computationally efficient space-marching procedure. The computational domain extends to approximately one body length away, where the pressure signature is then extrapolated using the Whitham method. Once the ground-level signature has been determined, an ad-hoc rise time is applied to the shock waves. Finally, the loudness in PLdb is determined using the Stevens Mark VII technique.

The next set of results is based on the AIRPLANE code. AIRPLANE solves the Euler equations in a time-relaxation approach on an unstructured grid. The ANET code is used to extrapolate the CFD results from a distance of one-third of a body length.

The final set of results from Ames are from the HFLO3 code. HFLO3 is also an Euler time-relaxation code that uses structured grids of H-H topology. The rise-time and loudness methods for both AIRPLANE and HFLO3 are the same as described for UPS3D.

CONTRIBUTED RESULTS - AMES

- **UPS3D**
 - PARABOLIZED NAVIER-STOKES METHOD TO APPROX. 1 LENGTH
 - WHITHAM THEORY EXTRAPOLATION
 - RISE TIME: AIR FORCE DATA REGRESSION ANALYSIS AND 3ms
 - LOUDNESS: STEVENS MARK VII
- **AIRPLANE**
 - UNSTRUCTURED EULER RELAXATION METHOD
 - ANET EXTRAPOLATION
 - RISE TIME: $T = 3\text{ms}/\Delta p$ ($\Delta p > .2$ psf);
 $T = 3\text{ms}(\Delta p)$ ($\Delta p \leq .2$ psf)
 - LOUDNESS: STEVENS MARK VII
- **HFLO3**
 - H-H EULER RELAXATION METHOD
 - ANET EXTRAPOLATION
 - RISE TIME: $T = 3\text{ms}/\Delta p$ ($\Delta p > .2$ psf);
 $T = 3\text{ms}(\Delta p)$ ($\Delta p \leq .2$ psf)
 - LOUDNESS: STEVENS MARK VII

The description of the methods from the Langley/Grumman and Boeing contributions is given below. The MIM3DSB code was developed by Grumman for efficient CFD solutions to sonic boom problems. MIM3DSB employs a multigrid implicit marching method to solve the Euler equations. The extrapolation, rise time, and loudness methods used in this exercise are the same as in the Ames contributions.

The contribution from Boeing was the only Modified Linear Theory (MLT) result. The characteristics of the MLT analysis are given below. The method is due to Middleton, but has been recently modified to account for camber and angle of attack in the equivalent area computation. The ARAP code is used to extrapolate the sonic boom signature to the ground.

CONTRIBUTED RESULTS GRUMMAN/LaRC AND BOEING

- **GRUMMAN/LANGLEY - MIM3DSB**
 - MULTIGRID IMPLICIT MARCHING EULER METHOD
 - ANET EXTRAPOLATION
 - RISE TIME: $3\text{ms}/\Delta p$
 - LOUDNESS: STEVENS MARK VII
- **BOEING**
 - MLT ANALYSIS (MIDDLETON)
 - CORRECTION TO GEOMETRY AND AREA FOR ANGLE OF ATTACK AND CAMBER
 - ARAP EXTRAPOLATION

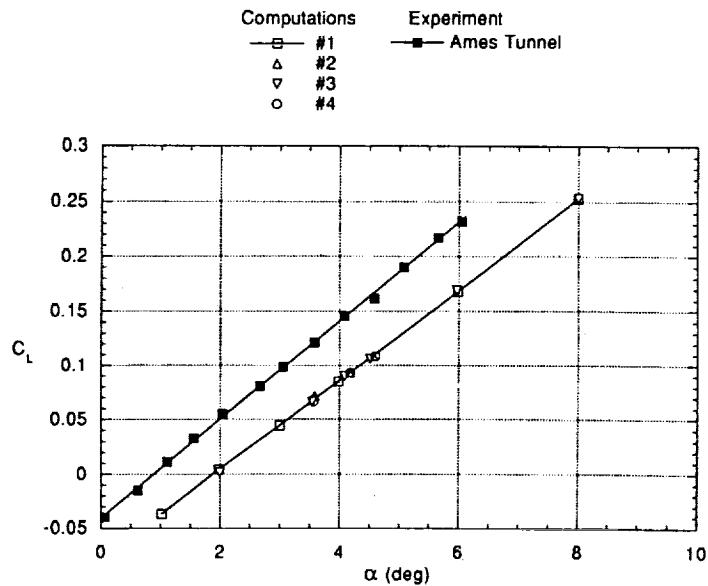
As of the Sonic Boom Workshop in June 1994, all of the computational results have been collected. The wind tunnel tests have also been conducted at the Ames Unitary Tunnel. However, due to calibration difficulties, only Test Case 2 (nacelle-on) data is usable for signature comparison purposes. Furthermore, there are significant differences between the initially planned and the post-test reported flow conditions. The reduced wind-tunnel test data showed an approximately 20% higher lift coefficient than originally planned. In order to account for the difference in lift, one of the methods contributed by Ames, UPS3D, was used to recompute Test Case 2 at the higher lift coefficient. Comparisons can therefore be made between all the computational methods and the experimental data with the two UPS3D cases used to assess the effect of the differences in lift.

CURRENT STATUS

- **ALL COMPUTATIONAL RESULTS COLLECTED**
- **WIND TUNNEL TEST COMPLETE**
 - TEST DATA OBTAINED FOR CASE 2: WITH NACELLES
 - DIFFERENCES BETWEEN COMPUTED AND TESTED FLOW CONDITIONS AND MEASUREMENT LOCATIONS
 - TEST DATA FOR CASE 1 (NO NACELLES) NOT USABLE FOR COMPARISONS
 - AMES MODEL 3 UNABLE TO BE RE-TESTED IN THE LANGLEY TUNNEL
- **COMPARISONS OF RESULTS USING AVAILABLE TEST DATA COMPLETE**

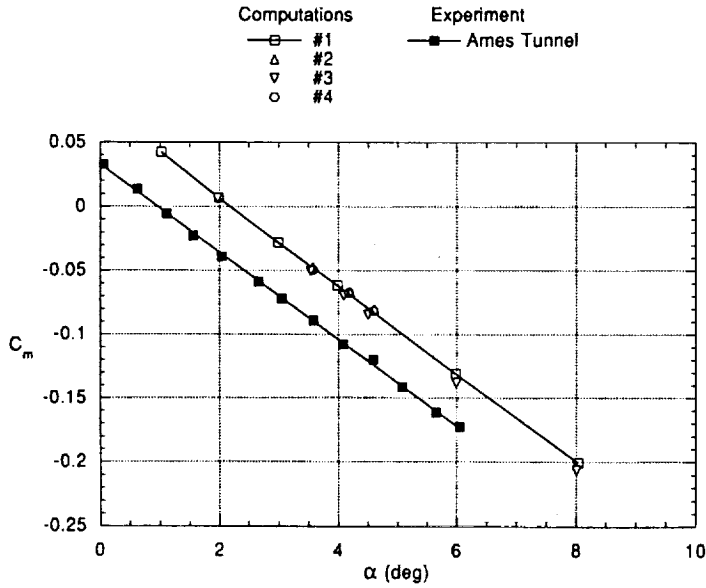
A comparison of computed and experimental lift curves is given in the figure below. The open symbols represent the computational predictions using the various methods and the solid (closed) symbols represent the experimental data. A least-squares curve fit is also shown through the computational and experimental data points. The figure shows excellent agreement between the computational methods, as well as good agreement in lift-curve slopes between the computations and experiment with the computations predicting a slightly lower slope. The shift in lift curves between the experiment and computations indicates the possible need for an angle-of-attack correction of approximately 1.2 deg.

LIFT CURVE COMPARISON, $M=1.68$



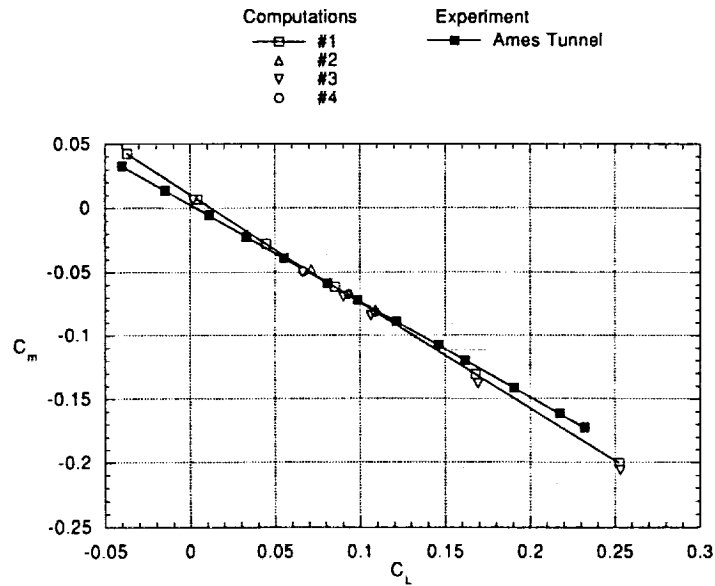
Pitching moment curves given in the figure below show similar comparison trends as the lift curves in the previous figure. A good comparison on pitching moment indicates that the lift distribution along the configuration is accurately predicted. This accuracy is important since the lift distribution is critical in the development of the sonic boom signature.

PITCHING MOMENT CURVE COMPARISON, M=1.68



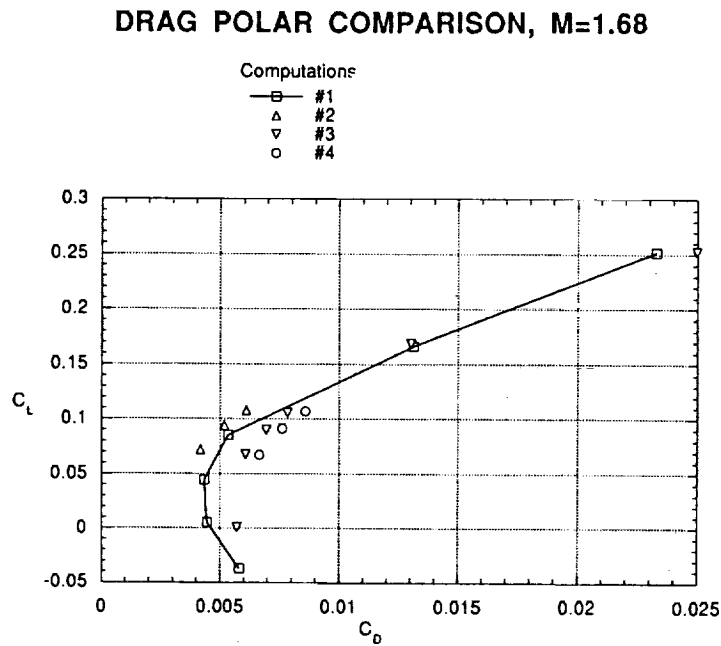
The shifts in the lift and pitching moment curves can be accounted for by plotting the predicted and measured pitching moments versus lift coefficients. The discrepancy in the slopes between the computations and experiment is due to the underpredicted lift-curve slope shown earlier.

PITCHING MOMENT CURVE COMPARISON, $M=1.68$ (C_m vs. C_L)



A comparison of CFD predicted drag polars is given in the figure below. Experimental drag measurements were not available for the prediction exercise. It is noted that all CFD predictions were made using the inviscid Euler equations and, therefore, drag due to viscous forces are not included.

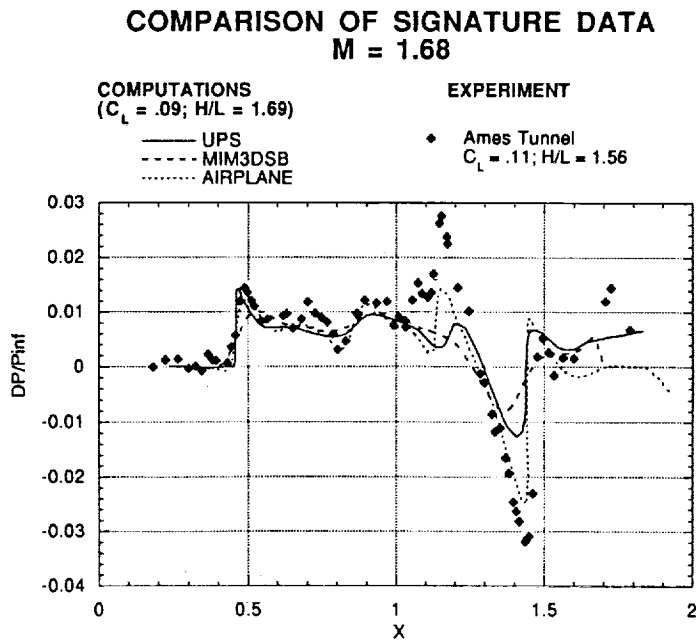
As expected, the drag polars show more scatter between the different methods. One major contributing factor to this scatter is the grid resolution in each method. As surface grids are generated, interpolated, or redistributed, the resolution of curved surfaces which contribute significantly to the drag varies.



A comparison of CFD predicted signatures with experimental measurements is given in the figure below for Test Case 2 (nacelle-on). The best available experimental signature measurements were made at a Mach number of 1.68, a lift coefficient of 0.11 and 1.56 body lengths below the model. For the CFD contributions, results from UPS3D, AIRPLANE and MIM3DSB are available at a 20% lower lift coefficient of 0.09 and a slightly further distance of 1.69 body lengths from the configuration.

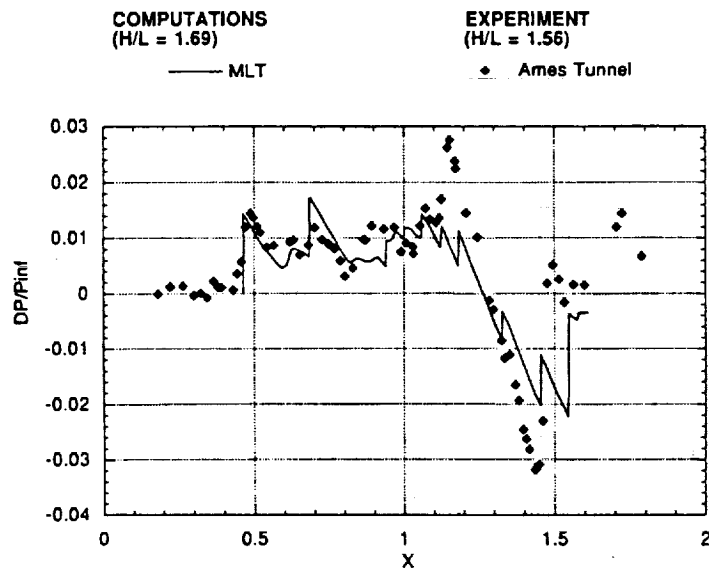
For the front portion of the configuration, the CFD predictions are in reasonable agreement with the experiment. In particular, the initial overpressure due to the bow shock is captured by the CFD methods. In general, further downstream from the bow shock, the predictions capture the basic flow features observed in the experiment. Due to grid resolution differences, some of the methods fail to capture the actual peaks of the over- or under-pressures.

At a normalized streamwise location (X) of 1.1 to 1.5, large discrepancies exist between the predictions and experiment. Possible sources of this discrepancy are examined further in the following figures.



A comparison of the MLT results with the experimental measurements is given below. The MLT prediction at this location gives numerous intermediate shocks but is also able to predict the overall trends in the signature at this location.

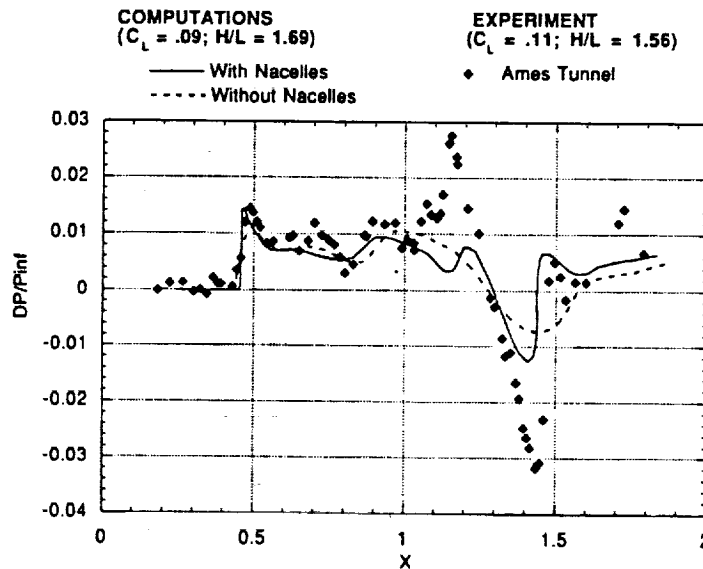
COMPARISON OF SIGNATURE DATA (CONT'D)
M = 1.68



In the results given in the last two figures, the computational predictions were unable to resolve the magnitude of the shock observed at $X = 1.1$ in the experiment. Several factors are investigated as possible contributions to the discrepancies between predictions and experiments. These factors include nacelle modeling, lift coefficient matching, and sting modeling.

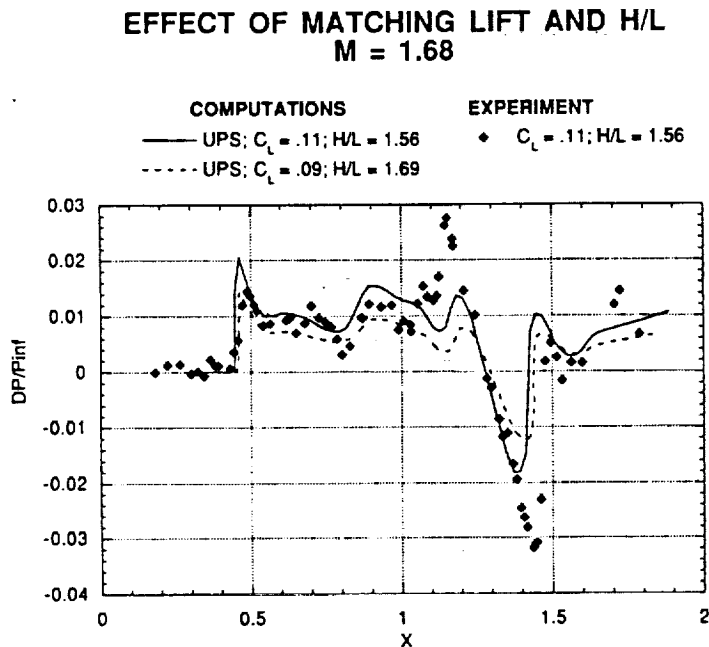
Although all of the presented computations included some form of nacelle modeling, it is instructive to evaluate the sensitivity of the predictions to nacelle effects. Using UPS3D, cases were recomputed at the same flow conditions with and without the presence of the nacelles. The nacelles were modeled in the computations as "flow-through," where inflow and matching outflow conditions are specified at the forward and aft faces, respectively, of the nacelles. Without actually computing the flow through the nacelles, and hence, neglecting nacelle blockage effects, the results given in the figure below demonstrate a stronger shock at $X = 1.1$ to 1.5 . Effects of the nacelles are also noted further upstream in the computational results. Flow blockage of the nacelles in either the computations or experiment would be expected to exaggerate the effects observed below.

EFFECT OF NACELLES ON SIGNATURE PREDICTION M = 1.68



As mentioned earlier, the final reported experimental conditions did not match the original computational flow conditions. Therefore, cases were recomputed using UPS3D to evaluate the relative effects of the differences in computed and measured lift coefficients on the signature data. Furthermore, the original call for computational contributions specified a distance of 1.69 body lengths for reporting computed signatures. A distance of 1.56 body lengths was the final reported experimental measurement position.

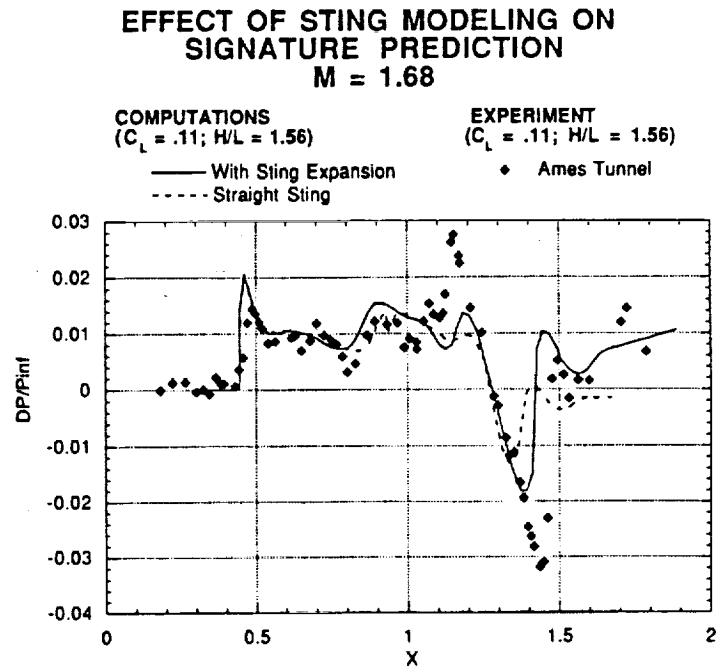
The figure below illustrates the effects of increasing lift coefficient (by 20%) and decreasing distance (by 8%) on the predicted signature of the configuration. Both effects will result in higher average overpressures and stronger shocks as observed in the figure.



The final effect investigated in this exercise is the effect of the sting modeling on the predicted results. The original computations were performed with stings extended straight back from the aft end of the configuration. The wind-tunnel sting consisted of a significant expansion (in sting radius) terminating at a forward-facing step. Both the expansion and step region of the sting are expected to contribute significantly to the shock structure.

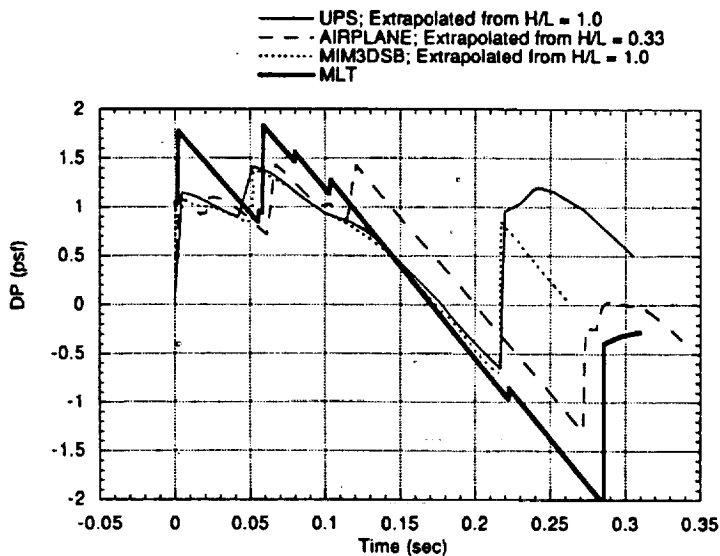
The comparison between a sting with and without expansion is given in the following figure. Due to the added computational gridding complexities, the forward-facing step was not included in this analysis. However, from the figure, it is clearly observed that the expansion of the sting radius has a significant effect on the shock strength and overall signature.

All three effects presented in this exercise, nacelle modeling, lift and distance matching, and sting modeling are shown to have significant effects on the predicted signatures of the configuration.



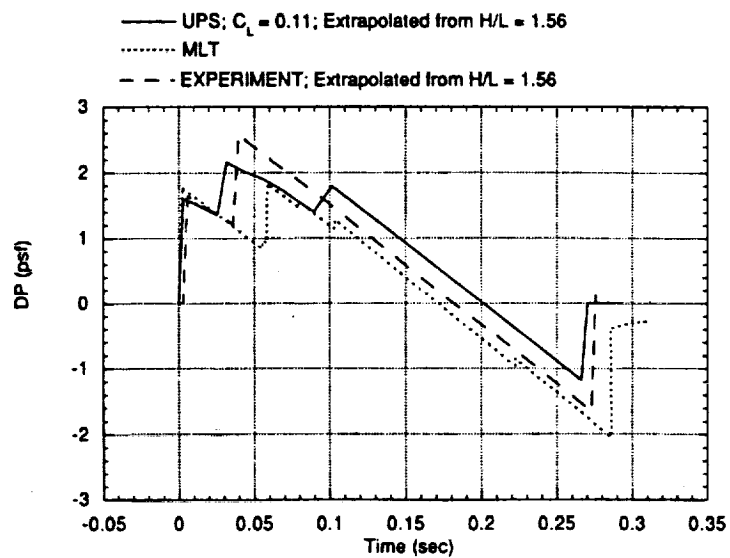
A comparison of predicted ground-level signatures is given in the following figure. The signatures predicted by UPS3D and MIM3DSB are quite comparable most likely due to similar nacelle treatments (flow-through) and similar extrapolation distances. The MLT result exhibits much stronger bow, wing and tail shocks and a longer overall signature length.

COMPARISON OF GROUND SIGNATURE WITH MLT M = 1.68



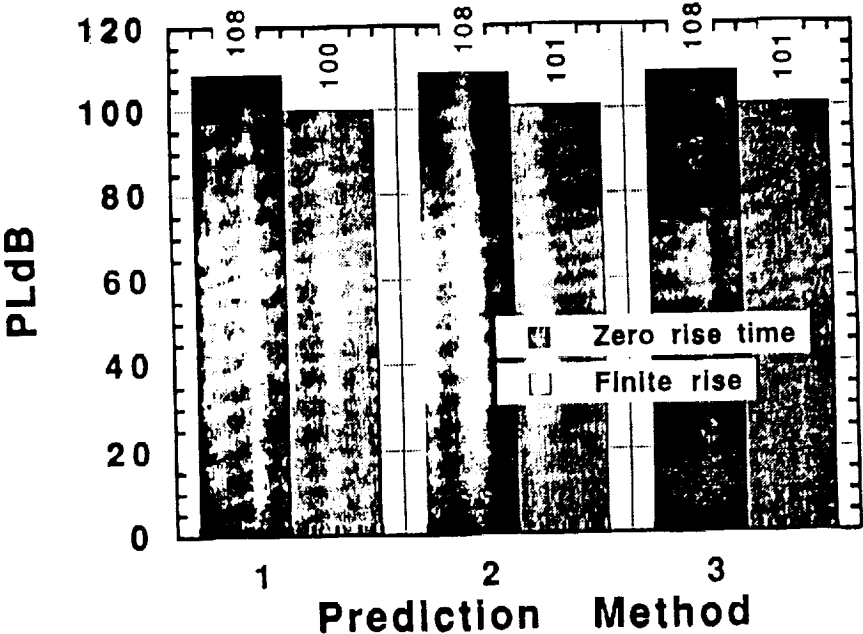
Although ground-level experiments are not available, the experimental data can be extrapolated using similar techniques as in the computational results. A plot comparing the ground-level signatures of the predictions (UPS3D and MLT) and experiment is given below.

COMPARISON OF GROUND SIGNATURE WITH EXPERIMENT M = 1.68



A collection of loudness results for all of the prediction methods is given in the following figure. Surprisingly, despite seemingly large differences in signature characteristics both in the near-field and at ground level, the integrated loudness levels are similar. This is primarily due to the effective filtering which results from using a PLdb metric, which generally determines loudness from macroscopic signature characteristics. These results indicate that comparative sonic boom loudness studies using the given computational methods should be reliable in predicting loudness levels.

Case 2, Loudness at Ground Level



The concluding remarks for the sonic boom prediction exercise are given below. In essence, prediction methods were able to accurately predict lift, pitching moment, and sonic boom loudness levels. The exercise also provided evidence that accurate predictions of near- and mid-field signatures are also anticipated when all pertinent flow and geometry conditions are properly modeled.

Significant variations in results due to differences in prediction methodologies were observed. In addition to physical modeling, differences in grid resolution and extrapolation distances are likely to provide significant variations in signature predictions, particularly absolute shock strength levels. However, sonic boom loudness levels are primarily dependent on macroscopic signature characteristics and appear to be relatively insensitive to many of the differences in the predicted signatures.

Recommendations resulting from this prediction exercise include a detailed study of the effects of grid resolution on the contributed computations. Various grids used in the CFD predictions should be analyzed and compared with the relative resolutions of the mid-field signature.

Further valuable information can also be gained from performing a more detailed study of the effects of nacelle and sting flow modeling. The sting analysis would also be useful in evaluating the differences between experimentally measured results and those expected in actual flight conditions.

Finally, the use of CFD in sonic boom analysis and design would improve with the development of error estimates in the CFD predictions and, based on those error estimates, development of guidelines for CFD modeling and the extrapolation of signatures.

CONCLUDING REMARKS

- LIFT AND PITCHING MOMENTS PREDICTED ACCURATELY BY ALL CFD METHODS
- DRAG SHOWS SIGNIFICANT VARIATION AND IS MORE SENSITIVE TO GRID RESOLUTION
- NEAR-FIELD SIGNATURE PREDICTIONS ARE IN GENERAL AGREEMENT
 - SIGNIFICANT VARIATIONS LIKELY DUE TO GRID RESOLUTIONS AND NUMERICAL DISSIPATION
 - LARGE EFFECT OF NACELLE AND STING MODELING OBSERVED IN SIGNATURE COMPARISON WITH EXPERIMENT
- EXTRAPOLATION TECHNIQUES INTRODUCE FURTHER VARIATIONS IN GROUND SIGNATURE PREDICTIONS
- LOUDNESS METRIC LESS SENSITIVE TO THESE DIFFERENCES

DESIGN AND COMPUTATIONAL/EXPERIMENTAL ANALYSIS OF LOW SONIC BOOM CONFIGURATIONS

Susan E. Cliff, Timothy J. Baker*, and Raymond M. Hicks
NASA Ames Research Center
Moffett Field, CA

*Princeton University
Princeton, NJ

INTRODUCTION

Recent studies have shown that inviscid CFD codes combined with a planar extrapolation method give accurate sonic boom pressure signatures at distances greater than one body length from supersonic configurations if either adapted grids swept at the approximate Mach angle or very dense non-adapted grids are used¹⁻⁵.

The validation of CFD for computing sonic boom pressure signatures provided the confidence needed to undertake the design of new supersonic transport configurations with low sonic boom characteristics. An aircraft synthesis code in combination with CFD and an extrapolation method were used to close the design.

The principal configuration of this study is designated LBWT (Low Boom Wing Tail) and has a highly swept cranked arrow wing with conventional tails, and was designed to accommodate either 3 or 4 engines. The complete configuration including nacelles and boundary layer diverters was evaluated using the AIRPLANE code⁶⁻⁸. This computer program solves the Euler equations on an unstructured tetrahedral mesh. Computations and wind tunnel data for the LBWT and two other low boom configurations designed at NASA Ames Research Center are presented. The two additional configurations are included to provide a basis for comparing the performance and sonic boom level of the LBWT with contemporary low boom designs and to give a broader experiment/CFD correlation study. The computational pressure signatures for the three configurations are contrasted with on-ground-track near-field experimental data from the NASA Ames 9x7 Foot Supersonic Wind Tunnel. Computed pressure signatures for the LBWT are also compared with experiment at approximately 15 degrees off ground track.

LOW BOOM CONFIGURATION DESIGN - LBWT

The LBWT configuration design⁹ was carried out using the HFLO4 code and iterative design procedures. HFLO4 is a finite volume Euler-equation solver that generates single block H-H meshes about configurations consisting of a fuselage and two lifting surfaces¹⁰⁻¹¹. It is a simple task to alter the HFLO4 input data set to run a new configuration. In particular, it is very easy to make systematic changes in geometric parameters such as planform, wing camber, and twist.

The HFLO4 grid used during design had 176 streamwise, 128 vertical, and 48 spanwise grid points. The computed sonic boom pressure signatures were obtained at distances of a quarter and a third body length from the configuration and extrapolated to the ground. The extrapolation code used for this study (designated ANET) is a waveform parameter method based on geometric acoustics¹². The maximum overpressure of the off-ground-track pressure signatures was constrained during design to be less than the on-ground-track overpressure.

The computational signatures of intermediate designs were extrapolated to the ground using ANET, then rise time was added to the shocks by ADDRISE¹³, and finally a perceived loudness level (PLdB)¹⁴ was calculated. An aircraft synthesis code, ACYSNT¹⁵⁻¹⁷, was used to determine if the proposed aircraft met the mission requirements. The design procedure is summarized below:

1. Perturb geometry
2. Obtain HFLO4 solution
3. Analyze near-field data (on and off ground track)
4. Extrapolate near-field signature to ground (on ground track)
5. Obtain PLdB (on ground track)
6. Evaluate performance - ACSYNT

This process was repeated until the design was terminated to permit manufacture and testing of the wind tunnel models by the project completion date. The resulting configuration is shown in Fig. 1.

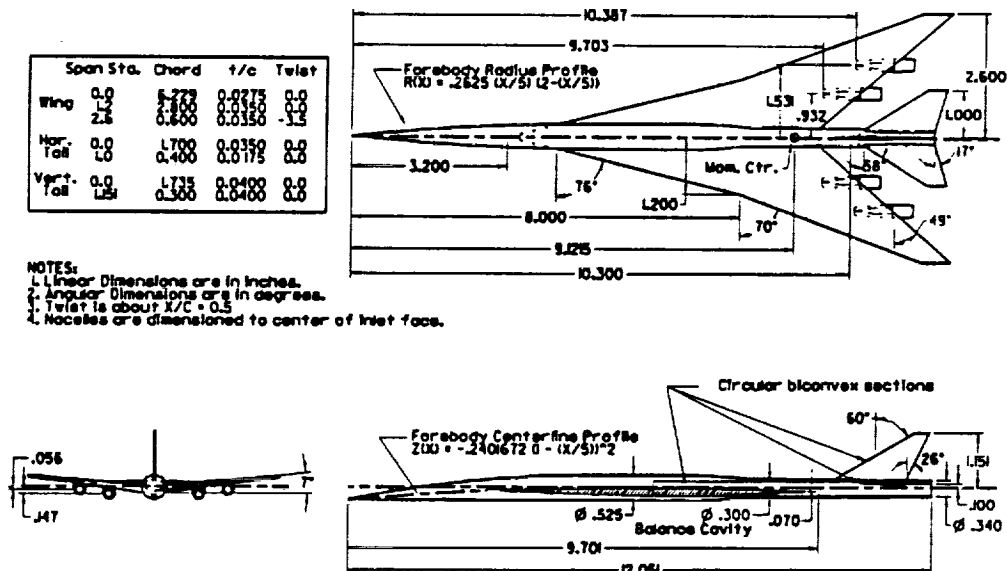


Figure 1. 3-view of the LBWT wind tunnel model.

REFERENCE PARAMETERS

The next generation supersonic transport configuration must meet performance criteria as well as environmental constraints. The design mission for the aircraft assumed a range of 5,500 nautical miles with 300 passengers. A PLdB of 95 or less was used as a goal for the design, assuming flight was restricted to designated corridors. Lower PLdB levels would be necessary if supersonic flight over populated areas were sought. 95 PLdB is assumed to be acceptable, but future legislation by Congress may dictate lower levels. The law currently states that commercial aircraft may not generate a sonic boom over the continental United States. The design was limited to conventional shapes so that the aircraft would be acceptable to the aviation community.

The reference areas for the three configurations studied are based on the planform areas of the main wing including the projected fuselage area between the root leading and trailing edges. The reference areas for the LBWT, LBWC (Low Boom Wing Canard), and LBW (Low Boom Wing) as well as the streamwise locations of the moment center, the average chord used in the moment calculations, and the reference body length are shown in Fig. 2.

	SREF	mom ctr	Cbar	length
LBWT	15.374	9.12	3.0	12.
LBWC	14.48	8.74	2.34	12.
LBW	15.788	8.22	3.97	11.18

Figure 2. Reference parameters.

TEST TECHNIQUES

Experimental pressure signatures from the NASA Ames 9x7 Foot Supersonic Wind Tunnel were obtained at approximately one body length from the LBWT, LBWC, and LBW configurations. The wing, body, and trimming surfaces of the models were machined from single billets of stainless steel. The aluminum nacelles and diverters were attached to the lower surfaces of the wing by screws. Pins were used to align the nacelles and diverters with the local flow direction at the inlet. The aft portion of the models were bored to accommodate an integral balance/sting. Lift and pitching moment values were measured using a 2-component force-moment balance. The reference lengths for the LBWT, LBWC, and LBW models were 12.0, 12.0, and 11.18 inches respectively.

The pressure signatures were measured using pressure transducers connected to 2 degree conical probes mounted on the wind tunnel walls. The reference pressure was measured by an absolute pressure transducer connected to a pressure probe in a non-interfering position in the tunnel. The overpressures were measured by differential pressure transducers connected to reference and overpressure probes. The manifold overpressure probe had four equally spaced radial orifices aligned with the Mach angle to ensure that the orifices lie within the shock layer for the design Mach number. The overpressure probes were located so that model and probe shock reflections did not interfere with the pressure signatures. Two overpressure probes were used to measure on- and off- ground track signatures simultaneously. The off-ground-track data were obtained at an azimuthal angle of approximately 15 degrees. The LBWT and LBWC configurations were tested at Mach 2, whereas the LBW configuration was tested at Mach 1.68. Total pressure was held constant at 30 in. Hg during testing. The moisture content of the air was difficult to control owing to leaking radiators and nozzle seals in the wind tunnel.

An installation photograph of the LBWT in the 9x7 Foot Supersonic Wind Tunnel is shown in Fig 3.

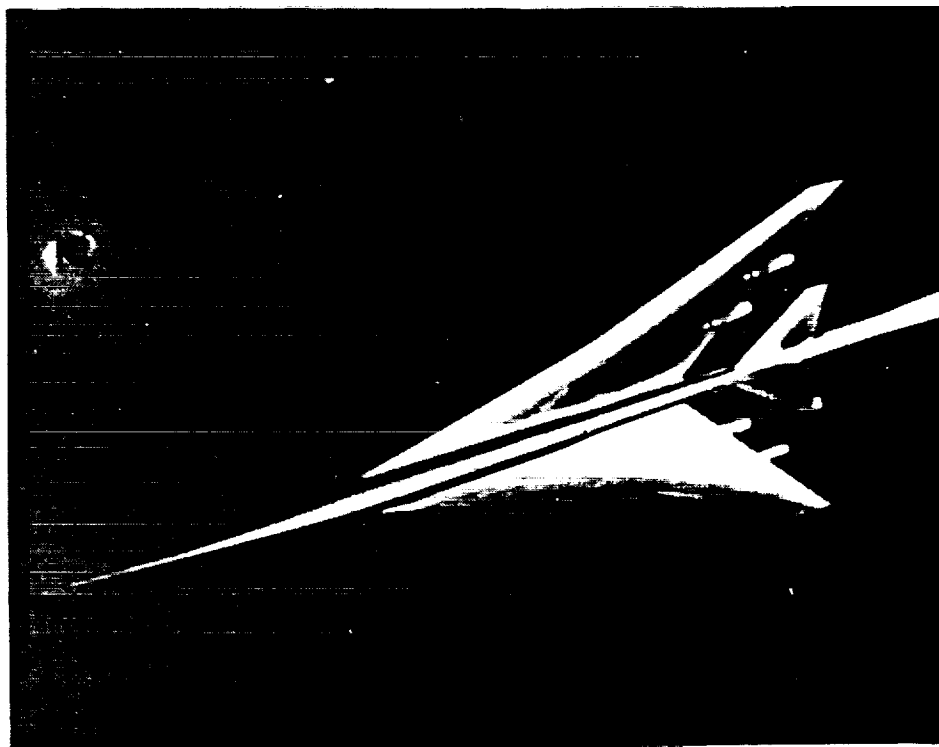


Figure 3. Installation photograph of the LBWT in NASA Ames 9x7 Foot Supersonic Wind Tunnel.

AIRPLANE SURFACE GRID: LBWT

AIRPLANE was used as an analysis code because of its demonstrated ability to give accurate flow field predictions and handle highly complex configurations. The generality afforded by AIRPLANE in treating arbitrary configurations precludes the designer from making systematic changes in geometric shape as easily as with HFLO4. Since AIRPLANE has been shown to give accurate sonic boom pressure signatures for many configurations it was therefore used to validate the results of the design code HFLO4 (The HFLO4 results can be found in Reference 9).

AIRPLANE⁶⁻⁸ assumes that a configuration is divided into a number of components defined by a series of planar or non-planar cross sections. The intersection between different components should be defined with one-to-one point matching for best results. AIRPLANE uses only the points given in the input data set since the true surface between points is not known. However, points are sometimes deleted which result in irregular surface triangles. Dividing the configuration into components is usually necessary to obtain exact intersections since the gridding algorithm contains logic to ensure that different components only connect along specified interfaces. If a configuration is not broken into different components the intersections between components may not be precise.

The AIRPLANE surface grid shown in Fig 4 has 8,295 points whereas the HFLO4 grid (not shown) used during design had 6,534 surface points.

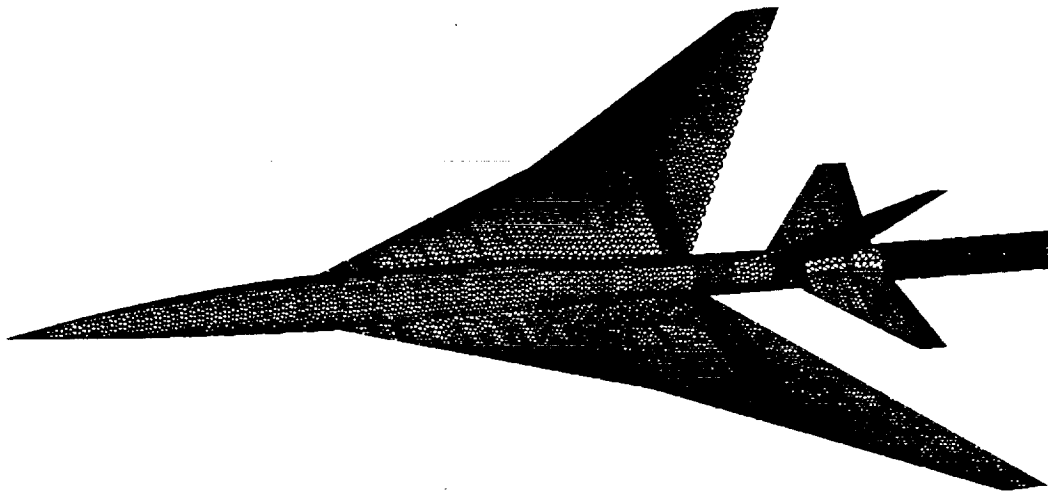


Figure 4. AIRPLANE unstructured tetrahedral surface grid of the LBWT without nacelles.

AIRPLANE SYMMETRY PLANE GRID: LBWT

AIRPLANE uses a staging of meshes that increase in density from the outer boundaries to the configuration surface by use of a sequence of nested boxes (Fig 5). The dense grid near the surface does not propagate to the outer boundaries, resulting in a more efficient use of points than the structured HFLO4 grid used during design. This dense grid near the surface of the configuration improved the shock definition of the pressure signatures compared with HFLO4 results ⁹.

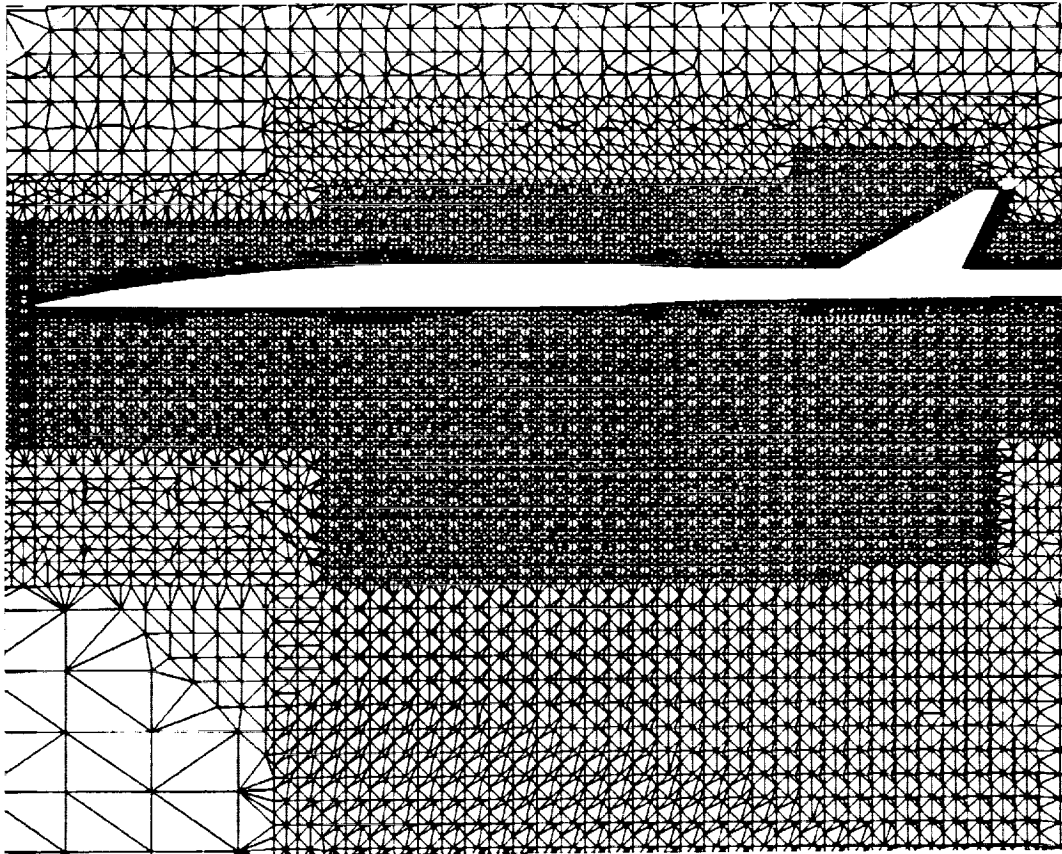


Figure 5. AIRPLANE symmetry plane grid for the LBWT without nacelles.

COMPUTATIONAL/ EXPERIMENTAL LIFT CURVES

The experimental lift curves are compared with AIRPLANE computations for the LBWT and LBWC configurations in Fig. 6a. The experimental data exhibits some non-linearity and scatter which may be due to model vibration and/or improper data sampling rate. The AIRPLANE lift curves have a slightly lower slope than the experimental data for the LBWT, but they are in close agreement for the LBWC. The experimental angle of attack is not known, because the model was tested in regions of the wind tunnel that have not been surveyed resulting in unknown stream angle.

The AIRPLANE computations for the LBWT and LBWC without nacelles are compared with an Euler marching solver developed by Siclari¹⁸ in Fig 6b. The computations from the marching scheme are in good agreement with the AIRPLANE results. The LBWT computations show minor differences resulting from neglecting the horizontal tail in the marching code calculations. The tail carries additional positive lift. The good agreement between AIRPLANE and the marching code gives additional confidence in the accuracy of the CFD predictions, and casts doubt on the accuracy of the experimental data. The poor correlation for zero lift angle is due to an inaccurate experimental angle of attack.

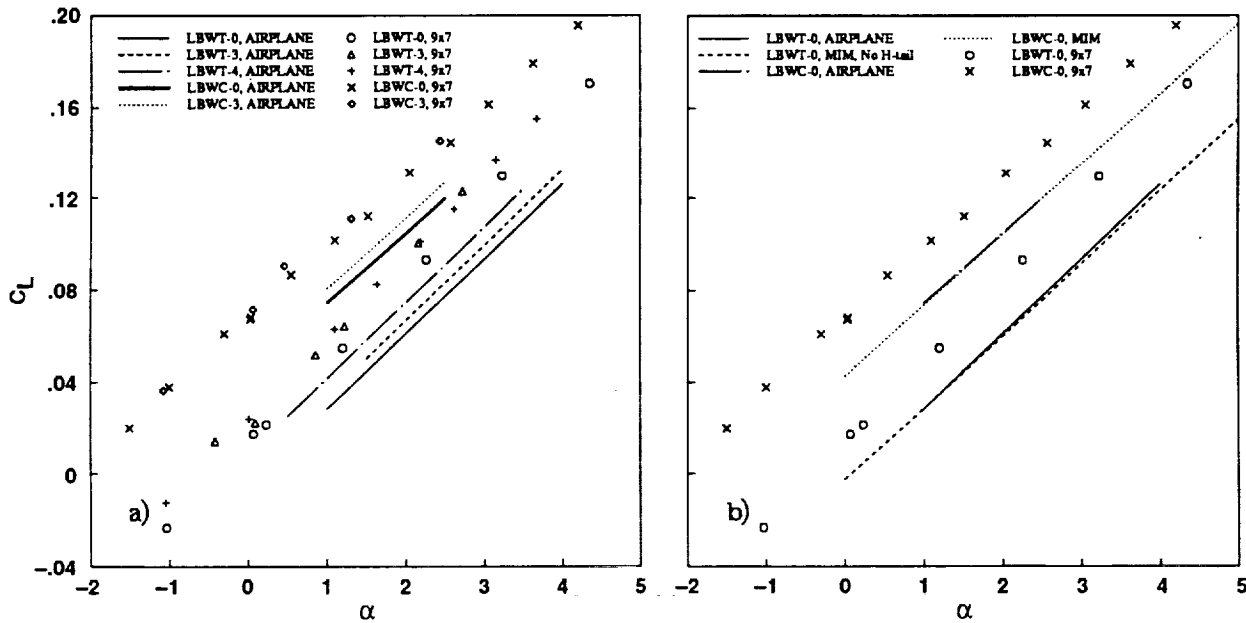


Figure 6. Experimental and computational lift curves, $M = 2.0$.

PRESSURE SIGNATURE CORRELATIONS: LBWT WITHOUT NACELLES

The pressure signatures for the LBWT configuration without nacelles are shown in Figs. 7a-d. The AIRPLANE computational data was taken at $1/4$ and $1/3$ body lengths (Y_S of 3 and 4) below the model and extrapolated to the experimental altitude of approximately 1 body length. Y_S is the computational sampling distance below the model in inches. Most of the shocks are under predicted by AIRPLANE. In particular, the tail shock is greatly underestimated which may be due to inaccurate modeling of the fuselage base and sting. The fuselage extended downstream approximately $1/4$ body length in the computational model. Accurate modeling of the sting and a boat-tail ramp at the base/sting intersection, to simulate the turning angle of the viscous wake, would have increased the tail shock strength. The comparisons improve with increasing lift and little effect from the computational sampling distance is observed.

The experimental data is questionable since the bow shock strength decreases with increasing lift coefficient (compare figs 7a and 7d). In addition, the free-stream pressure level upstream of the bow shock shows fluctuations which define a scatter band width and make it difficult to determine an accurate reference level for the pressure signatures. The first data point was assumed to be the free stream level. These anomalies also appear related to the tunnel moisture level and will be discussed later. Numerical dissipation may be partly responsible for the weakening of the computational shocks. However, obtaining the signature in the dense grid near the model should have minimized the effects of dissipation.

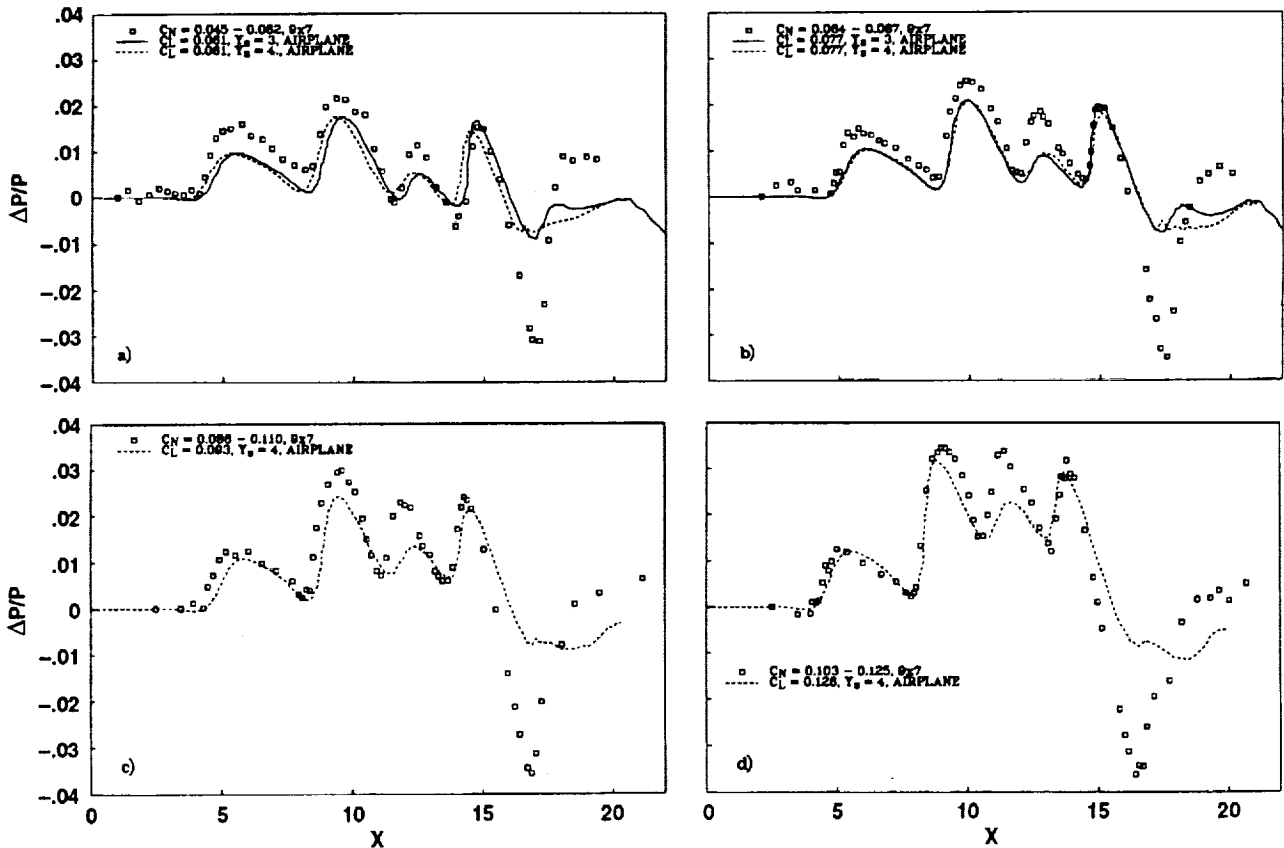


Figure 7. Pressure signatures for the LBWT without nacelles, $M = 2.0$, $h = 14$ in.

AIRPLANE SURFACE GRID: LBWT- 4 NACELLES

The effects of nacelles and boundary layer diverters on the pressure signatures were determined by AIRPLANE. A conventional 4 engine configuration was studied first. The orientation of the nacelles in both pitch and yaw was determined from the stream angles calculated by HFLO4. The interior of the nacelles diverged 1 degree between the inlet and exit which allows for boundary layer growth to help "start" the nacelles during wind tunnel testing. The surface grid of the LBWT configuration complete with nacelles/diverters and horizontal and vertical tails is shown in Fig. 8.

The increased density of points in the nacelle/diverter region was used to more accurately compute the complex flow field in this region. A nearly uniform distribution of grid points was used to improve the quality of the surface grid. The nacelles analyzed with AIRPLANE had constant area ducts to simulate the divergent ducts with boundary layer growth in the wind tunnel. This results in the large base area shown in the figure.

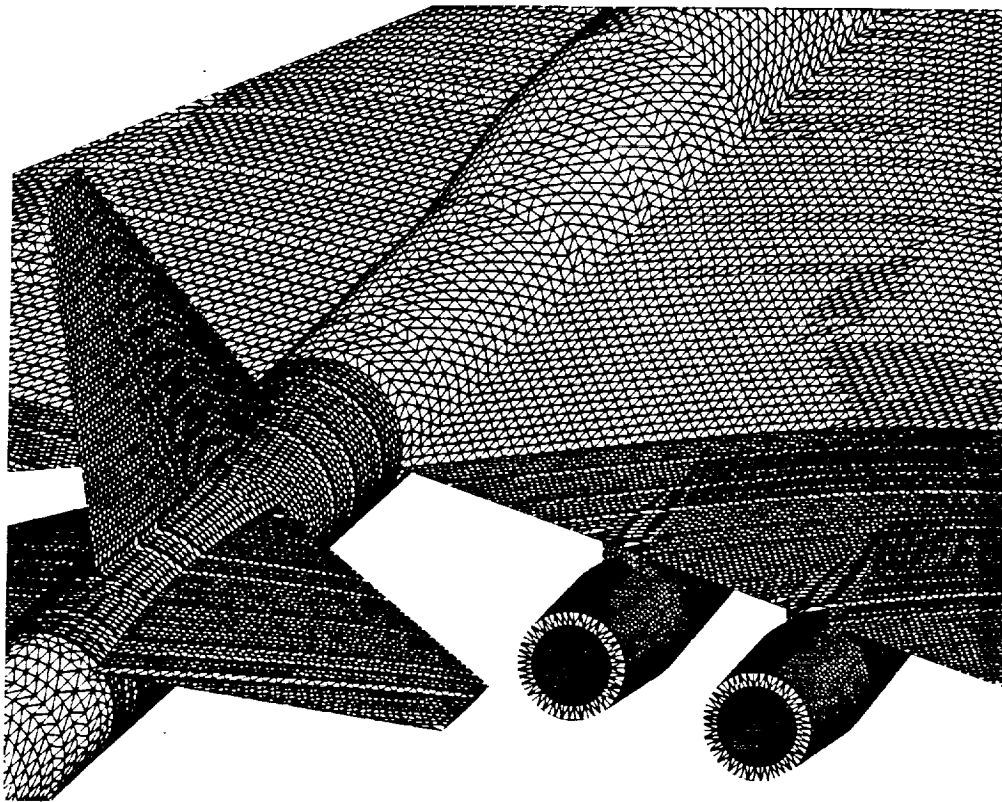


Figure 8. AIRPLANE unstructured surface grid for the aft portion of the LBWT with 4 nacelles.

PRESSURE SIGNATURE CORRELATIONS: LBWT - 4 NACELLES

The results for LBWT configuration with 4 open nacelles are shown in Figs. 9a-c. Here, the comparisons are acceptable for the two lower lift cases with the strength of the bow and inboard shock fairly accurately predicted. The outboard wing and nacelle shocks are slightly under predicted which may be due to spillage. The high lift case (Fig. 9c) shows poor correlation. The poor agreement may be due to inaccurate experimental data, since the bow shock increases with lift at a larger rate than would be expected for the slender nose. Another explanation for the poor correlation may be an unstart condition with reduced mass flow ratio at the high lift coefficient. A stronger computational tail shock is observed when nacelles are present (Figs. 7 and 9). This may be the result of using an increased number of grid points, 580,762 compared with 443,930 for the LBWT configuration without nacelles.

The open nacelles were filled with dental plaster to simulate choked nacelles in the experimental model and by gridding the inlet and exit faces of the nacelle in the computational model. The AIRPLANE/Experiment comparison with blocked nacelles is shown in Fig. 9d. The bow and inboard wing shocks are in good agreement, but the blocked-nacelle/outboard-wing shock is under predicted by AIRPLANE.

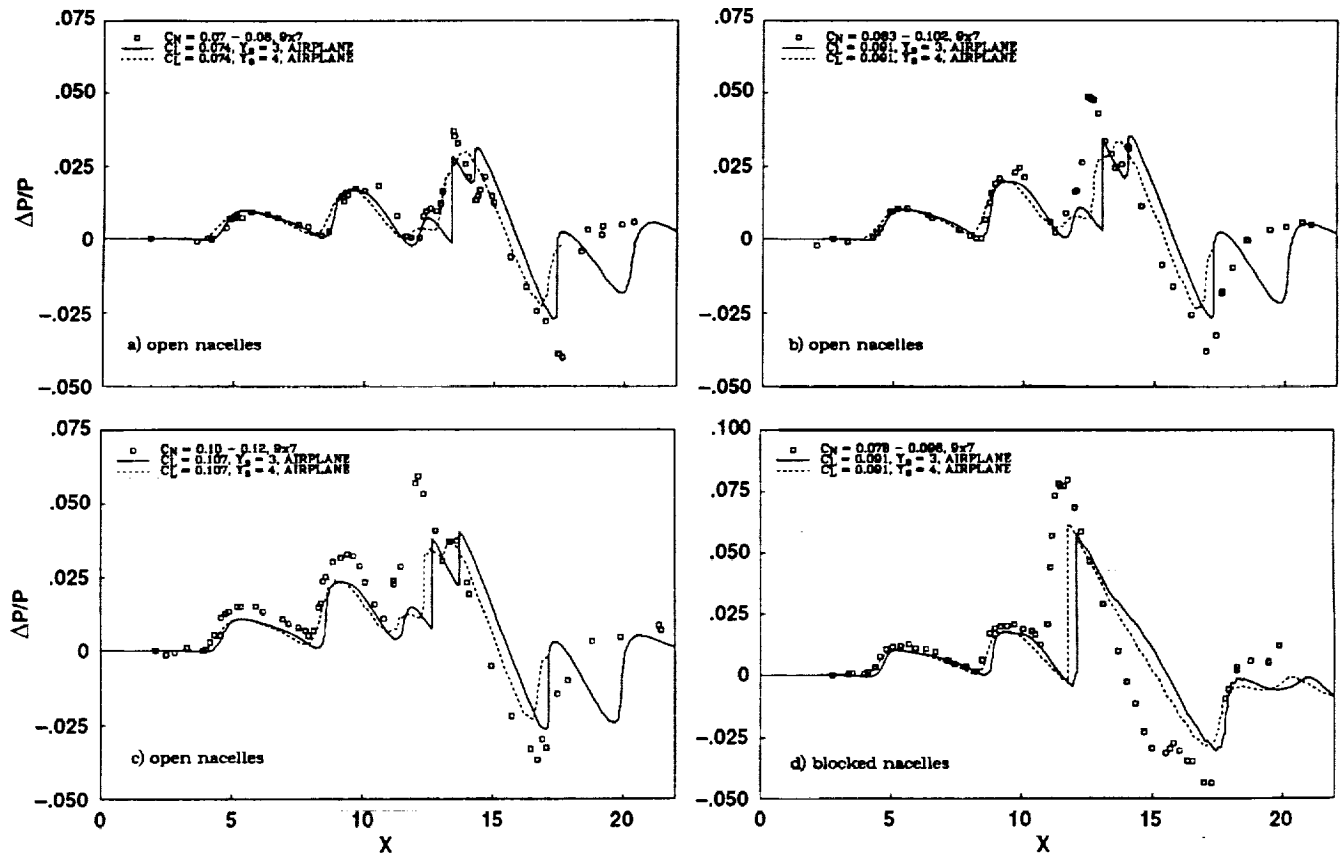
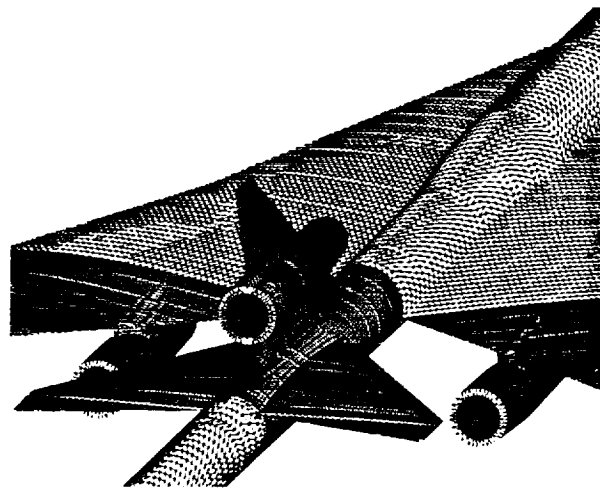


Figure 9. Pressure signatures for the LBWT with 4 nacelles, $M = 2.0$, $h = 14$ in.

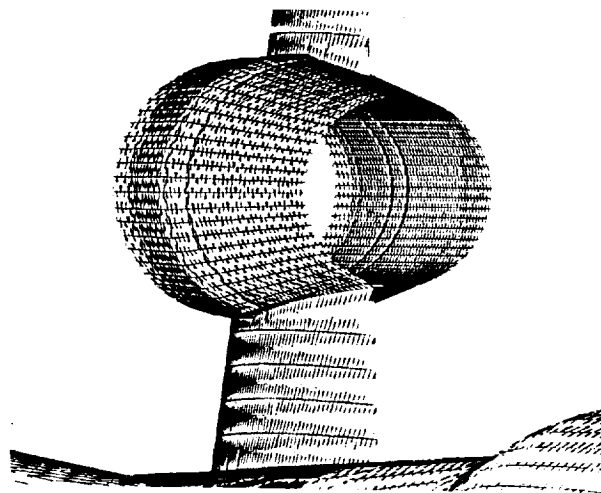
AIRPLANE SURFACE GRID: LBWT - 3 NACELLES

The 3 engine LBWT configuration used the same wing, fuselage, and horizontal tail components for input to AIRPLANE as the 4 engine configuration. The added thrust required per engine for the 3 engine configuration resulted in larger nacelles than the 4 engine configuration. The inboard nacelle and diverter on the 4 engine configuration were replaced and the outboard nacelle/diverter removed.

The third nacelle was mounted on the vertical tail (Fig 10a). An enlarged view of the inlet region of the nacelles on the vertical tail is shown in Fig 10b. The grid density of the empennage is increased in the nacelle region for improved computational accuracy.



a)



b)

Figure 10. AIRPLANE unstructured surface grid for the LBWT with 3 nacelles.

PRESSURE SIGNATURE CORRELATIONS: LBWT 3 NACELLES

The LBWT comparisons with 3 open nacelles are shown in Figs. 11a-d. The open nacelle computations have a weaker nacelle/outboard wing shock than experiment. The strength of the bow and inboard shocks range from good agreement (Fig 11b) to poor agreement (Fig. 11c). The experimental bow shock strength oscillates with increasing lift coefficient. The shock directly up-stream of the tail shock is under predicted by AIRPLANE for all cases. The tail shock was more accurately predicted for the 4-nacelle configuration than the 3- or 0- nacelle cases. This may be due to coarser grids used for this and the 0-nacelle configuration. The comparison for the blocked nacelle case is shown in Fig. 11e. The bow and inboard wing shock correlation is acceptable, but the nacelle/outboard wing and tail shocks are under predicted. Extrapolating from 1/4- rather than 1/3-body length results in a stronger computational nacelle shock.

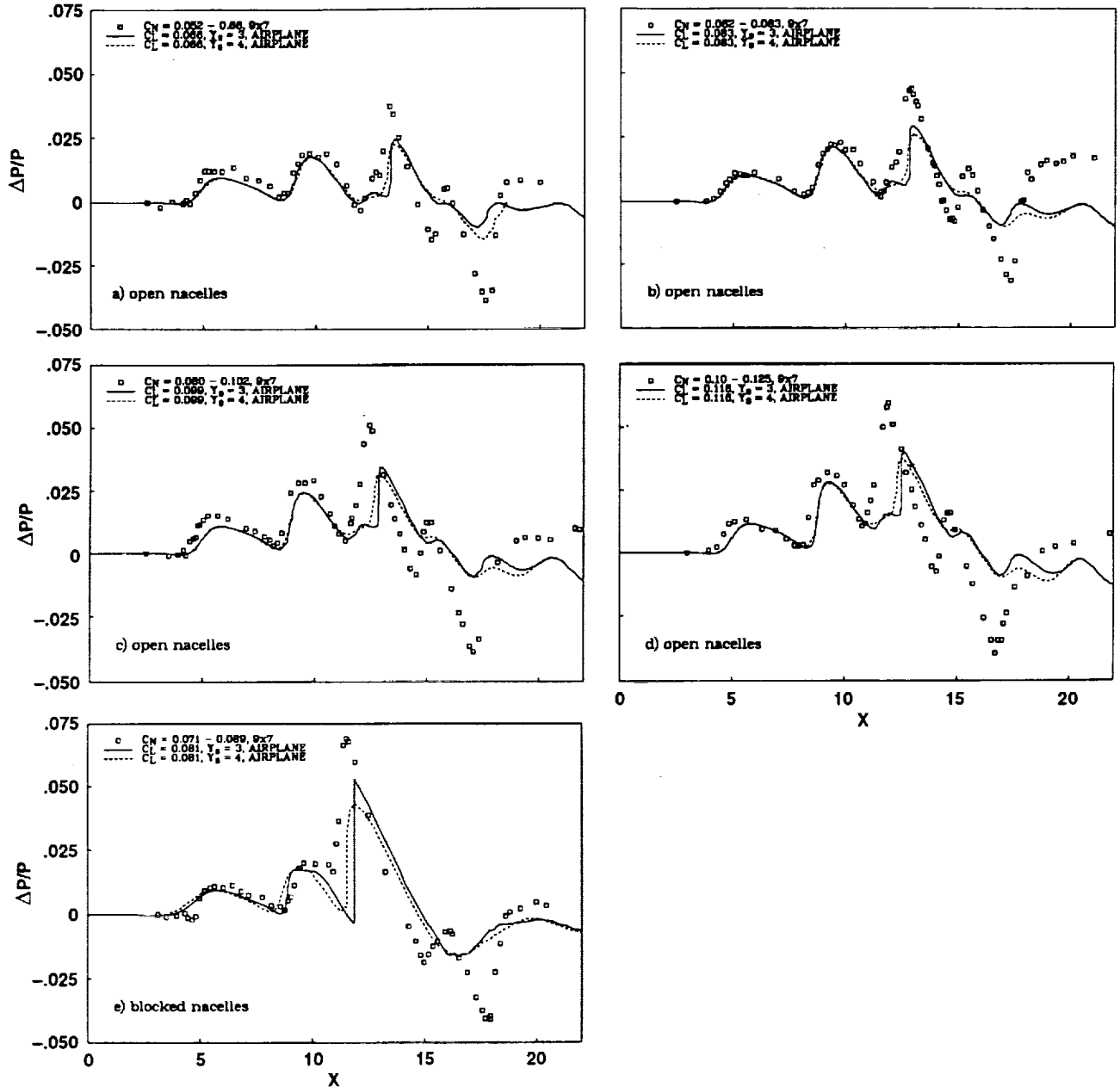


Figure 11. Pressure signatures for the LBWT with 3 nacelles, $M = 2.0$, $h = 14$ in.

BOW SHOCK STRENGTH COMPARISONS

The experimental and computational bow shock strength has been plotted as a function of normal force coefficient in Fig. 12a. The AIRPLANE results show the expected slight increase of shock strength with increasing normal force coefficient. Clearly, the 4 nacelle configuration should have a weaker bow shock than the 3- or 0- nacelle models due to a more positive C_{L0} and hence lower angle of attack for a given lift coefficient. The larger C_{L0} is due to the added lift obtained by an increase in pressure from the nacelle shocks impinging on the wing lower surface. The experimental results indicate large changes in bow shock strength for relatively small changes in lift coefficient. The 4 nacelle configuration has the correct slope but the magnitude is larger than expected. Data from past 9x7 wind tunnel tests 19-21 for several models which have distinct bow shocks show the expected slight increase in shock strength with increasing normal force coefficient (Fig. 12b). This suggests that the current wind tunnel data is questionable. Note that the scales for the two figures differ, the changes in shock strength with normal force for the current data are plotted to a finer scale.

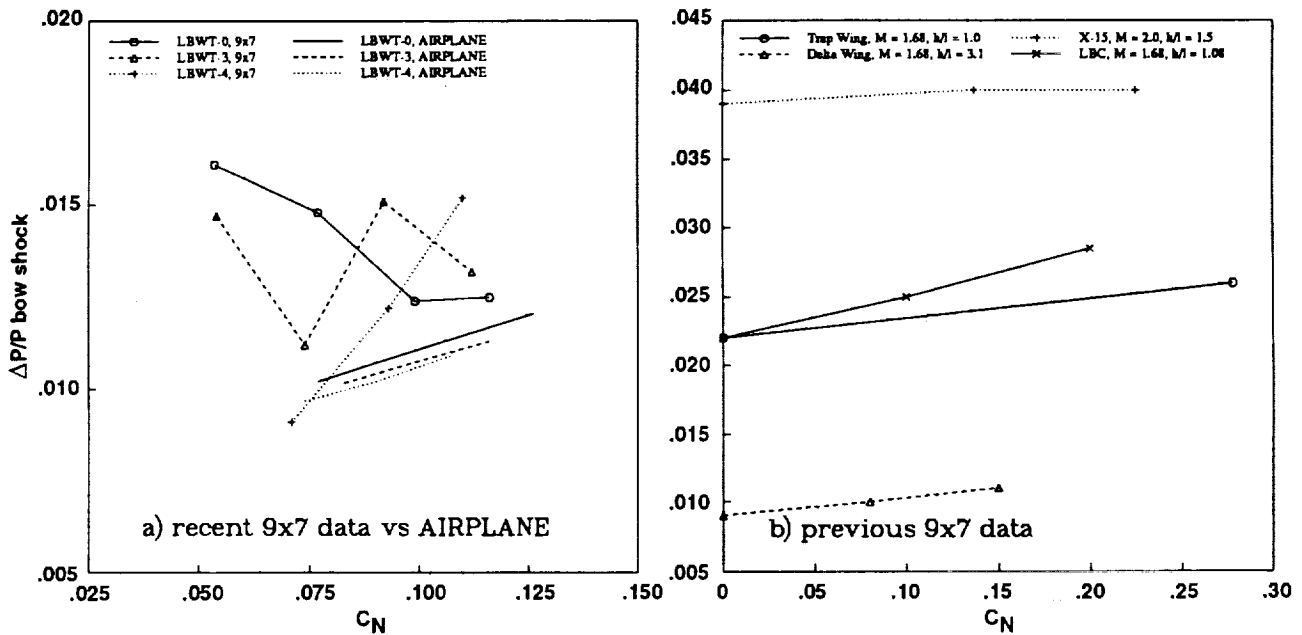


Figure 12. Bow shock strength as a function of normal force coefficient.

MOISTURE LEVEL/BOW SHOCK STRENGTH CORRELATION: LBWT

Bow shock strength appears to vary inversely with moisture level (Fig. 13a-b). The shock strength decreases in magnitude with increasing moisture content. The data from past wind tunnel tests were obtained at moisture levels below 300 PPM. This moisture level could not be attained during this test owing to radiator and nozzle seal leaks. The computational results correlate better at the higher moisture level. The correlations would probably have been more consistent if the moisture level were held constant. These inconsistencies in the data make it difficult to compare the three low boom models.

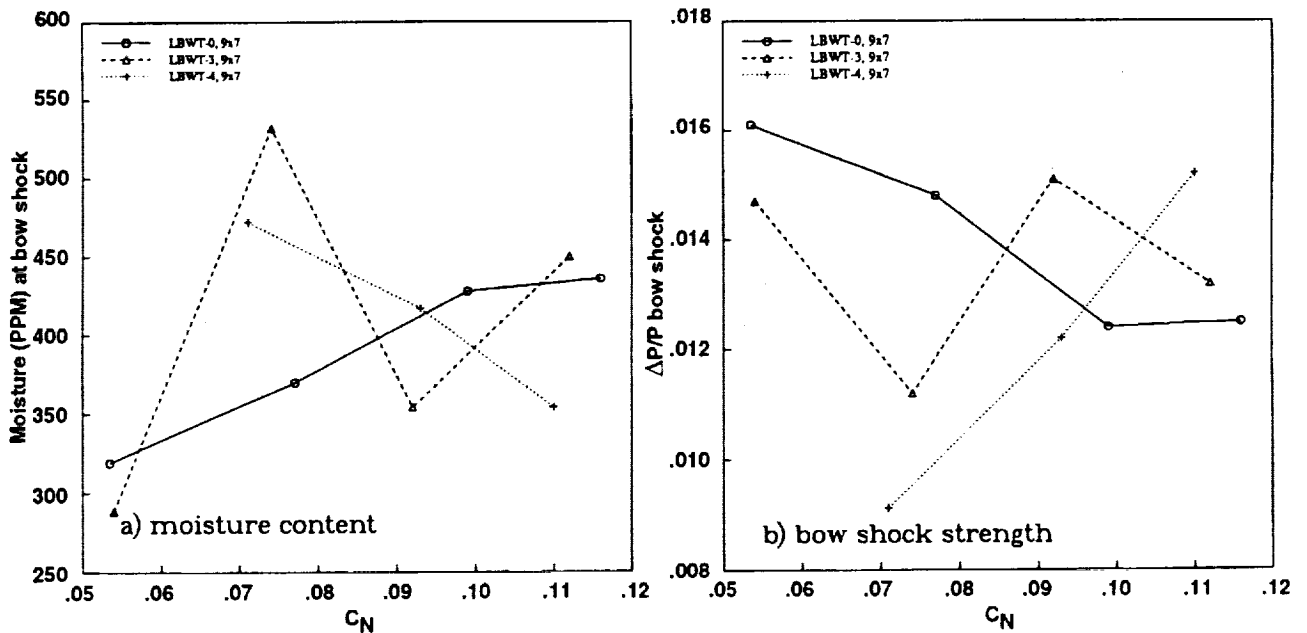


Figure 13. Wind tunnel moisture levels and bow shock strength for the LBWT.

OFF GROUND TRACK PRESSURE SIGNATURES: LBWT

The AIRPLANE off-ground-track pressure signatures at an azimuthal angle of approximately 15 degrees are compared with experiment in Figs. 14a-c. The shock locations shown in the pressure signatures for the LBWT without nacelles (Fig. 14a) correlate better with experiment than with nacelles (Fig 14b-c). The nacelle shocks should be closer to the bow shock off track than on track, a trend not observed in the computational data (compare figs. 14b and 9a). The difference in nacelle shock position on- and off-track can be explained by the following argument based on Mach cutting planes: The lateral distance from the centerline to the nacelles is greater than the vertical distance from the centerline to the nacelles. This difference in distance causes off-track cutting planes to pick-up the nacelles before the on-track cutting planes giving rise to the forward shift in the position of the nacelle shocks. The AIRPLANE computations do not show the correct forward shift due, in part, to the computational sampling distance, Y_S . Characteristic lines emanating from the nacelles are not captured by the planar extrapolation method near the configuration. The sampling distance should be further from the model to accurately capture nacelle effects. However, grid density limitations and dissipation in the numerical scheme render the data at larger distances inaccurate.

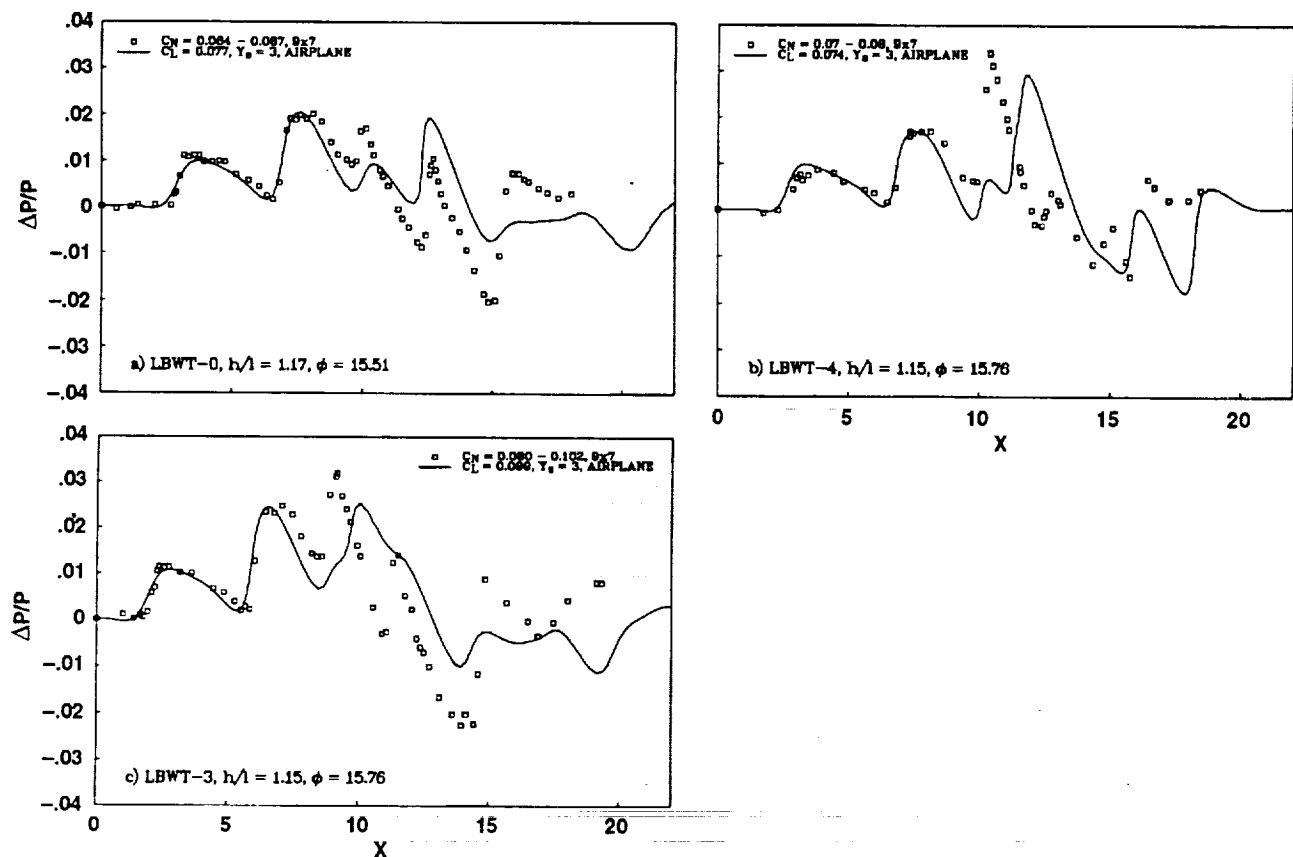


Figure 14. Off-ground-track pressure signatures for the LBWT, $M = 2.0$, nominal $\phi = 15.5$ deg.

AIRPLANE SURFACE GRID: LBWC - 3 NACELLES

The surface triangulation for the LBWC configuration is shown in Fig. 15. The LBWC was designed using the same method as the LBWT configuration²¹. The integral nacelle/vertical tail geometry is identical to that used for the LBWT configuration. A narrow re-entrant corner occurs where the trailing edge of the wing attaches to the bottom of the fuselage which required additional surface grid points to accurately triangulate the surface in this region.

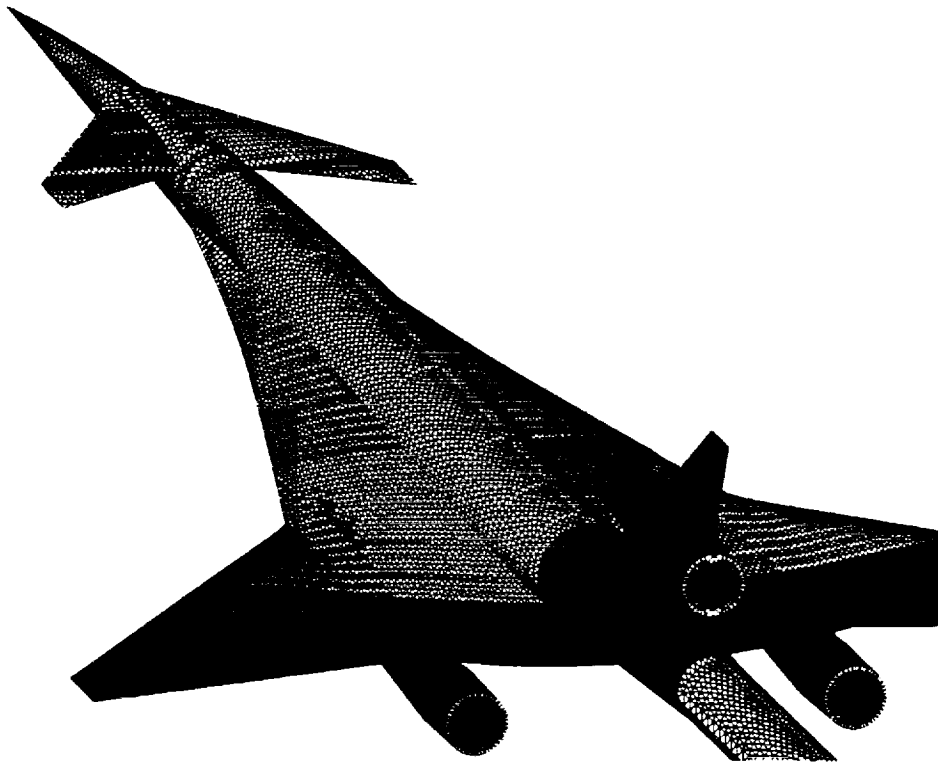


Figure 15. AIRPLANE unstructured surface grid for the LBWC with 3 nacelles.

PRESSURES SIGNATURE CORRELATIONS: LBWC WITHOUT NACELLES

The pressure signatures for the LBWC configuration without nacelles are shown in Figs 16a-c. Here, the experimental and computational data show a weak shock from the nose of the fuselage that has not coalesced with the canard shock. The bow shock appears as a small finite rise at the front of each signature, consistent with the $X^{5/2}$ area growth of the fuselage. The computational data shows weaker canard and wing shock strength than experiment. The moisture levels in PPM range from 350-430, 350-425, and 460-525 for nominal lift coefficients of .07, .09, and .11. It is not desirable to have this much variation in moisture level during a run.

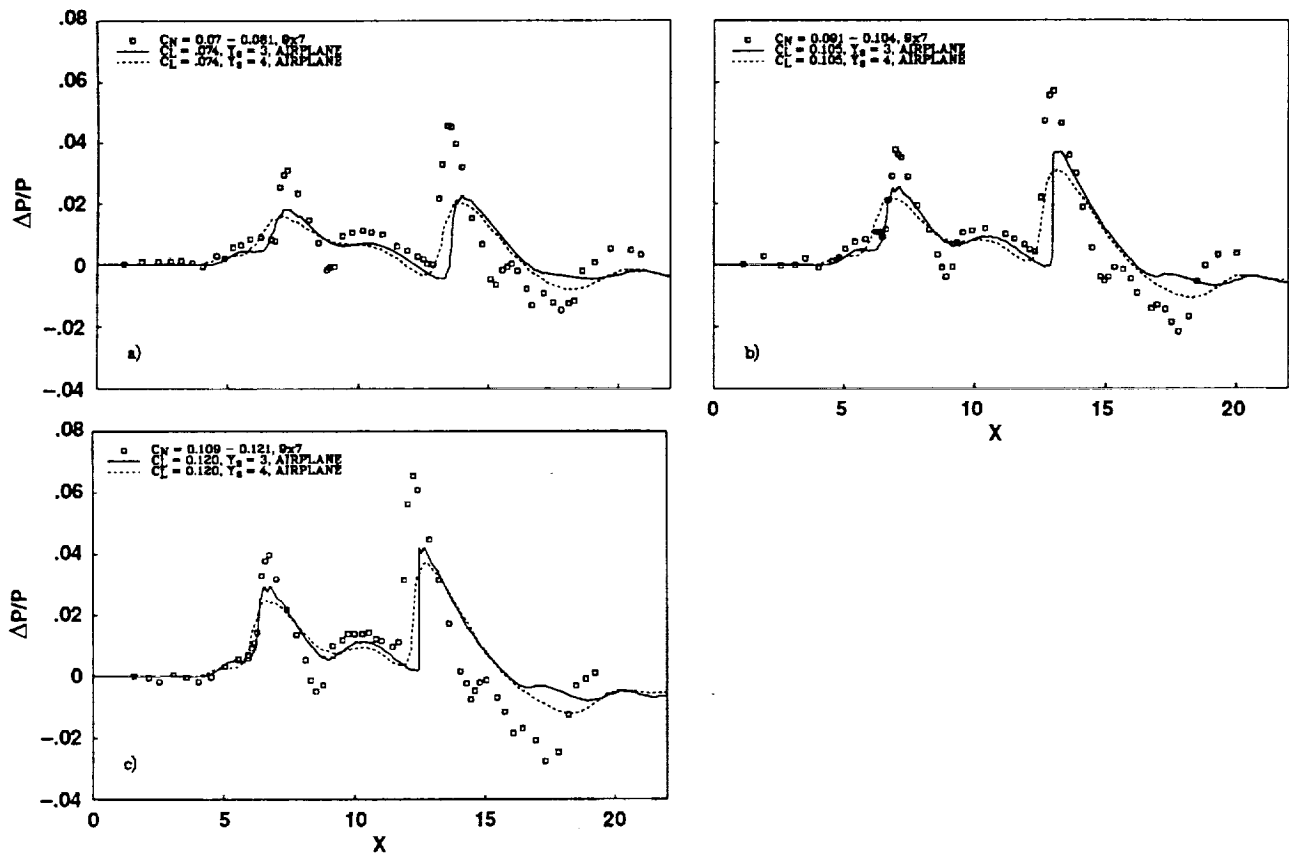


Figure 16. Pressure signatures for the LBWC without nacelles, $M = 2.0$, $h = 14$ in.

PRESSURE SIGNATURE CORRELATIONS: LBWC - 3 NACELLES

Results for the 3 nacelle configuration are shown in Figs 17a-c. Fairly good correlation is observed for the two lower lift coefficients. In particular, the computational data shown in Fig 17b correlates well with experiment with the exception of the tail shock. The moisture levels for the three runs range from 475-640, 370-470, and 480-575 for the nominal lift coefficients of .07, .09, and .11. The moisture levels are larger and change more rapidly during each signature than desired. A larger difference in the pressure signatures is seen for the two computational data sampling distances than previously observed. The correlation with experiment improves at the smaller computational sampling distance ($Y_S=3$). This is probably due to not maintaining a sufficiently dense grid to $1/3$ body length from the model.

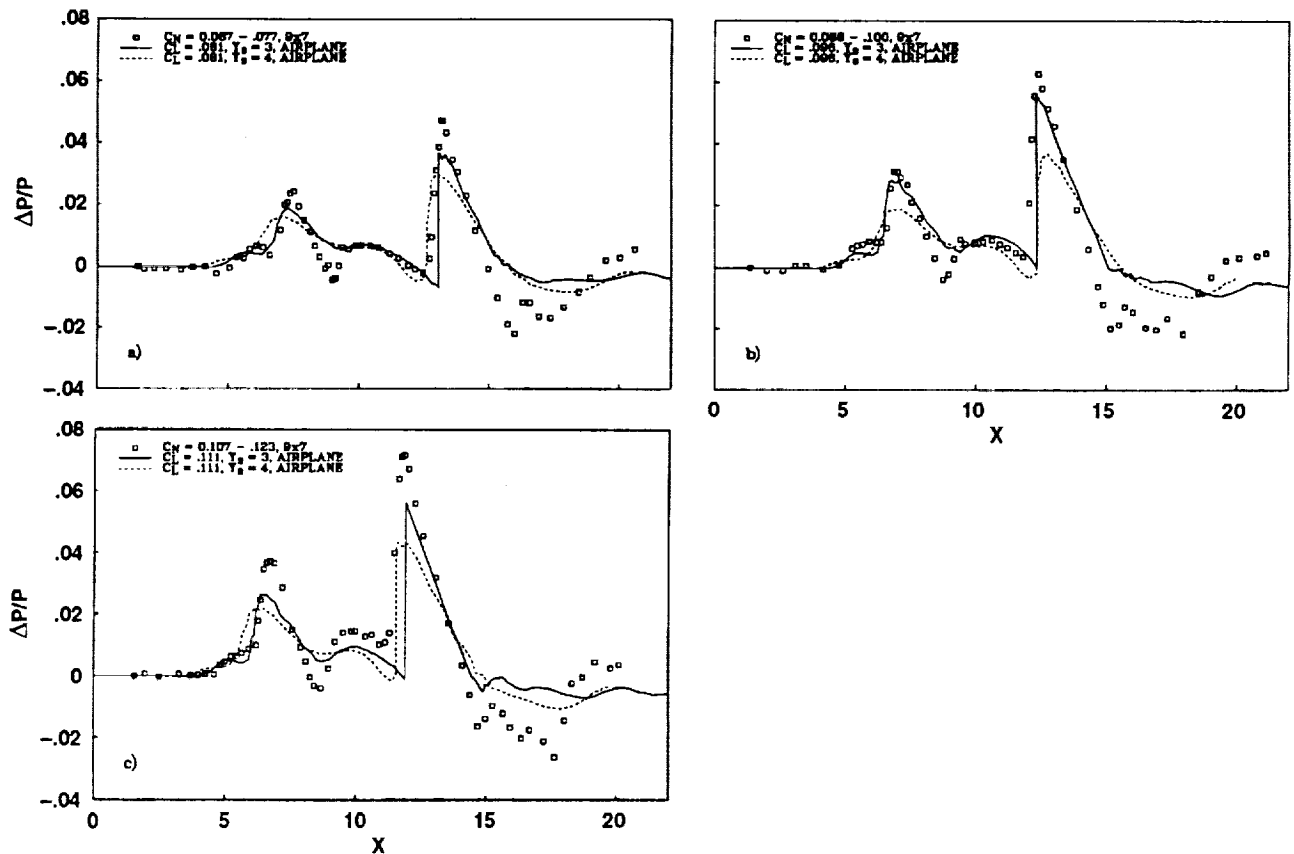


Figure 17. Pressure signatures for the LBWC with 3 nacelles, $M = 2.0$, $h = 14$ in.

AIRPLANE SURFACE GRID: LBW 4 NACELLES

The triangulated surface grid for the LBW configuration is shown in Fig. 18. Details of the design methodology can be found in References 22-23. The waviness in the fuselage is the result of area ruling for the staggered nacelles. The nacelles on this configuration are smaller than those on the 4 engine LBWT configuration, but have constant area ducts with no allowance for boundary layer growth. This results in a smaller base area than for the LBWT and LBWC nacelles.

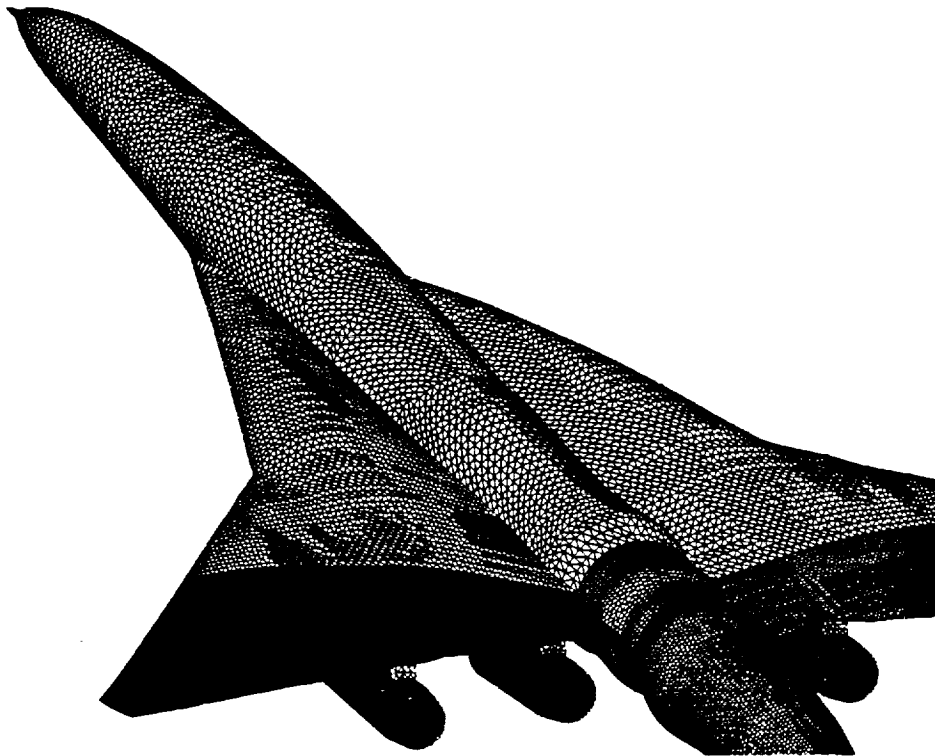


Figure 18. AIRPLANE unstructured surface grid for the LBW with 4 nacelles.

PRESSURE SIGNATURE CORRELATIONS: LBW - 4 NACELLES

The computational/experimental comparisons for the LBW configuration with 4 nacelles are shown in Figs 19a-c. The correlations are good. The multiple weak shocks following the bow shock are accurately captured with AIRPLANE. The magnitude of the tail shock correlates well with experiment for this configuration where poor agreement was found for the LBWT and LBWC configurations. The better experiment/CFD correlation for this configuration may be due to a more dense computational grid. A larger number of grid points were used on this model than the other configurations. The number of grid points ranged from 428,673 used on the LBWC configuration without nacelles to 600,590 on this model. A table is given in reference 9 showing the number of points, cells and computational resource used for the computations shown here.

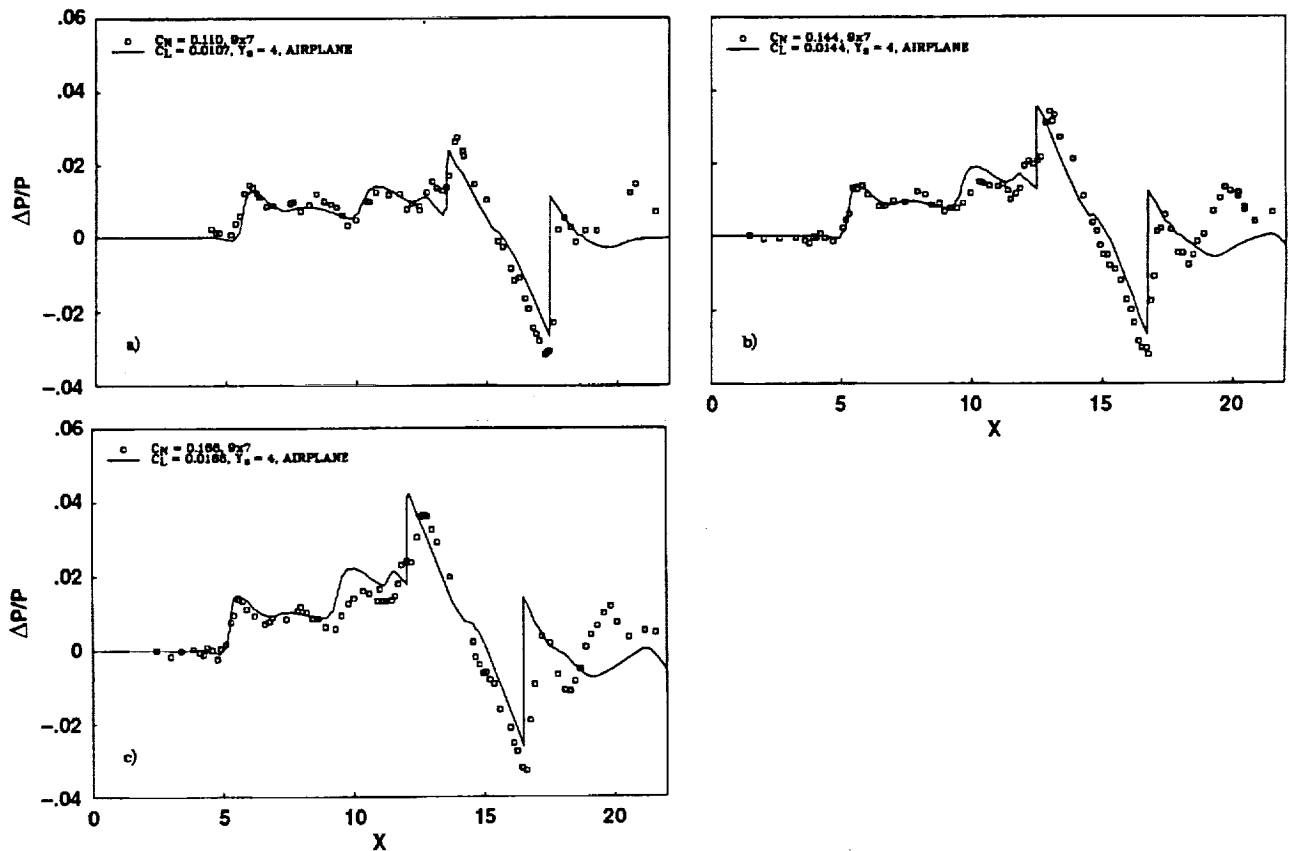


Figure 19. Pressure signatures for the LBW with 4 nacelles, $M = 1.68$, $h = 17.44$ in.

MOISTURE LEVEL/ BOW SHOCK STRENGTH COMPARISONS: LBW - 4 NACELLES

The bow shock strength as a function of normal force coefficient is shown in Fig 20a. The slight decrease in strength with increasing lift may be due to inaccurate determination of free-stream pressure level upstream of the model or bow shock. The moisture level as a function of normal force coefficient is plotted in Fig 20b. The moisture content was relatively high (> 400 PPM) for the 3 cases shown. The reason for the good correlations may be due in part to high moisture levels which may have caused greater attenuation of the experimental signatures combined with the dense computational grid that should give more accurate pressure signatures with reduced numerical dissipation. In addition, the reduced Mach number (1.68 as opposed to 2.0) results in the tail shocks intersecting the computational sampling line closer to the model where the grid density is greater.

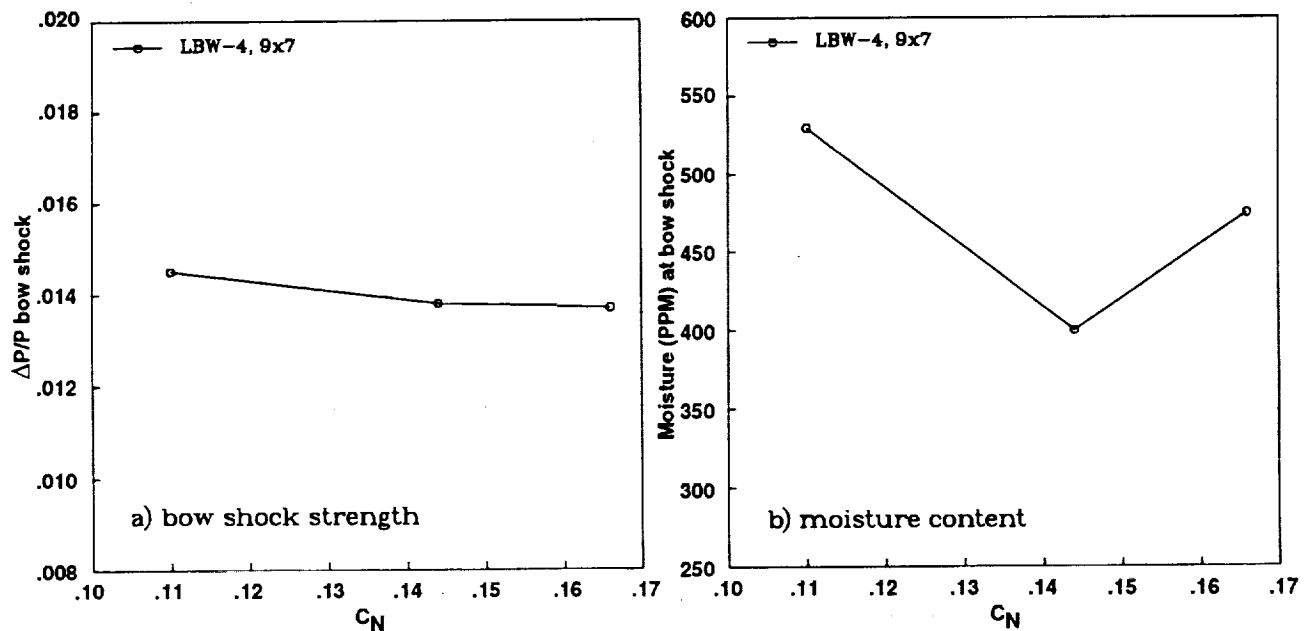


Figure 20. Wind tunnel moisture levels and bow shock strength for the LBW.

FUSELAGE CLOSURE

The LBWT and LBWC configurations were designed with open bodies to accommodate a balance/sting assembly. The fuselage of the configurations were subsequently closed as illustrated in Figure 21 to assess the aerodynamic characteristics of more realistic airplanes.

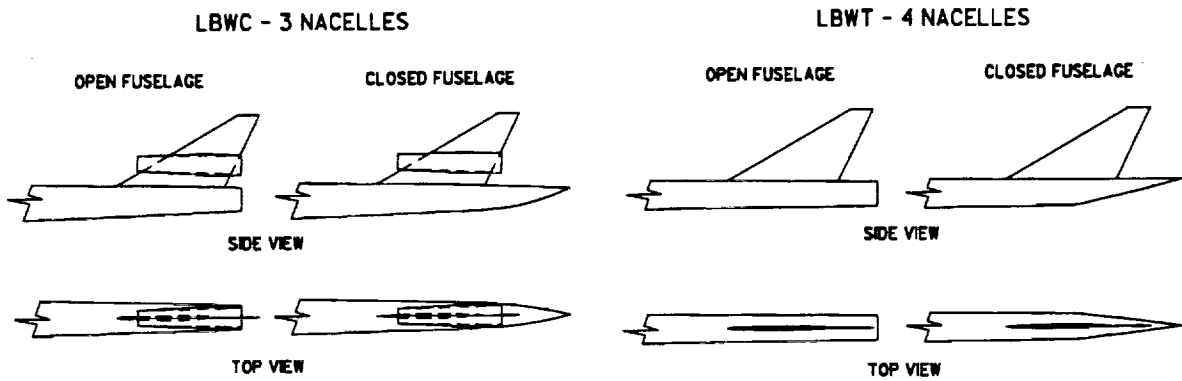


Figure 21. Side view of the LBWT and LBWC configurations with and without fuselage closure.

FORCE AND MOMENT COEFFICIENTS: LBWT AND LBWC

The AIRPLANE force and moment coefficients for the LBWT and LBWC configurations with fuselage closure are shown in Fig 22a. The nacelle and diverter base drag coefficients and drag associated with the interior surface of the nacelles were subtracted from the computational results. The LBWT has lower wave drag as would be expected at the cruise Mach number due to the highly swept wing. The LBWT with 3 engines would be expected to have less wave drag than the 4 engine configuration.

The LBWC is predicted by AIRPLANE to have less wave drag at Mach .9 than the LBWT due to increased wing camber (not shown).

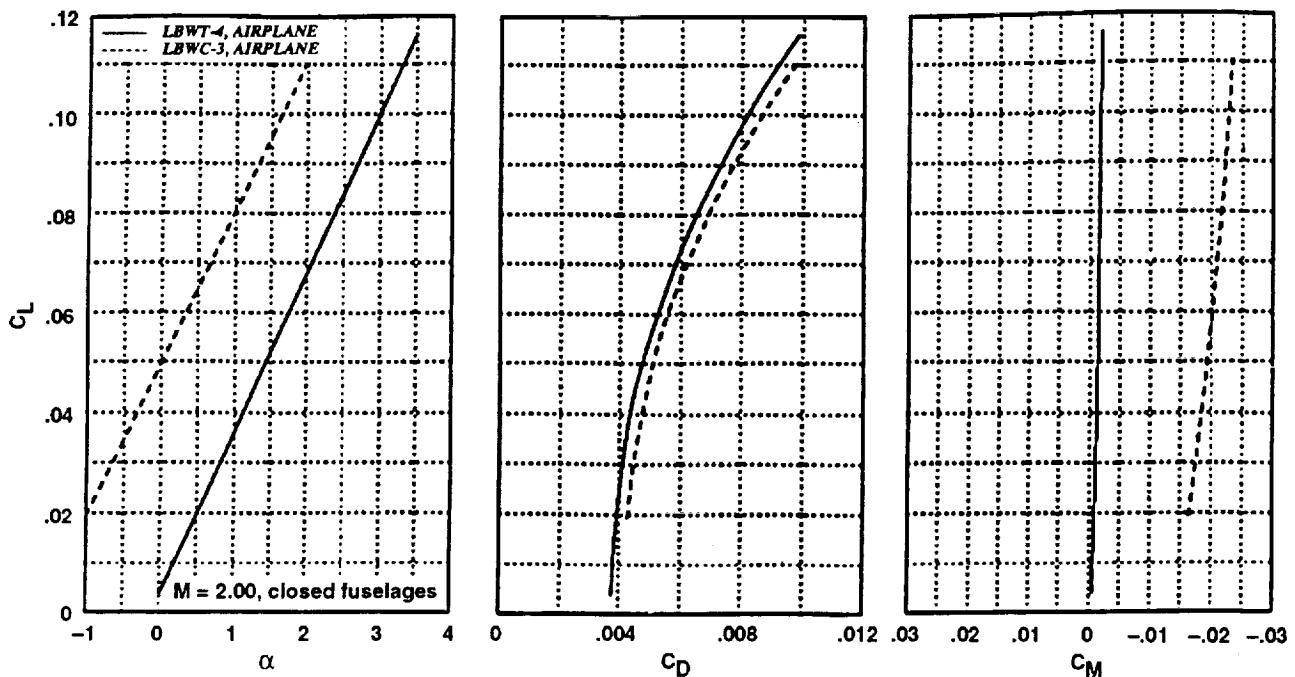


Figure 22. Force and moment coefficients of the LBWT and LBWC with fuselage closure, M = 2.0.

CONCLUDING REMARKS

1. The forward portion of the signatures was generally better predicted than the aft portion, due in part to not modeling the fuselage base or sting. However, the shocks associated with the aft model are not representative of realistic aircraft.
2. The LBW-4 nacelle results correlate well with experiment, due to a larger number of computational grid points and a lower Mach number than the LBWT and LBWC configurations.
3. Free stream pressure fluctuations cause data scatter, making accurate shock strength determination difficult.
4. The moisture content of the air was poorly controlled during testing owing to leaking radiators and nozzle seals in the wind tunnel, resulting in data scatter.
5. The strengths of the bow shocks for the LBWT were found to vary inversely with moisture content of the air during testing. The bow shock strength decreased with increasing moisture level. The comparisons were good when the moisture levels were high, and poor when the moisture levels were low. High moisture appears to act like dissipation in the CFD code.
6. The shock locations for the LBWT without nacelles at 15 deg. off-ground-track correlate better with experiment than with nacelles present. The computational nacelle shocks off-ground-track do not exhibit the forward shift observed in the experimental data.
7. Experimental data scatter makes it difficult to compare the sonic boom levels of the three models.

REFERENCES

- ¹Cliff, Susan E., and Thomas, Scott D., "Euler/Experiment Correlations of Sonic Boom Pressure Signatures," AIAA paper 91-3276-CP, Baltimore, MD, September 23-25, 1991.
- ²Cliff, Susan E., "Computational/Experimental Analysis of Three Low Sonic Boom Configurations with Design Modifications", High Speed Research: Sonic boom Vol II, NASA Conference Publication 3173, Langley Research Center, Hampton, VA, February 25-27, 1992.
- ³Cheung, S. H., Edwards, T.A., and Lawrence, S.L., "Application of Computational Fluid Dynamics to Sonic Boom Near- and Mid-Field Prediction," Journal of Aircraft, vol 29, Number 5, Sept-Oct 1992, pp. 920-926.
- ⁴Madson, Mike D., "Sonic Boom Predictions for Three Generic Models Using a Solution-Adaptive Full Potential Code," AIAA paper 91-3278, 1991.
- ⁵Siclari, M.J., "Ground Signature Extrapolation of Three-Dimensional Near-Field CFD Predictions for Several HSCT Configurations" High Speed Research: Sonic boom Vol I and II, NASA Conference Publication 3173, Langley Research Center, Hampton, VA, February 25-27, 1992.
- ⁶Baker, Timothy J., "Automatic Mesh Generation for Complex Three-Dimensional Regions Using a Constrained Delaunay Triangulation," Engineering with Computers 5, 1989, pp. 161-175.
- ⁷Baker, Timothy J., "Generation of Tetrahedral Meshes Around Complete Aircraft," 2nd International Conference on Numerical Grid Generation in Computational Fluid Dynamics, Dec 5-8, 1988.
- ⁸Jameson, A., and Baker, T. J., "Improvements to the Aircraft Euler Method," AIAA Paper 87-0452, 1987.
- ⁹Cliff, Susan E., "On The Design and Analysis of Low Sonic Boom Configurations" High Speed Research: Sonic Boom Vol II, NASA Conference publication 10133, NASA Ames Research Center, Moffett Field, CA, May 12-14, 1993, pp. 37-80.
- ¹⁰Baker, Timothy J., "Single Block Mesh Generation for a Fuselage Plus Two Lifting Surfaces," 3rd International Conference on Numerical Grid generation, Barcelona, Spain, June 3-7, 1991.
- ¹¹Jameson, A., "A Vertex Based Multigrid Algorithm for Three Dimensional Flow Calculations," Proceedings on Numerical Methods for Compressible Flows—Finite Difference and Volume Techniques, edited by T. E. Tezduar and T. J. R. Hughes, AMD-Vol. 78, ASME, 1986, pp. 45-73.
- ¹²Thomas, Charles, "Extrapolation of Sonic Boom Pressure Signatures by the Waveform Parameter Method," NASA TN D-6832, 1972.
- ¹³Needleman, Kathy E., "A Study of Loudness as a Metric for Sonic Boom Acceptability," AIAA paper 91-0496, Reno, NV, January 7-10, 1991.
- ¹⁴Shepherd, Kevin, P., and Sullivan, Brenda M., "A Loudness Calculation Procedure Applied to Shaped Sonic Booms", NASA TP-3134, November, 1991.

¹⁵Gregory, T. J., "Computerized Preliminary Design at the Early Stages of Vehicle Definition", NASA TMX-62,303, 1973.

¹⁶Wampler, S. G., Myklebust, A., Jayaram, S., and Gelhausen, P., "Improving Aircraft Conceptual Design- A PHIGS Interactive Graphics Interface for ASYNT", presented at the AIAA/AHS/ASEE Aircraft Design, Systems and Operations Meeting, September 7-9, 1988, Atlanta, Georgia (paper no. AIAA-88-4481)

¹⁷Jayaram, S., Myklebust, A., and Gelhausen, P. "ASYNT-A Standards Based System for Parametric Computer Aided Conceptual Design of Aircraft", presented at the AIAA 1992 Aerospace Design Conference, Irvine, California, February 3-6, 1992 (paper no. AIAA 92-1268)

¹⁸Siclari, M.J., and Fouladi, K. "A CFD Study of Component Configuration Effects on the Sonic Boom of Several High-Speed Civil Transport Concepts", High Speed Research: Sonic Boom Vol II, NASA Conference publication 10133, NASA Ames Research Center, Moffett Field, CA, May 12-14, 1993, pp. 227-299.

¹⁹Mendoza, Joel P., and Hicks, Raymond M. "Further Studies of the Extrapolation of Near-Field Overpressure Data", NASA TM X-2219, March 1971.

²⁰Hunton, Lynn W., Hicks, Raymond M., and Mendoza, Joel P. "Some effects of Wing Planform on Sonic Boom", NASA TN D-7160, January 1973.

²¹Goodsell, Aga M., Lee, Christopher A., and Hicks, Raymond M. "Use of CFD in the Design of Low Sonic Boom Aircraft", High Speed Research: Sonic Boom Vol II, NASA Conference publication 10133, NASA Ames Research Center, Moffett Field, CA, May 12-14, 1993, pp. 143-168.

²²Haglund, George T., "Two HSCT Mach 1.7 Low Sonic Boom Designs", High Speed Research: Sonic boom Vol II, NASA Conference Publication 3173, Langley Research Center, Hampton, VA, February 25-27, 1992.

²³Cheung, Samson, "Design Process of Ames Wind-Tunnel Model 3" High Speed Research: Sonic Boom Vol II, NASA Conference publication 10133, NASA Ames Research Center, Moffett Field, CA, May 12-14, 1993, pp. 95-123.

Wind-Tunnel Overpressure Signatures From A Low-Boom HSCT Concept With Aft-Fuselage-Mounted Engines

Robert J. Mack

NASA Langley Research Center

Hampton, Virginia

SUMMARY

A 1:300 scale wind-tunnel model of a conceptual High-Speed Civil Transport (HSCT) designed to generate a shaped, low-boom pressure signature on the ground was tested to obtain sonic-boom pressure signatures in the Langley Research Center Unitary Plan Wind Tunnel at a Mach number of 1.8 and a separation distance of about two body lengths or four wing-spans from the model. Two sets of engine nacelles representing two levels of engine technology were used on the model to determine the effects of increased nacelle volume. Pressure signatures were measured for (model lift)/(design lift) ratios of 0.5, 0.63, 0.75, and 1.0 so that the effect of lift on the pressure signature could be determined. The results of these tests were analyzed and used to discuss the agreement between experimental data and design expectations.

INTRODUCTION

A conceptual low-boom HSCT configuration with four aft-fuselage-mounted engines was described at the Second Workshop on Sonic Boom (ref. 1) held at the Ames Research Center in May, 1993. The four engine nacelles were mounted on the aft fuselage to: (1) give the configuration a "clean" wing with ample room for flaps and control surfaces, (2) reduce the need for inboard "gull-wing" dihedral to accommodate engine-nacelle clearance, (3) balance the aircraft from takeoff to landing, (4) remove the sonic-boom, nacelle-wing, interference-lift contribution, leaving only the nacelle volume as a flow-field disturbance source, (5) reduce engine-out problems on takeoff, (6) locate engines well behind the passenger cabin, and (7) place the nacelle-inlet shocks generated during the low-boom part of the cruise mission in the expansion region of the aircraft's volume-and-lift-disturbed flow field where their effects on the overall ground signature could be appreciably reduced. Of particular importance from an engine-integration and sonic-boom point of view is the consideration of nacelle volume disturbance source (factor 4) because previous sonic-boom wind-tunnel tests of a Mach 2.0 low-boom

validation model (ref. 2) demonstrated that the nacelle integration problem had not been satisfactorily solved. Thus, the HSCT-10B concept, with its aft-fuselage nacelle design, was developed so that the effects of nacelle volume on the flow field could be isolated, the newly-developed nacelle-integration methods could be readily applied, and the resulting design concept could be tested.

A 1:300 scale model of the HSCT-10B concept was built for tests in the Unitary Plan Wind Tunnel at a Mach number of 1.8, a total temperature of 125 degrees Fahrenheit, and a Reynolds number per foot of two million. Two sets of engine nacelles were used during the tests. The first set with small nacelles represented an advanced-technology, high thrust-to-weight ratio engine (ref. 3) while the second set, with larger nacelles, represented a more conservative-technology, reduced thrust-to-weight ratio engine which would be similar to that used on a first-generation HSCT.

In this paper, a brief description of the conceptual HSCT-10B design and wind-tunnel model geometry is given along with the analysis of the surface geometry that provided predictions of the aircraft's F-function and ground-level pressure signature. Pressure signature data, measured at a model-probe separation distance of about 24 inches, with the model having small and large nacelles and at four lifting conditions are also presented. Correlation between experimental data and design expectations is discussed.

SYMBOLS

C_L	lift coefficient
$F(y)$	Whitham F-function
h	model-probe separation distance, in
l	aircraft or model overall length, ft or in
l_e	effective length, ft or in
M	Mach number
p	flow-field pressure, psf
p_a	ambient pressure, psf
Δp	$p - p_a$, psf
x	distance along the horizontal axis, ft or in
y	effective length parameter, ft or in
β	Mach number parameter equal to $\sqrt{M^2 - 1.0}$

CONFIGURATION DESCRIPTION

A three-view drawing of the conceptual HSCT-10B (ref. 1), with four aft-fuselage-mounted engine nacelles arranged in a V-pattern, is shown in figure 1. The design was guided by well-established low-boom design principles as documented in a number of reports (references 4 through 9).

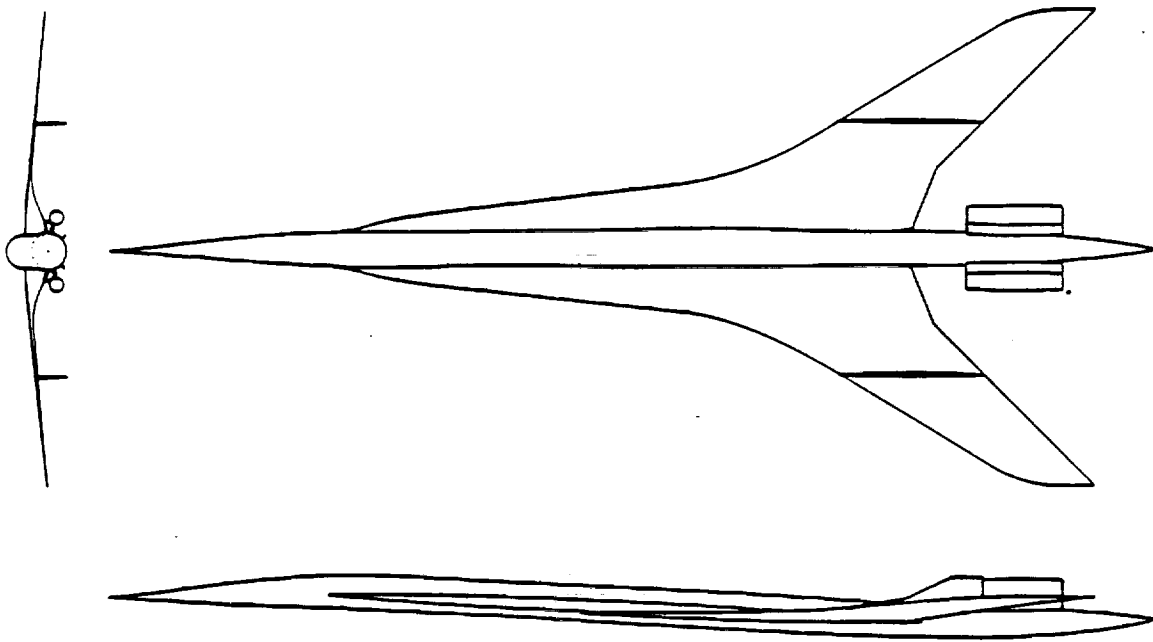


Figure 1. Three-view of the HSCT-10B concept.

The 1:300 scale wind-tunnel model had an integral sting balance attached to the aft fuselage at a location which corresponded to the 300 foot fuselage station on the full-scale conceptual aircraft. A lift-moment balance, consisting of four flush-mounted strain gages mounted in 180-degree-separated pairs, was built into the rear of the sting. As previously mentioned, special attention was paid to the lessons learned from the low-boom Mach 2.0 validation model results reported in reference 2. An application of these lessons to the HSCT-10B concept required that the nacelles be moved further aft from their usual position (under the wings and slightly behind the mid-point of the aircraft) to a location on the aft fuselage. In this aft location, the nacelle's positive pressure disturbances would be superimposed on the flow-field expansion region caused by the fuselage approaching closure and the wing lift gradients decreasing toward the wing-tip trailing edge. A Whitham F-function that demonstrates this approach is presented in figure 2, and the predicted ground-level pressure signature obtained from this F-function is shown in figure 3.

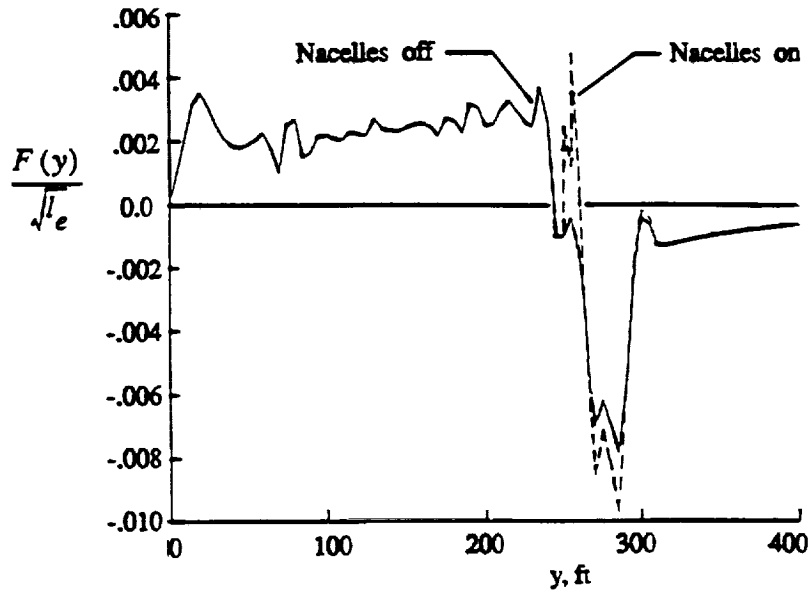


Figure 2. Whitham F-function of the complete HSCT-10B wind-tunnel model.

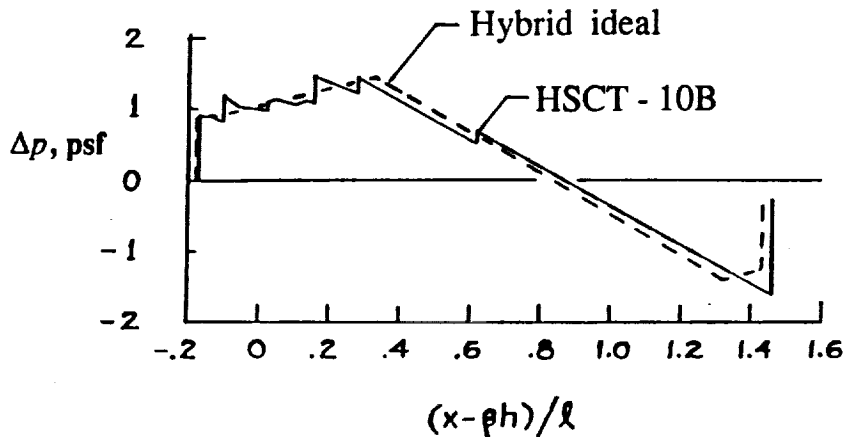


Figure 3. Predicted ground-level pressure signature from the HSCT-10B cruising at $M = 1.8$, $h = 48,600$ ft., and start-of-cruise weight of about 618,000 lb.

The most noticeable feature in figure 3, after making some allowances for computationally-induced extraneous small shocks, is the *absence of a prominent shock* from the nacelle inlets. This control over the flow-field disturbances generated by the nacelle inlets is due entirely to the aft-fuselage engine-nacelle location indicated on the F-function of the HSCT-10B concept (figure 2). While these theoretical predictions were encouraging, it was obvious that wind-tunnel tests, which would provide measured flow-field pressure signatures from the HSCT-10B concept, were needed to verify this low-boom and engine-integration design methodology.

DISCUSSION OF RESULTS

Wind-Tunnel Data

The wind-tunnel model of the HSCT-10B concept was used to generate pressure signatures at the designed low-boom Mach number of 1.8 in Test Section I of the Langley Research Center Unitary Plan Wind Tunnel. One of the initial pressure signatures, measured with the small-nacelles and with the wind-tunnel model at about one-half the beginning-cruise lift, is shown in figure 4.



Figure 4. Initial pressure signature from the HSCT-10B model with small nacelles at $M = 1.8$, $h = 24$ inches, and $C_L = 0.0519$.

This measured pressure signature as well as the following pressure signatures includes several ambient pressure points upstream of the nose shock for reference. The measured pressure signature does not have the prominent pressure spike due to the nacelle inlets that was observed in the measured pressure signature of the Mach 2.0 validation model (ref. 2). Therefore, the signature is a validation of the nacelle-integration methodology used to design the conceptual aircraft since previous experimental results have shown that the usual engine-nacelle inlet shocks would have been readily observed, even at this lower lift coefficient. When flow-field pressures were measured with the model, having the small nacelle pack, at the designed cruise lift coefficient, $C_L = 0.1022$, the pressure signature shown in figure 5 was obtained.



Figure 5. Pressure signature of the HSCT-10B model with small nacelles at $M = 1.8$, $h = 24$ inches, and $C_L = 0.1022$.

The noticeable pressure jump on the aft part of the positive section of the signature destroyed the almost flat-top shape. If it were not for the flatness in the measured signature in figure 4, this pressure jump (or shock) might have been incorrectly attributed to the engine-nacelle inlets.

Following these tests, the small nacelles were removed and the large nacelles were installed. These new nacelles had increased diameters and lengths to represent engines of a more conservative technology level. A pressure signature of the model with large nacelles is presented in figure 6.

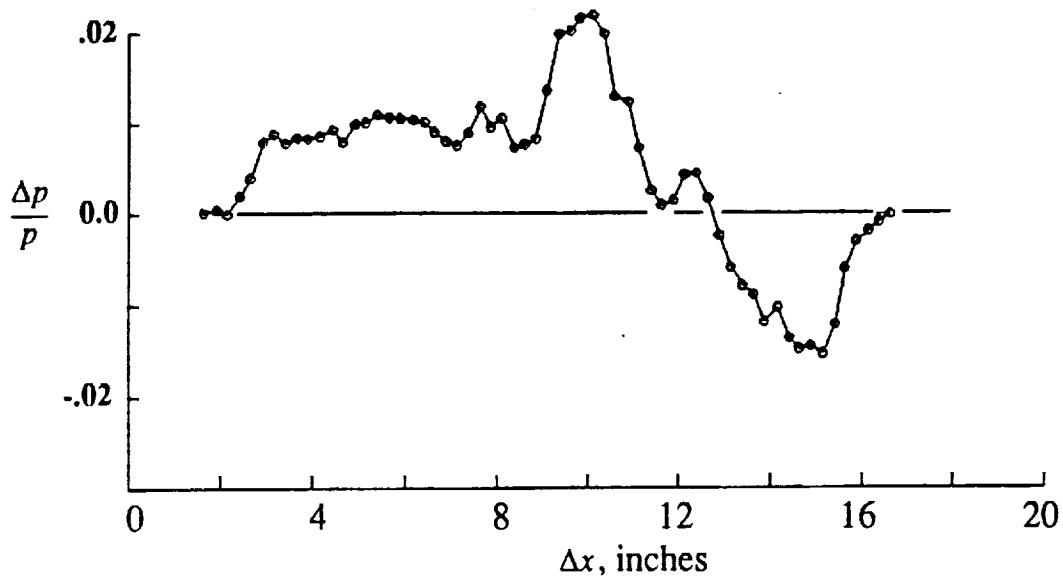


Figure 6. Pressure signature of the HSCT-10B model with large nacelles at $M = 1.8$, $h = 24$ inches, and $C_L = 0.1022$.

A comparison of the signatures in figures 5 and 6 led to the conclusion that there was little difference between the small- and large-nacelle HSCT-10B model pressure signatures. This is surprising because the large nacelles are about 20 percent longer and wider than the small nacelles. Theoretically, the F-function value from the inlet lip of the large nacelle was about one-third larger than that from the small nacelle, yet the pressure signatures (figures 5 and 6) are almost identical. Moreover, when the model with the large nacelles was tested at the same lift coefficient as that used to obtain figure 4, virtually the same pressure signature (figure 7) was measured.

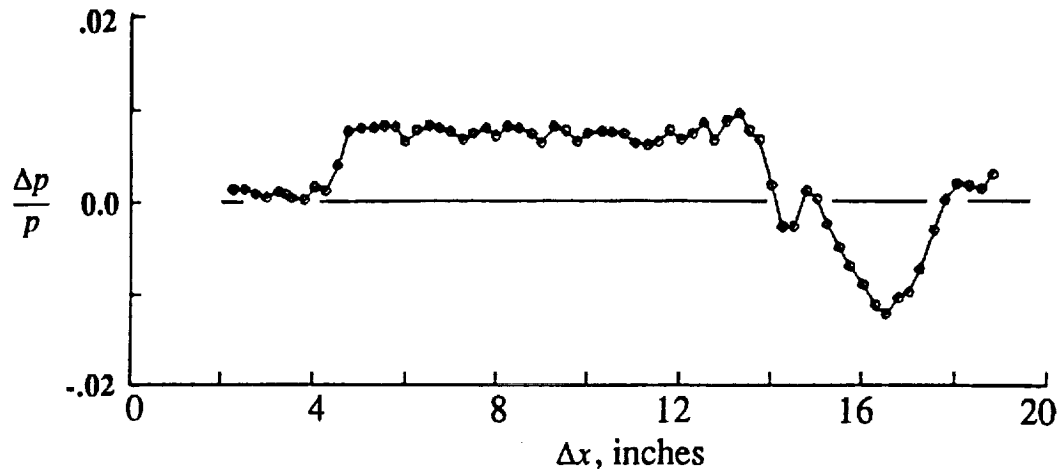


Figure 7. Pressure signature of the HSCT-10B model with large nacelles at $M = 1.8$, $h = 24$ inches, and $C_L = 0.0511$.

The strong similarity found in the comparison of these pressure signatures (figures 4 and 7) reinforced the conclusion that the pressure jumps seen in figures 5 and 6 were caused by the higher lift rather than by nacelle inlet and volume-induced disturbances. This conclusion led to measuring pressure signatures at lift coefficients of 0.0639 and 0.0767 which are 62.5 and 75 percent of the beginning-of-cruise lift coefficient, respectively. These additional pressure signatures are presented in figures 8 and 9.

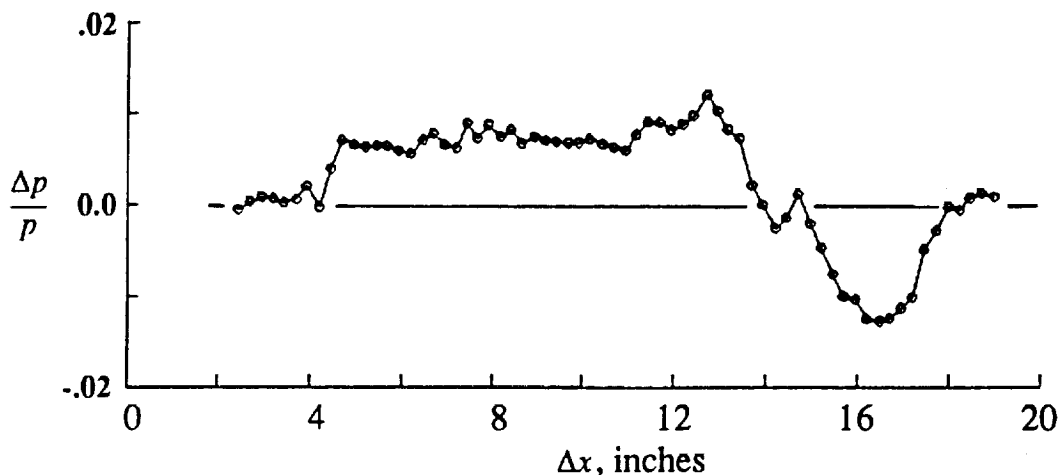


Figure 8. Pressure signature of the HSCT-10B model with large nacelles at $M = 1.8$, $h = 24$ inches, and $C_L = 0.0639$.

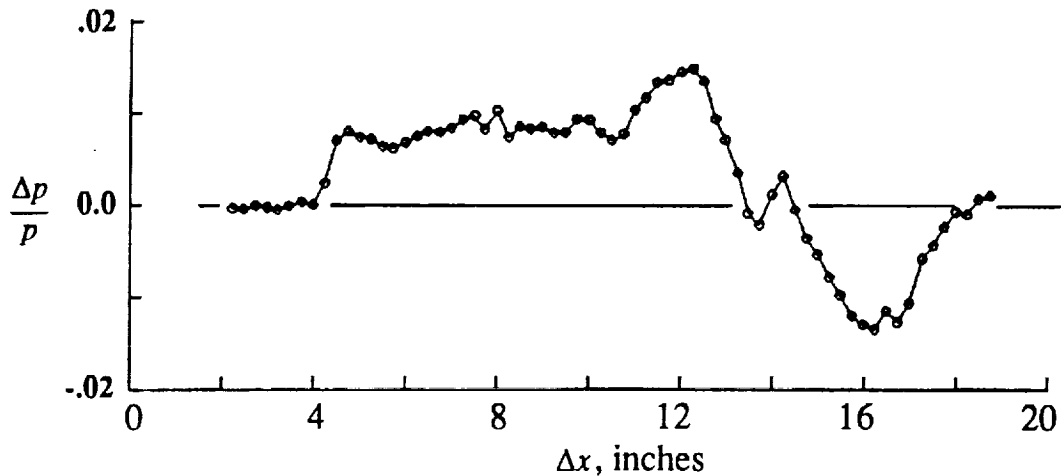


Figure 9. Pressure signature of the HSCT-10B model with large nacelles at $M = 1.8$, $h = 24$ inches, and $C_L = 0.0767$.

The pressure signatures in figures 6 through 9 for the model with large nacelles showed a steady increase in the strength of the pressure disturbance which preceded the expansion -- a disturbance triggered by an increase in angle of attack and wing lift. This nonlinear growth in disturbance strength suggested that the onset of these pressure perturbations occurred rather suddenly after the lift on the model exceeded between 50 and 62.5 percent of the beginning-of-cruise lift.

In the following sections, these perturbations to the flat-topped pressure signatures (figures 4 and 7) are discussed. Data from an additional set of wind-tunnel tests are presented and included in the discussion. Finally, the results from a theoretical flow-angularity analysis and those from a comparison of theoretical and experimental pressure signatures were added to the analysis of experimental data so that causes of the unpredicted pressure disturbances might be identified.

Lift-Induced Pressure Disturbances

Two of the measured pressure signatures, figures 4 and 7, suggest that the design goal of integrating the nacelles with the wing-body-fin was successfully achieved. This conclusion is based on the results of previous wind-tunnel tests where conspicuous inlet shocks from nacelles located under the wings were readily observed at several lifting conditions.

A second goal of obtaining a shaped pressure signature at the design lift coefficient was not realized. The onset location of the pressure-signature disturbances, observed in figures 5, 6, 8, and 9, was traced to the section of the wing leading-edge where the sweep angle was changing from 84.3 to 59.0 degrees. The first appearance of a small pressure perturbation is noted at a (model lift)/(design lift) ratio of 0.625 although it must have begun earlier at a lift ratio somewhat larger than 0.50. The pressure perturbation had developed fully at a lift ratio of 0.75, and a noticeable shock was observed in the measured signature when the lift ratio reached 1.0. This phenomena is not unique to this model and wind-tunnel test. Wind-tunnel pressure signatures with very similar pressure perturbations and shocks were obtained in previous tests from other theory-validation

wing-body models (ref. 10 and 11).

In figure 10, an overlay of these measured pressure signatures, obtained at the four values of (model lift)/(design lift) ratio, shows this pressure perturbation and its growth toward becoming a shock.

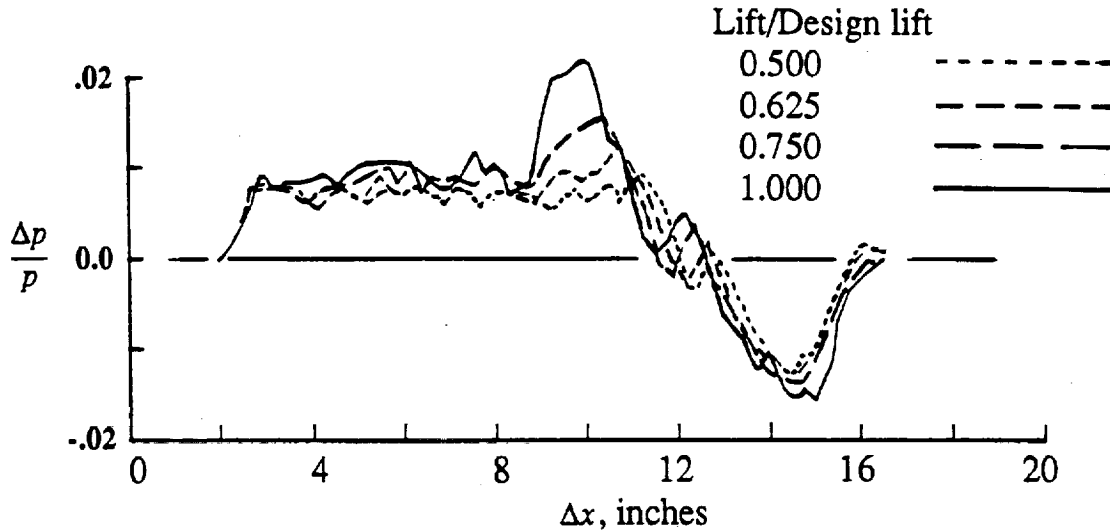


Figure 10. Comparison of pressure signatures for lift ratios of 0.5, 0.625, 0.75, and 1.0.

Note that as the lift coefficient increased, the mean slope of the unperturbed top of the pressure signature also increased to approach the signature slope predicted in figure 3. At the same time, the multiple small perturbations coalesced into a few moderate-sized perturbations and one shock as the lift increased. In the expansion region of the signature, the small nacelle-boattail shock moved forward, but did not grow in strength, as the angle of attack and the lift increased.

There are at least two possible explanations why the low-boom design methodology did not account for these lift-induced pressure disturbances on the measured pressure signatures: (1) flow separation effects, and (2) flow-accommodation distance effects, i.e., the lift disturbances from the upper and the lower surfaces have not merged to form cylindrical or quasi-cylindrical propagation wave fronts. In the following sections, wind-tunnel data are analyzed and these possible explanations are examined for validity.

Analysis of Wind-Tunnel Data

Both of the foregoing explanations of why the low-boom design methods did not predict the lift-induced pressure disturbances needed to be explored so that the causes for the transition from the desired signature shape (figures 4 and 7) to the perturbed signature shape (figures 5 and 6) could be determined. To further investigate the possibilities of flow separation and insufficient flow-field accommodation distance, additional wind-tunnel tests were made and two theoretical analyses were conducted.

Additional Wind-Tunnel Tests

(1) Leading-edge-gritted signatures. Several pressure signatures were measured with grit (applied with the information from reference 12) on the leading edges of the HSCT-10B model wing. If the flow over the wings were laminar and separated, then the leading-edge grit should induce turbulence and reattachment. However, no decrease in the size of the perturbation on the pressure signature with the (model lift)/(design lift) ratio of 1.0 (figure 6) was noted. The same negative results were obtained on pressure signatures measured at (model lift)/(design lift) ratios of 0.625 and 0.75.

(2) Oil-flow study. Pictures of the oil-dye flow patterns (using the method of reference 13) on the upper surface of the model's wing were obtained to determine the flow characteristics. Only one flight condition was observed: design Mach number of 1.8 and a $C_L = 0.1022$, i.e., (model lift)/(design lift) ratio of 1.0. The observed patterns across the upper wing surfaces were fairly smooth and regular in spacing and dye density, strongly indicating fully attached, rather than separated, flow.

Theoretical Analysis

(1) Comparison of leading-edge geometry with upwash. The methods in references 14 and 15 were used to predict differences between the leading-edge camber angle and the upwash angle along the entire wing panel. The calculation predicted the differences to be less than one to two degrees, again suggesting that there was attached flow.

(2) Comparison of measured and predicted pressure signatures. Figure 4 shows a pressure signature with the desired shaping (although at a $C_L = 0.0519$), while figure 5 shows a similar pressure signature for the design lift ($C_L = 0.1022$), but with an additional lift-induced shock. In figure 11, these pressure signatures are compared with a Whitham-theory signature predicted for a wind-tunnel distance of 24 inches and a $C_L = 0.1022$.

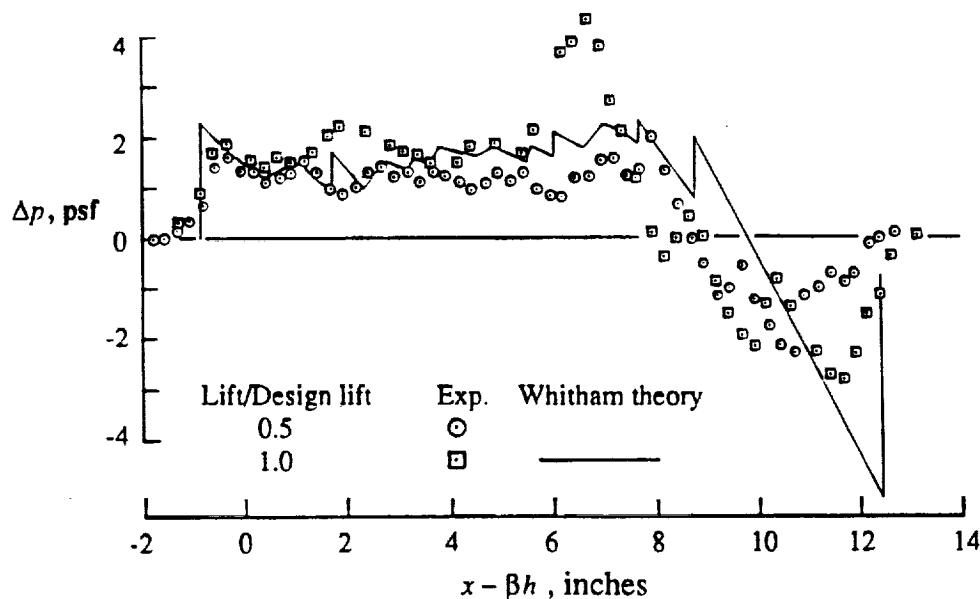


Figure 11. Comparison of HSCT-10B measured and predicted pressure signatures at $M = 1.8$; $C_L = 0.0519$ and 0.1022 , theoretical signature at $C_L = 0.1022$, $h = 24$ inches.

As mentioned in the *Configuration Description* section, low-boom design methods were used to develop the HSCT-10B concept and model. These methods are based on the small disturbances felt at separation distances from 150 to 200 body lengths (300 to 400 wing spans). At these distances, flow-field disturbances generated by the aircraft have changed from complex and three-dimensional to cylindrical, i.e., two-dimensional, in nature. Thus, these design methods are applied outside the scope of their limitations when employed to predict *full-length* near-field pressure signatures generated by aircraft with wing spans that are nearly half of their overall length. It must, therefore, be emphasized at this point that the comparisons of the near-field pressure signatures shown in figure 11 are valid *only for the first third to first half of the pressure signature*. Over this length, the disturbances are due to forward-fuselage volume, forward-wing volume, and a small amount of wing lift. The resemblance between these combined configuration components and a slender body of revolution is very good. Measured pressure signatures were adjusted to account for wind-tunnel characteristics as discussed in Appendix B of reference 16. A comparison of the nose-shock strengths in the HSCT-10B model data with the predicted fore-body signature pressures showed reasonably good agreement. The pressures in the small "hump" between $x - \beta h$ values of 1.0 and 3.0 inches on the signature with the lift ratio of 1.0 did not agree with theory as well as the pressures on the signature with the lift ratio of 0.50. This "hump" is a lift-induced effect as is the shock that is centered at a $x - \beta h$ value of about 6.4 inches. So its forward position would seem to preclude a separated-flow explanation. Further aft on the model, where the leading-edge sweep is increasing rapidly, the local span is still small and the leading-edge curvature is mathematically smooth and continuous. These model geometry features would also seem to promote attached, rather than separated flow at the low cruise-altitude angle of attack.

Discussion of Additional Tests and Theoretical Analysis

These follow-on wind-tunnel tests and theoretical analyses gave two types of results. The two wind-tunnel tests strongly suggested that *flow separation was not present*. This conclusion was corroborated by the first of the theoretical calculations. In the second analysis, a comparison of a theoretically predicted signature with two measured signatures, the reasonably good agreement indicated that the flow *was probably attached* over the whole model at the lift coefficient corresponding to a (model lift)/(design lift) ratio of 0.50, and that flow could have stayed attached at the higher lift coefficient where the lift ratio was 1.0. In spite of this conclusion, however, there was insufficient evidence to conclude further that incomplete flow-field accommodation was the definite cause of both the growth of pressure perturbations and the extra pressure signature shock at the higher of the two lift levels. Sonic-boom tests in a supersonic-flow wind-tunnel facility with a larger test section would be the best way to look for evidence of this effect. Unfortunately, these facilities are few in number and are very expensive to use.

Reasonably good agreement between theory and experiment was found in the comparison of pressure signatures (figure 11) *for the part of the model that conformed to the Whitham theory limitations*. If it could be demonstrated that the near-field measurement distances, i.e., lack of flow-field accommodation, were the cause of the observed lift-induced disturbances, then *the Whitham-Walkden theory could be trusted to predict ground signatures for HSCT-type aircraft*. Whatever may be hypothesized, the wind-tunnel pressure signature measurements, the follow-on wind-tunnel tests, and the theoretical analyses already reported should serve as guidelines and sources of data.

CONCLUDING REMARKS

An evaluation of measured near-field pressure signatures and theoretical analysis for a conceptual low-boom HSCT configuration with four aft-fuselage mounted nacelles has led to the following conclusions:

1. The measured near-field pressure signatures indicate that both large and small nacelles were successfully integrated on the conceptual HSCT-10B configuration so as to prevent inlet shocks from appearing. However, at the design lift, a pressure disturbance developed that was believed to be caused by the lift being increased from an initial level of about 50 percent of the design lift to a level of 100 percent of the design lift.

2. Two possible causes of the growth in localized pressure perturbations which led to the formation of a lift-induced shock were investigated. The first possibility, flow separation effects, was not found. The second, insufficient flow-field accommodation, might have been the cause but could not be verified due to a lack of direct evidence. Further testing in supersonic wind-tunnel facilities with larger test sections is suggested so that this hypothesis can be tested.

REFERENCES

1. Mack, Robert J.: Low-Boom Aircraft Concept With Aft-Fuselage-Mounted Engine Nacelles. High Speed Research: Volume II, NASA Conference Publication 10133, 1992.
2. Mack, Robert J.: Some Considerations on the Integration of Engine Nacelles Into Low-Boom Aircraft Concepts. High-Speed Research: Sonic Boom, Volume II, NASA Conference Publication 3173, 1992.
3. Fenbert, James W.; Ozoroski, Lori P.; Geiselhart, Karl A.; Shields, Elwood W.; and McElroy, Marcus O.: Concept Development of a High-Speed Civil Transport, NASA/TP-1999-209694, 1999.
4. Seebass, R.; and George, A. R.: Sonic-Boom Minimization. Journal of the Acoustical Society of America, vol. 51, no. 2, pt. 3, February 1972, pp. 686-694.
5. Carlson, Harry W.; Barger, Raymond L.; and Mack, Robert J.: Application of Sonic-Boom Minimization Concepts in Supersonic Transport Design. NASA TN D-7218, June 1973.
6. Darden, Christine M.: Sonic-Boom Minimization With Nose-Bluntness Relaxation. NASA TP-1348, 1979.
7. Mack, R.; and Needleman, K.: The Design of Two Sonic-Boom Wind-Tunnel Models from Conceptual Aircraft Which Cruise at Mach Numbers of 2.0 and 3.0, Thirteenth AIAA Conference, Tallahassee, Florida, October 22-24, 1990.

8. Mack, Robert J.; and Needleman, Kathy E.: A Methodology For Designing Aircraft To Low Sonic-Boom Constraints. NASA TM-4246, February 1991.
9. Mack, Robert J.; Haglund, George T.: A Practical Low-Boom Overpressure Signature Based on Minimum Sonic-Boom Theory. High-Speed Research: Volume II, NASA Conference Publication 3173, 1992.
10. Mack, Robert J.; and Darden, Christine M.: Wind-Tunnel Investigation of the Validity of a Sonic-Boom-Minimization Concept. NASA TP-1421, 1979.
11. Mack, Robert J.; and Darden, Christine M.: Limitations on Wind-Tunnel Pressure Signature Extrapolation. High-Speed Research: Volume II, NASA Conference Publication 3173, 1992.
12. Braslow, Albert L.; Hicks, Raymond M.; and Harris, Roy V., Jr.: Use of Grit-Type Boundary-Layer-Transition Trips on Wind-Tunnel Models. NASA TN D-3579, 1966.
13. Corlett, William A.: Operational Flow Visualization Techniques in the Langley Unitary Plan Wind Tunnel. Flow Visualization and Laser Velocimetry for Wind Tunnels, William W. Hunter, Jr., and Jerome T. Foughner Jr., eds., NASA CP-2243, 1982, pp. 65-73.
14. Carlson, Harry W.; and Walkley, Kenneth B.: Numerical Methods and a Computer Program for Subsonic and Supersonic Aerodynamic Design and Analysis of Wings With Attainable Thrust Considerations. NASA CR-3808, 1984.
15. Carlson, Harry W.; and Mack, Robert J.: Estimation of Wing Nonlinear Aerodynamic Characteristics at Supersonic Speeds. NASA TP-1718, 1980.
16. Carlson, Harry W.: Correlation of Sonic-Boom Theory With Wind-Tunnel and Flight Measurements. NASA TR R-213, 1964.

This page intentionally left blank.

LOW SONIC BOOM DESIGN ACTIVITIES AT BOEING*

George T. Haglund
Boeing Commercial Airplane Group
Seattle, WA

INTRODUCTION

Low sonic boom studies have continued during the last year with the goal of exploring the ability of practical airplane designs to achieve significantly reduced sonic boom loudness with reasonable performance penalties. At the 1993 Sonic Boom Workshop (Ref. 1), improvements to the low-boom design methods were described and early results of two low-boom configurations (-935 and -936) were presented. Now that the low boom design methods are reasonably mature, recent design activities have broadened somewhat to explore refinements to the -935 and -936 designs.

In this paper the results are reported of a detailed systems study and performance sizing of the -935 (Hybrid sonic boom waveform) and the -936 (Flat-top waveform). This analysis included a second design cycle for reduced cruise drag and balance considerations. Another design study was of a small-wing version of the -935. Finally, some preliminary results of the recent LaRC UPWT test of the -935 configuration are given, along with a proposed alternative method for extrapolating wind tunnel pressure signatures to the ground.

Figure 1 summarizes the various configurations studied. The topics covered by this paper are as follows:

- Systems study results of the Baseline -939 and low boom configurations -935 and -936.
- Small wing derivative of the -935.
- Wind tunnel test results of the -935.
- Test-derived F-function and propagation to the ground.
- Future considerations (boom-softened baseline, overwater issues, and operations).

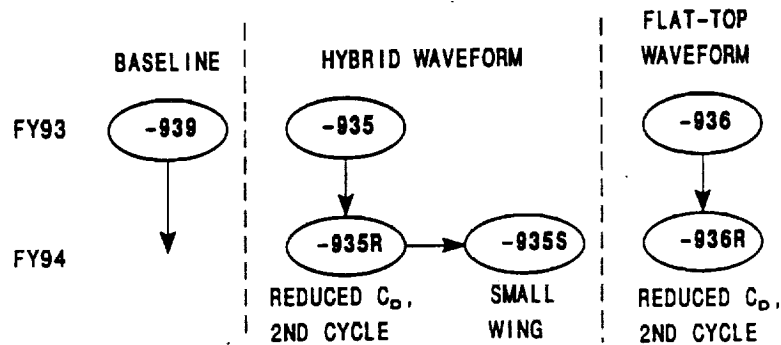


Figure 1. Configuration Relationships and History.

* This work was done under Contract NAS1-19360, Tasks 6 and 25.

BASELINE CONFIGURATION, -939

The -939 is a conventional baseline design used to assess the relative performance of the low-boom configurations. The -939 is similar to the well-known "Reference H", and has the following general characteristics:

- Unblended wing-body and low-wing integration.
- Three-post landing gear.
- Four GE 21/F15-A17 Mixed-Flow Turbofan (MFTF) engines, with bypass ratio 0.7.

Figure 2 is a configuration drawing of the -939, and gives additional airplane characteristics.

The low-boom airplanes share the above characteristics (and many other systems components) of the baseline, and are designed to be as realistic as possible within the sonic boom constraint. The MFTF engine concept selected is one of the better engine cycles, having excellent fuel flow characteristics at both Mach 1.7 (overland cruise speed) and Mach 2.4 (overwater cruise speed).

Fuselage Length:	314.0 ft
Wing Span:	137.1 ft
Wing Area:	7960.0 ft ²
L.E. Wing Sweep:	76.0 / 68.5 / 48.0 deg
Aspect Ratio:	2.367
Tri-Class Pax:	309
Cruise Speed	
Overland:	M 0.9
Overwater:	M 2.4

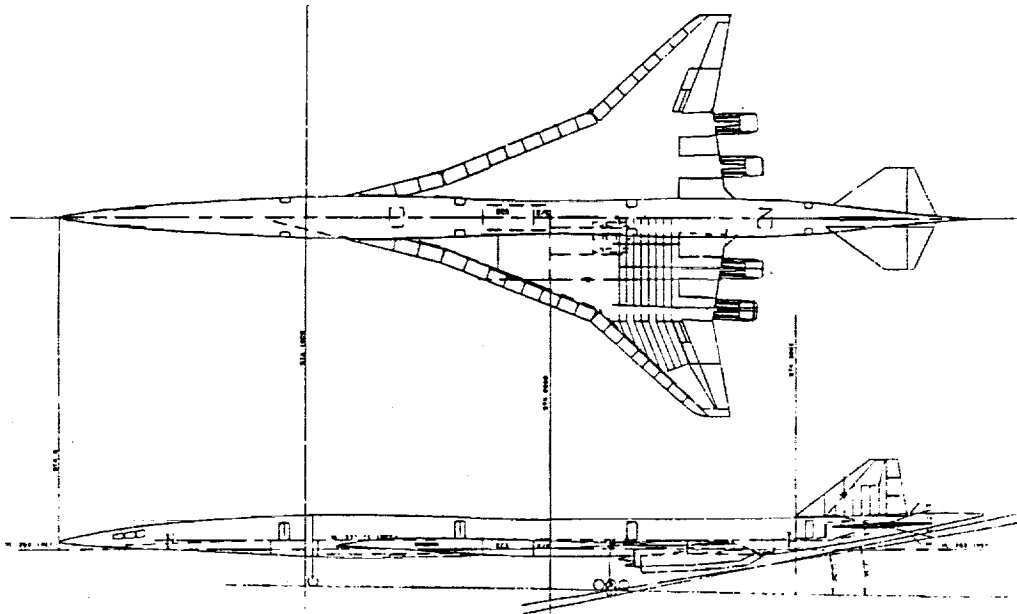


Figure 2. Configuration Drawing of the Baseline Configuration, Model 1080-939.

Figure 3 is the performance sizing "thumbprint" that allows selection of the minimum MTOW-sized airplane considering the effects of OEW, payload, aerodynamics, and more specifically the following design requirements:

- Design Mach = 2.4
- Design Range = 5000 nm with a 750 nm subsonic leg
- Takeoff field length = 11,000 ft
- Approach speed = 155 KEAS
- Climb thrust margin = 0.1.

The performance-sizing method used by Boeing includes a technology projection for a 6% improvement in drag. This drag reduction gives a significant reduction in the sized MTOW (about 10%) for the mission, and accounts for most of the difference in MTOW when compared to the results in Reference 2. In addition, the climb speed schedule has recently been revised which gives a significant reduction in MTOW of about 5%. Community noise levels were not evaluated.

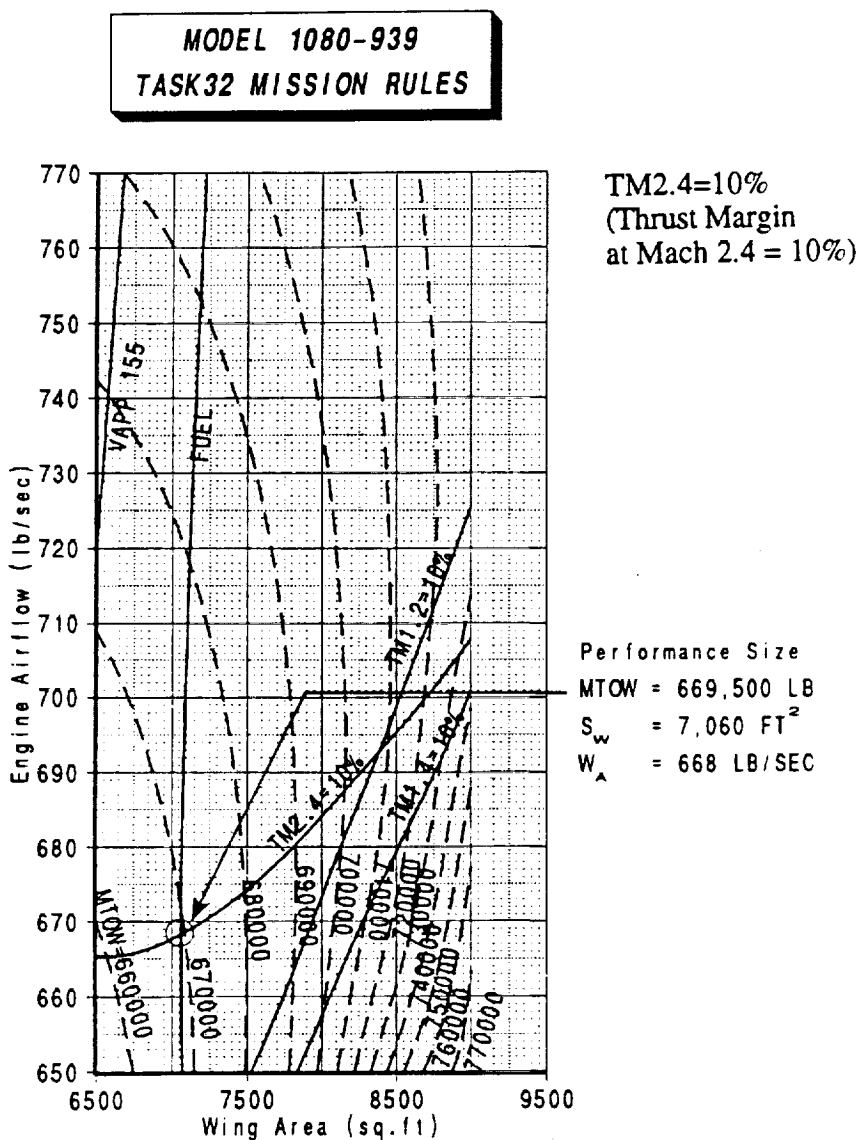


Figure 3. Performance Sizing Chart, Model 1080-939.

-935 LOW-BOOM CONFIGURATION (HYBRID WAVEFORM)

The -935, -935R, and -935S low-boom configurations were designed to the "Hybrid" waveform shown in Figure 4. The Hybrid waveform is a combination of the flat-top and ramp (or minimum shock) waveforms, and has desirable features in terms of configuration design, sonic boom propagation, and loudness (Refs. 3 and 4).

The -935R wing planform is compared to the baseline in Figure 5. Both mid-wings have the same leading edge sweep angle of 68.5 deg. The outboard leading edge sweep angles are quite different, however, 63.5 deg for the -935 and 48.0 deg for the baseline. Figure 6 is the -935 configuration drawing.

The initial mission-performance sizing of the -935 in June, 1993, resulted in a MTOW that was about 26,000 lb heavier than the baseline. This small weight penalty was very encouraging. This was also the first Boeing low-boom design for which the start-of-cruise weight closely matched the sonic boom design weight. However, this initial analysis revealed some design deficiencies that were corrected in a second design cycle during 1994, as follows:

- Wing shifted 45 inches aft for balance
- Empennage sized for adequate control
- Inboard wing thickness increased for adequate landing gear volume
- Wing camber and twist redesigned at Mach 2.4 instead of Mach 1.7 and with more positive C_{M0}

The performance sizing chart for the -935R in Figure 7 shows two sized airplanes, one at the optimum performance size ($S_{REF} = 7200 \text{ ft}^2$), and the other at the sonic boom design wing area of 9000 ft^2 . The MTOWs are 651,000 lb and 707,000 lb, respectively, compared to the baseline MTOW of 669,500 lb. A noise assessment was not done at this time since total success was not achieved in reaching the reduced boom loudness goal with a small MTOW penalty. However, the reduced aspect ratio, more highly swept wing, would present a more severe challenge than the baseline.

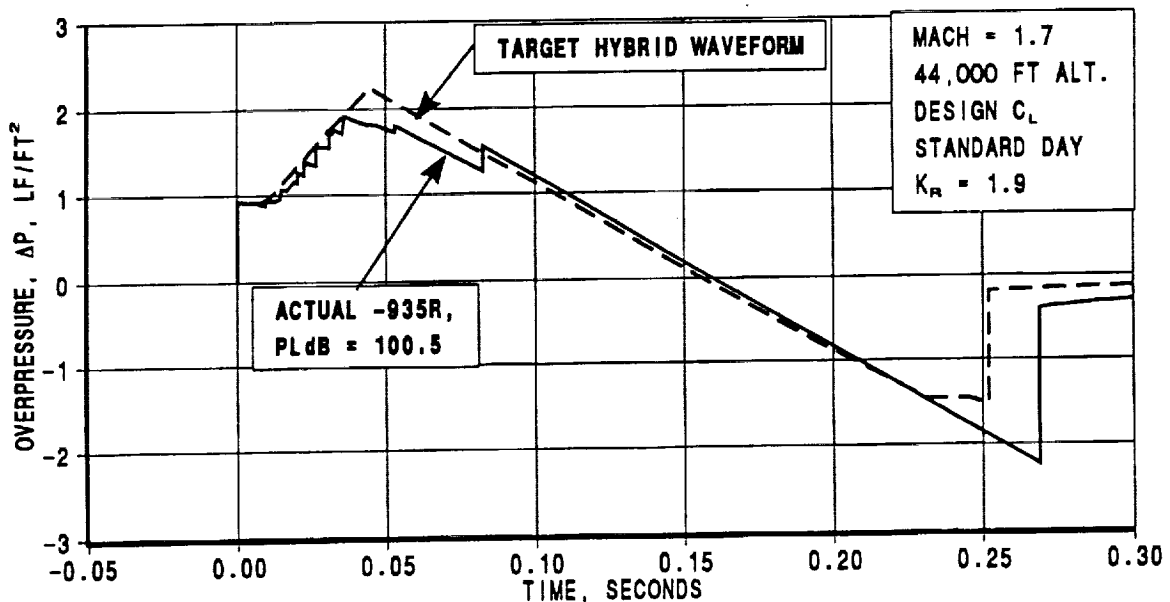


Figure 4. Target and Calculated Hybrid Waveform for -935R.

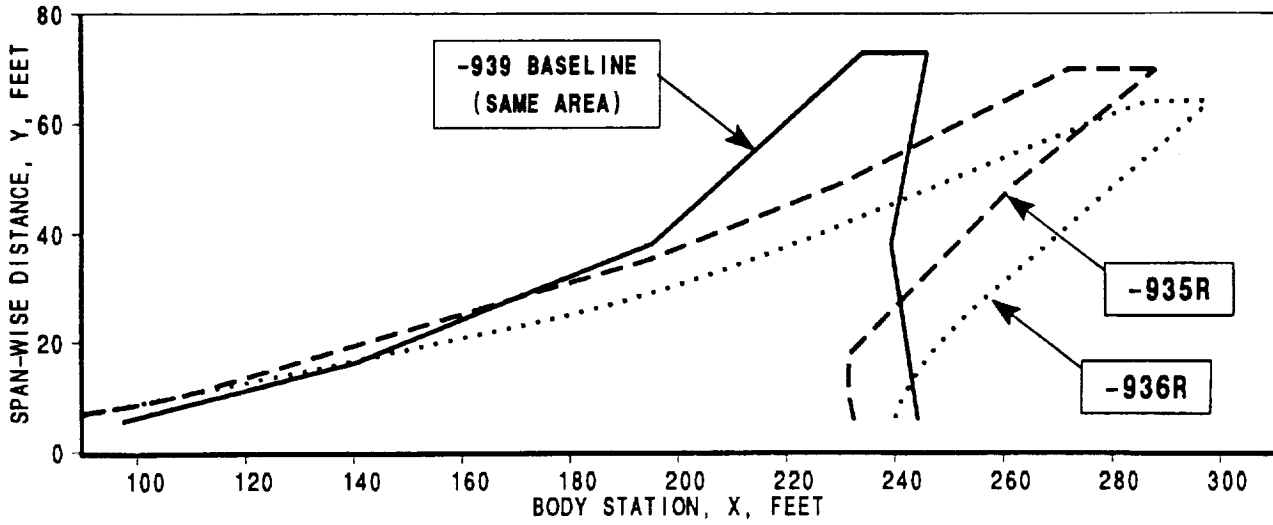


Figure 5. Planform Comparison, -935R, -936R, and Baseline -939.

Fuselage Length: 317.5 ft
 Wing Span: 140.0 ft
 Wing Area: 9000.0 ft²
 L.E. Wing Sweep: 74.0 / 68.5 / 63.4 deg
 Aspect Ratio: 2.18
 Tri-Class Pax: 300
 Cruise Speed
 Overland: M 1.7
 Overwater: M 2.4

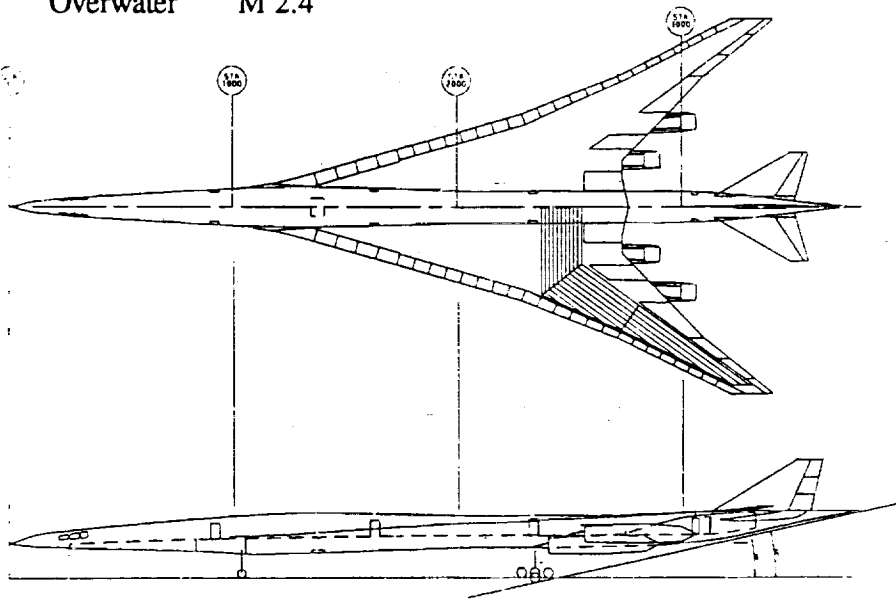


Figure 6. Configuration Drawing of Low-Boom Model -935.

MODEL 1080-935R
GE 21/F15-A17
TASK 32 MISSION RULES

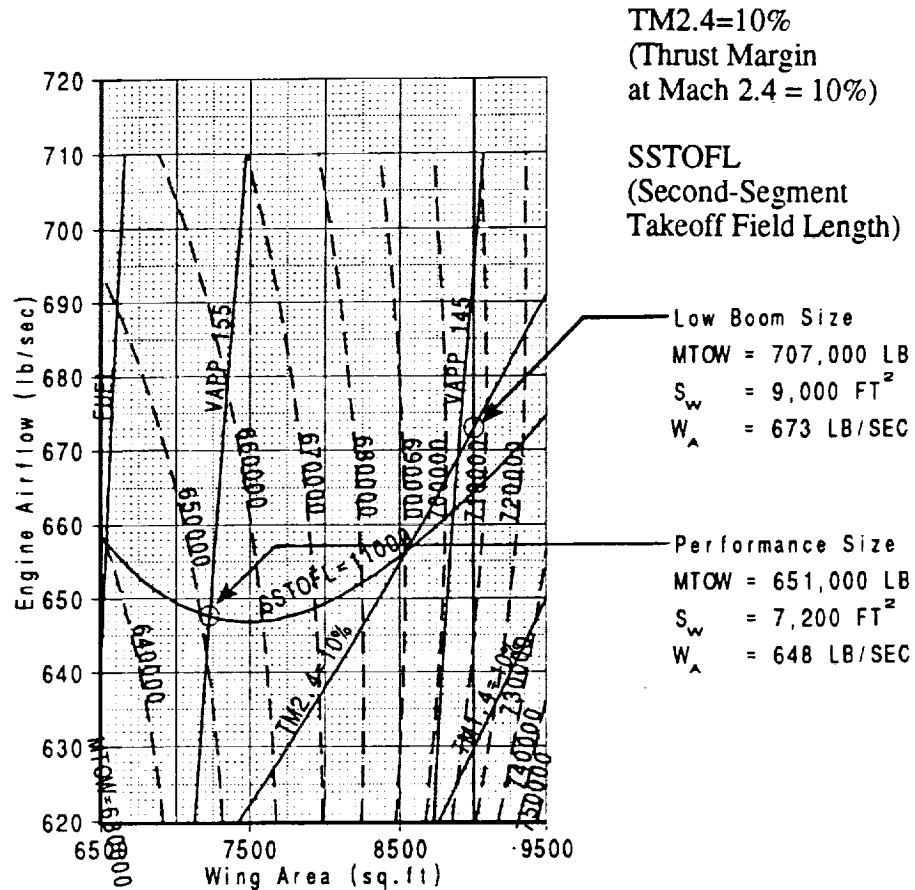


Figure 7. Performance Sizing Chart, Model 1080-935R.

SMALL WING VERSION OF THE -935R

A big wing is very helpful in low-boom design since the low wing loading gives reduced pressure levels for the lift contribution to sonic boom. Earlier Boeing designs (Ref. 5) had wing areas of about 10,000 ft², while the more recent -935 and -936 have wing areas of about 9,000 ft². The -935S is a "small" wing derivative of the -935R to explore the benefits of a smaller wing in terms of reduced OEW and improved overall performance. The -935S has the following characteristics relative to the -935R:

- Scaled down wing planform and thickness by 10% ($S_{REF} = 8100 \text{ ft}^2$).
- Same wing sweep angles and aspect ratio
- No change to wing camber and twist
- Redesigned fuselage (slightly fatter)
- OEW reduced by 7230 lb
- L/D worse by 3.5% at Mach 2.4

Figure 8 shows a comparison of the planforms for the -935R and -935S, and Figure 9 compares the calculated pressure signatures for the -935R and -935S. The -935S signature has a slightly higher pressure peak. In the performance sizing chart for the -935S in Figure 10, the optimum performance size occurs at a MTOW of 660,000 lb and a wing area of 7350 ft², while the sonic boom design wing area of 8100 ft² gives a MTOW of 680,000 lb, which is only 10,500 lb heavier than the baseline.

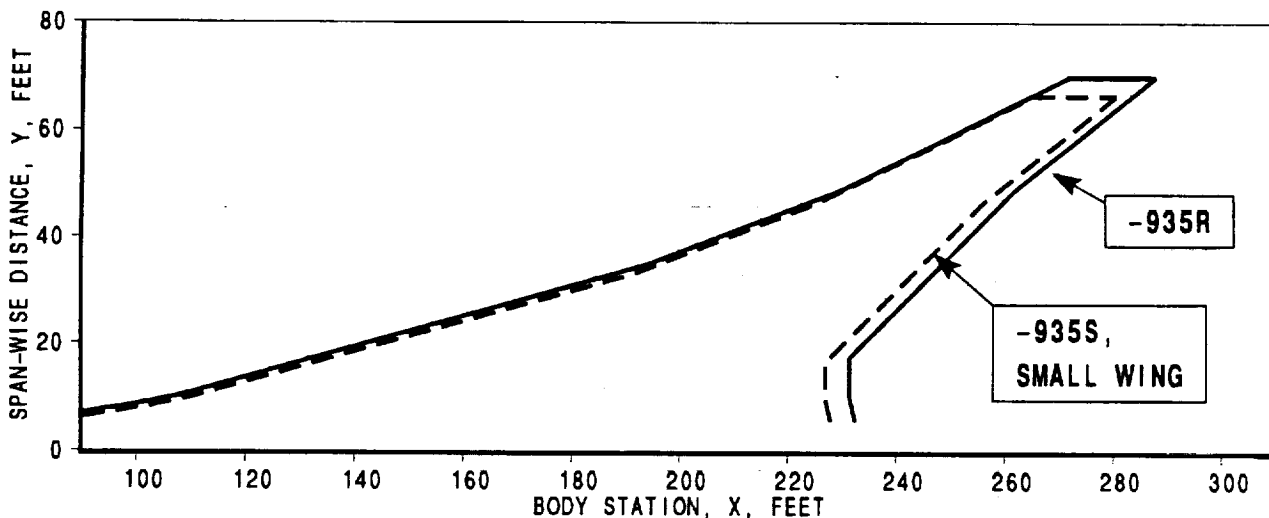


Figure 8. Planform Comparison, -935S and -935R.

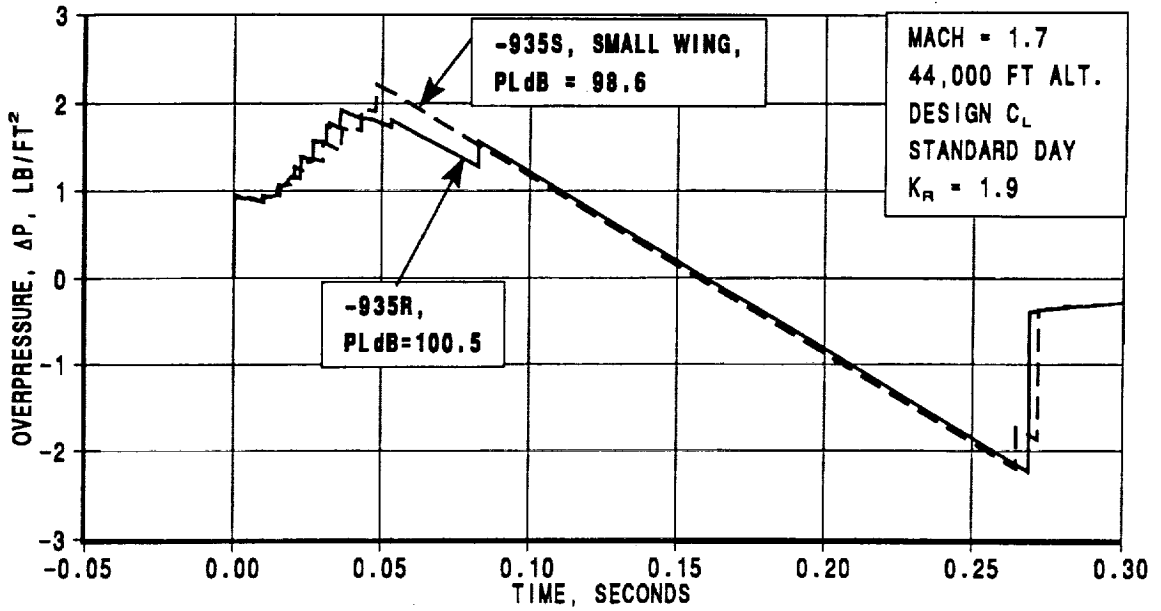


Figure 9. Calculated Sonic Boom Pressure Signatures, -935R and -935S.

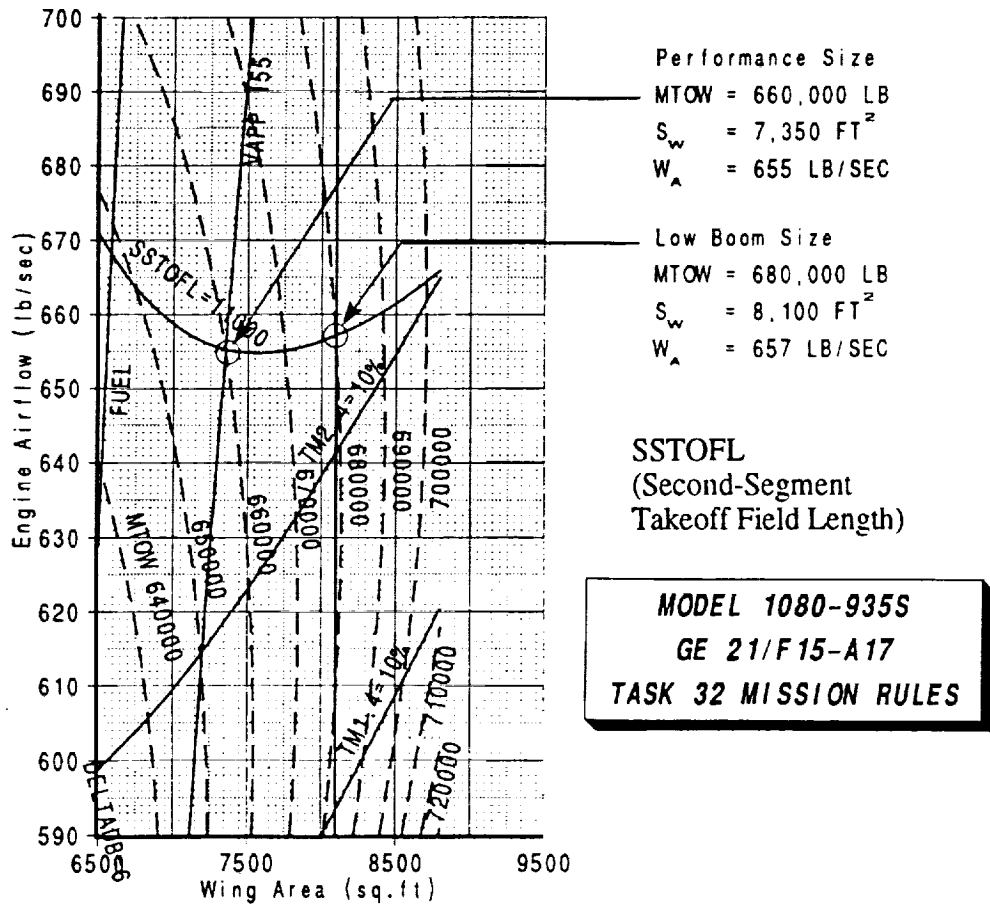


Figure 10. Performance Sizing Chart, Model -935S.

-936 LOW-BOOM CONFIGURATION (FLAT-TOP WAVEFORM)

The -936 low-boom configuration was designed to the "flat-top" waveform, shown in Figure 11. The flat-top waveform is attractive since its low peak pressure may provide reduced loudness for indoor observers. From an airplane design standpoint, however, the flat-top waveform is a more difficult proposition, since it requires more wing sweep and a more aft wing location. Figure 5 compares the -936 planform with the baseline and the -935R planforms. Due to these rather severe constraints, the initial performance-sizing of the -936 in June 1993 resulted in a MTOW that was significantly heavier (about 189,000 lb) than the baseline. Figure 12 is the configuration drawing.

In 1994 a second design cycle on the configuration (-936R) resulted in a significant performance improvement, primarily through drag reduction. However, it was necessary to depart from a true flat-top waveform, as shown in Figure 11. The changes from the -936 to the -936R are as follows:

- Wing shifted forward 74 inches for balance
- Revised fuselage camber and forebody shape
- New wing camber and twist design (at M 2.4 instead of M 1.7 and more positive C_{M0})
- L/D improved by 12% at Mach 2.4
- Payload reduced from 325 to 300 passengers
- Revised sonic boom waveform (maximum $\Delta P = 1.5$ psf instead of 1.0 psf).

The -936R performance-sizing chart in Figure 13 shows a MTOW of about 720,000 lb for the optimum performance size and 725,000 lb for the sonic boom design wing area of 8790 ft². As with the -935R, a noise assessment was not done; however, meeting a noise constraint would be more difficult than on the baseline due to the increased wing sweep and lower aspect ratio.

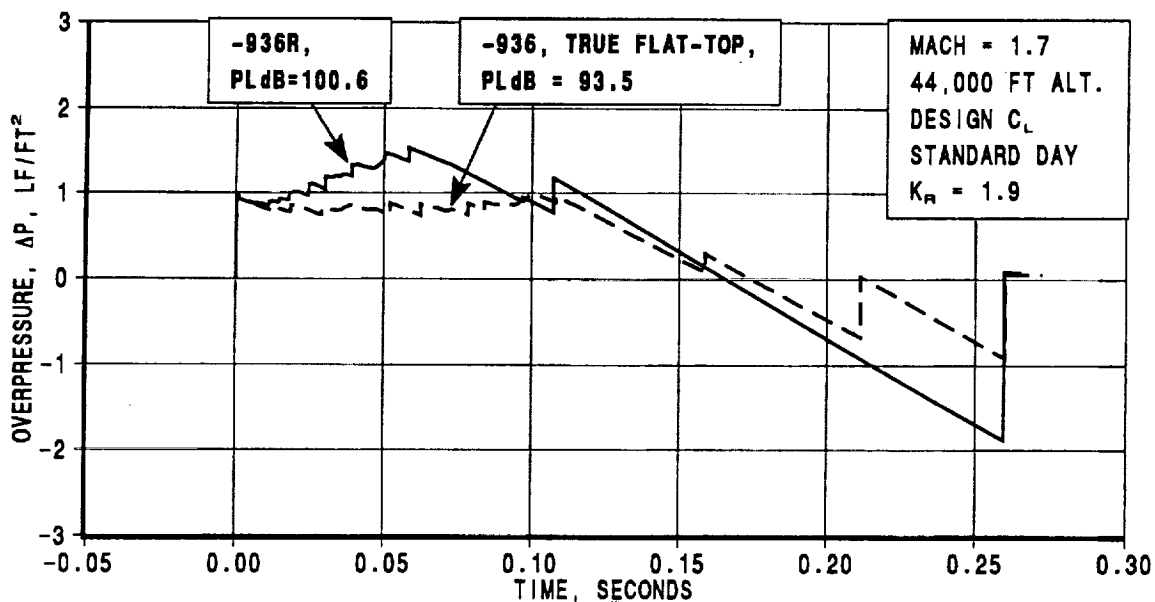


Figure 11. Calculated Sonic Boom Pressure Signatures, -936 and -936R.

Fuselage Length: 317.5 ft
 Wing Span: 128.3 ft
 Wing Area: 8790.0 ft²
 L.E. Wing Sweep: 78.7 / 68.0 deg

Aspect Ratio: 1.87
 Tri-Class Pax: 325
 Cruise Speed
 Overland: M 1.7
 Overwater: M 2.4

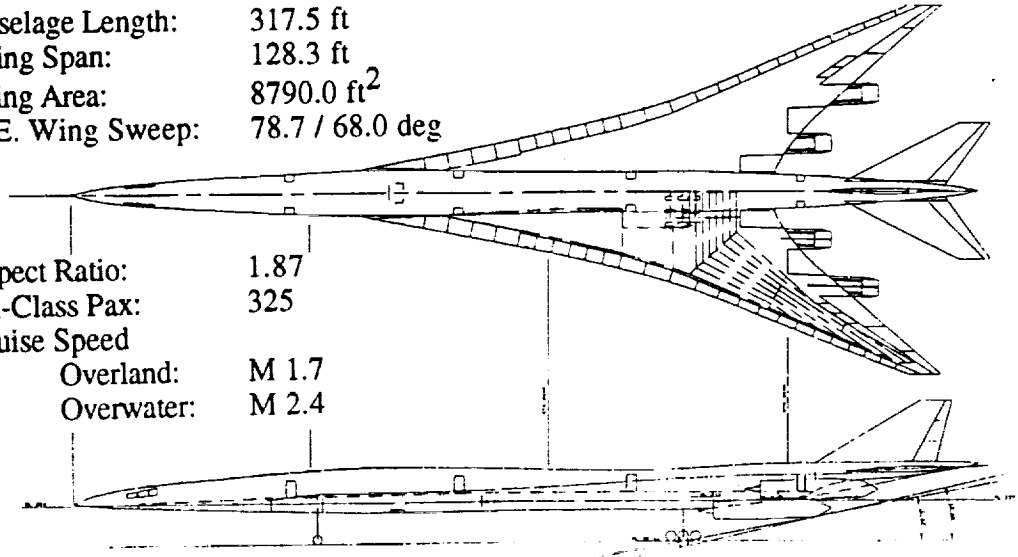


Figure 12. Configuration Drawing of Low-Boom Model -936.

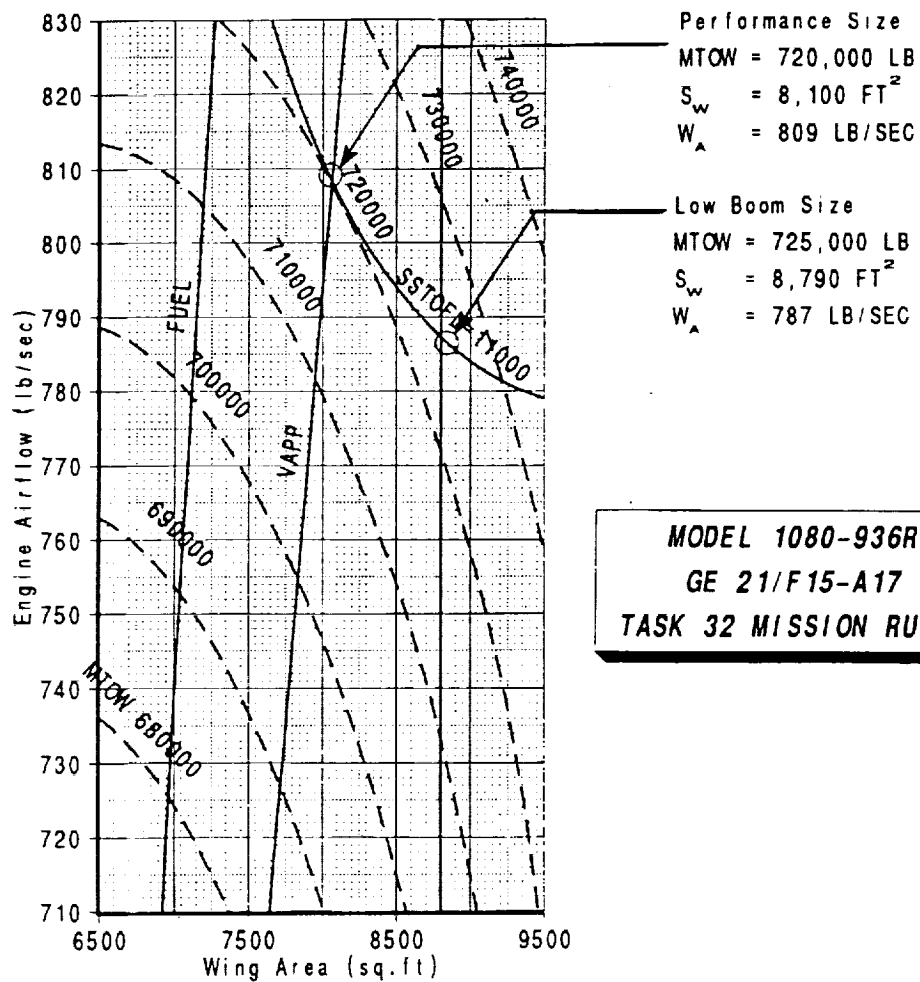


Figure 13. Performance Sizing Chart, Model -936R.

SUMMARY OF CURRENT LOW-BOOM DESIGNS

The figure-of-merit for assessing various configurations is the performance-sized Maximum Takeoff Weight (MTOW) for the 5000 nm mission. For configurations with different passenger capacities, however, a more convenient metric is MTOW per passenger. Figure 14 summarizes the MTOW/PAX for the various configurations relative to the baseline, and Figure 15 shows the sonic boom loudness for these configurations. A significant conclusion is that it takes severe arrow-wing planforms with much increased risk to achieve fairly minor noise reductions with a significant MTOW penalty. For the two up-dated low boom airplanes -935S and -936R, the loudness goal of 94 PLdB was exceeded by 5 and 7 dB, respectively, and the performance penalties in terms of MTOW/PAX were +4.6 % and +11.4 %. Increased risk is associated with low speed performance, takeoff noise, and wing structural characteristics.

The attempts to reduce drag and improve performance have tended to result in an increase in the sonic boom loudness, primarily because of an increase in the strength of the tail shock. If the tail shock could be reduced to about 1.0 lb/ft², the loudness could be reduced by about 6 dB, but would require a more exotic planform with significant lift carried further aft.

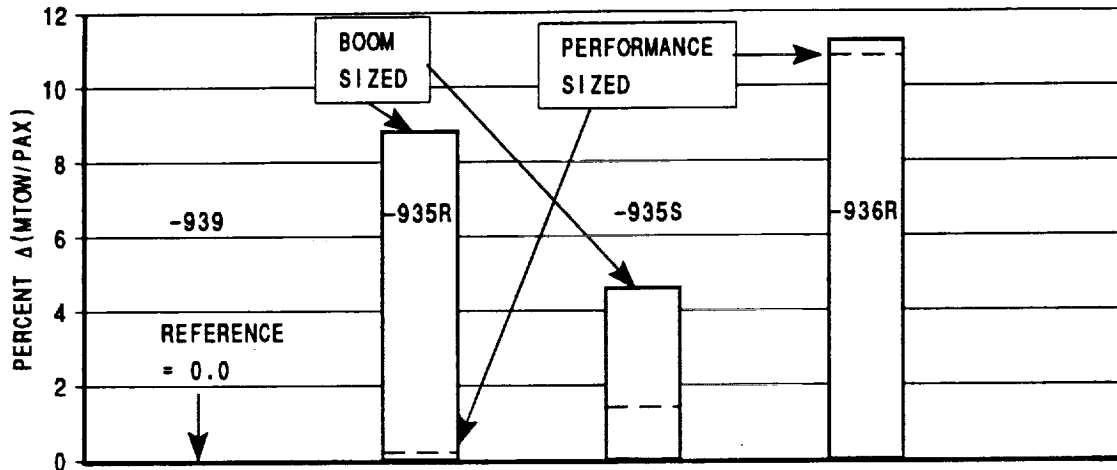


Figure 14. Comparison of Overall Performance (MTOW / PAX).

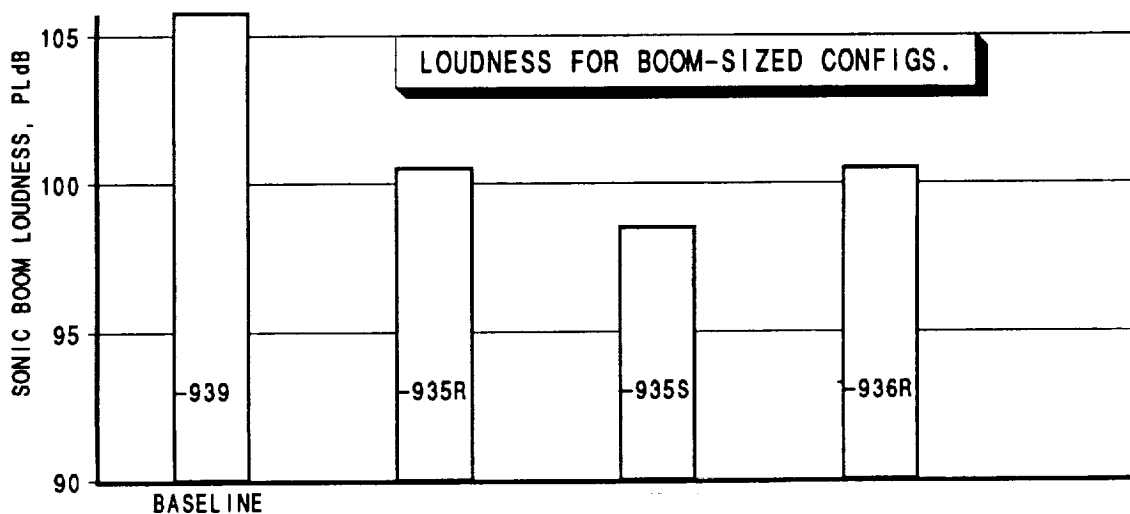


Figure 15. Sonic Boom Loudness.

-935 PRELIMINARY WIND TUNNEL RESULTS

A 12-inch model of the -935 was tested in the LaRC Unitary wind tunnel in March and April, 1994. Test conditions included a range of C_L in addition to the design C_L of 0.11. Data were obtained at distances of 12 and 24 inches from the model. Figure 16 compares the theoretical Whitham $\Delta P/P$ (calculated for the geometry and the wind tunnel conditions) and the test $\Delta P/P$ at 12 and 24 inches away. Although there are differences in the details of the signatures, the pressure levels and pressure peaks agree well. Differences are to be expected in this comparison because the Whitham theory applies in the far-field, while the wind tunnel data at this close-in distance may have strong non-linear effects.

TRANAIR results are also given in Figure 16, and are somewhat disappointing. Great care was taken to preserve the shocks by using dense gridding near shocks and the second-order upwind method. The shocks are rounded, however, and the nacelle influence appears muted.

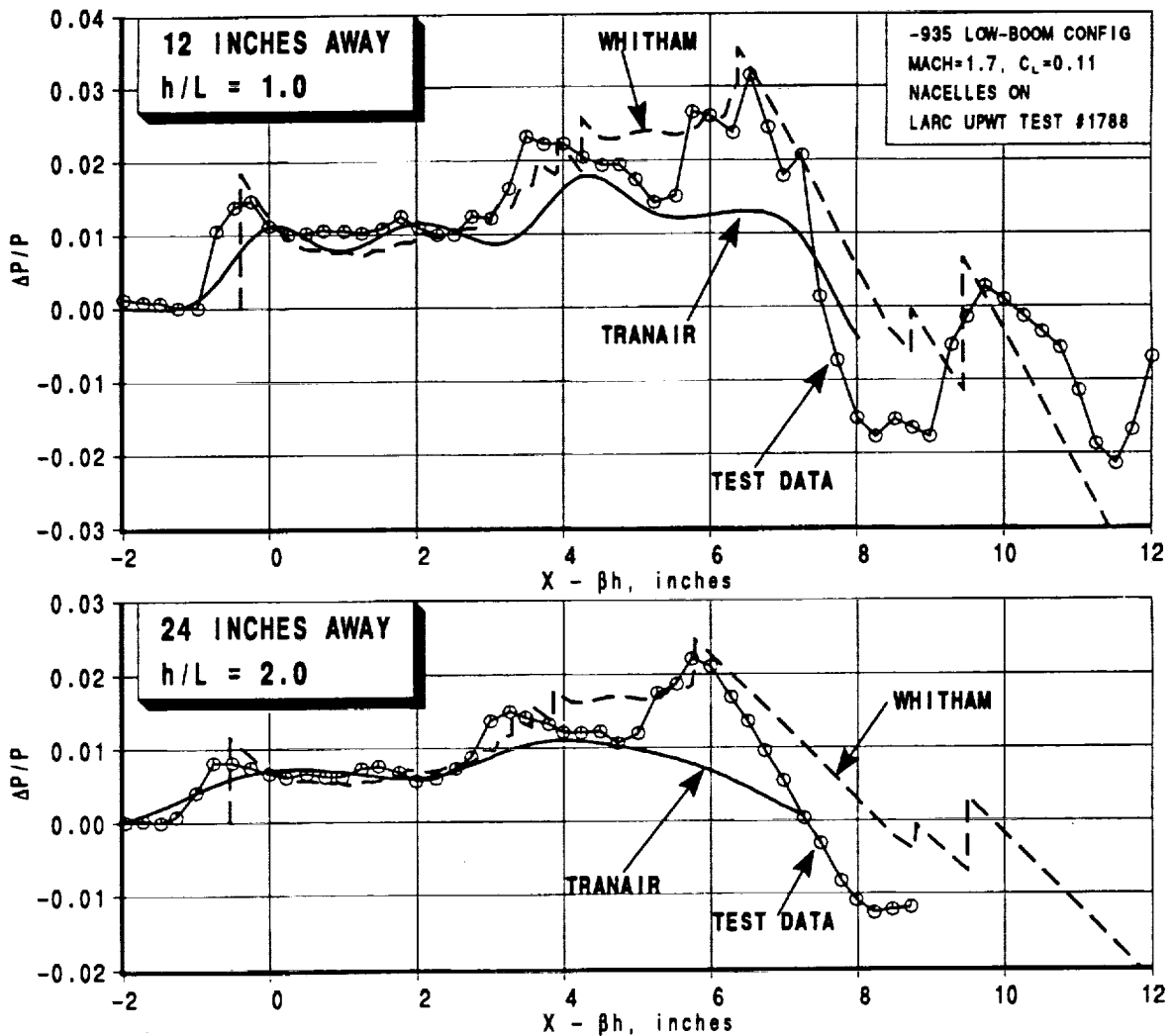


Figure 16. Wind Tunnel Versus Theory at $h/L = 1.0$ and 2.0 .

DERIVED F-FUNCTION AND PROPAGATION TO THE GROUND

For pressure signatures measured in the wind tunnel (or calculated by CFD methods) for low-boom shaped vehicles, an accurate method is required for waveform extrapolation to the ground in the real atmosphere. The Thomas method (Ref. 7) has been widely used; however, it does not account for the different waveform "aging" (non-linear advance) between the wind tunnel (or CFD) uniform conditions and the real atmosphere. In addition, the "reverse propagation" method suggested by Hayes (Ref. 6, pg. 50) was used to adjust the test data $\Delta P/P$ to the airplane and then to convert the measured $\Delta P/P$ to an F-function. The procedure is as follows:

1) Match the age variable, τ , in the wind tunnel and the atmosphere. The well-known "Hayes freeze" means that in the real atmosphere (with density increasing downward), the aging is retarded compared to the uniform wind tunnel conditions. To match the wind tunnel age at $h/L = 1.0$, for example, the real atmosphere waveform must propagate to h/L of 1.53. Similarly, at $h/L = 2.0$ in the wind tunnel, the age match occurs at $h/L = 3.08$ in the real atmosphere.

2) Correct the measured $\Delta P/P$ for the h difference in (1). Alternatively, the amplitude could have been matched, which would require a more difficult correction to the age. Since we have matched the age at different h values, there needs to be a correction to the measured $\Delta P/P$, as follows:

$$(\Delta P/P)_{\text{corr}} = (\Delta P/P)_{\text{WT}} (h_{\text{WT}}/h_{\text{corr}})^{1/2} \quad (1)$$

where "WT" denotes wind tunnel conditions and "corr" denotes the corrected value for the real atmosphere. The following table summarizes the wind tunnel / atmosphere matching for the Mach 1.7 test conditions of the LaRC Unitary wind tunnel and for the Standard atmosphere conditions at 44,000 feet altitude.

Wind tunnel h/L	h/L in real atmosphere to match WT age	$\Delta P/P$ Factor
1.0	1.53	0.808
2.0	3.08	0.806

3) "Reverse propagate" the measured $\Delta P/P$ from the wind tunnel h/L to the airplane. Since the wind tunnel conditions are uniform, the reverse propagation is according to the well-known equations for phase shift due to aging and for converting $\Delta P/P$ to an F-function, as follows:

$$F(x) = (\Delta P(x)/P) (2h\beta)^{1/2} / (\gamma M^2) \quad (2)$$

$$y = x - \beta h + k h^{1/2} F(x), \quad \text{where } k = (\gamma+1) M^4 (2\beta^3)^{-1/2} \quad (3)$$

4) Propagate the "test-derived" F-function to the ground in the normal manner (Ref. 6 or 7).

Figure 17 shows the ground-extrapolated pressure signatures calculated with the above method and also calculated directly from the geometry using the ARAP method of Reference 6. Figure 18 compares the "reverse propagation F-function" method to the Thomas method (Ref. 7), and it's clear that the Thomas method gives pressure levels that are too high. The Thomas method would agree with the new method if the $\Delta P/P$ factor of 0.808 were applied.

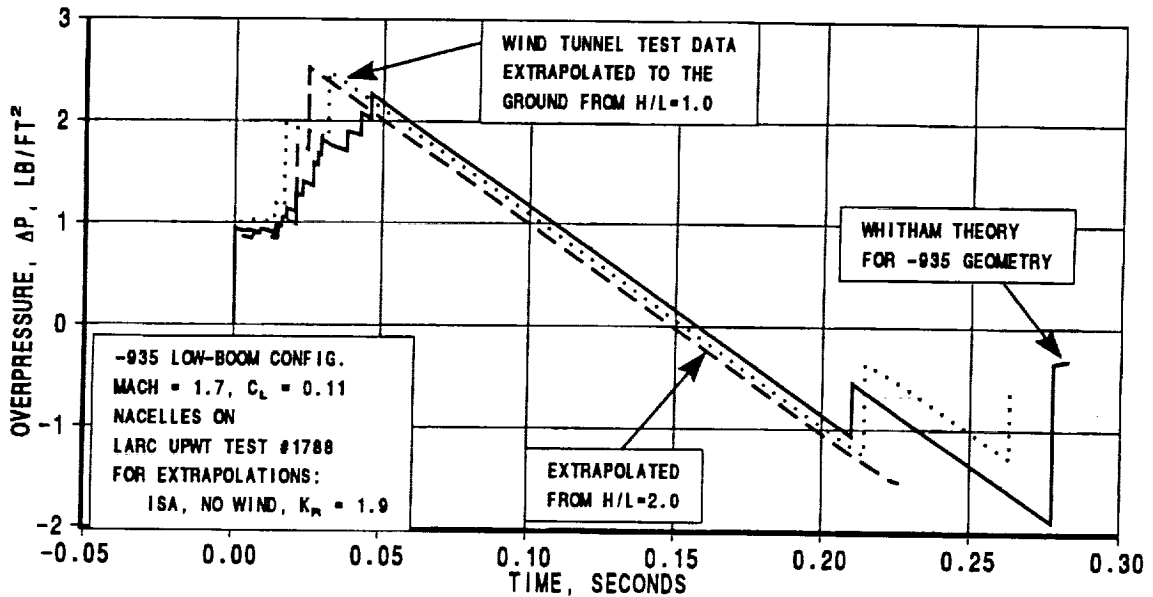


Figure 17. Extrapolated Signatures to the Ground From $h/L = 1.0$ and 2.0 .

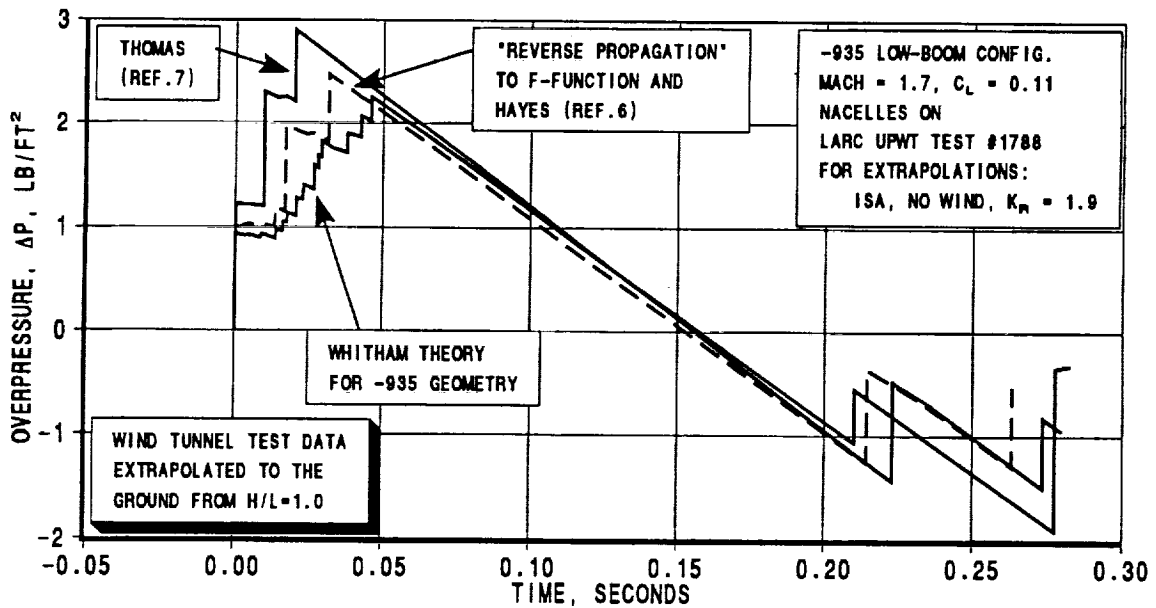
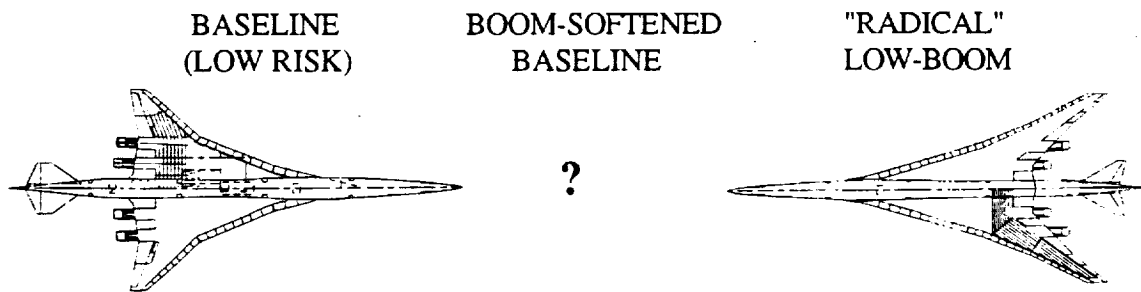


Figure 18. Comparison of Extrapolated Signatures (Thomas Method and "Test-Derived" F-Function Method).

FUTURE CONSIDERATIONS

Despite the significant progress in low boom design, it appears that even radical arrow wing concepts achieve only modest noise reductions (5 to 7 dB) at a significant performance penalty (5 to 12% in MTOW/PAX). Accordingly, boom design efforts will be directed toward small reductions in sonic boom of the baseline configurations with minimal penalties. Fortunately, what we have learned in our low-boom design work applies directly to this boom "softening". The boom-softened baseline can be thought of as being an intermediate design between the baseline and the current "radical" low-boom designs (-935 and -936), as illustrated below.

Other areas of future study include operational considerations, the focused booms produced by accelerations and turns, secondary booms, and overwater issues.



REFERENCES

1. Haglund, George T.: Low Sonic Boom Studies at Boeing. High Speed Research: Sonic Boom, Volume II, NASA CP 10133, 1994.
2. Baize, Daniel G., et al.: A Performance Assessment of Eight Low-Boom High-Speed Civil Transport Concepts. NASA High Speed Research: Sonic Boom, NASA/CP-1999-209699, 1999.
3. Mack, Robert J., and Haglund, George T.: A Practical Low-Boom Overpressure Signature Based on Minimum Sonic Boom Theory. High Speed Research: Sonic Boom, Volume II, NASA CP 3173, 1992.
4. Haglund, George T.: Nacelle and Forebody Considerations in Design for Reduced Sonic Boom. High-Speed Research: Sonic Boom, Volume II, NASA CP-3173, 1992.
5. Haglund, George T.: High Speed Civil Transport Study of Two Mach 1.7 Low Boom Designs. NASA CR 191138, September 1993.
6. Hayes, Wallace D., et al.: Sonic Boom Propagation in a Stratified Atmosphere, with Computer Program. NASA CR-1299, 1969.
7. Thomas, Charles L.: Extrapolation of Sonic Boom Pressure Signatures by the Waveform Parameter Method. NASA TN D-6832, 1972.

This page intentionally left blank.

SONIC BOOM SOFTENING OF REFERENCE-H

Samson Cheung
MCAT Institute, NASA Ames Research Center
Moffett Field, CA

INTRODUCTION

For the past four years, various low-boom configurations have been designed and tested in wind tunnels. However, recent consideration of high speed civil transport (HSCT) flying over water reveals the possibility of a high performance aircraft flying within a specific corridor. Boeing's Reference -H, which is a performance aircraft cruising at Mach 2.4 over-water, is considered as a baseline configuration for the HSCT. Typically, a performance aircraft has higher lift coefficient than a low-boom configuration.

It is known to the industry that it is difficult to reduce the sonic boom of a performance aircraft to the noise level of a low-boom aircraft. In the present study, effort was spent to find out what factors make the reduction of loudness level of a performance aircraft so difficult, and to investigate the possibility of reducing the loudness level of Reference-H.

AIMS

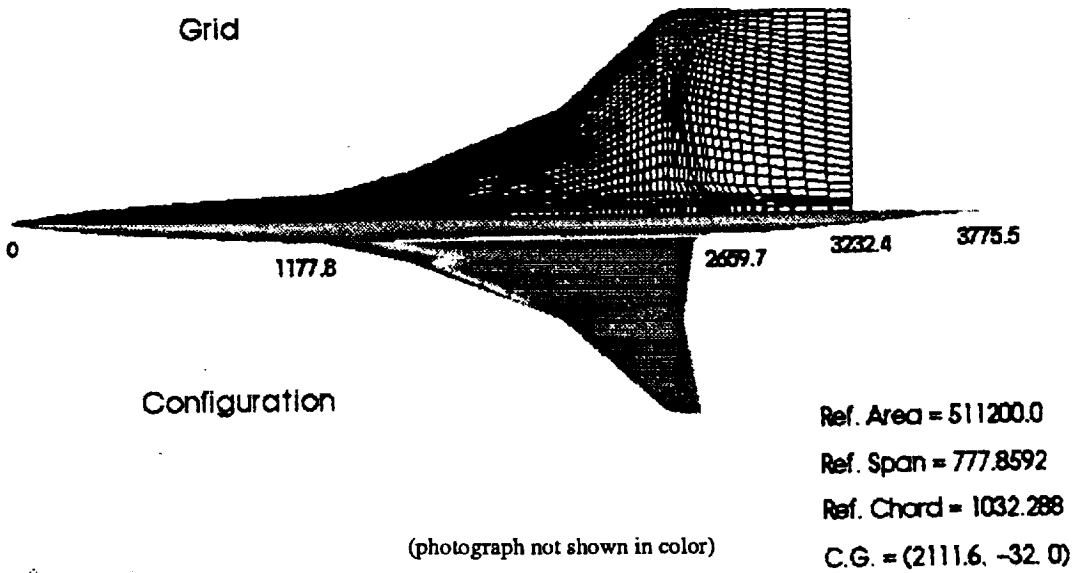
First is to combine two computational fluid dynamics (CFD) codes to form an accurate and efficient flow analysis tool for near-field flow calculation in airplane design cycle. The characteristics of the codes will be described later.

Second is to reduce the sonic boom of Reference-H by the above CFD codes and the optimization package developed in the past [1,2].

- Combining two CFD codes (Inviscid calculations)
Upwind Parabolized Navier-Stokes code: UPS3D
Thin-Layer Navier-Stokes code: OVERFLOW
- Reducing sonic boom loudness of Ref-H

REFERENCE-H

The figure below is the surface grid and geometry of Reference-H. The free-stream Mach number is 2.4, angle of attack is 4.5 degrees, and the lift coefficient CL is 0.124.



CODES

Two CFD codes are combined to calculate the near-field solution of Reference-H. The first one is an upwind Parabolized Navier-Stokes code (UPS3D) [3]. It is a very efficient space-marching code, which solves the Parabolized Navier-Stokes (PNS) equations. However, it fails in subsonic flow that often occurs near the nacelle/wing region. Furthermore, the gridding for such complex geometry is such that UPS3D cannot handle.

Another CFD code is a time iterative thin-layer Navier-Stokes code (OVERFLOW) with overset grid method [4]. It is a good CFD flow solver, which can handle almost any complex geometry. However, time iterative code is relatively slow and computationally expensive.

Therefore, the flow in the wing/nacelle region is calculated by OVERFLOW, but the rest of the flow is calculated by UPS3D code.

- Upwind Parabolized Navier-Stokes Code (UPS3D)
 - Space-Marching Code
 - Roe Scheme
 - High Efficiency
 - Difficulty in Complex Configuration (Wing/Nacelle)
 - Failing in Subsonic Regions

- Thin-Layer Navier-Stokes Code (OVERFLOW)
 - Time-Iterative Code
 - Beam-Warming Implicit Three-Factor Central Difference Scheme
 - Overset Grid
 - Relatively Slow

GRID DIMENSIONS

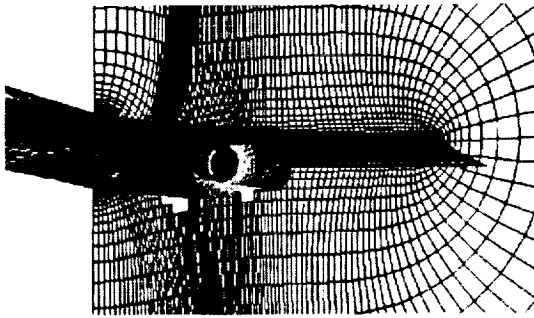
The figure below shows the computational grids used by OVERFLOW and UPS3D codes. In the wing/nacelle region, five grids are used, namely, one for wing/body, two for the outer part of the two nacelles, and two for the inner part of the nacelles.

OVERFLOW

32x203x101 for partial wing/body

46x43x21 for outer nacelles (two)

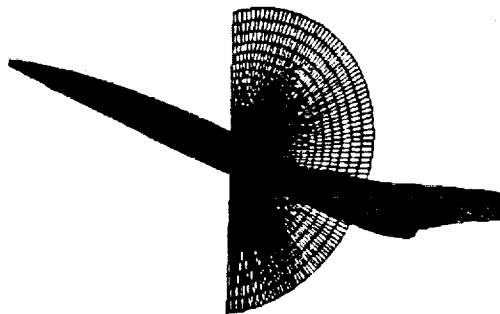
43x8x8 for inner nacelles (two)



UPS3D

111x121

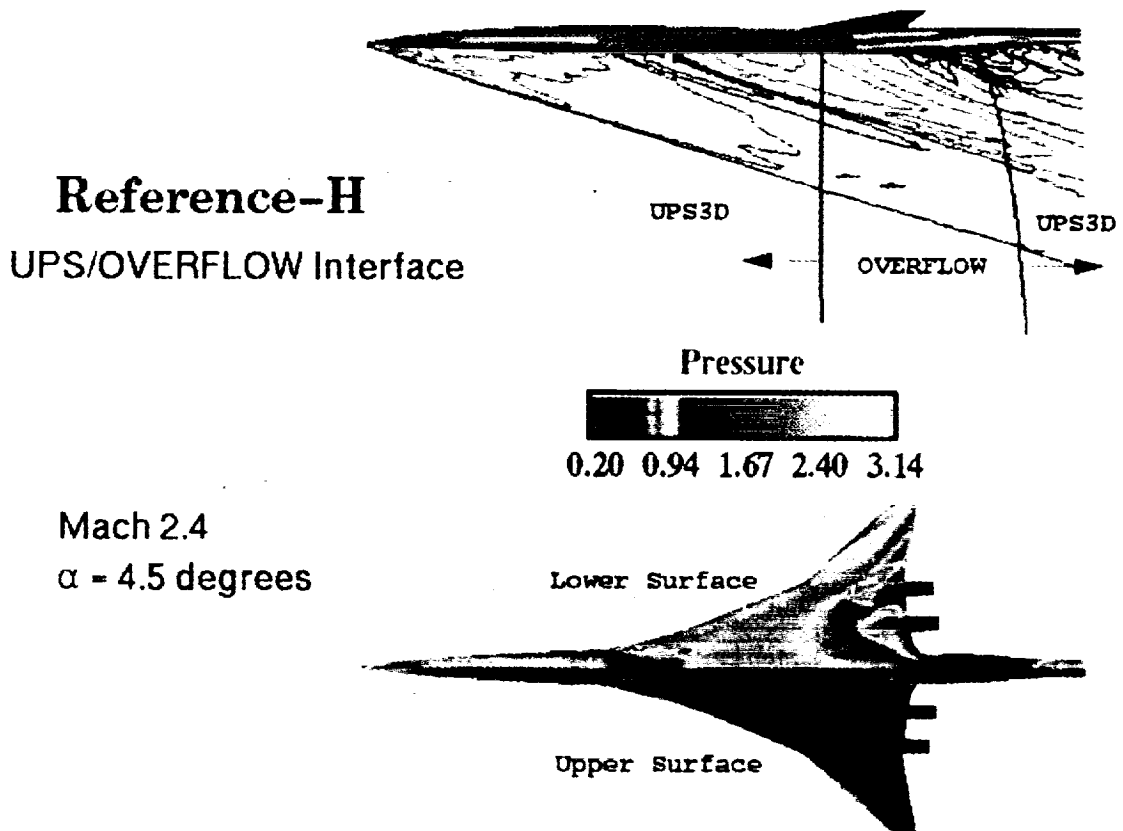
step size 0.01 body lengths



(photograph not shown in color)

UPS/OVERFLOW INTERFACE

The figure below shows the flow solution calculated from the two CFD codes. The upper diagram shows the interfaces of the codes. The continuity of the pressure contours suggests that the interfacing routine between the two CFD codes is satisfactory. The lower diagram shows the upper and lower surface pressure fields.

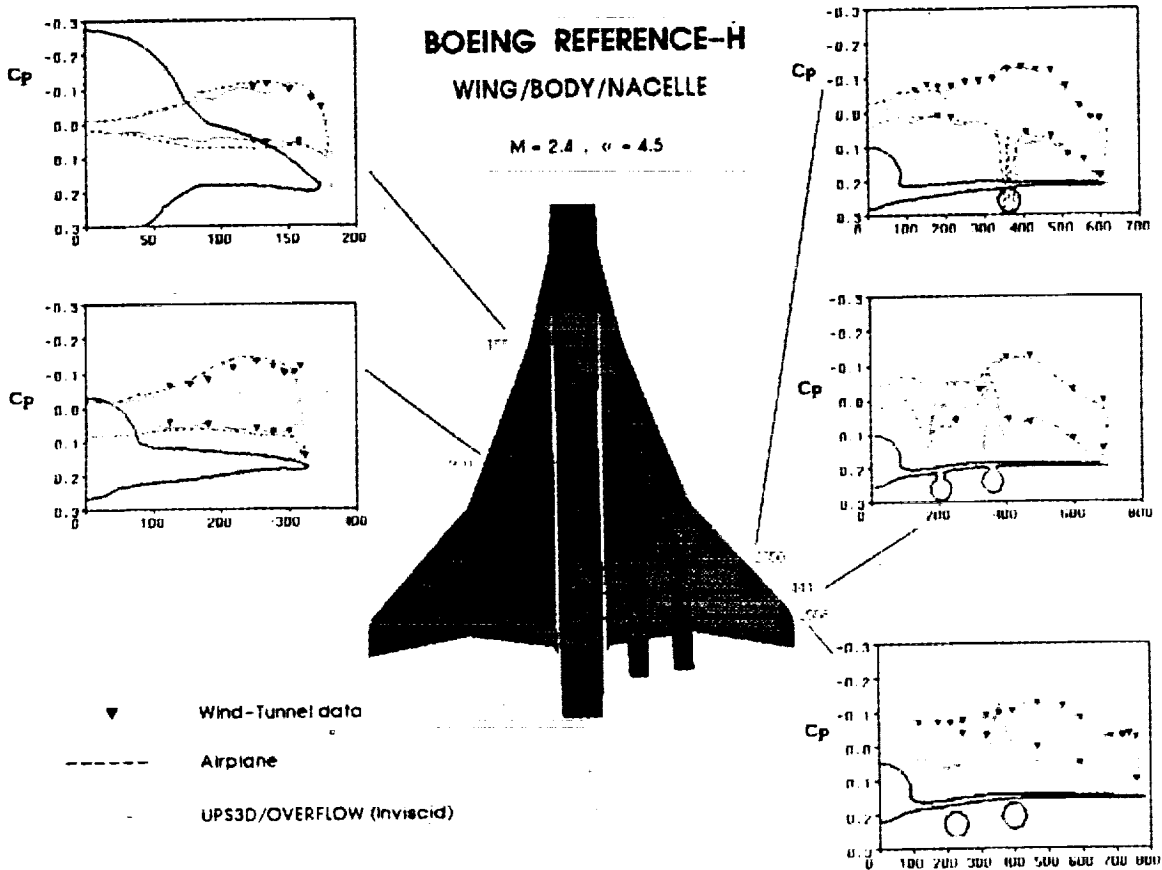


SHC 94/2

(photograph not shown in color)

PRESSURE DATA

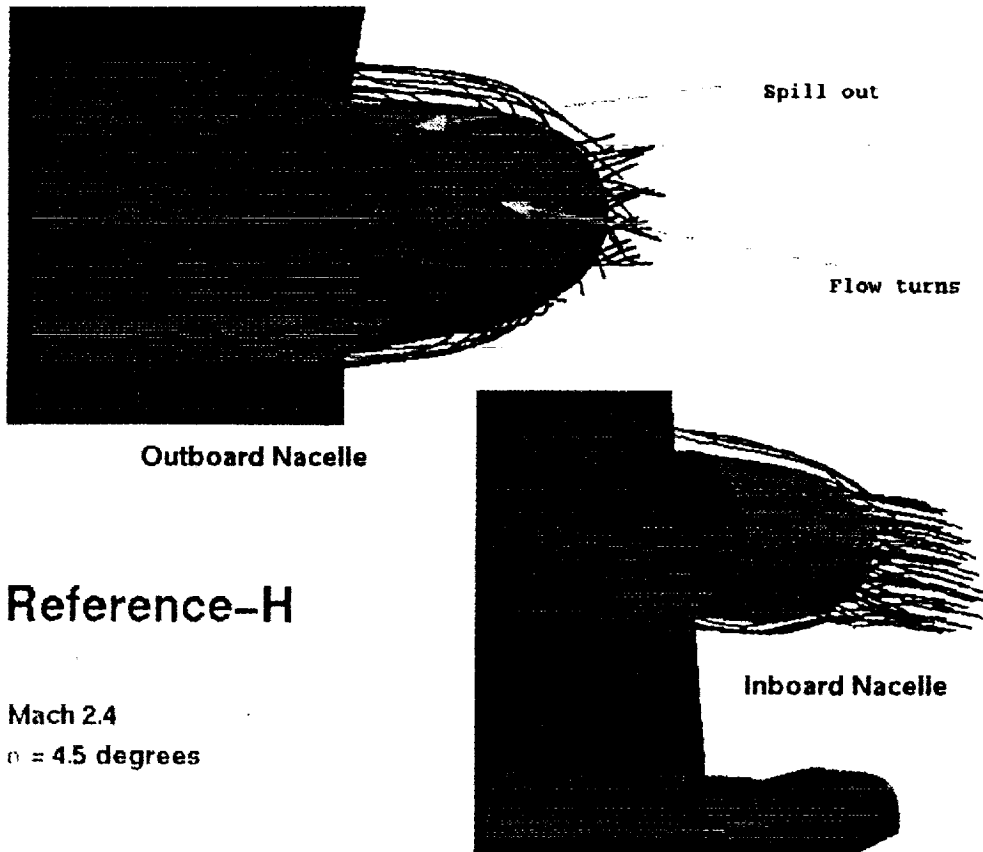
The figure below shows the comparison of the CFD computational data and the wind-tunnel data. The triangle represents the wind-tunnel data, the solid line represents the computational result from UPS3D/OVERFLOW, and the dotted line represents the computational result from Airplane. Airplane solves the Euler equations with unstructured grid concept. It took UPS3D/OVERFLOW less than 45 mins. in Cray-YMP to generate the solution; whereas, it took Airplane more than 3.5 hours in the same machine. The C_p plots suggest that UPS3D/OVERFLOW is a good tool to compute the near-field solution of Reference-H, although more grid points seem to be needed to resolve the leading edge tip. Nevertheless, present grid density in the circumferential direction is sufficient for sonic boom prediction.



(photograph not shown in color)

NACELLES REGIONS

The figure below shows the particle traces in the wing/nacelle regions. The lower diagram shows that the flow is smooth over/into the inboard nacelle. On the other hand, the upper diagram shows a significant turning of the flow. This turn could be due to mass spilling from the inlet of the nacelle. The figure suggests that there is room for improvement in aerodynamics for the Reference-H.



Reference-H

Mach 2.4
 $\alpha = 4.5$ degrees

(photograph not shown in color)

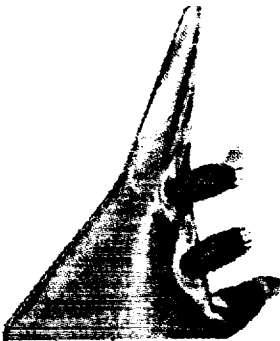
FLOW UNDER THE WING

The figure below shows the flow under the wing. The spill out in the outboard nacelle may be due to the sweep leading edge.

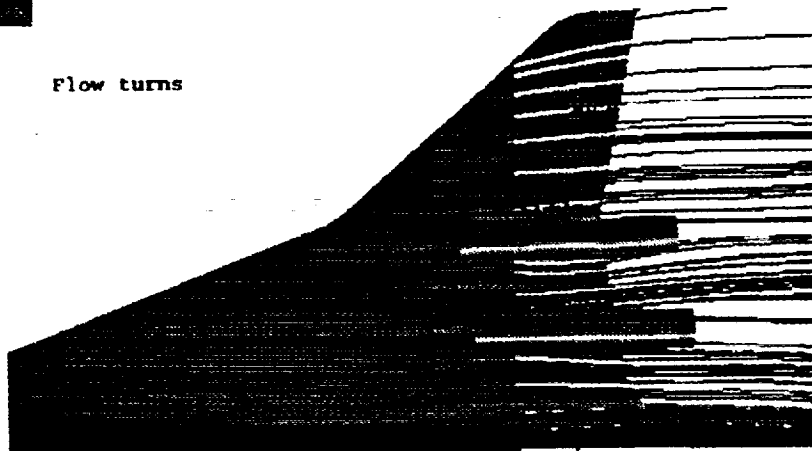


Reference-H Flow under the wing

Mach 2.4
 $\alpha = 4.5$ degrees



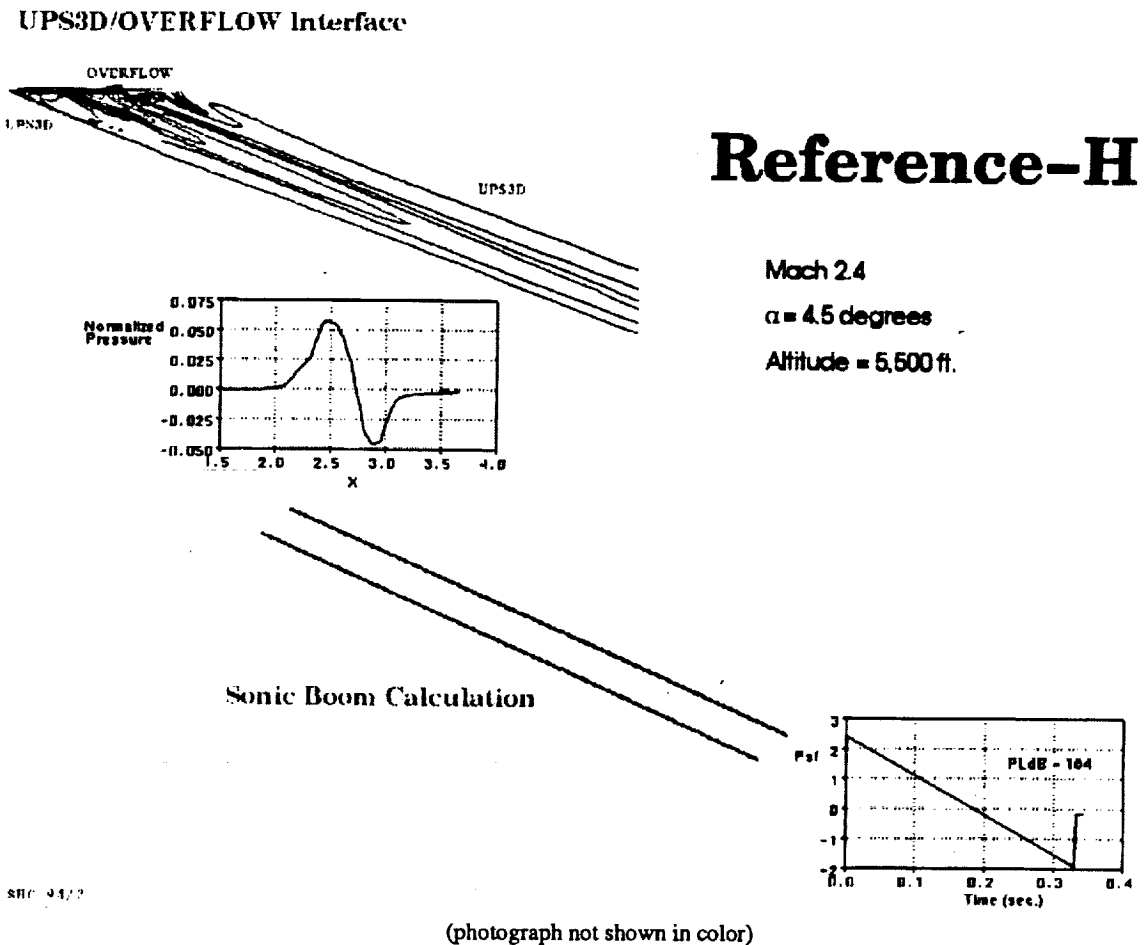
Flow turns



(photograph not shown in color)

SONIC BOOM EXTRAPOLATION

The figure below gives an idea how the sonic boom created by Reference-H is calculated. The overpressure at one body-lengthy ($H/L=1$) under the flight track is first obtained from the near-field solution. The near-field signal is then extrapolated to the ground by Whitham's F-function theory [5]. It is noticed that at $H/L=1$, the signal is almost an N-wave. This fact gives almost no room to design a shaped signature for Reference-H.

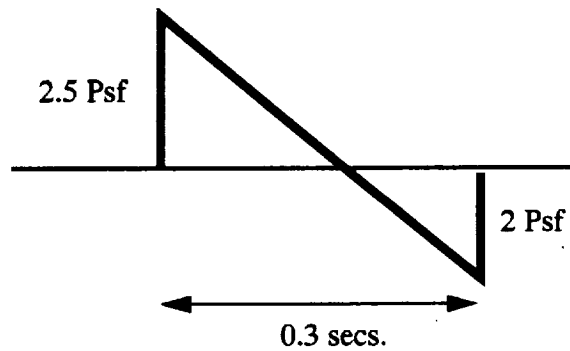


SONIC BOOM OF REFERENCE-H

The sonic boom at the present flow condition (Mach 2.4 and angle-of-attack 4.5°) of Reference-H is an N-wave. The initial shock is as strong as 2.5 Psf. This is no weaker than the current supersonic civil transport, the Concord. The perceived loudness of the boom is 104 PLdB.

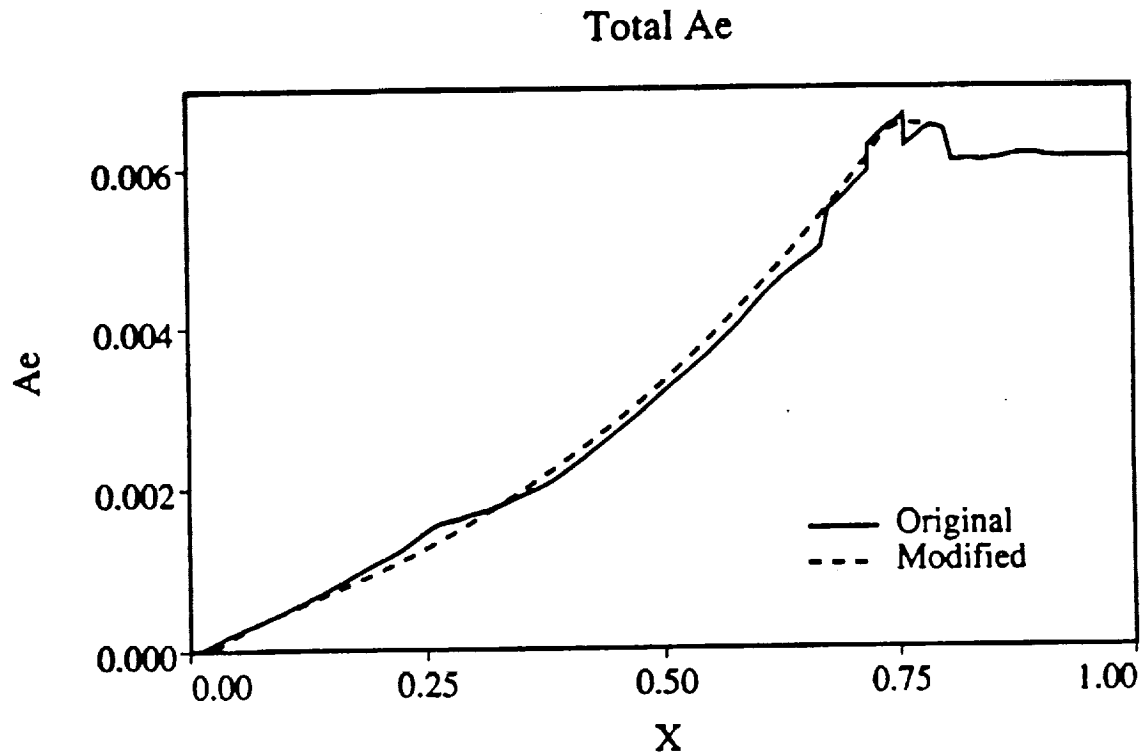
SONIC BOOM

- N-Wave
- 2.5 Psf
- 104 PLdB



TOTAL EQUIVALENT AREA

The figure below shows a typical total equivalent area (A_e) of a low-boom configuration. Note that the total equivalent area is the sum of the equivalent area due to volume and lift [6]. The solid line is the equivalent area of a previously designed low-boom configuration, and the dashed line is that generated from an optimization package [1]. Since the curve is very generous, modification is possible without adding or deleting too much volume, which will affect the performance and structure of the aircraft.

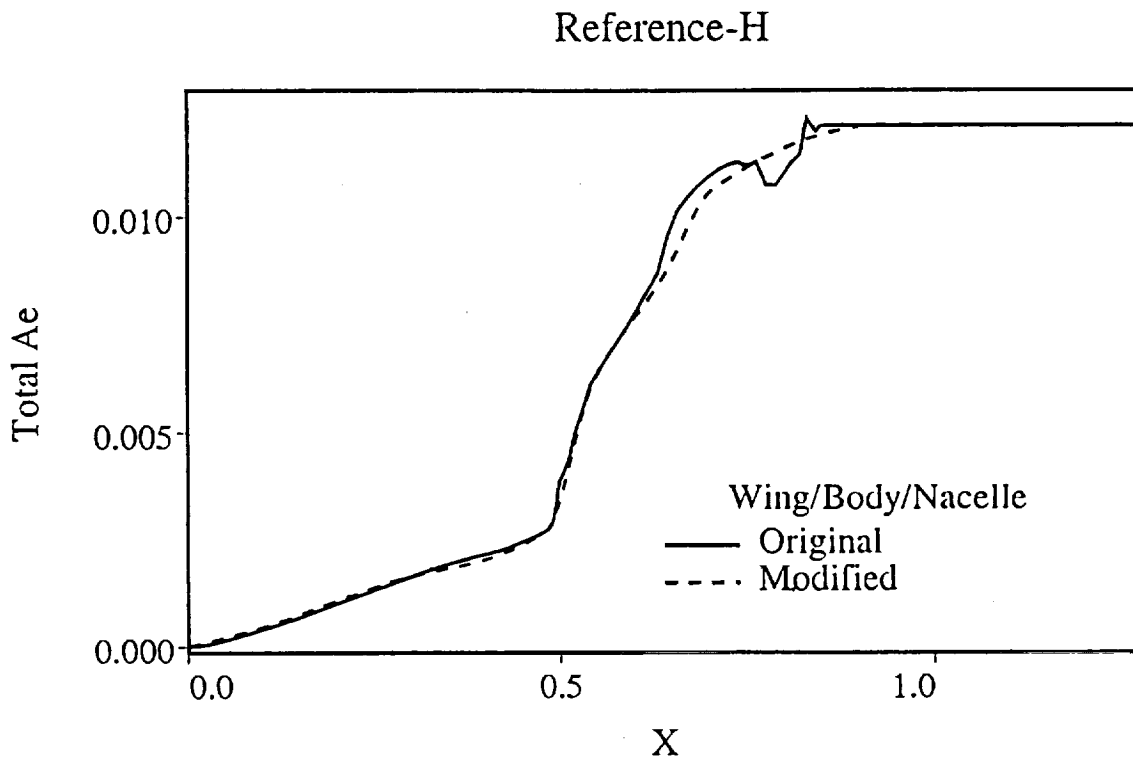


TOTAL EQUIVALENT AREA OF REFERENCE-H

The solid line in the figure below shows the A_e of Reference-H. It is noted that there is a big turn at about $x=0.5$. The curve is not as moderate as the one from the previous page. This is due to the sudden change of lift from the wing. According to Whitham's theory, the F-function is related to the integral of the second derivative of A_e . The sharp turn at $x=0.5$ creates a big wing shock, which quickly coalesces to the bow shock and forms an N-wave as near as one body-length under the airplane.

At this point, previous optimization technique for low-boom configuration is not applicable. In this study, I am trying to make use of Whitham's theory which states that second derivative of A_e is important. The dashed line in the figure is a modified A_e of Reference-H, so that the second derivative of A_e is "smooth."

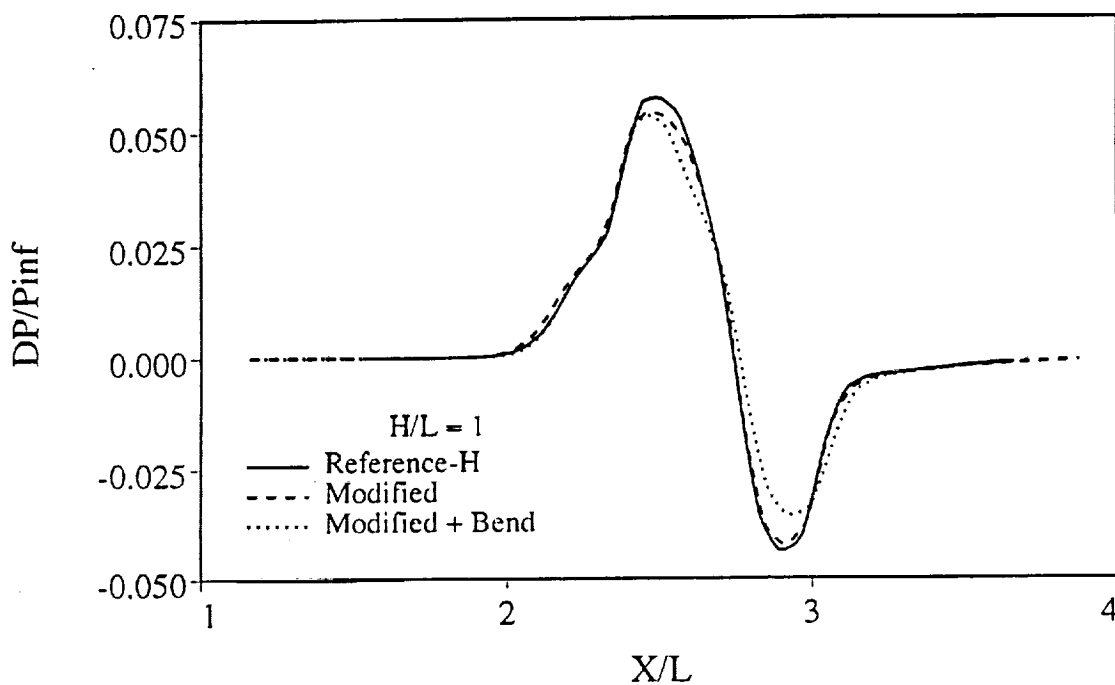
The modification has taken place by changing the fuselage and keeping the wing untouched. Note that such a small change in fuselage does not have a big effect on aerodynamic and structure, likewise.



PRESSURE SIGNAL OF REFERENCE-H

The figure below shows the overpressure of Reference-H at one body-length ($H/L=1$) under the airplane. The solid line is from the original Reference-H, which is almost an N-wave. The dashed line is the modified Reference-H as discussed on the previous page. It is noticed that small change in A_e does reduce the shock strength from the wing. The dotted line is the modified configuration with a dihedral wing (the tip is bended up 4 feet from the original place). The bended wing helps to reduce the tail shock of the signature.

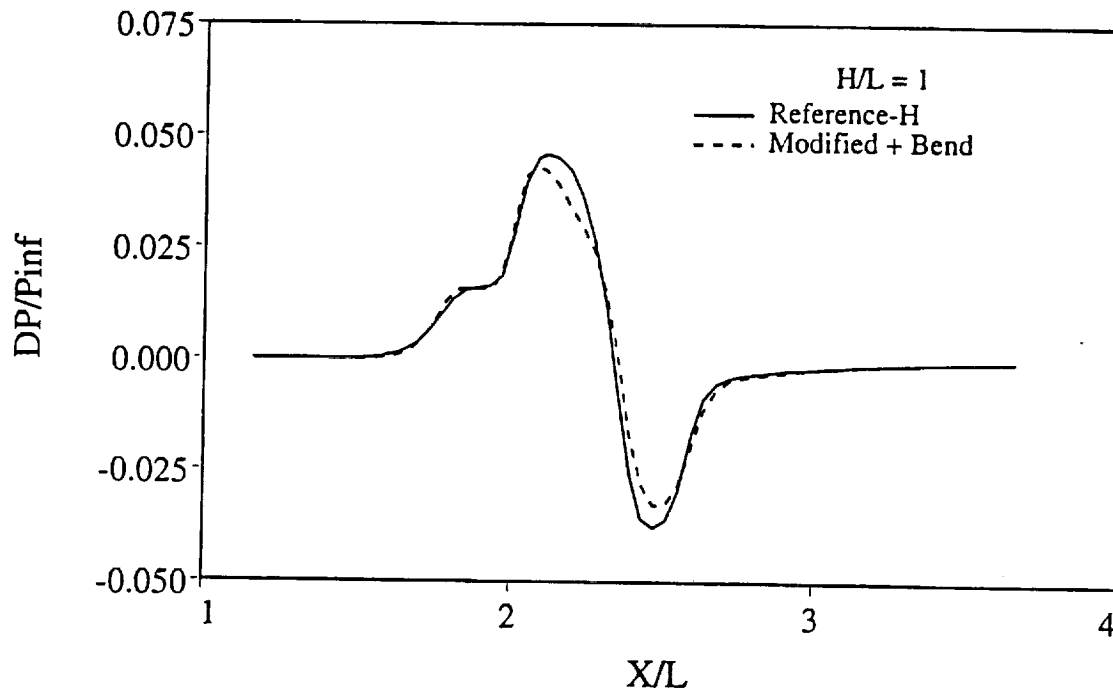
After extrapolation to the ground, the modified sonic boom is still an N-wave, but the loudness is reduced by 2 PLdB, i.e., 102 PLdB, with shock strength of 2.3 Psf.



PRESSURE SIGNAL AT M=2.0

Nevertheless, the basic structure of the modified signal is still an N-wave. In order to look for room for improvement, changing the flow condition is proposed. Now, the angle-of-attack is 4.5 degrees as before, but the free-stream Mach number is reduced to 2.0.

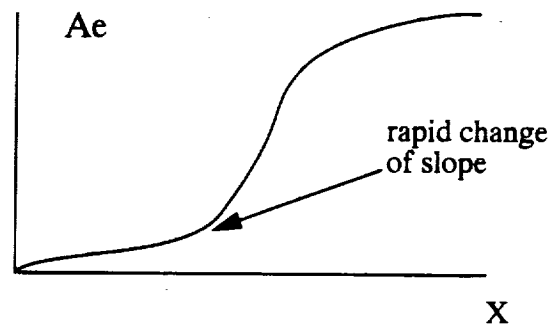
The figure below shows the signal at $H/L=1$. At this point, the bow and wing shocks can be distinguished. However, the wing shock is still too strong, it coalesces the bow shock, and the signature becomes an N-wave at the ground.



DIFFICULTIES

The main difficulty I encountered was that the signal was already an N-wave at $H/L=1$, this left me almost no room for modification. The reason to have an N-wave at such a close distance is due to the strong wing shock, which is due to the high Mach number, high lift coefficient, and the sweep angle of Reference-H.

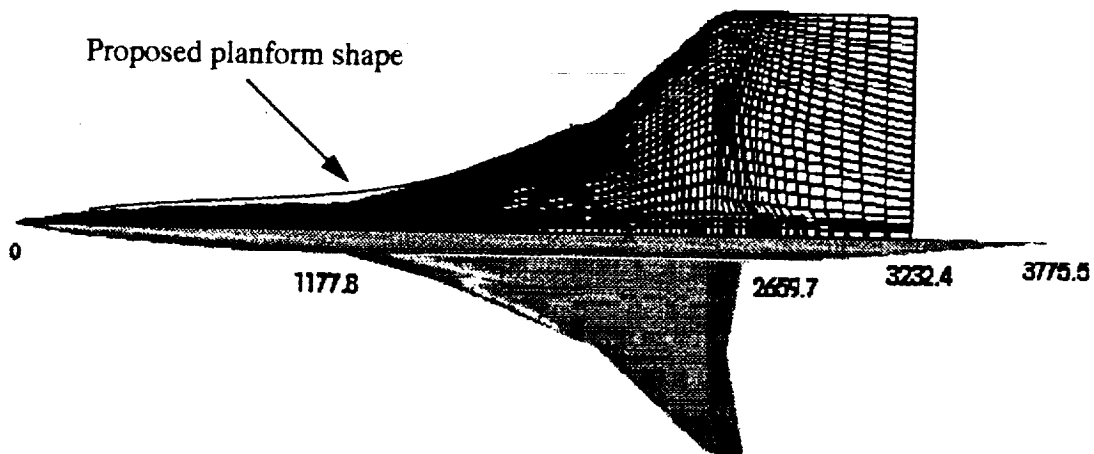
- High Lift Coefficient
- High Mach Number



POSSIBLE SOLUTION

In order to reduce the rate of change of the slope in the Ae-curve, the following wing modifications are needed:

- increase leading edge sweep angle
- increase wing planform area
- add a platypus (such as SR-71, Langley Mach 2 model in 1991) as shown in figure



(photograph not shown in color)

REFERENCES

- 1 Cheung, S., Edwards, T., "Supersonic Design Optimization Method for Aerodynamic Performance and Low Sonic Boom," High Speed Research: Sonic Boom Workshop, Vol. 2, NASA CP-3173, 1992.
- 2 Cheung, S. "Design Process of Ames Wind-Tunnel Model 3," High Speed Research: Sonic Boom Workshop, Vol. 2, NASA CP-10133, 1993.
- 3 Lawrence, S., Chaussee, D., and Tannehill, J., "Application of an Upwind Algorithm to the 3-D Parabolized Navier-Stokes Equations," AIAA paper 87-1112, June 1987.
- 4 OVERFLOW Manual. Contact Pieter Buning at NASA Ames Research Center, e-mail: buning@nas.nasa.gov
- 5 Whitham, G., "The Flow Pattern of a Supersonic Projectile," Comm. and Pure and Applied Math., Vol. 5, No.3, 1952.
- 6 Brown, J., Haglund, G., "Sonic Boom Loudness Study and Airplane Configuration Development," AIAA paper 88-4467, Sept., 1988.

THE ANALYSIS AND DESIGN OF LOW BOOM CONFIGURATIONS USING CFD AND NUMERICAL OPTIMIZATION TECHNIQUES⁺

Michael J. Siclari
Northrop Grumman Research & Development Center
Bethpage, NY

INTRODUCTION

The use of computational fluid dynamics (CFD) for the analysis of sonic booms generated by aircraft has been shown to increase the accuracy and reliability of predictions. CFD takes into account important three-dimensional and nonlinear effects that are generally neglected by modified linear theory (MLT) methods. Up to the present time, CFD methods have been primarily used for analysis or prediction. Some investigators have used CFD to impact the design of low boom configurations using trial and error methods. One investigator (Ref. 1) developed a hybrid design method using a combination of Modified Linear Theory (e.g. F-functions) and CFD to provide equivalent area due to lift driven by a numerical optimizer to redesign or modify an existing configuration to achieve a shaped sonic boom signature. A three-dimensional design methodology has not yet been developed that completely uses nonlinear methods or CFD.

Constrained numerical optimization techniques have existed for some time (e.g. see Ref. 2). Many of these methods use gradients to search for the minimum of a specified objective function subject to a variety of design variable bounds, linear and nonlinear constraints. Gradient based design optimization methods require the determination of the objective function gradients with respect to each of the design variables. These optimization methods are efficient and work well if the gradients can be obtained analytically. If analytical gradients are not available, the objective gradients or derivatives with respect to the design variables must be obtained numerically. To obtain numerical gradients, say, for 10 design variables, might require anywhere from 10 to 20 objective function evaluations. Typically, 5-10 global iterations of the optimizer are required to minimize the objective function. In terms of using CFD as a design optimization tool, the numerical evaluation of gradients can require anywhere from 100 to 200 CFD computations per design for only 10 design variables. If one CFD computation requires an hour of computational time on a Cray computer, one can see that the use of constrained numerical optimization quickly becomes impractical.

Hence, in order to practically couple a numerical design optimization technique with a CFD method, the CFD method must be extremely efficient with running times on the order of only minutes. The CFD Euler code developed under NASA sponsorship and referred to as MIM3D-SB (Ref. 3) for the most part fulfills these efficiency requirements. Analysis of wing-body configurations can be computed in a matter of a few minutes. The present study will

⁺ This work was sponsored by NASA Langley Research Center, Dr. C. Darden

concentrate on the feasibility of the use of this CFD code in conjunction with a numerical design optimization technique for the sonic boom reduction of candidate HSCT configurations. A preliminary supersonic aircraft design system has been established that utilizes the numerical design optimization code NPSOL (Ref. 2) developed at Stanford University coupled with the supersonic MIM3D-SB CFD code.

Many questions still need to be answered in regard to using CFD and numerical optimizers as design tools. There are difficulties related to both the CFD codes and the numerical optimizers. Numerical optimizers can converge to a local minima rather than a global minima. This behavior is largely a function of the initial guess in the design space. The optimizer also is searching for a minimum of the function in terms of its derivative without any regard to the actual function value. Numerically (i.e. CFD) determined gradients can also generate spurious numerical local minima. In addition, for the sonic boom problem, grid fineness will also determine the accuracy of the final design solution. Design optimization methods work well on problems defined by continuous objective functions. The sonic boom signature design problem is not necessarily defined by a continuous objective function. The signature can have a variety of shapes; i.e. from N-wave to multiple shocks. The far-field or ground signature may not transition continuously from one shape to another and hence, may exhibit discontinuous behavior. This is also a source of difficulty in using design optimization methods.

In the following sections, several low boom and one reference aircraft configuration will be analyzed to predict their sonic boom signature characteristics. Modifications to some of these designs will also be presented to demonstrate the feasibility of using CFD as a design tool and to demonstrate the feasibility of designing shaped sonic boom signatures. Design modifications to some configurations will be presented to demonstrate the feasibility of achieving shaped signatures with reduced levels and not necessarily to represent realistic or aerodynamically efficient design modifications. Fuselage volume or camber are used as design variables in order to have a minimal effect on the primary wing aerodynamics. The paper will also seek to demonstrate whether a hybrid or ramped signature is feasible to achieve. For the low-boom configurations, the CFD predicted signatures will be compared qualitatively to their MLT design signatures.

DESIGN SYSTEM

The CFD code MIM3DSB uses a simple wave drag geometry input data format to describe the input geometry. MIM3DSB internally enhances this geometry to generate smooth continuous surfaces. A grid is then generated at each marching station or crossflow plane. The computation is carried out to a specified distance beyond the aircraft. Near-field pressure signatures are then interpolated from data below the aircraft. These pressure signatures then become input to a waveform parameter code (Ref. 4) which extrapolates these near-field signatures to the ground through a specified atmosphere given an altitude and Mach number to generate the aircraft's far-field sonic boom signature.

This entire process has been automated within the MIM3DSB code. To couple this method with a design code required several additional modifications. Firstly, the output generated for a single CFD run must be reduced to a minimum since scores of CFD runs will be necessary for the design problem. Secondly, a mechanism is needed to automatically regenerate geometry based on a finite number of design variables. It was decided to remain with the wave drag format primarily for convenience since the geometry of a variety of configurations was already available in this format. This geometry format defines the wing as a series of airfoils with thickness and camber and the fuselage as a series of cross sections. The primary drawback to this definition is the use of a finite number of airfoils and fuselage cross sections to define the vehicle. As a result, a sufficient number of sections must be used to accurately define the geometry.

Cubic splines with matched first and second derivatives are used for simplicity to describe the geometric design variables. The design variables could be fuselage volume or radii, fuselage camber, wing thickness, dihedral, etc. The practical implementation of the method requires the use of a small number of design variables. A small number of design variables might be as little as three variables or as many as fifteen. The gradient based optimization method will require one or two evaluations of the objective function for each design variable depending upon whether one-sided or central derivatives are used to evaluate the objective function gradients. Hence, for example, if 10 design variables are used, the design methodology will require 10 to 20 CFD runs to evaluate the objective function gradients. If 10 global iterations of the design method are implemented, this amounts to 100 to 200 CFD runs. Even though the CFD code, MIM3DSB, can take as little as 5 minutes of CPU time per run on a Cray computer, 100 to 200 runs can still take a significant amount of computational effort. Hence, cubic splines are used to minimize the number of design variables.

Figure 1 shows the implementation of the overall CFD sonic boom design optimization system. The overall system is controlled by the optimization code NPSOL which calls three subroutines, the geometry wave drag data set generator, the CFD analysis code MIM3DSB, and finally, a subroutine which utilizes the CFD results to evaluate the sonic boom signature objective function and any nonlinear aerodynamic constraints. In the present preliminary study, to determine the feasibility or utility of the design system, aerodynamic constraints were not implemented. Hence, given an initial guess for the geometric design variables, the geometry generator will read an existing wave drag data set and replace the desired portion of the geometry with geometric data generated by the cubic spline fits with the same resolution as the initial wave drag input data. The geometric data is then rewritten to the same wave drag data file. The CFD code then reads this wave drag data set and carries out the computation to a specified distance below and downstream of the aircraft. New enhanced surface geometry required by the CFD code and a new grid are then generated automatically within the CFD code conforming to the new surface geometry of the new data set. A subroutine to the CFD code calls the Thomas ANET wave propagation method to extrapolate the near-field data through the atmosphere down to the ground. Aerodynamic coefficients and ground sonic boom signatures are then returned to the design program. At this point, the design program contains a subroutine which uses this information to evaluate the user specified objective function and constraints. The design program will use this information to generate gradients and to further predict new values of the design

variables. The entire system has been automated and hundreds of CFD runs can be performed without any user intervention. User interactivity comes in the form of specifying appropriate geometric design variables, objective functions, and constraints on the geometric design variables. Care must be taken in specifying the proper constraints on the design variables, otherwise, totally unrealistic geometries can result. In addition, the constraints that govern the design variables will also ultimately govern the goodness of the geometry and prevent the CFD code from "blowing up". For example, if fuselage camber is to be optimized, the constraints must be such that the wing root remains within the fuselage. In other words, the fuselage camber can not be allowed to grow unbounded and upper and lower limits must be prescribed accordingly.

CFD Sonic Boom Design System

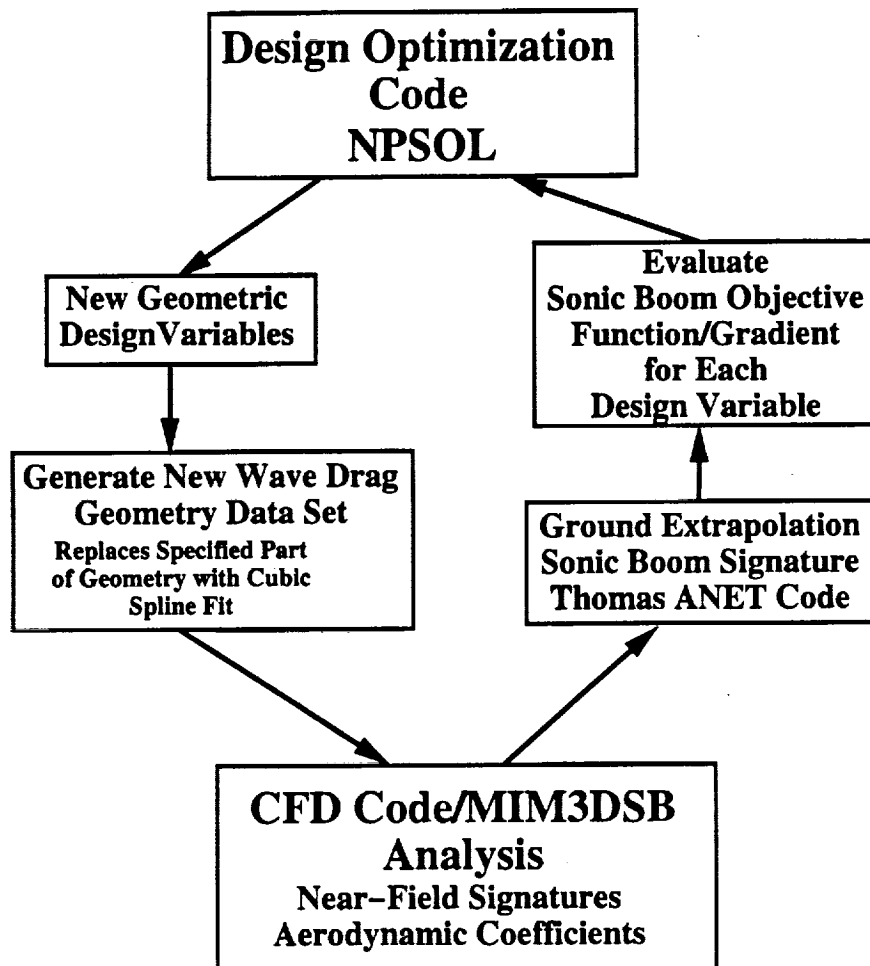
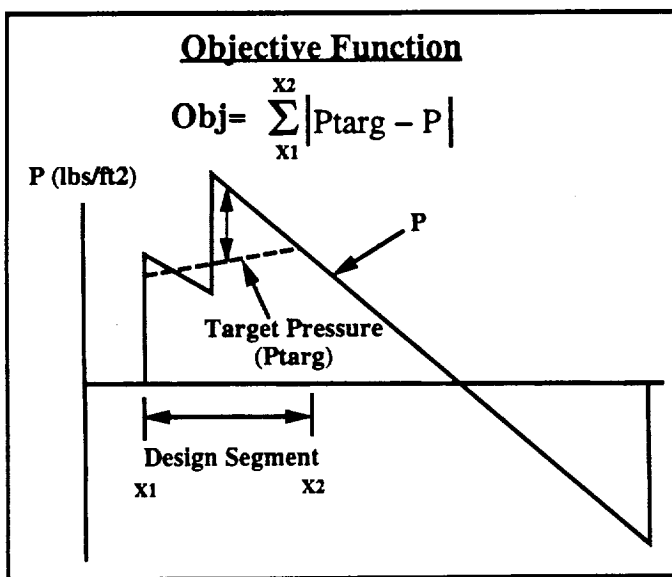


Figure 1 CFD Sonic Boom Design System.

Figure 2 illustrates the definition of the objective function used in this study for seeking shaped or hybrid sonic boom signatures. Given a baseline geometry, the baseline sonic boom ground signature is established. The objective is to modify this signature either by "softening" or by a general reduction in level over a specified portion of the signature. A target level and shape are then prescribed. The objective function is evaluated numerically as the sum of the absolute value of the difference between the target signature and current signature over a specified portion of the signature. The objective function is evaluated on a fixed Cartesian grid from the output of the Thomas extrapolation code. In addition, in order to evaluate the objective function with multiple shocks, a finite rise time is added to the ground signature for numerical definition. The purpose of the design method is to find the minimum of the objective function and the corresponding design variables. If the objective function vanishes or goes to zero, then the target signature and current signature will coincide.

As will be discussed throughout this paper, many problems and difficulties arise in this design procedure. Two of the biggest problems are that the objective function is not necessarily continuous and that many local minima may exist. The design methodology is seeking a minimum to the objective function in terms of its derivative and not the minimum value of the function. Hence, if the initial guess is near a local minimum, the design process will determine this to be the optimal solution. This leads to a trial and error game, where several initial guesses must be specified to try to converge to a global minimum of the objective function. There is also no guarantee that the objective function will vary continuously or smoothly as the character of the signature changes from an N-wave to a multiple shock or smooth distribution. This property of the objective function also wrecks havoc on the design methodology. Lastly, there is no way of knowing whether an optimal solution even exists for a given target signature and specified set of geometric design variables.



- Design specified portion of ground pressure signature
- Minimize absolute difference between target and current signature
- Both target and current signature interpolated to same Cartesian grid
- Finite rise time added to shocks prior to interpolation

Figure 2 Objective function definition for shaped signature design.

BASELINE CONFIGURATIONS

Figure 3 shows four HSCT configurations. Three of these configurations correspond to low-boom modified linear theory (MLT) designs and the fourth corresponds to a reference aerodynamic configuration. The two Boeing low-boom configurations are designed for Mach 1.7 overland flight at an altitude of 44000 feet (see Ref. 5). The Boeing-936 configuration was designed to have a flat-top signature with an overpressure of about 1.0 lbs/ft². The Boeing-935 configuration was designed for the same overland Mach number and altitude for a hybrid or ramped signature from about 1 to 2 lbs/ft². The Boeing-936 wing configuration is more highly swept in comparison to the Boeing-935. The third Boeing configuration is a baseline aircraft referred to as Reference H and exhibits an N-wave signature at Mach 2.4. In addition, the NASA Langley low-boom design referred to as LB18-10B (see Ref. 6) was also designed by MLT to have a hybrid signature at Mach 1.8. The following sections will present the CFD analysis of these configurations and their sonic boom characteristics and attempts at design modifications to "soften", shape, or generally reduce the level of the sonic boom signatures. In all cases, only clean wing-body configurations are analyzed in the absence of engine nacelles and other devices. As will be demonstrated in the subsequent studies, CFD analysis does not indicate the attainment of the MLT target signature.

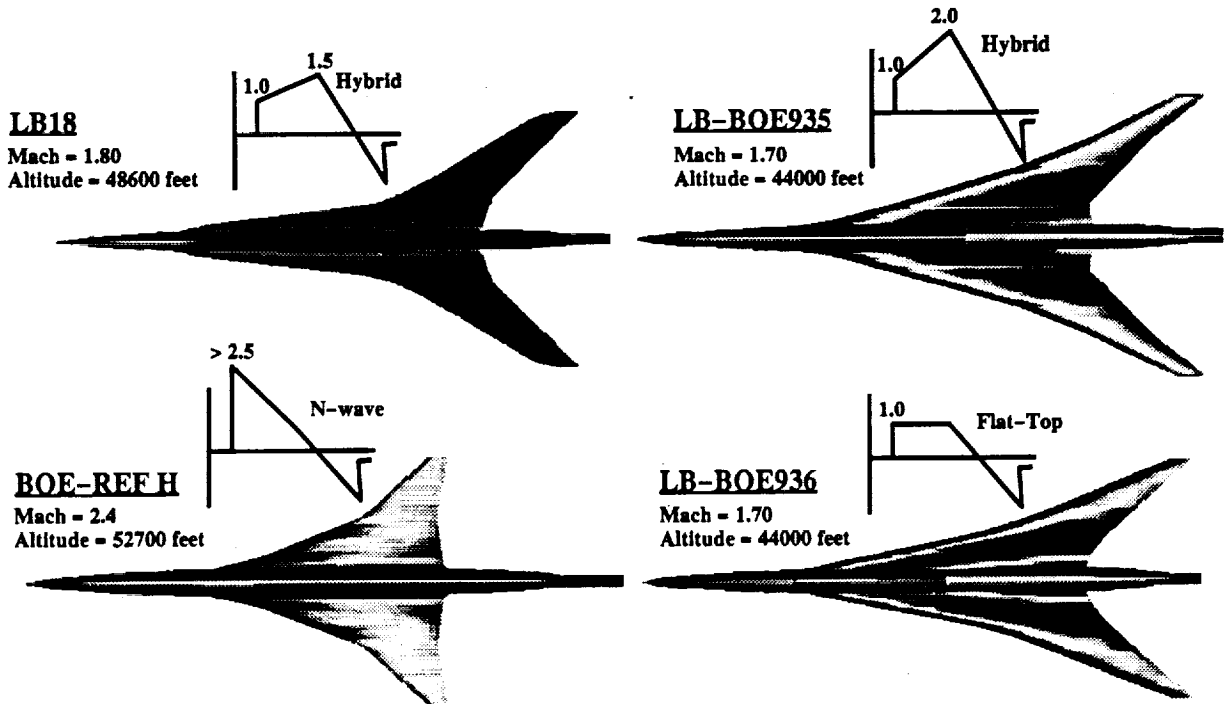
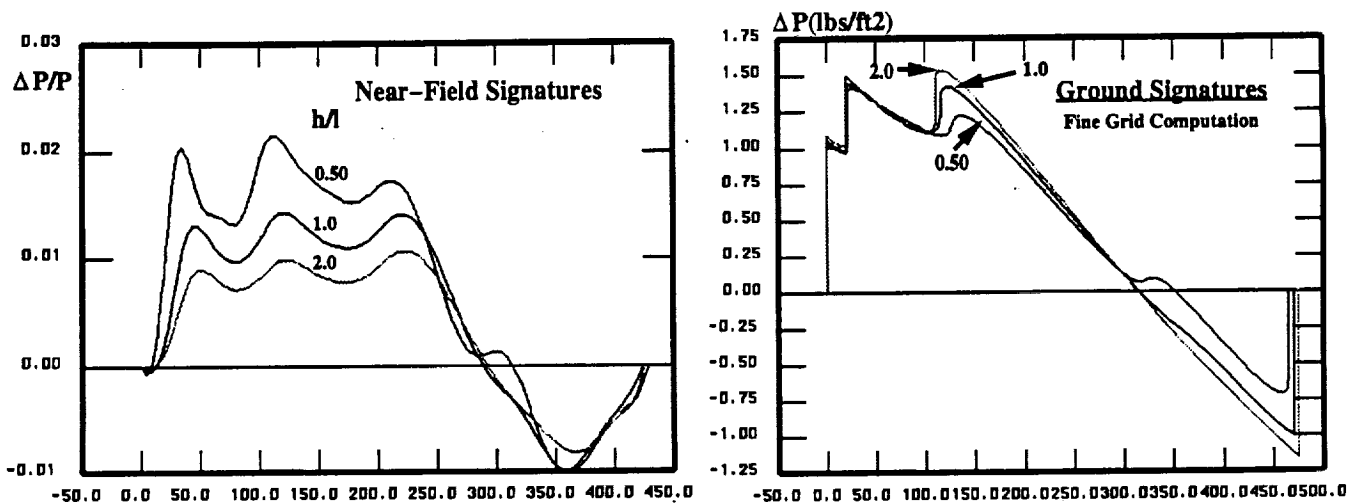


Figure 3 Several low-boom HSCT configurations and their MLT target signatures in comparison to a reference aircraft.

NASA LANGLEY LB18-10B

Baseline Analysis

Figure 4 shows the results of the CFD analysis for the NASA Langley LB18-10B low-boom configuration. The left side of the figure shows the near-field signatures computed by the CFD code at $h/l = 0.50, 1.0,$ and 2.0 . The right side of the figure shows the results of extrapolating the computed near-field signatures to the ground from an altitude of 48,600 feet using the Thomas ANET extrapolation code. An interesting feature of this configuration is the secondary shock that increases in strength with increasing extrapolation distance from the aircraft. This third shock in the signature increases from about 1.2 to 1.5 lbs/ft². This is most likely due to three-dimensional effects. This can be seen also in the near-field signatures where the second shock strength is diminishing faster with extrapolation distance in comparison with the third shock. This configuration was originally designed to have a hybrid or ramped signature from about 1.0 to 1.5 lbs/ft². As is indicated by figure 4, the CFD analysis does not indicate a hybrid or ramped shape to the far-field signature although the MLT target pressure levels (i.e. 1 to 1.5 lbs/ft²) have been achieved.



LB18-10B Configuration
Mach = 1.8 Alpha = 2.06 Altitude = 48,600 feet

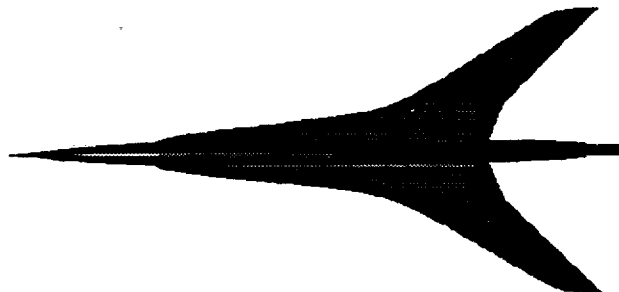


Figure 4 CFD analysis of near-field and extrapolated ground signatures for the LB18-10B.

Design Modifications

Modifications to the 10B configuration were undertaken to determine if a hybrid signature could be recovered with some minor revisions to the shape of the aircraft. Fuselage volume was chosen as the candidate for design modification. Several steps had to be taken to modify the existing signature. The fuselage radii were fitted with cubic splines while the existing fuselage camber line was maintained. For the design process, a cruder baseline grid is desired for computational efficiency which still maintains the characteristics and shape of the baseline signature. It is also desirable to extrapolate the signature from the closest possible distance to the aircraft while also maintaining the characteristics and shape of the baseline signature. The cruder grid and closer distances are required simply to reduce the amount of computational effort throughout the design process which might require as many or more than 100 CFD runs. The cruder grid could be used in this case but the closer extrapolation distance could not because of the buildup of the strength of the third shock. In order to modify or soften this shock it must exist in the ground signature that is used to evaluate the objective function.

Since a certain amount of trial and error as well as intuition must be used in the design process, the design cycles used to modify this configuration will be presented in their entirety. An attempt was made to recover a hybrid or ramped signature. Figure 5 documents the design cycles used for this configuration. Initially, an attempt was made to modify and reduce the strength of the second shock of the signature by modifying the volume of the forward part of the fuselage. 12 design variables in terms of fuselage radii were used at 20 foot intervals on the fuselage. To let the design process have as much flexibility as possible a three-dimensional elliptical fuselage shape was also allowed. 6 radii were used for the maximum side width and 6 radii described the upper and lower centerline with the original fuselage camber maintained during the design process. Stations in between were fitted with cubic splines. It was determined in earlier trials that allowing three-dimensionality to the fuselage yielded much more flexibility and prevented fuselages from becoming too slender. The three-dimensionality to the fuselage also allows for more flexibility in canceling out waves since the centerline can be expanding while the side could be compressing. RUN1 of figure 5 shows the initial ground signature obtained with the cruder design grid extrapolated from $h/l = 1.0$ and also the initial target ground pressure signature distribution specified for the forward part of the signature to be used in evaluating the objective function. The initial prescribed target pressure distribution was consistent with the 1.0 to 1.5 lbs./ft² MLT design goal. The unmarked curve shows the final result of the design process. In most cases, the objective function could not be made to vanish yet a significant reduction in the objective function could be achieved. Hence, the target pressure distribution was not completely achieved. In the second design run, or RUN2, the target pressure distribution was modified to include more of the signature. A further reduction in the objective function was achieved using the same design variables. For the third run or RUN3 it was desired to modify the strength of the third remaining shock. Since this shock was definitely coming from the aft end of the configuration, the latter half of the fuselage radii were used as design variables as indicated on the figure as well as a new target pressure distribution. The third shock was completely eliminated in RUN3 although the target pressure distribution was not totally achieved as indicated by the bump in the signature at about 75 feet. The intention of the last design run or RUN4 was to remove this bump in the signature by redesigning the mid portion of the fuselage. As indicated by the figure, the bump was significantly reduced with only some discrepancy in the target versus attained

signature in the forward part of the signature. These four design runs were comprised of at least 100 CFD runs for the overall design process. One must ask why not design the entire fuselage all at once. At least 25 to 30 design variables would probably be necessary to do this instead of 12. That means that upwards of 50 CFD runs would have to be made for just one design iteration for each design run.

Hence, the design process is shown to be capable of recovering a signature similar to a hybrid or ramped shape although the increase in pressure of the new hybrid signature is less than that of the original MLT design. Now, the ultimate test is to analyze the modified design using a

LB18-10B DESIGN CYCLES

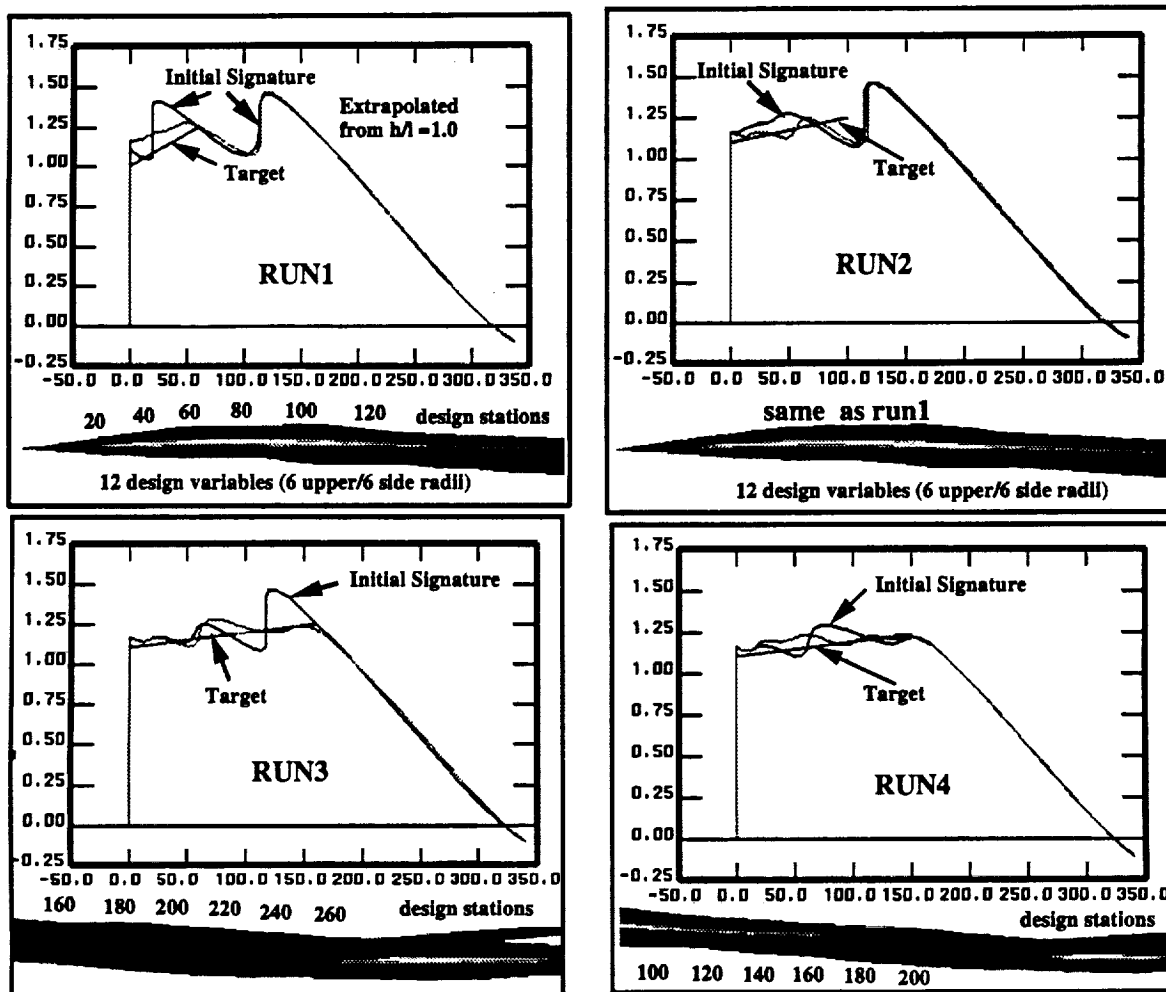


Figure 5 Fuselage volume modifications and target signatures for the LB18-10B Configuration

fine grid for the CFD computation. Figure 6 shows the result of such a fine grid analysis computation for the ground signature extrapolated from $h/l = 1.0$ in comparison to the signature obtained on the cruder design grid. The fine grid analysis indicates a slightly lower initial shock overpressure but two steep compressions have arisen due to the fine grid analysis in comparison to the smooth crude grid design signature. The steep compressions or steps in the signature were not represented as shocks in the Thomas ANET extrapolation code. To further determine how well the design signature will hold up, the fine grid analysis was also extrapolated from $h/l = 2.0$ as shown in figure 7 and compared to the fine grid signature of the original configuration. The steep pressure gradients in the design signature obtained at an extrapolation distance of $h/l = 1.0$ have diminished at the extrapolation distance of 2.0. A further increase in pressure signature level appears at this extrapolation distance at about 150 feet due to the initial effect of the increase in strength of the third shock previously observed for the original design. Whether this design signature could be made into a linear ramp is still unknown because fine grids would have to be used in the design process which would require significantly more computational effort. This study may be conducted in the near future. If a linear ramp can not be achieved, the question will always be whether the bumps in the signature really represent weak shocks not being resolved by the CFD analysis or truly shockless compressions.

LB18 Modified Design
Mach = 1.80, Alpha = 2.06, Altitude = 48,600 feet

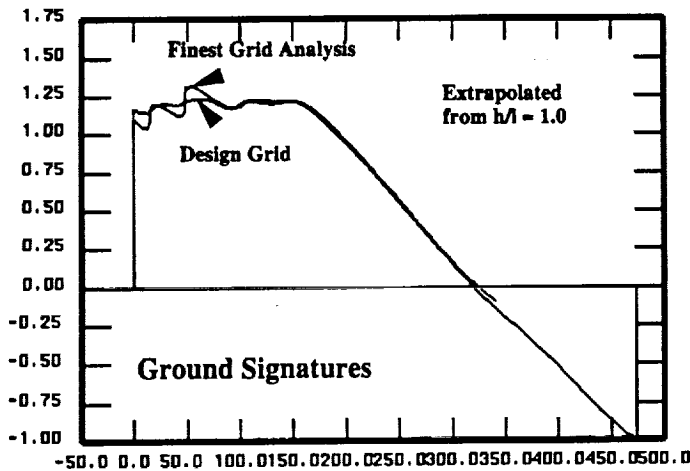


Figure 6 Comparison of ground signatures for crude design and fine grid analysis of modified LB18-10B extrapolated from $h/l = 1.0$.

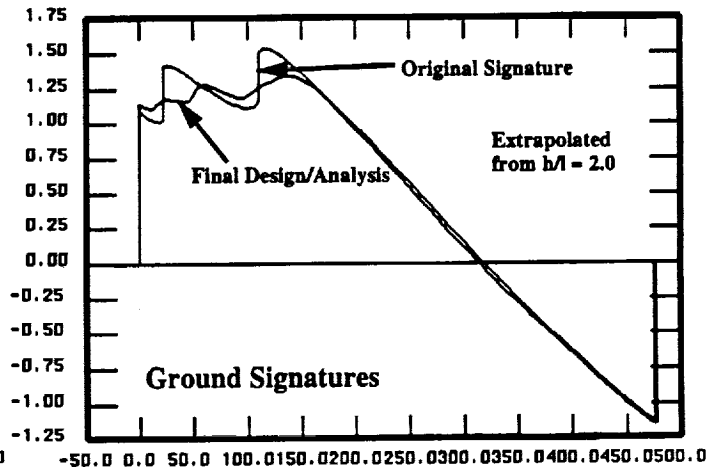


Figure 7 Comparison of ground signatures for modified and original LB18-10B configuration extrapolated from $h/l = 2.0$.

Figure 8a shows the fuselage area modification to the design. Several bumps in the fuselage area can be observed. Two additional bumps in the fuselage area distribution were created by the design process. The fourth bump already present in the original configuration was diminished. Figure 8b further shows the three-dimensional contouring of the fuselage area modifications by plotting maximum half width radii and centerline plane radii versus the original radii of the circular fuselage. Figure 9 further shows a comparison of the near-field pressure signatures of the original design and the modified design. At $h/l = 0.25$, the modified design shows a series of shocks partially due to the bumps in the fuselage area. At further distances below the aircraft, the modified design exhibits a flatter character in comparison with the original design. Evidently, these additional shocks are necessary to achieve the hybrid or ramped signature.

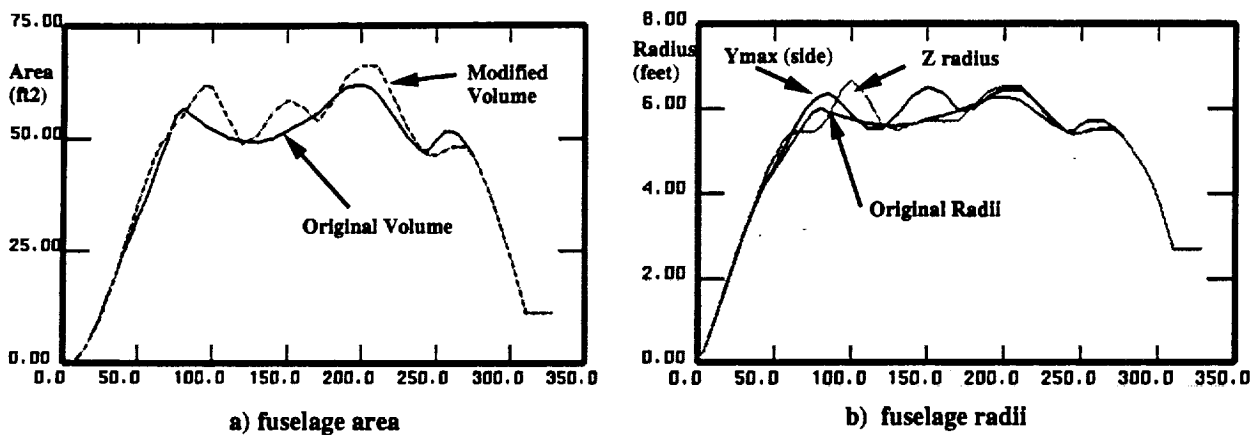


Figure 8 Fuselage volume and radius modifications to the LB18-10B configuration.

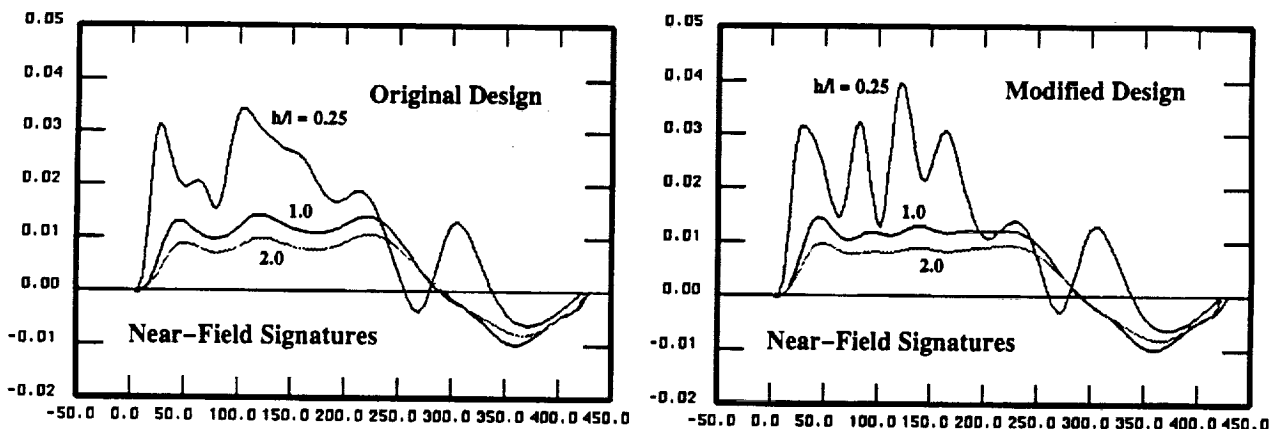


Figure 9 Comparison of near-field signatures for the original and modified LB18-10B configuration.

BOEING-936 CONFIGURATION

Baseline Analysis

Figure 10 shows computed CFD near-field and extrapolated far-field or sonic boom signatures for the Boeing-936 configuration flying at Mach 1.7 and an altitude of 44000 feet. This configuration was designed by MLT to have a flat-top signature with an initial shock overpressure of about 1 lbs/ft². The fine grid CFD analysis indicates a multi-shock signature with shock strengths of about 1.2 and 1.7 lbs/ft². Very little variation in the ground signature was obtained as a function of extrapolation height. Hence, to save computational effort, the signature extrapolated from $h/l = 0.25$ or 75 feet below the aircraft was used in the design process on a cruder grid.

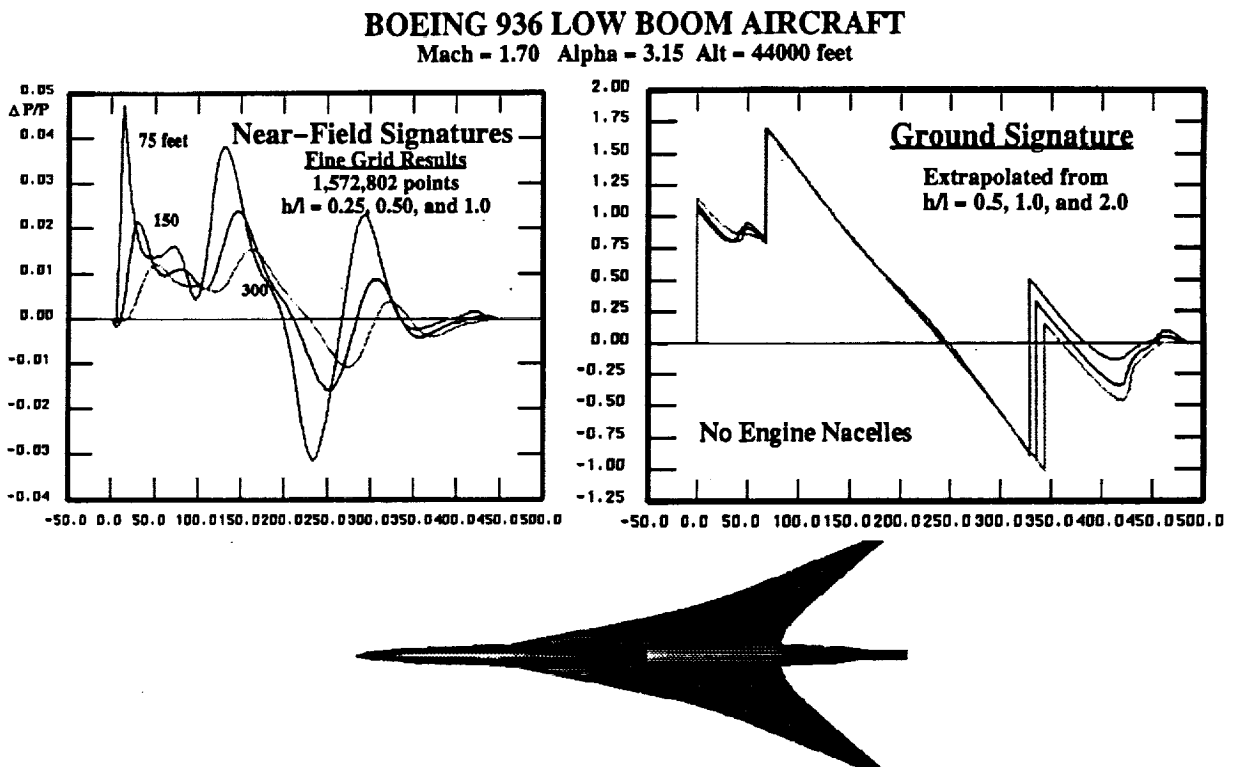


Figure 10 CFD analysis of near-field and extrapolated ground signatures for the low-boom Boeing-936 configuration.

Design Modifications

The first attempt at redesigning and shaping this ground signature consisted of modifications to the fuselage volume while preserving the fuselage camber. A three-dimensional elliptical representation of the fuselage was again chosen for flexibility and 10 design variables were used, 5 for the upper and lower radii and 5 for the side or maximum width radii. Cubic

splines were used again to fit the fuselage between design variable stations and the forward two-thirds of the fuselage was chosen to be modified. The target signature was to recover the flat-top signature of the original MLT design. The left side of figure 11 shows the final results of the design process on the crude design grid in comparison to the original fine grid signature. The second shock was virtually eliminated at the slight expense of the initial shock. A fine grid analysis of the modified design was then carried out for verification and the results are shown on the right side of figure 11 at various extrapolation heights. At extrapolation heights beyond $h/l = 0.25$, a smooth nearly flat-top signature is indicated although the 1 lbs/ft² level could not be achieved. The growth to the fuselage volume to attain this signature was unacceptable. To determine if this solution was unique, 12 design variables were used and the design process was continued. Figure 12 shows the final fine grid results of this design modification. A slightly different shape to the ground signature was obtained but the growth to the fuselage volume was still similar and unacceptable placing an undesirable hump at mid-section. Evidently, to fill in the expansion region prior to the second shock and also to negate the strength of the second shock, a compression followed by an expansion in fuselage area is necessary.

The unacceptable fuselage growth led to a third try at modifying this configuration using fuselage camber while maintaining or preserving the original volume. The left side of figure 13 shows the original signature and the target signature applied during the design iteration process on the crude grid using an extrapolation distance of $h/l = 0.25$. A ramped target pressure distribution

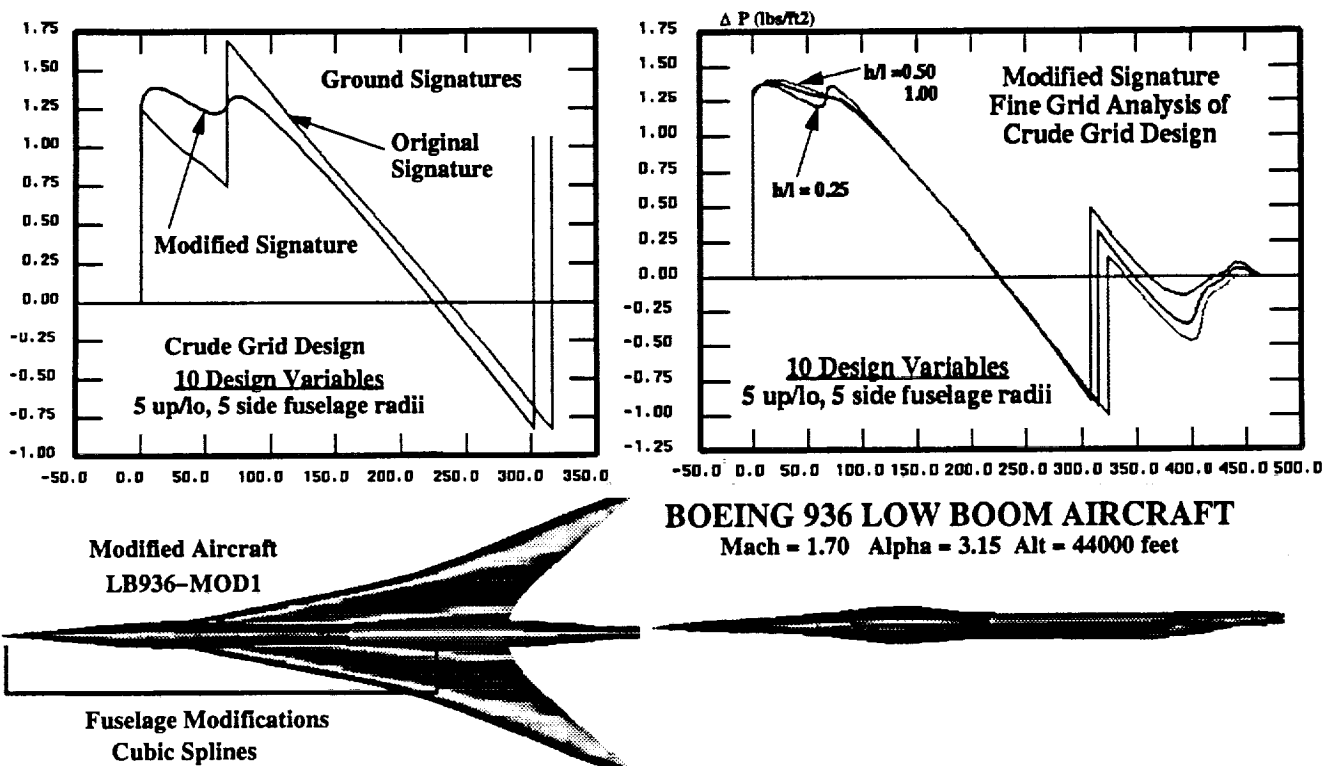


Figure 11 Fuselage volume modification to ground signatures using 10 design variables for the Boeing-936 configuration.

was used for the design in an attempt to lower the strength of the initial shock. The results of the design split the second shock into two smaller shocks but could not diminish the initial shock overpressure. The right side of figure 13 shows the results of a fine grid analysis of this modification at several extrapolation distances. Unfortunately, the second shock coalesces with the initial shock with increasing extrapolation distance somewhat increasing the initial shock overpressure above the 1 lbs/ft² level. Figure 14 shows the extent of the fuselage camber modifications in comparison to the original camber of the configuration. Additional camber was added near the nose and diminished near the mid-section of the fuselage.

BOEING 936 LOW BOOM AIRCRAFT

Mach = 1.70 Alpha = 3.15 Alt = 44000 feet

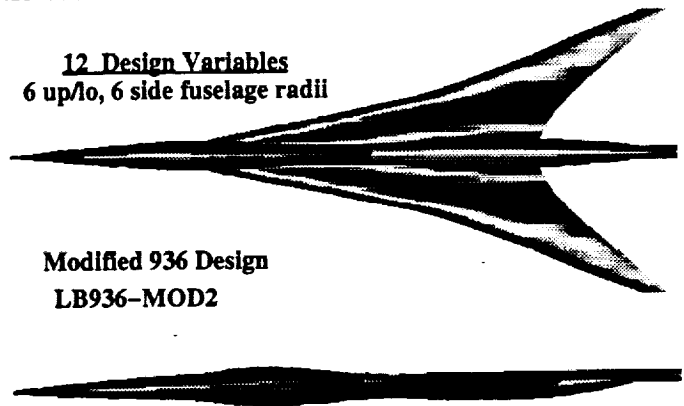
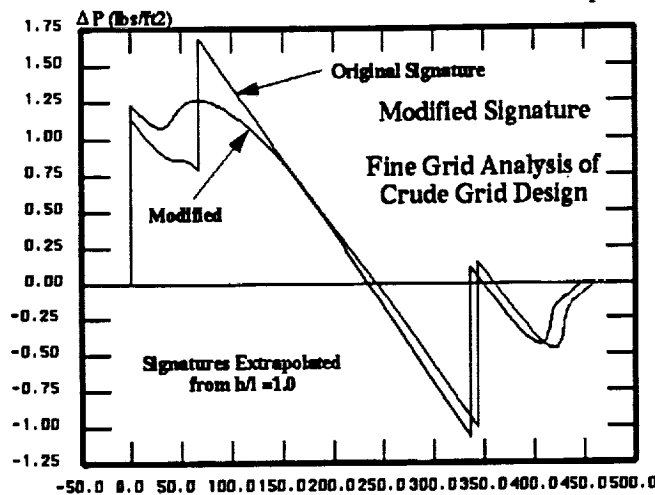
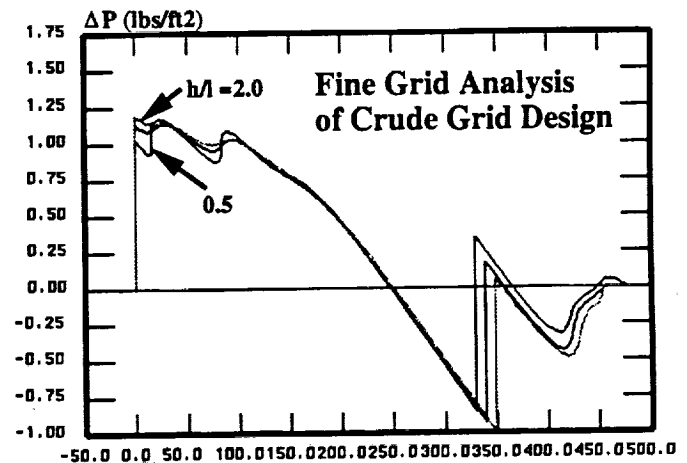
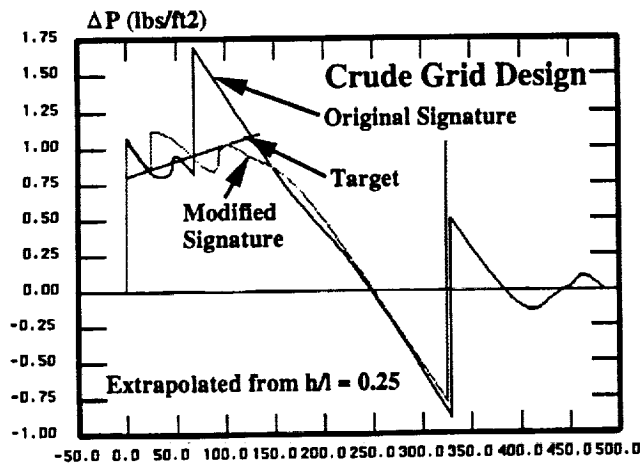


Figure 12 Fuselage volume modifications to ground signature using 12 design variables for the Boeing-936 configuration.

BOEING 936 LOW BOOM AIRCRAFT

Mach = 1.70 Alpha = 3.15 Alt = 44000 feet



Fuselage Camber Mod

Figure 13 Fuselage camber modification to ground signature of the Boeing-936 configuration.

A further attempt was now made to improve and smooth the signature characteristics using the fuselage volume. Figure 15 shows an interesting comparison indicating the sensitivity of the overall process to the geometry. Figure 15 shows a comparison of the ground signature obtained for the fuselage camber modification with the same design but with the fuselage radii now fitted with cubic splines for the stations in between. Significant changes to the signature were computed just by fitting the fuselage radii with cubic splines every 20 to 30 feet. Apparently, there is a sensitivity to the geometry, its derivatives, and to the type of analytical fit used to represent it. This is an important issue and must be addressed sometime in the near future. The left side of figure 16 shows the result of applying some minor fuselage volume modifications to the configuration. The target pressure distribution was flat-top in an attempt to eliminate the second shock and smooth the pressure signature. This was not fully obtained although the strength of the second shock was diminished as well as the expansion region. The right side of figure 16 shows the results of a further fine grid analysis for the additional fuselage volume modification for several different extrapolation heights. As before, the second shock coalesces with the first shock giving rise to an increase in the initial overpressure with increasing extrapolation distance. At extrapolation distances of $h/l = 1.0$ and greater, the ground pressure signature essentially becomes a flat top. Figure 17 shows a comparison of the two design modifications for the pressure signatures in the near field at $h/l = 1.0$ and in the far-field signatures. In the near-field, it is quite evident that the fuselage camber modification virtually eliminates the second shock or wing shock. The additional fuselage volume modification led to a more flat-top signature in comparison to the fuselage camber alone modification.

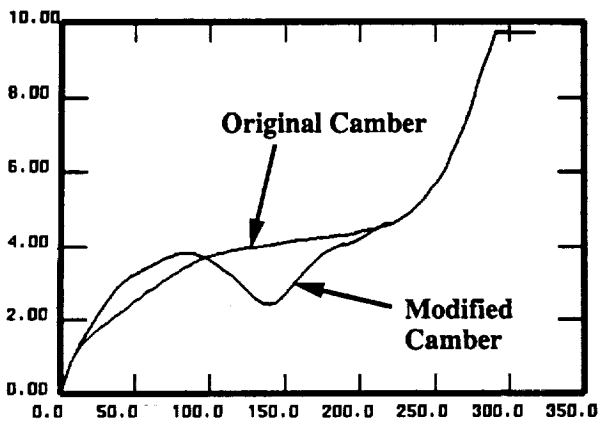


Figure 14 Fuselage camber modifications to the Boeing-936 configuration.

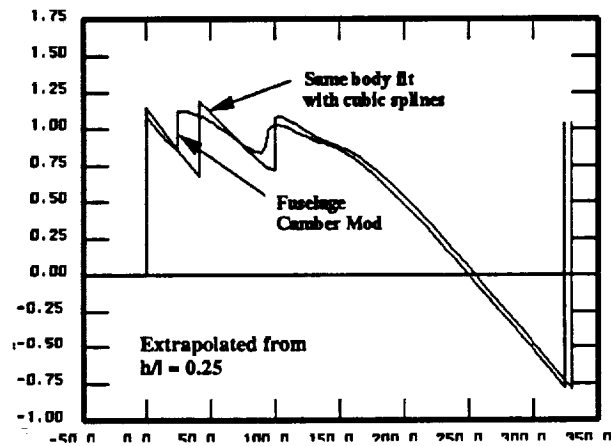


Figure 15 Comparison of original fuselage volume ground signature with signature from the same fuselage fitted using cubic splines.

BOEING 936 LOW BOOM AIRCRAFT

Mach = 1.70 Alpha = 3.15 Alt = 44000 feet

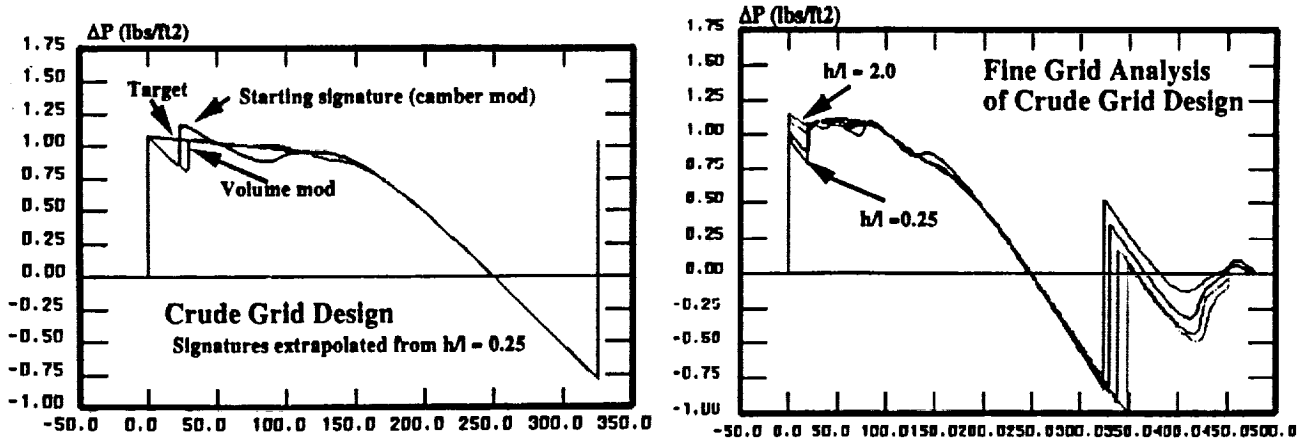


Figure 16 Ground signatures computed for the Boeing-936 configuration with additional fuselage volume modifications.

BOEING 936 LOW BOOM AIRCRAFT

Mach = 1.70 Alpha = 3.15 Alt = 44000 feet

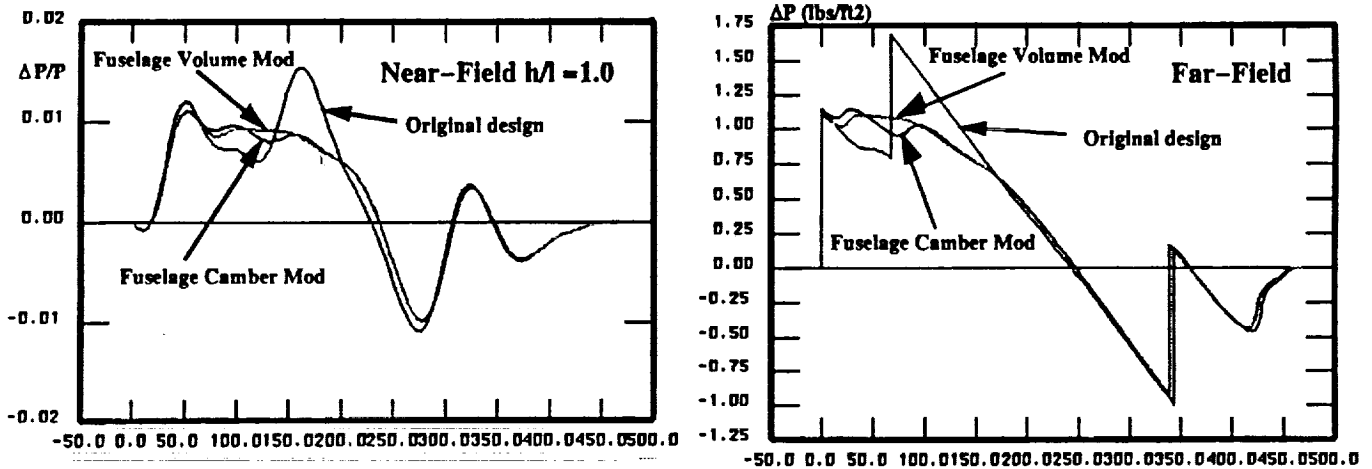


Figure 17 Near-field and extrapolated ground signatures for fuselage camber and volume modifications to the Boeing-936 configuration.

BOEING-935 CONFIGURATION

Baseline Analysis

Figure 18 shows the results of the CFD analysis for the near-field and extrapolated ground signatures for the Boeing-935 low-boom configuration at Mach 1.7 and an altitude of 44000 feet. As mentioned earlier, this configuration was designed by MLT for a target ramp signature from 1.0 to 2.0 lbs/ft². As is typical for most configurations designed by MLT for a ramped or hybrid signature, a multi-shock signature (in this case almost an N-wave) is obtained when analyzed by CFD. The second stronger shock is caused by the more highly loaded wing planform. The discrepancy between MLT and the CFD analysis is largely due to the nonlinear and three-dimensional effects of the highly loaded wing that are neglected by MLT.

Initial attempts at shaping this signature with fuselage volume were found to be completely ineffectual. Fuselage camber was used in an attempt to modify the signature and separate the two leading shocks. A shaped signature objective function was abandoned and the sonic boom objective function was specified to simply minimize the maximum shock overpressure. This was partially successful and led to a reduction in level of the second shock. Unfortunately, continuation of this design process was leading to extreme fuselage camber shapes. The design process was terminated and a less extreme fuselage camber shape was chosen that reduced the level of the second shock. This is illustrated in figure 19 where the original fuselage camber is

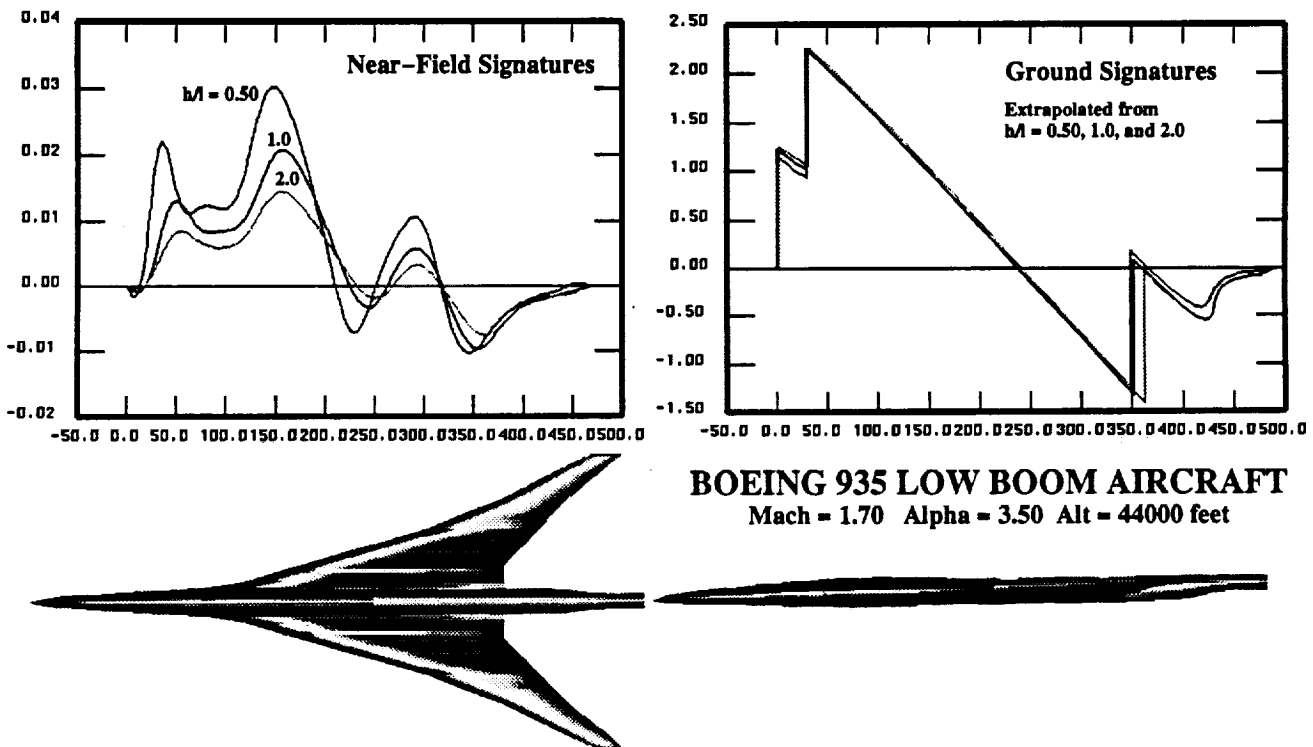


Figure 18 CFD analysis of near-field and extrapolated ground signatures for the Boeing-935 low-boom configuration.

plotted versus the modified camber line. Positive values of the camber line were completely eliminated for the forward half of the fuselage. Figure 20 shows the final ground signatures obtained with a fine grid CFD analysis. A significant reduction in level of the overall signature from about 2.25 to 1.7 lbs/ft² was achieved. The design modifications also significantly reduced the strength of the tail shock. A further attempt at this point to reduce the level was carried out using fuselage volume. Figure 20 also shows the result of this design process. The overall level was reduced from about 2.3 to about 1.5 lbs/ft².

Major changes to the fuselage camber might alter the lift coefficient. Since this preliminary study did not include aerodynamic constraints, a check on the lift coefficient for the modified design showed a reduction in lift coefficient from .121 to .105. Figure 21 shows the effect of lift coefficient. The signature of the original design is plotted versus the modified design at the design angle of attack with a lower lift coefficient and at a higher angle of attack corresponding to a lift coefficient of .124 similar to the original design. Some of the reduction gained during the design process is lost at the higher lift coefficient. In future studies, the lift coefficient will be a constraint and hence, the angle of attack will become a design variable.

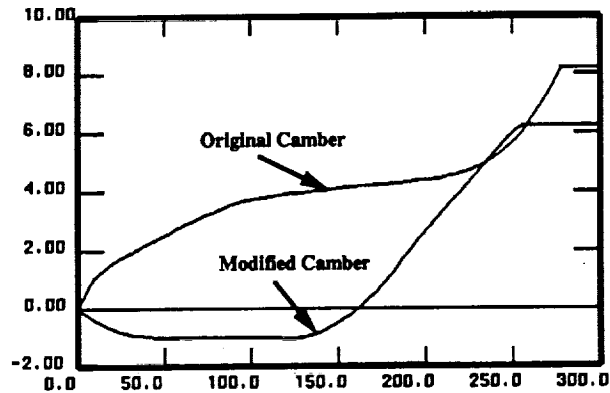


Figure 19 Modified fuselage camber distribution for the Boeing-935 configuration.

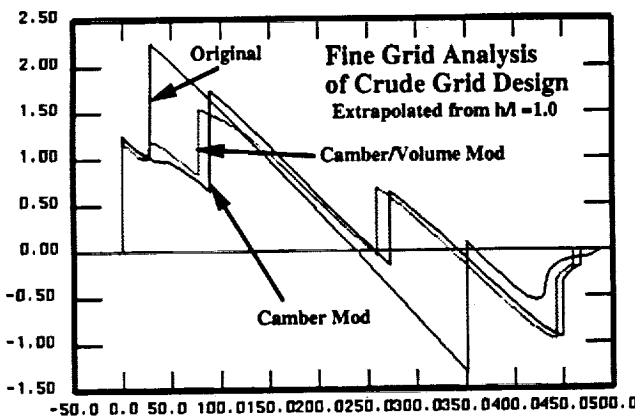


Figure 20 Fuselage camber and volume effects on ground signatures for the Boeing-935 configuration.

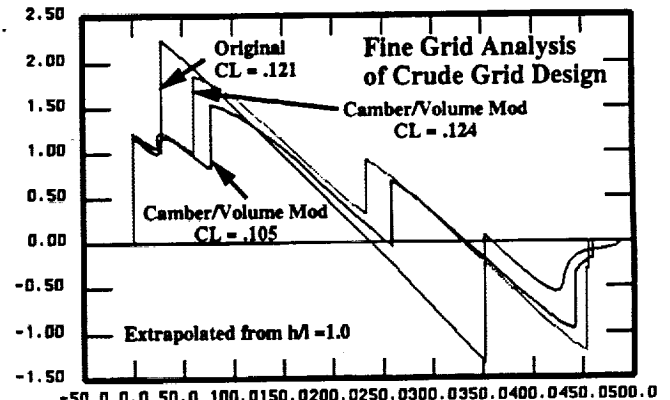


Figure 21 Effect of lift coefficient on modified signature for the Boeing-935 configuration.

BOEING REFERENCE H CONFIGURATION

Baseline Analysis

Figure 22 shows the results of a CFD analysis of the Boeing Reference H configuration at Mach 2.4, angle of attack of 4.5 degrees, and an altitude of 52700 feet. The near-field signatures indicate the dominance of the highly loaded wing generated shock. Extrapolation to the far-field yields an N-wave with an initial overpressure of almost 3 lbs/ft². The far-field signature is longer than previous configurations reaching almost 700 feet in length. At 4.5 degrees angle of attack, the lift coefficient was computed to be about 0.12. The ground signature is relatively invariant with extrapolation distance although the signature becomes slightly longer with a slight increase in initial shock overpressure.

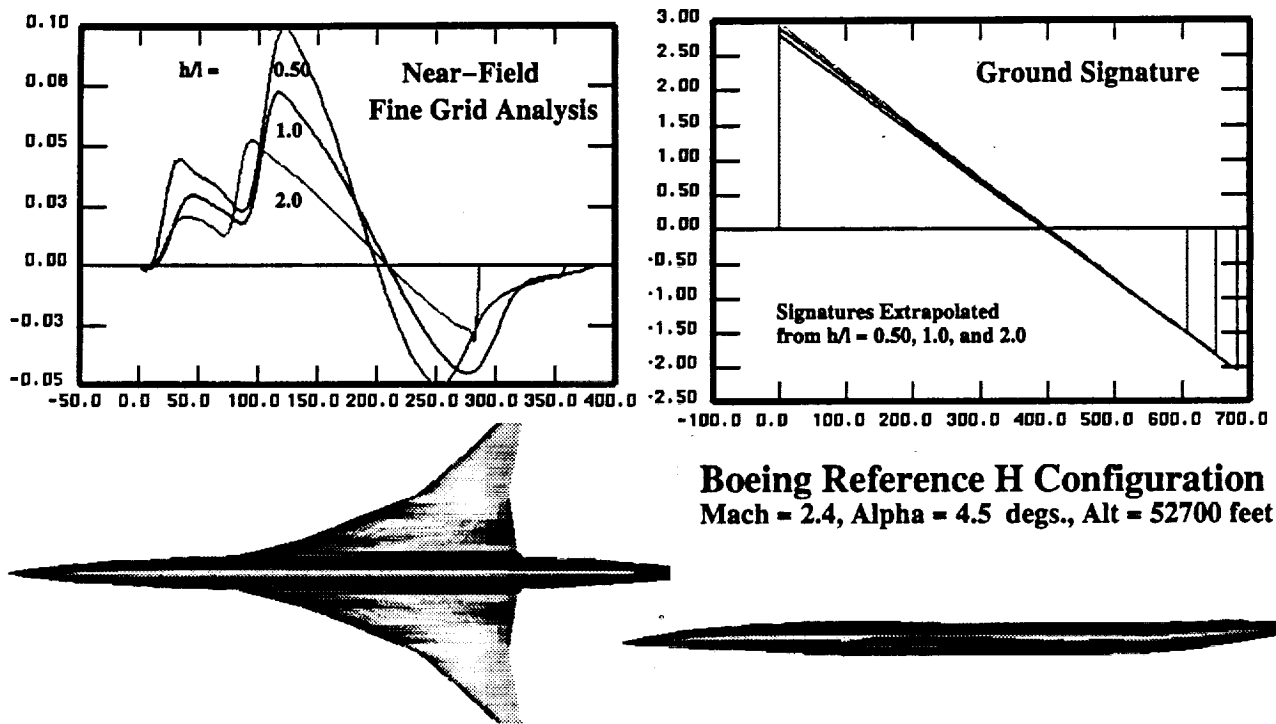
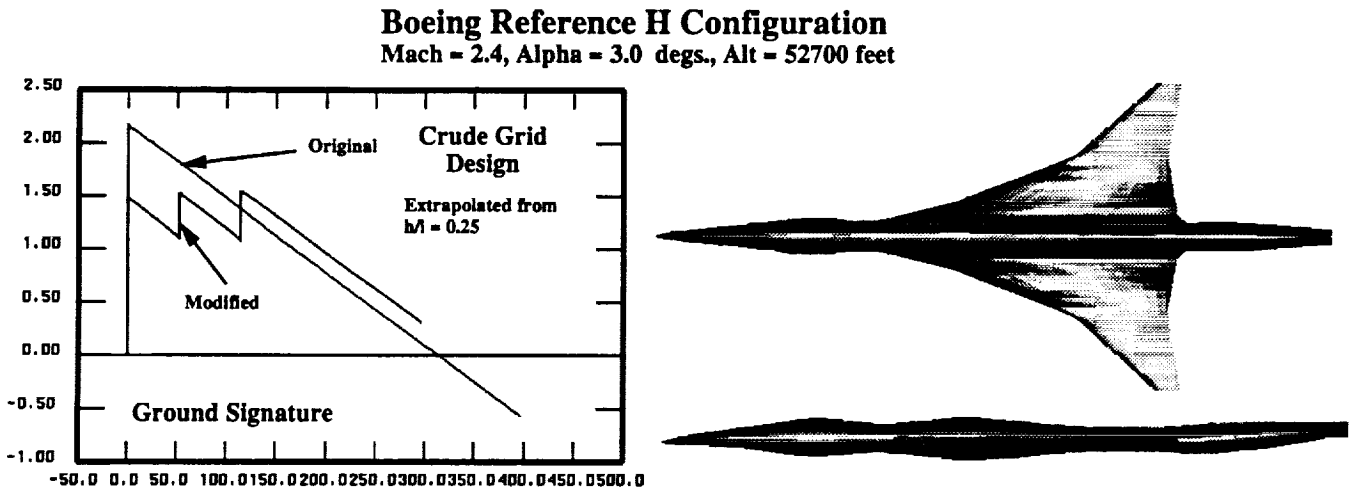


Figure 22 CFD analysis of near-field and extrapolated ground signature for the Boeing Reference H configuration.

Design Modifications

As before with the Boeing-935 configuration, the signature shape based objective function can not be used initially if the configuration exhibits an N-wave signature. The first objective is to break up the N-wave into a multiple shock signature. To accomplish this, the objective function is specified to minimize all shock strengths. If just the initial shock overpressure is used in the objective function, a second stronger shock would result in the design process. Hence, the objective function is specified to detect and minimize all shock waves for the positive or forward half of the signature.

Figure 23 shows the results of an initial attempt to modify the N-wave of the Boeing Reference H configuration using fuselage volume at a lower lift coefficient corresponding to 3.0 degrees angle of attack. As indicated, the strong nose shock is separated into three shocks of almost equal strength, hence, resulting in an overall reduction in boom level. The right side of figure 23 shows the resulting "coke bottle" fuselage shape required to produce the multi-shock signature. Work is currently in progress to further modify this configuration to produce shaped signatures at higher lift coefficients.



SUMMARY

A preliminary CFD design system using an efficient Euler code in conjunction with a numerical optimizer has been developed for the optimization of High-Speed Civil Transports. The design system can be used for inviscid aerodynamic optimization and for sonic boom signature shaping and reduction. The design system is coupled to an extrapolation code to obtain ground sonic boom signatures that are used in evaluating a user specified objective function. The system has also been automated so that geometric and grid generation take place automatically during the design process. The geometry utilizes a simple wave drag input format.

The CFD analysis of several low-boom configurations demonstrated the departure of MLT from its specified sonic boom signature design goals. This was particularly apparent for configurations designed using MLT with a hybrid or ramped sonic boom signature. It is evident from the CFD analysis of these configurations that MLT does not properly account for the three-dimensional nonlinear wing aerodynamics. Preliminary application of the design system has demonstrated its capability in modifying surface geometries of baseline configurations in order to achieve desired sonic boom shapes and signatures. It was found that flat-top shaped signatures and signatures with a small rise in pressure (i.e. hybrid or ramped) could be recovered using the present design system and with fuselage volume and/or camber as the design variables. In some cases, these modifications may have been unacceptable in terms of aerodynamic efficiency.

For configurations exhibiting close to N-wave signatures, the pressure shape objective function approach had to be abandoned during initial attempts to modify the design. Instead, a simpler objective function designed to minimize the strength of all shocks over the forward half of the signature was utilized.

Further work on the design system will be to include aerodynamic constraints in the overall design process.

REFERENCES

1. Cheung, S., "Design Process of Ames Wind-Tunnel Model 3," presented at the NASA HSR Sonic Boom Workshop, pp 95-123, Volume II, held at Ames Research Center, Moffett Field, CA, May 12-14, 1993.
2. Gill, P.E., Murray, W., Saunders, M.A., and Wright, M.H., "User's Guide for NPSOL (Version 4.0): A Fortran Package for Nonlinear Programming," Technical Report SOL 86-2, January 1986, Department of Operations Research, Stanford University.
3. Siclari, M.J. and Fouladi, K., "A CFD Study of Component Configuration Effects on the Sonic Boom of Several High-Speed Civil Transport Concepts," presented at the NASA HSR Sonic Boom Workshop, pp 227-299, Volume II, held at Ames Research Center, Moffett Field, CA, May 12-14, 1993.
4. Thomas, C.L., "Extrapolation of Sonic Boom Pressure Signatures by the Waveform Parameter Method". NASA TN D-6832, 1972.
5. Haglund, G.T., "Low Sonic Boom Studies at Boeing", presented at the NASA HSR Sonic Boom Workshop, pp 81-93, Volume II, held at Ames Research Center, Moffett Field, CA, May 12-14, 1993.
6. Mack, R.J., "Low-Boom Aircraft Concept with Aft-Fuselage-Mounted Engine Nacelles", presented at the NASA HSR Sonic Boom Workshop, pp 18-35, Volume II, held at Ames Research Center, Moffett Field, CA, May 12-14, 1993.

MID-FIELD SONIC BOOM EXTRAPOLATION METHODOLOGY

Samson Cheung, Sanford Davis, and Eugene Tu
NASA Ames Research Center
Moffett Field, CA

INTRODUCTION

In the design cycle of low-boom airplanes, sonic boom prediction must be accurate and efficient. The classical linear method, Whitham's F-function theory [1], has been widely applied to predict sonic boom signatures. However, linear theory fails to capture the nonlinear effects created by large civil transport. Computational fluid dynamics (CFD) has been used successfully to predict sonic boom signals at the near and mid fields [2]. Nevertheless, it is computationally expensive in airplane design runs [3].

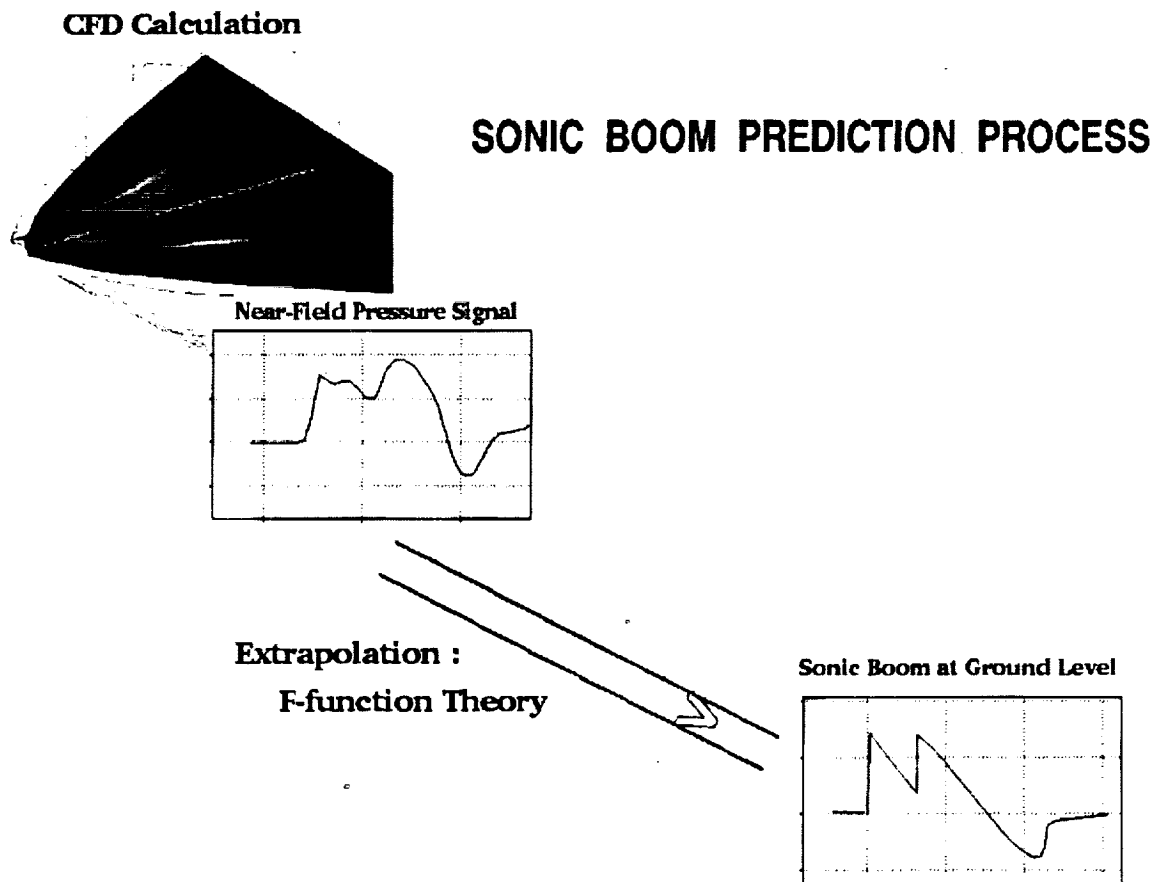
In the present study, the method of characteristics is used to predict sonic boom signals in an efficient fashion. The governing equations are the axisymmetric Euler's equations with constant enthalpy. Since the method solves Euler's equations, it captures more nonlinear effects than the classical Whitham's F-function technique. Furthermore, the method of characteristics is an efficient marching scheme for initial value problems.

In this study, we will first review the current CFD extrapolation technique and the work previously done in sonic boom extrapolation [2]. Then, we will introduce the governing equations and the method of characteristics. Finally, we will show that the present method yields the same accurate results as previous CFD techniques, but with higher efficiency.

SONIC BOOM EXTRAPOLATION PROCESS

This paragraph describes the CFD sonic boom prediction technique in Ref. [2].

The near-field solution of a supersonic vehicle is calculated by the UPS3D code [4] which solves the Parabolized Navier-Stokes (PNS) equations. This near-field solution is then interfaced to an extrapolation code for sonic boom prediction. In Ref. [2], Whitham's F-function theory [1] and an axisymmetric finite-volume PNS code (PNSYM) were used to extrapolate the solution to mid and far fields. Since the F-function theory is based on linear potential theory, the nonlinear effects are not taken into account. Although the PNS code captures the nonlinear effects, it is computational expensive for optimization runs, even in an axisymmetric case.

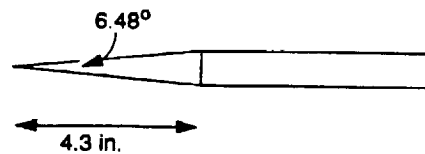


REVIEW: CONE-CYLINDER

A technique of sonic boom prediction used in Ref. [2] has been described on the previous page. A cone-cylinder configuration was chosen because wind-tunnel data [5] were available. Since the geometry is axisymmetric, two points are needed in the circumferential direction. An axisymmetric PNS code (PNSYM) was used to obtain the pressure signals.

Cone-Cylinder

- $M = 1.68, \alpha = 0$
- 10 and 20 cone-lengths
- Grid dimensions:
 - 2 points in circumferential direction
 - 340 points in normal direction
 - 1% cone length in step size

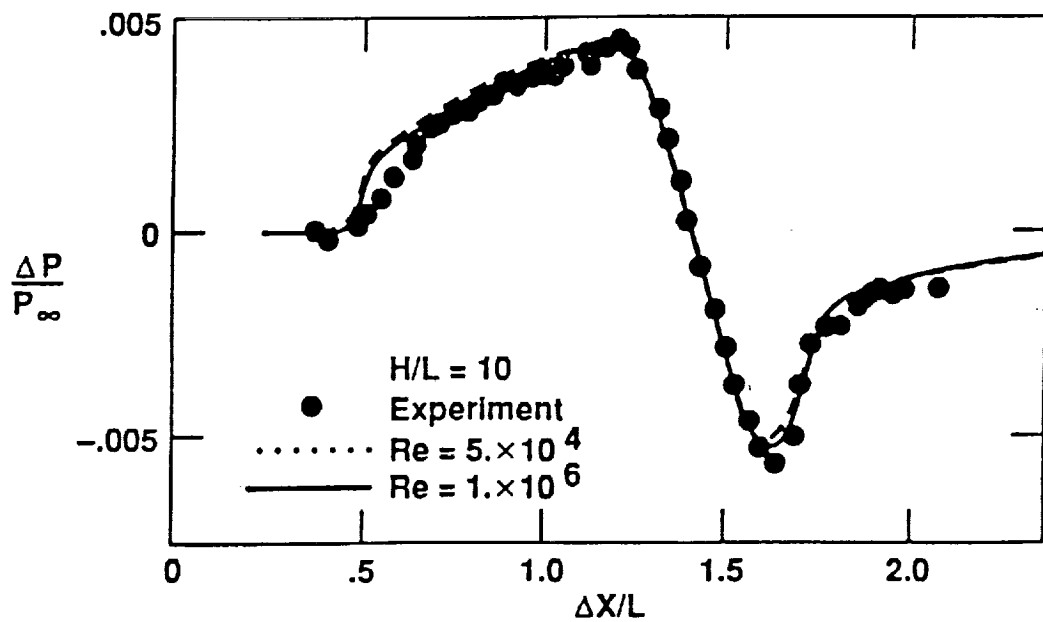


PRESSURE SIGNAL AT H/L=10

The figure below shows the pressure signal at 10 cone lengths ($H/L=10$) obtained from the axisymmetric PNS code (PNSYM). This shows that the CFD code is capable of obtaining a sonic boom signal if enough grid points are used.

PRESSURE SIGNAL AT H/L = 10

Viscous calculation

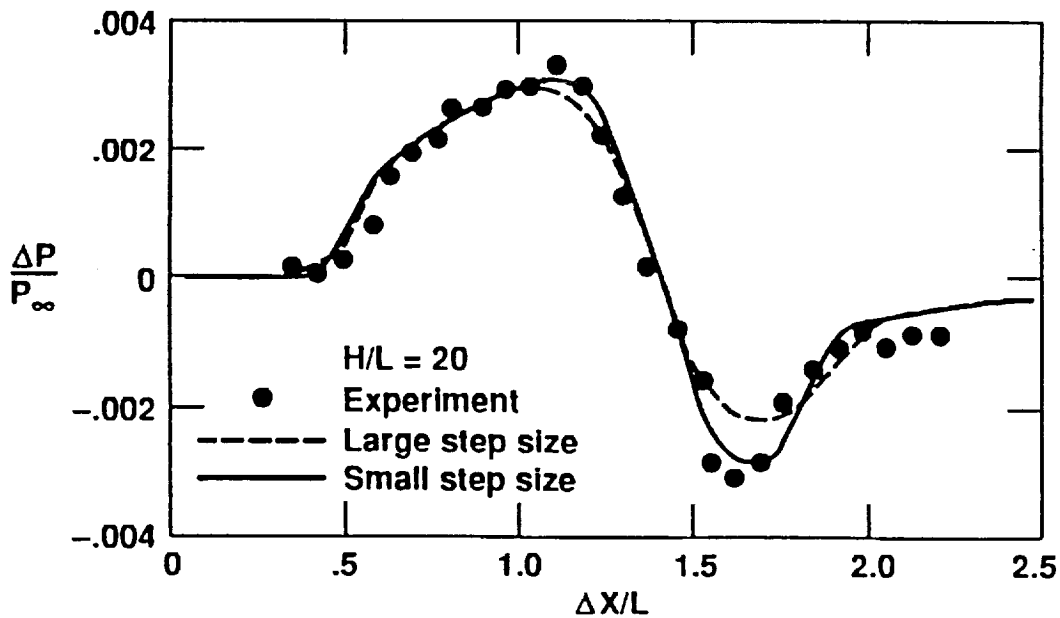


PRESSURE SIGNAL AT H/L=20

The figure below shows the pressure signal at 20 cone lengths ($H/L=20$) obtained from the axisymmetric PNS code (PNSYM). Note that viscosity was turned off for these calculations. This shows that the CFD code is capable of obtaining a sonic boom signal if matching step size is small enough.

PRESSURE SIGNAL AT H/L = 20

Cone-cylinder: $M_\infty = 1.68$, Euler calculation, Grid = 340



REVIEW: DELTA-WING BODY

Another geometry chosen to be studied in Ref. [2] is a delta-wing body whose wind-tunnel data [6] were available. In this case, the near-field solution is first computed by the 3-D CFD code (UPS3D); then the solution is interfaced with the axisymmetric PNS code (UPSYM) for sonic boom extrapolation.

Delta-Wing Body

- $M = 2.7$

- UPS3D:

40 points in circumferential

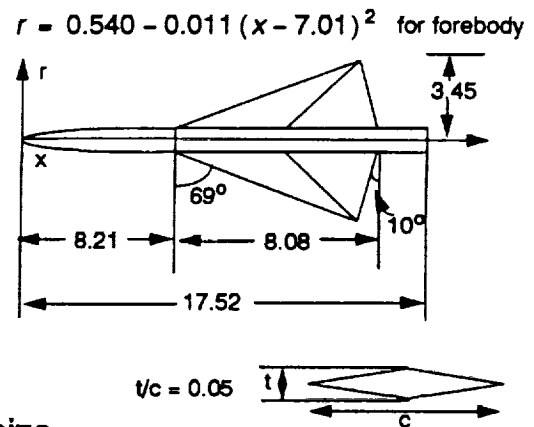
140 points in normal

0.06-0.18% body length in step size

- UPSYM

2 points in circumferential

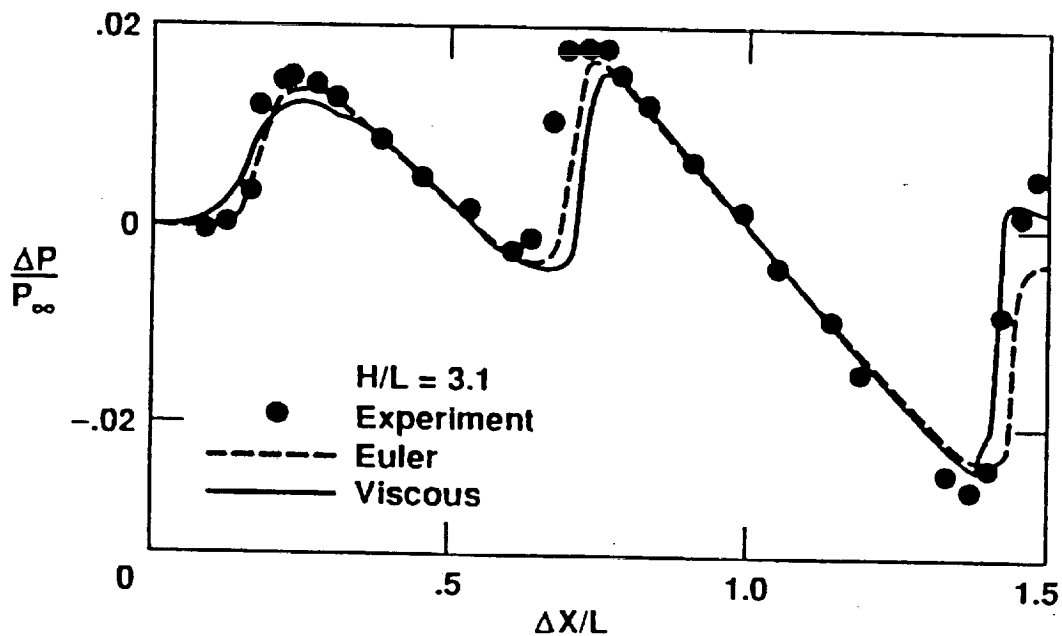
400 points in normal



PRESSURE SIGNAL AT H/L=3.1 BY CFD

The figure below shows the pressure signal at 3.1 body lengths ($H/L=3.1$) obtained by both viscous and inviscid calculations. The differences between the calculations are due to the boundary layer displacement. Detailed explanation can be found in Ref. [2]. The near-field inviscid calculation took 20 CPU mins. in Cray-YMP, and the inviscid extrapolation (to 3.1 body lengths) took 40 mins.

PRESSURE SIGNAL AT $H/L = 3.1$ Viscous and inviscid calculation

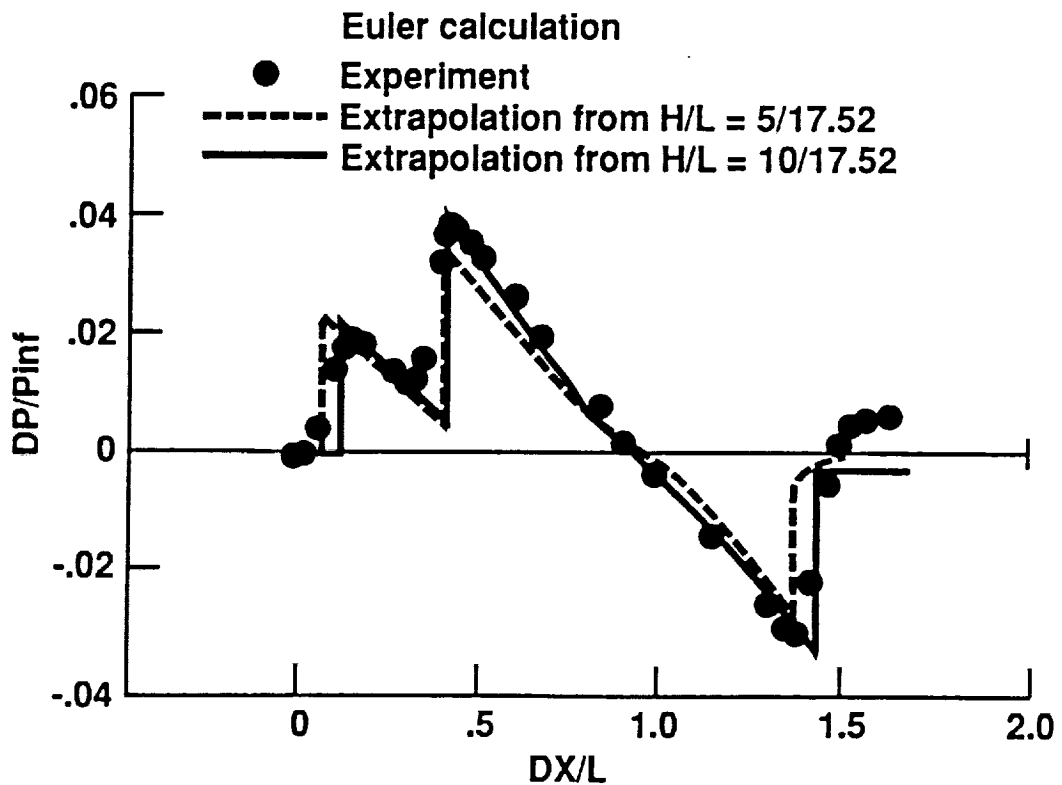


PRESSURE SIGNAL AT H/L=3.1 BY F-FUNCTION

The figure below shows the pressure signal at 3.1 body lengths ($H/L=3.1$) obtained by Whitham's F-function (linear) theory. The extrapolation interfacing with the near-field CFD solution at two different distances gave two different results. This shows that nonlinear effects still played a significant role in these distances. In general, this is hard to determine where are the good places to start the linear extrapolation.

PRESSURE SIGNAL AT $H/L = 3.1$

Wind-body: $M_\infty = 2.7$, $C_L = 0.08$ ($\alpha \approx 3.3$)



FORMULATION

So much about the review of previous sonic boom extrapolation results. Let us change gear and consider the formulation of the present methodology. Below is the formulation of Euler equations with constant enthalpy.

Formulation

The non-conservation form in cylindrical coordinates of Euler equations with constant enthalpy is

$$u \frac{\partial \rho}{\partial x} + v \frac{\partial \rho}{\partial r} + \rho \frac{\partial u}{\partial x} + \rho \frac{\partial v}{\partial r} = -\frac{\rho v}{r}$$

$$u \frac{\partial u}{\partial x} + v \frac{\partial u}{\partial r} + \frac{1}{\rho} \frac{\partial p}{\partial x} = 0$$

$$u \frac{\partial v}{\partial x} + v \frac{\partial v}{\partial r} + \frac{1}{\rho} \frac{\partial p}{\partial r} = \frac{v^2}{r}$$

where u and v are velocity components in the x and r directions respectively, ρ is density, and p is pressure.

FORMULATION (CONT.)

The idea is to convert the governing equations into a form of Burger Equation. The trick is to introduce a variable R , such that R is the natural logarithm of density, ρ . Note that for sonic boom extrapolation, a small perturbation theory can be assumed.

Formulation (Cont.)

Let R be $\ln(\rho)$, therefore,

$$\frac{1}{\rho} \frac{\partial \rho}{\partial x} = \frac{\partial R}{\partial x} \qquad \frac{1}{\rho} \frac{\partial \rho}{\partial x} = \frac{1}{\rho} \frac{\partial \rho}{\partial \rho} \frac{\partial R}{\partial x} = a^2 \frac{\partial R}{\partial x}$$

where a is the local speed of sound.

Small perturbation $u = U(1+u')$ and $v = Uv'$

where U is free-stream velocity.

FORMULATION (CONT.)

With previous assumption and substitution, the system of Euler equations can be written as a system of Burger equations. Note that the prime in u' and v' is dropped for convenience. To solve this system of equations, a method of characteristics is used.

Formulation (Cont.)

The form of Burger Equation (System)

$$Aq_x + Bq_r = c$$

$$A = \begin{bmatrix} 1+u & 1 & 0 \\ M^2 & 1+u & 0 \\ 0 & 0 & 1+u \end{bmatrix}, B = \begin{bmatrix} v & 0 & 1 \\ 0 & v & 0 \\ M^2 & 0 & v \end{bmatrix}, c = \begin{bmatrix} v/r \\ 0 \\ v^2/r \end{bmatrix}, q = \begin{bmatrix} p \\ u \\ v \end{bmatrix}$$

where $M^2 = (a/U)^2$. The primes are dropped.

METHOD OF CHARACTERISTICS

A and B are 3×3 matrices. Look for a 3×3 matrix T , such that $TA = \Lambda TB$ where Λ is a diagonal matrix which consists of the eigenvalues of the system, as shown below.

Method of Characteristics

Governing Equations $Aq_x + Bq_r = c$

Look for $T \in \mathfrak{R}^3$, $\ni TA = \Lambda TB$, therefore

$$TAq_x + TBq_r = Tc$$

or
$$\Lambda TBq_x + TBq_r = Tc$$

- Obtain Λ by solving $\det(A - \lambda B) = 0$
- Obtain T by solving $(A^T - \lambda_i B^T)t_i = 0$, t_i is i^{th} row of T

METHOD OF CHARACTERISTICS (CONT.)

Suppose initial conditions at Q, T, and S are given. The solution at point P in the next step is needed to be found. There are three characteristic curves passing through P from Q, T and S. Let these curves be $\alpha=\text{constant}$, $\beta=\text{constant}$, and $\gamma=\text{constant}$, respectively, as shown below.

Along each characteristic, we have $\lambda \frac{\partial}{\partial x} + \frac{\partial}{\partial r} = \frac{1}{r_\alpha} \frac{\partial}{\partial \alpha}$ etc.

The left-handed side of this equation fits the left-handed side of the Burger equation

$$\Delta TBq_x + TBq_r = Tc$$

Therefore, each of the three equations has the form shown at the bottom of the viewgraph.

Method of Characteristics (Cont.)

$$\Delta TBq_x + TBq_r = Tc$$

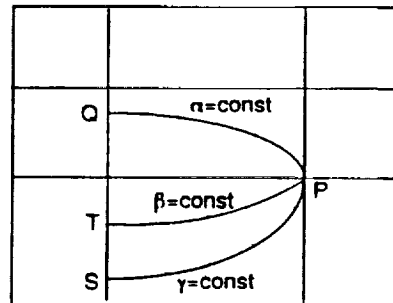
Let α , β , and γ be the characteristics of the corresponding eigenvalue's λ s.

Along α characteristic, $\alpha=\text{const}$.

$$\lambda \frac{\partial}{\partial x} + \frac{\partial}{\partial r} = \frac{1}{r_\alpha} \frac{\partial}{\partial \alpha}$$

For each λ

$$C_1 \frac{\partial R}{\partial \alpha} + C_2 \frac{\partial U}{\partial \alpha} + C_3 \frac{\partial V}{\partial \alpha} = (Tc)_\lambda$$



METHOD OF CHARACTERISTICS (CONT.)

So far we have three equations, but six unknowns (R , u , v , and three λ 's). The other three equations become the characteristic equations.

Method of Characteristics (Cont.)

- Unknowns: R , u , v , and λ s
- Three characteristic equations plus

$$\frac{dx}{dr} = \lambda \quad \Rightarrow \quad \frac{\partial x}{\partial \alpha} = \lambda \frac{\partial r}{\partial \alpha} \text{ for all } \lambda$$

- Six equations and six unknowns

METHOD OF CHARACTERISTICS (CONT.)

Six equations and six unknowns are shown below.

Method of Characteristics (Cont.)

$$a_1 \frac{\partial R}{\partial \alpha} + a_2 \frac{\partial u}{\partial \alpha} + a_3 \frac{\partial v}{\partial \alpha} = a_4 \frac{\partial r}{\partial \alpha}$$

$$b_1 \frac{\partial R}{\partial \beta} + b_2 \frac{\partial u}{\partial \beta} + b_3 \frac{\partial v}{\partial \beta} = b_4 \frac{\partial r}{\partial \beta}$$

$$c_1 \frac{\partial R}{\partial \gamma} + c_2 \frac{\partial u}{\partial \gamma} + c_3 \frac{\partial v}{\partial \gamma} = c_4 \frac{\partial r}{\partial \gamma}$$

$$\frac{\partial x}{\partial \alpha} = \lambda_1 \frac{\partial r}{\partial \alpha}, \quad \frac{\partial x}{\partial \beta} = \lambda_2 \frac{\partial r}{\partial \beta}, \quad \frac{\partial x}{\partial \gamma} = \lambda_3 \frac{\partial r}{\partial \gamma}$$

a 's, b 's, and c 's are functions of R , u , and v .

DISCRETIZATION

Suppose we are looking for the solution (R , u , and v) at point P , and the solution at current points Q , T , and S are known. Consider one of the three governing equations at α -characteristic, as shown below. Denote $R(P)$ to be the value of R at point P , etc.

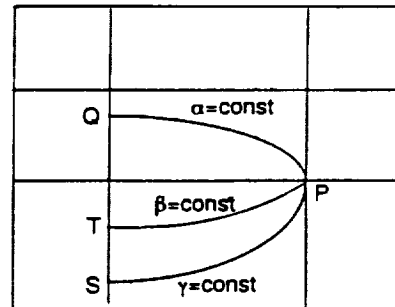
We discretize $\delta f / \delta \alpha$ by $(f(P) - f(Q)) / \Delta \alpha$, and we average a_i by $(a_i(P) + a_i(Q)) / 2$. Note that $\Delta \alpha$ are cancelled out in the discretized equation. The six discretized equations are solved iteratively.

Method of Characteristics (Cont.)

Discretization

$$a_1 \frac{\partial R}{\partial \alpha} + a_2 \frac{\partial u}{\partial \alpha} + a_3 \frac{\partial v}{\partial \alpha} = a_4 \frac{\partial r}{\partial \alpha}$$

\swarrow \swarrow $(R(P) - R(Q))$
 $\frac{(a_1(P) + a_1(Q))}{2}$



Solve the system iteratively.

POSSIBLE PROBLEMS

The values of λ 's are given below.

The first problem occurs when $v=0$ (note v is v'). This can be solved easily as shown.

The second problem occurs when $Mv=1$. In application of sonic boom propagation in civil transport, M is in the range of 1.5 to 3. On the other hand, v' is much less than $1/3$ for low angle-of-attack civil transport. Therefore, the problem will not occur.

Possible Problems

$$\lambda_1 = \frac{1+u}{v}$$

$$\lambda_{2,3} = \frac{M^2 v(1+u) \pm \sqrt{M^2(v^2 + (u+1)^2) - 1}}{M^2 v^2 - 1}$$

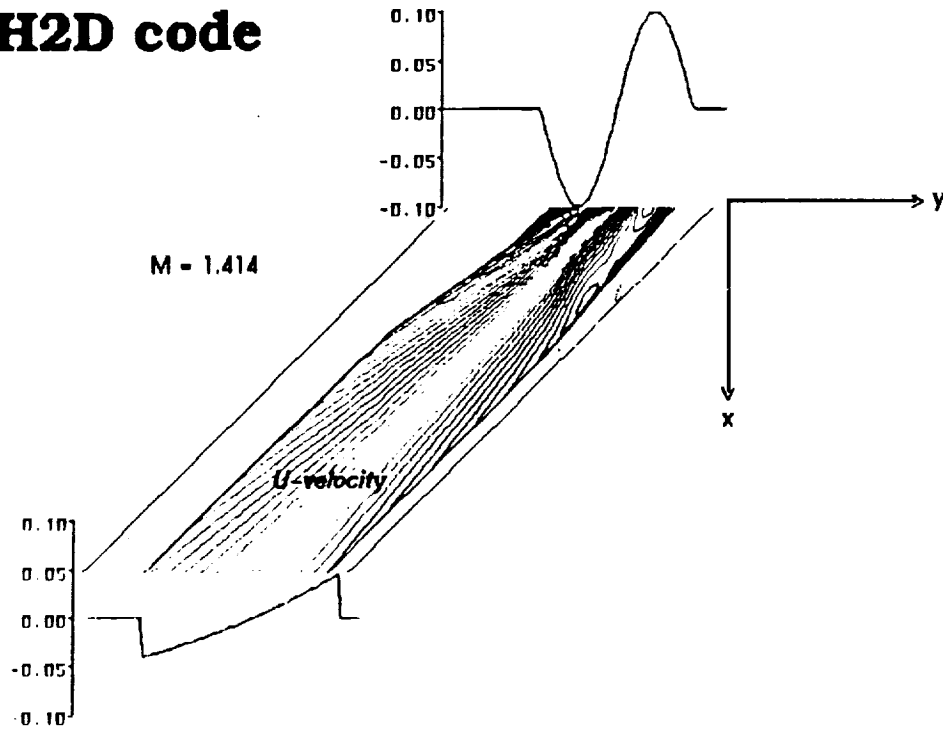
- For λ_1 , problem occurs at $v=0$
$$\frac{\partial x}{\partial \alpha} = \lambda_1 \frac{\partial r}{\partial \alpha} \quad \rightarrow \quad \frac{\partial r}{\partial \alpha} = \lambda_1^{-1} \frac{\partial x}{\partial \alpha}$$
- For $\lambda_{2,3}$, problem occurs at $Mv = \pm 1$

In application of supersonic flow; therefore $M > 1$.

APPLICATION (2-D)

This is a 2-D application. Initial signal is a sine curve. At supersonic flow (Mach 1.414), we can see the formation of the shock waves in space.

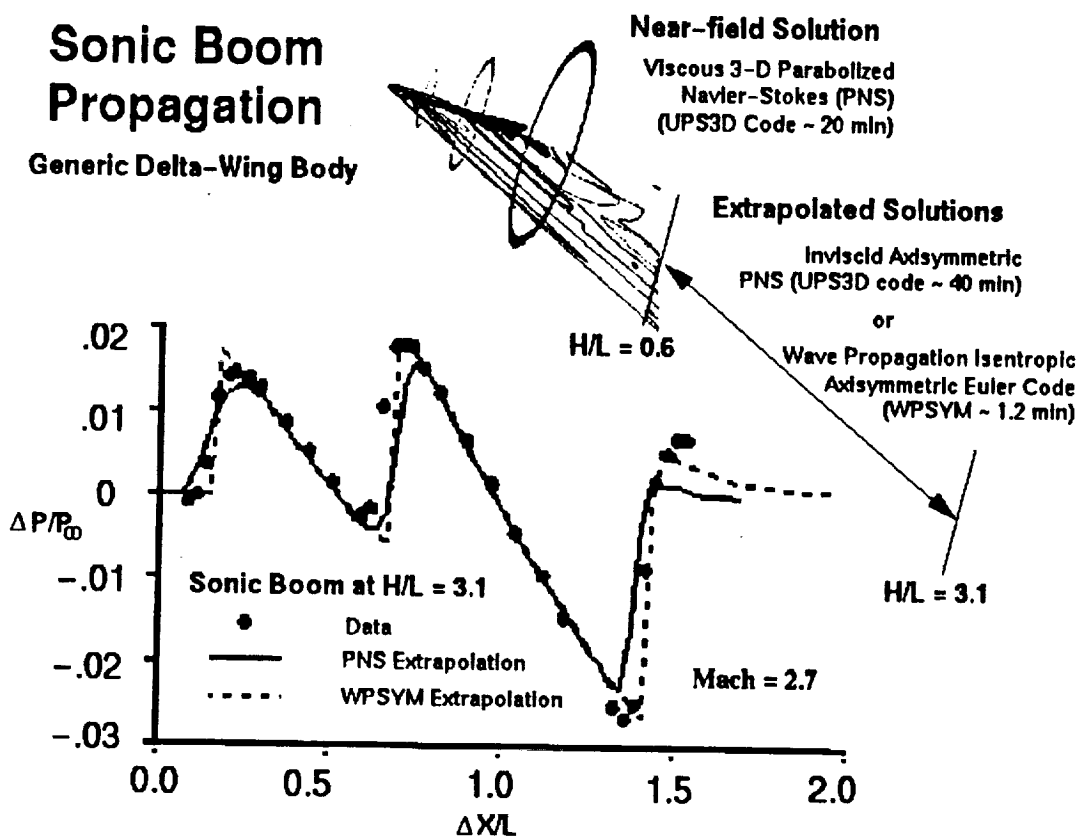
CH2D code



APPLICATION (AXISYMMETRIC)

The name of this code solving the Euler equations with constant enthalpy by method of characteristics is WPSYM (wave propagation - symmetric).

The geometry is the delta-wing body described previously. The near-field solution is obtained by UPS3D code at about 0.6 body length under the flight track. This calculation took 20 CPU mins. in Cray-YMP. At this point, the solution was interfaced with two extrapolation codes; namely, the axisymmetric PNS code mentioned before and WPSYM. The axisymmetric PNS code took 40 mins. to obtain the pressure signal at $H/L=3.1$; whereas, WPSYM took 1.2 mins. in the same machine. The x - y plot below also shows the new method sharply defines the shock points with high efficiency.



References

- 1 Whitham, G., "The Flow Pattern of a Supersonic Projectile," *Comm. and Pure and Applied Math.*, Vol. 5, No. 3, 1952.
- 2 Cheung, S., Edwards, T., and Lawrence, S., "Application of CFD to Sonic Boom Near and Mid Flow-Field Prediction," *J. of Aircraft*, Vol. 29, No. 5, 1992.
- 3 Cheung, S., Edwards, T., "Supersonic Design Optimization Method for Aerodynamic Performance and Low Sonic Boom," *High Speed Research: Sonic Boom Workshop*, Vol. 2, NASA CP-3173, 1992.
- 4 Lawrence, S., Chaussee, D., and Tannehill, J., "Application of an Upwind Algorithm to the 3-D Parabolized Navier-Stokes Equations," *AIAA paper 87-1112*, June 1987.
- 5 Mendoza, J. and Hicks, R., *NASA TM X-2219*.
- 6 Hunton, L. and Hicks, R., *NASA TN D-7160*.

A PERFORMANCE ASSESSMENT OF EIGHT LOW-BOOM HIGH-SPEED CIVIL TRANSPORT CONCEPTS

Daniel G. Baize, Marcus O. McElroy, James A. Fenbert, and Peter G. Coen
NASA Langley Research Center
Hampton, Virginia

Lori P. Ozoroski, Chris S. Domack, Kathy E. Needleman, and Karl A. Geiselhart
Lockheed Engineering & Sciences Company
Hampton, Virginia

INTRODUCTION

A performance assessment of eight low-boom high speed civil transport (HSCT) configurations and a reference HSCT configuration has been performed. Although each of the configurations was designed with different engine concepts, for consistency, a year 2005 technology, 0.4 bypass ratio mixed-flow turbofan (MFTF) engine was used for all of the performance assessments. Therefore, all original configuration nacelles were replaced by a year 2005 MFTF nacelle design which corresponds to the engine deck utilized. The engine thrust level was optimized to minimize vehicle takeoff gross weight. To preserve the configuration's sonic-boom shaping, wing area was not optimized or altered from its original design value. Performance sizings were completed when possible for takeoff balanced field lengths of 11,000 ft and 12,000 ft, not considering FAR Part 36 Stage III noise compliance. Additionally, an arbitrary sizing with thrust-to-weight ratio equal to 0.25 was performed, enabling performance levels to be compared independent of takeoff characteristics. The low-boom configurations analyzed included designs from the Boeing Commercial Airplane Group, Douglas Aircraft Company, Ames Research Center, and Langley Research Center. This paper discusses the technology level assumptions, mission profile, analysis methodologies, and the results of the assessment. The results include maximum lift-to-drag ratios, total fuel consumption, number of passengers, optimum engine sizing plots, takeoff performance, mission block time, and takeoff gross weight for all configurations. Results from the low-boom configurations are also compared with a non-low-boom reference configuration. Configuration dependent advantages or deficiencies are discussed as warranted.

This paper is divided into the six sections shown in the outline below. The technology assumptions and propulsion system are discussed first. The full mission profile simulated for all of the configuration sizings is presented, followed by a brief discussion of the methodology employed to arrive at the results. The performance results for a non-boom constrained reference configuration are shown first, then the results for the eight low-boom configurations are presented. The sonic-boom characteristics of each low-boom configuration are assumed to be as designed (refs. 1-7). Finally the results are compiled, when applicable, into three differently constrained sizing tables. The final page of this report contains conclusions which can be drawn from this assessment.

The method of analysis and assumptions used are constant for each of the configurations evaluated. When assumptions are made that affect the relative sizing of the concepts differently, the advantage is always given to the heavier configuration, since sonic-boom shaping and design closure inherently become less certain as the configuration's weight grows. In addition, the heavier designs are unlikely to be selected for further study, and slight performance assumption advantages gained over more efficient configurations are, therefore, moot. One example of this philosophy is the method for estimation of available fuel volume. All configurations are assumed to have the same size landing gear bay as the reference configuration. As the low-boom configurations grow in takeoff gross weight (TOGW), this assumption becomes less and less valid, giving the heaviest configurations a slight advantage in fuel capacity.

Outline

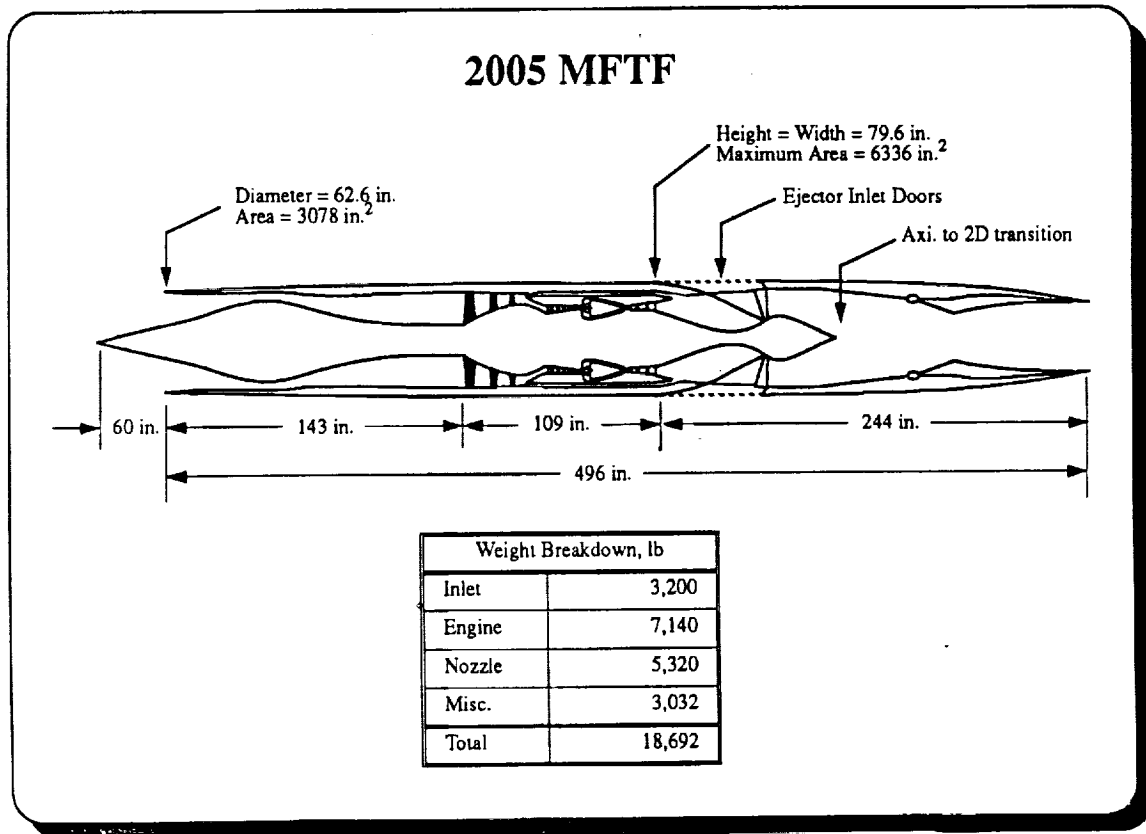
- I. Technology Assumptions
- II. Mission Schematic
- III. Methodology
- IV. Reference Configuration Results
- V. Individual Low-Boom Configuration Results
- VI. Tabular Comparisons & Conclusions

The technology assumptions shown below are used for all of the performance analyses. A year 2005 Entry-Into-Service (EIS) date is assumed. Major weight savings are achieved by utilizing advanced composite materials, structural designs, and aeroelastic tailoring. Synthetic vision is used to eliminate the weight penalty of a variable geometry nose section. Cockpit multipurpose displays and advanced flight control systems provide additional weight savings. Computer-controlled flap schedules allow for aerodynamic shape optimization during takeoff and landing, which minimizes the net thrust required for final vehicle sizing. The takeoff distance computations are reported as balanced field lengths and are not constrained by FAR Part 36 Stage III noise certification compliance. The eight low-boom configurations were developed over a time span of years, with some originating before the High-Speed Research (HSR) mission requirements were well defined, or year 2005 engine technologies well understood. The changes in technology level assumptions and mission requirements, along with the severe challenges of sonic-boom shaping, cause a significant variance between the low-boom concepts' passenger load, propulsion system layout, and assumed engine cycle. Though not all of these inconsistencies can be removed for these analyses, a single engine cycle must be selected to remove the large possible TOGW variance directly proportional to engine weight and performance. Therefore, a year 2005 EIS, 0.4 bypass ratio MFTF is used for all of the concept analyses. Since none of the configurations were designed with this engine, all original configuration nacelle geometries were replaced with the nacelle of the year 2005 MFTF. This change impacted the wave drag of the reference and all low-boom configurations differently, and is discussed on a case by case basis later in this paper.

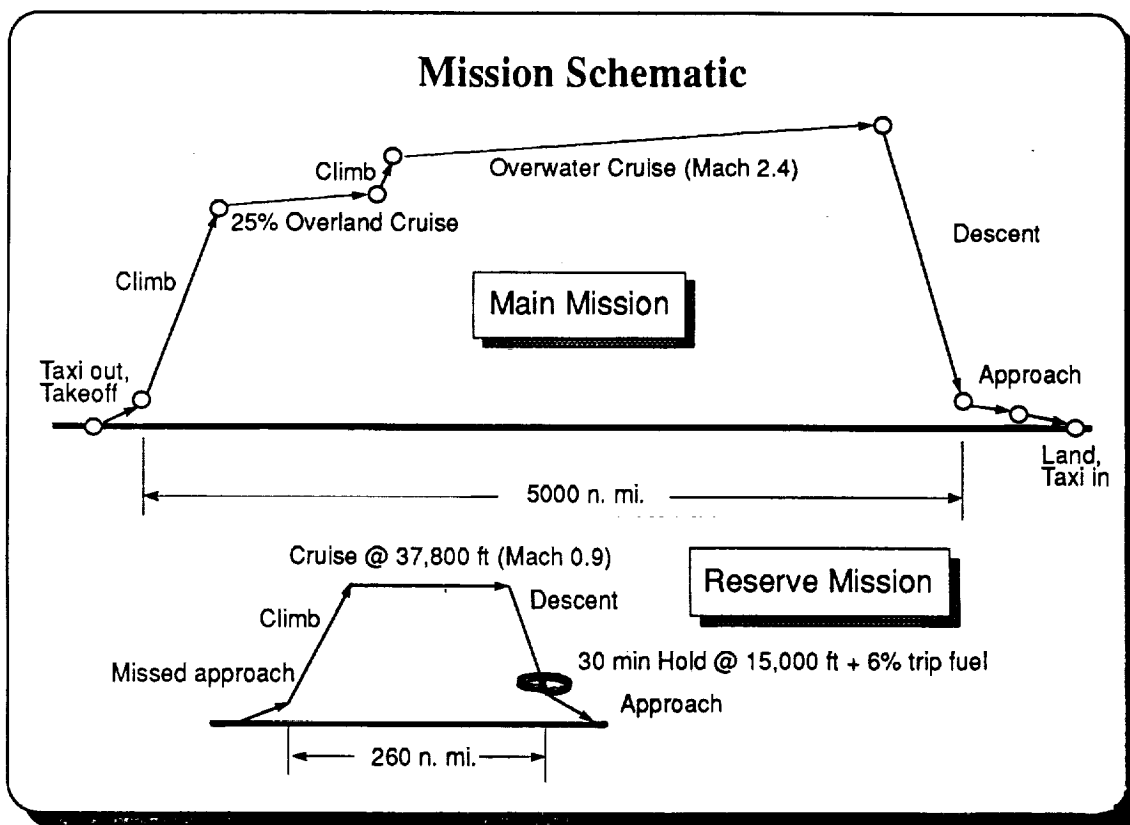
Technology Assumptions

- ❖ 2005 Entry-Into-Service (EIS) Date
- ❖ Advanced Composite Materials and Structural Designs
- ❖ Aeroelastic Tailoring
- ❖ Synthetic Vision and Cockpit Multipurpose Displays
- ❖ Computer-Controlled Flap Schedules for Takeoff and Landing
- ❖ Balanced Field Length with NO Noise Constraint Applied
- ❖ 0.4 Bypass Ratio, Mixed Flow Turbofan (MFTF) Engines

When replacing the original propulsion system with that of the year 2005 MFTF engine shown below, every effort was made to preserve the originally assumed boundary layer offset, lateral spacing, and longitudinal positioning of the nacelles. However, if for a particular configuration this placement would result in greater than one third of the nacelle overhanging the wing, the MFTF nacelles were moved forward, averaging damage tolerance (engine face behind rear spar) and overhang constraints. The MFTF propulsion system performance, weight, and dimensional data were generated using a modified version of the Navy/NASA Engine Program (NNEP, ref. 8), with temperature, structural, and material limits established by HSR industry partners and Lewis Research Center. The MFTF has a bypass ratio of 0.4 and an overall pressure ratio of 21.9. The inlet is an axisymmetric, mixed compression, translating centerbody inlet, and is started for Mach numbers greater than 1.6. An axisymmetric/two-dimensional hybrid mixer ejector (ME) nozzle is used to reduce takeoff noise associated with the high jet velocity typical of this cycle. The ME nozzle entrains an additional 120 percent ambient air over the MFTF's inlet air. The ambient air mixes with the engine air to reduce the jet velocity at the exit of the nozzle, thereby reducing noise. Acoustic lining is used inside the nozzle to reduce mixing noise. The baseline engine has a design corrected mass flow of 650 lb/s and develops 47,000 lb of sea-level static thrust. The total propulsion system (inlet, engine, nozzle, nacelle, firewall, mounts, diverter, etc.) weighs 18,692 lb and is scaled linearly with thrust for all analyses. Installation effects included in the propulsion system data are inlet spillage, bleed, and bypass drags. Because of this engine's early development, boattail drag is not in the engine deck, but is included with the far-field wave drag data.



The mission profile illustrated in the schematic below was utilized for the performance assessment. Instead of the usual HSR mission profile which has an all Mach 2.4 overwater cruise leg, a mixed mission is used in the current study that incorporates an initial 25 percent overland segment. The non low-boom reference configuration flies subsonically during the overland segment at Mach 0.9 while the low-boom configurations' overland Mach numbers vary from 1.6 to 2.0. The remaining 75 percent of the 309 passenger, 5000 n.mi. range mission is assumed to be overwater at Mach 2.4. Main mission trip fuel allowances include fuel for 10 minutes of warm-up and taxi at idle power, takeoff and climb, cruise at optimum altitude, and descent. Reserves include fuel for a missed approach, climb to 37,800 ft, cruise at Mach 0.9 and 37,800 ft for 260 n.mi. to an alternate airport, a 30-minute hold at 15,000 ft, descent from hold condition, plus an additional 6 percent of the trip fuel allowance. Since most of the low-boom arrow-wing type planforms are significantly challenged in the low-speed arena, up to three different constant wing area performance sizings are presented for each configuration. These include an 11,000 ft takeoff field length (TOFL) constrained sizing, a 12,000 ft TOFL constrained sizing, and an arbitrary 0.25 thrust-to-weight ratio sizing. This last sizing is presented to provide a relative comparison of the configurations independent of their takeoff characteristics which could be improved by future design cycles, or by improving high-lift augmentation capabilities.

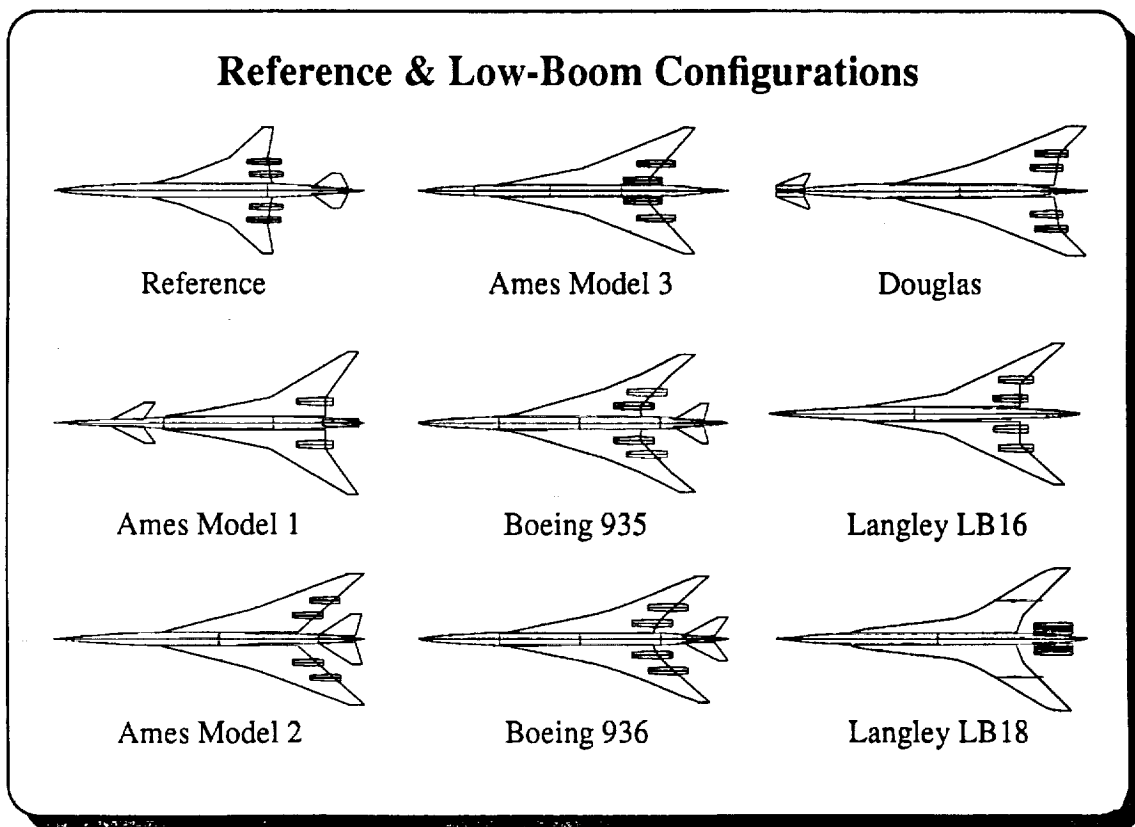


The performance analysis methodology used in this study closely follows the well documented method of reference 9. All methods are linear, modified-linear, or empirical in nature. Zero-lift drag analysis consists of skin-friction, roughness, and volume-wave drag computations with base drag assumed negligible for all configurations. Skin-friction drag is calculated using the T' method of Sommer and Short (CDF1, ref. 10), and roughness drag is empirically calculated as a percentage of skin-friction drag. Zero-lift far-field wave drag is estimated using a slightly refined method of reference 11 (AWAVE). Supersonic lift-dependent drag calculations are performed with the modified-linear theory method of reference 12 (WDES), with the empirical corrections of reference 13 applied. Supersonic trim-drag increments are obtained from the linear results of the UDP (ref. 14) code. Nacelle interference effects are calculated in the lift analysis module of the System for Aerodynamic Design and Analysis of Supersonic Aircraft (SDAS, refs. 15,16) code. AERO2S (ref. 17) is used for subsonic and trimmed takeoff drag polar development. A configuration's weight and balance are estimated using the Flight Optimization System (FLOPS, ref. 18). Fuel volume is determined by laying out wing and aft fuselage fuel tanks utilizing the Configuration Development Module (CDM) of reference 19, with a final empirical factor applied. Passenger count estimation, a linear curve fit based on numerous previously documented supersonic transport studies, utilizes available fuselage volume and assumes a fixed volume for galleys, lavatories, etc., plus volume per passenger. Final constant wing area sizing and full mission simulation are accomplished with FLOPS.

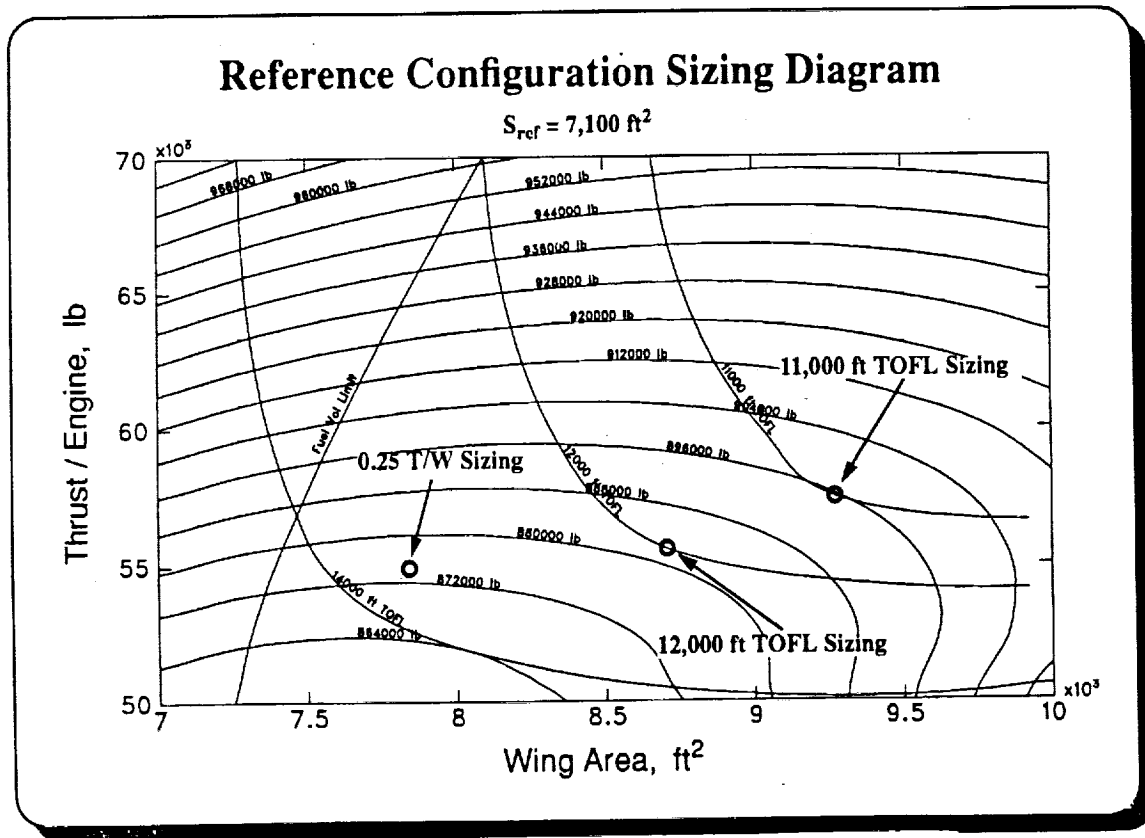
Performance Assessment Methodology

- ❖ Zero-Lift Drag: CDF1, AWAVE
- ❖ Subsonic & Takeoff Lift-Dependent Drag Calculations: AERO2S
- ❖ Supersonic Lift-Dependent Drag Calculations: WDES
- ❖ Supersonic Trim Drag Increments: UDP
- ❖ Supersonic Nacelle Interference Effects: SDAS
- ❖ Mass Properties: FLOPS
- ❖ Fuel Volume, Passenger Count, Center-of-Gravity: CDM, FLOPS
- ❖ Mission Simulation & Configuration Sizing: FLOPS

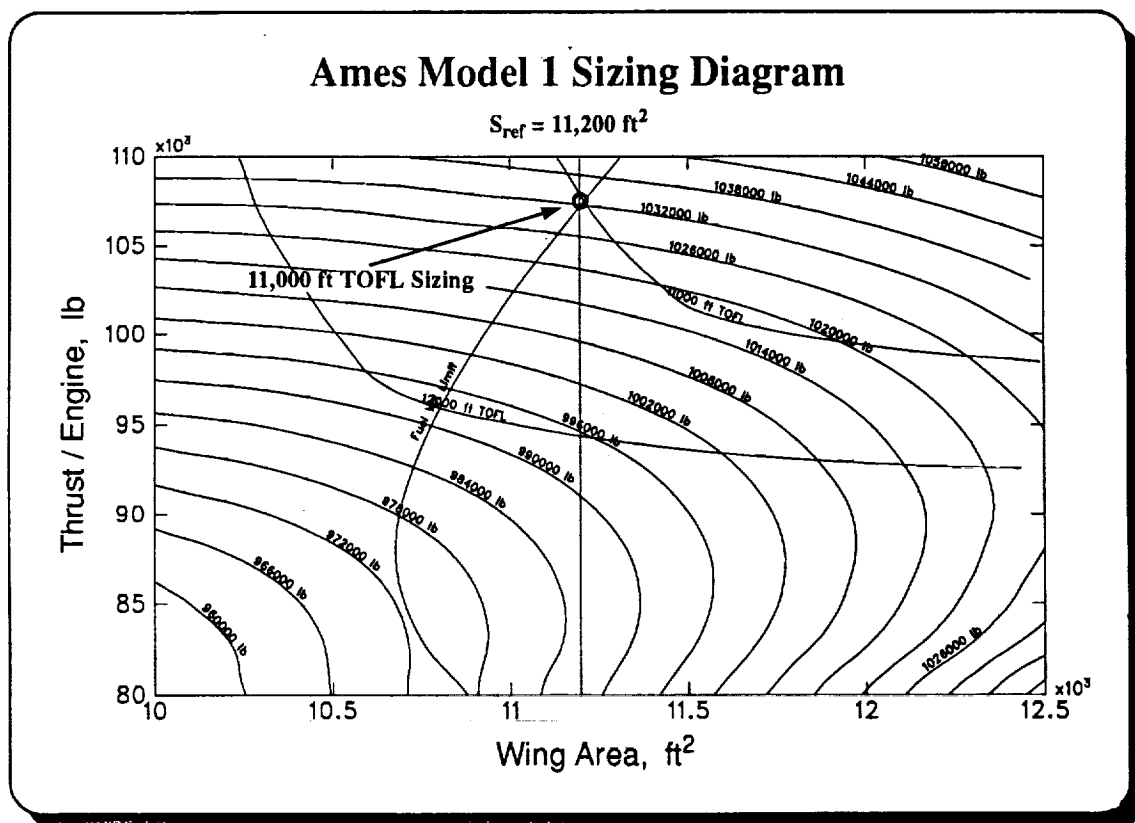
Plan-views of the reference configuration and the eight low-boom concepts assessed in this study are presented below. Although the reference configuration has the same planform as Boeing's Reference H, the propulsion system and aerodynamic performance assumptions differ. As shown, the low-boom configurations have more aerodynamically aggressive (and structurally challenging) arrow-wing planforms than the double delta of the reference. This is a direct result of applying the low-sonic-boom constraint (traditionally a smooth, elongated lift distribution) during the design process. Three of the low-boom designs incorporate a horizontal tail, two include a canard, and three use single lifting surfaces. Adherence to the HSR programmatic assumptions of a 309 passenger Mach 2.4 overwater mission with four underwing engines varies. Design variations include: the Ames Model 1, designed as a trijet; the Langley LB16, designed to accommodate only 250 passengers at an overwater Mach number of 2.0; and the Langley LB18, designed with aft fuselage mounted engines to ensure sonic-boom shaping. Such radically different characteristics could bias the analysis results either for or against these particular concepts. Therefore, care must be taken when comparing the final results of these three low-boom designs because differences in performance could be highly dependent on cruise Mach number or propulsion system layout. Additionally, because the individual designers used several different methods of calculating reference area, a calculation of planform area carried to the centerline using a consistent method is presented for each configuration.



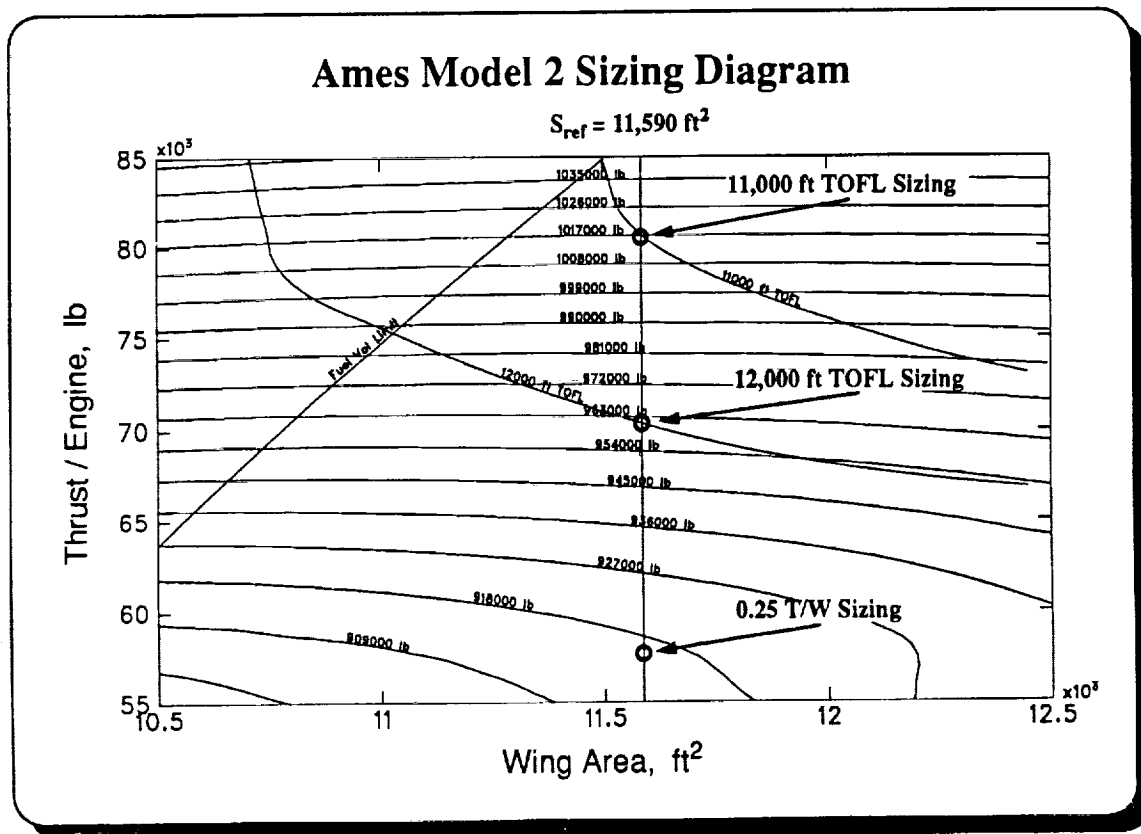
Shown below is the sizing diagram for the reference configuration. This concept is an HSCT designed without any consideration for the loudness of the sonic-boom signature. Although the configuration was originally designed for an all Mach 2.4 overwater cruise, this sizing study includes an initial 25 percent subsonic leg simulating overland operation. The incorporation of the 25 percent 0.9 Mach number segment results in a penalty of approximately 30,000 lb in TOGW and 1.4 hr in block time. The original design incorporated four turbine bypass engines. When the original engine nacelles were replaced with the larger year 2005 MFTF engine nacelles for this study, the result was a wave drag penalty of 3.0 counts at the overwater cruise Mach number. The maximum lift-to-drag ratio for Mach 2.4 at 40,000 ft is 7.9. Illustrated on the diagram below are the three different sizing points. At the 11,000 ft TOFL sizing point, the vehicle is estimated to have a TOGW of 895,600 lb with a reference wing area of 9,270 ft² (calculated wing area of 9,760 ft²) and a thrust per engine of 57,500 lb resulting in a mission fuel burn of 448,000 lb. For the 12,000 ft TOFL sizing, the vehicle has a TOGW of 881,000 lb at a wing area of 8,700 ft² (calculated wing area of 9,200 ft²) and 55,500 lb thrust per engine with the mission fuel burn reduced 4,600 lb. At a thrust-to-weight ratio of 0.25, the minimum TOGW sized configuration drops to 873,000 lb at a reference wing area of 7,800 ft² (calculated wing area of 8,300 ft²) and 54,600 lb thrust per engine. The TOFL for this configuration increases to an estimated 13,500 ft while the mission fuel burn remains roughly the same as for the 12,000 ft sized vehicle. The required fuel volume was not a factor in any of the sizings for this vehicle, resulting in a full passenger load of 309 for all cases.



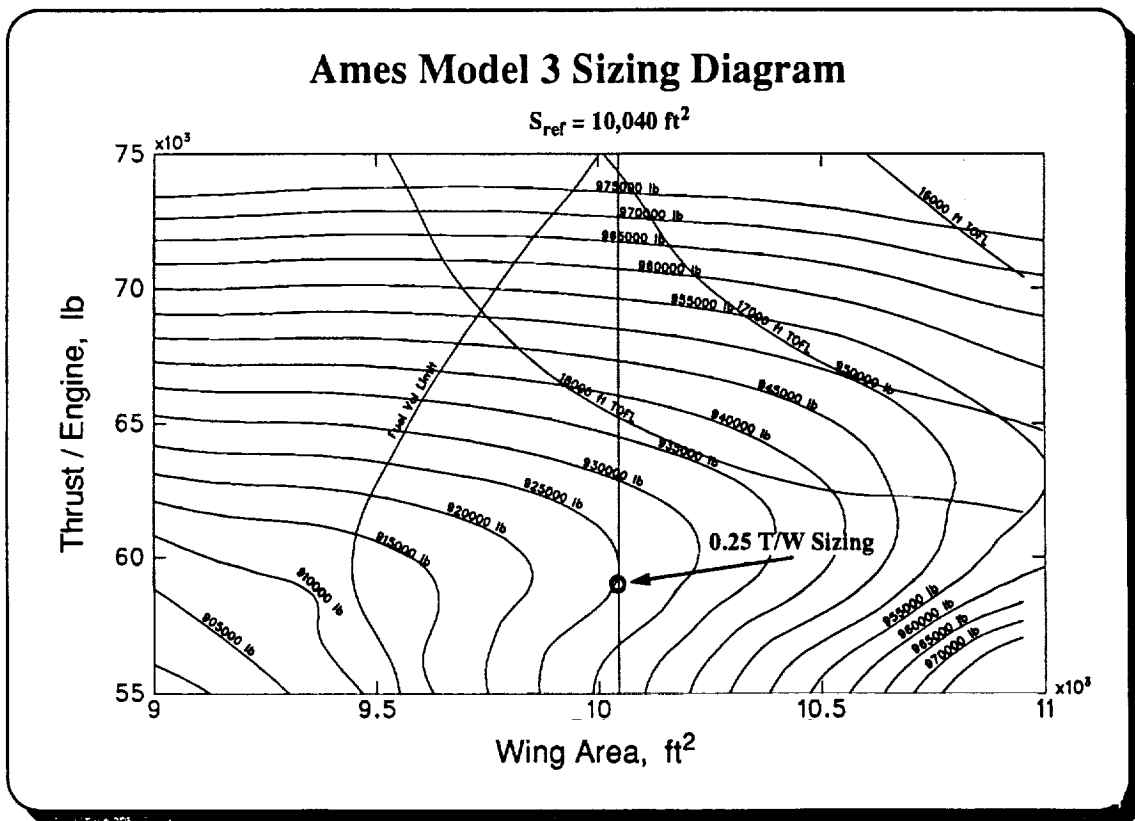
A sizing diagram for the Ames Model 1 low-boom configuration is shown below. Of the eight low-boom configurations, the Ames Model 1 is the only trijet, configured with two wing-mounted engines and one tail-mounted engine. A canard is used as a second lifting surface. The wing reference area is 11,200 ft² while the calculated planform area is 600 ft² smaller. The year 2005 MFTF engine nacelles are significantly larger than the original propulsion system nacelles and have an excessive overhang when installed at the original longitudinal position. Therefore, the wing-mounted MFTF nacelles are shifted forward approximately 5 ft while there is no change in the positioning of the tail-mounted nacelle. As a result there is a wave drag increase of 1.2 counts at the low-boom cruise Mach number of 2.0 and 0.8 counts at the overwater cruise Mach number of 2.4. At an altitude of 40,000 ft, the maximum lift-to-drag ratios are 8.1 and 8.8 for Mach numbers 2.4 and 2.0, respectively. As shown in the diagram below, this vehicle satisfies the 11,000 ft TOFL constraint at a thrust per engine of 107,400 lb. This sizing results in a TOGW of 1,032,400 lb and a trip fuel burn of 536,000 lb to carry 260 passengers. The 12,000 ft TOFL constraint can be satisfied for 12,400 lb less thrust per engine. The corresponding fuel burn is reduced by 13,000 lb, lowering the TOGW to 999,500 lb while allowing 4 more passengers on board. At a thrust-to-weight ratio of 0.25, the vehicle's TOGW is 988,200 lb for 82,200 lb of thrust per engine; however, the TOFL would be over 15,000 ft. This sizing requires slightly more mission fuel than the 12,000 ft sizing and therefore carries one less passenger.



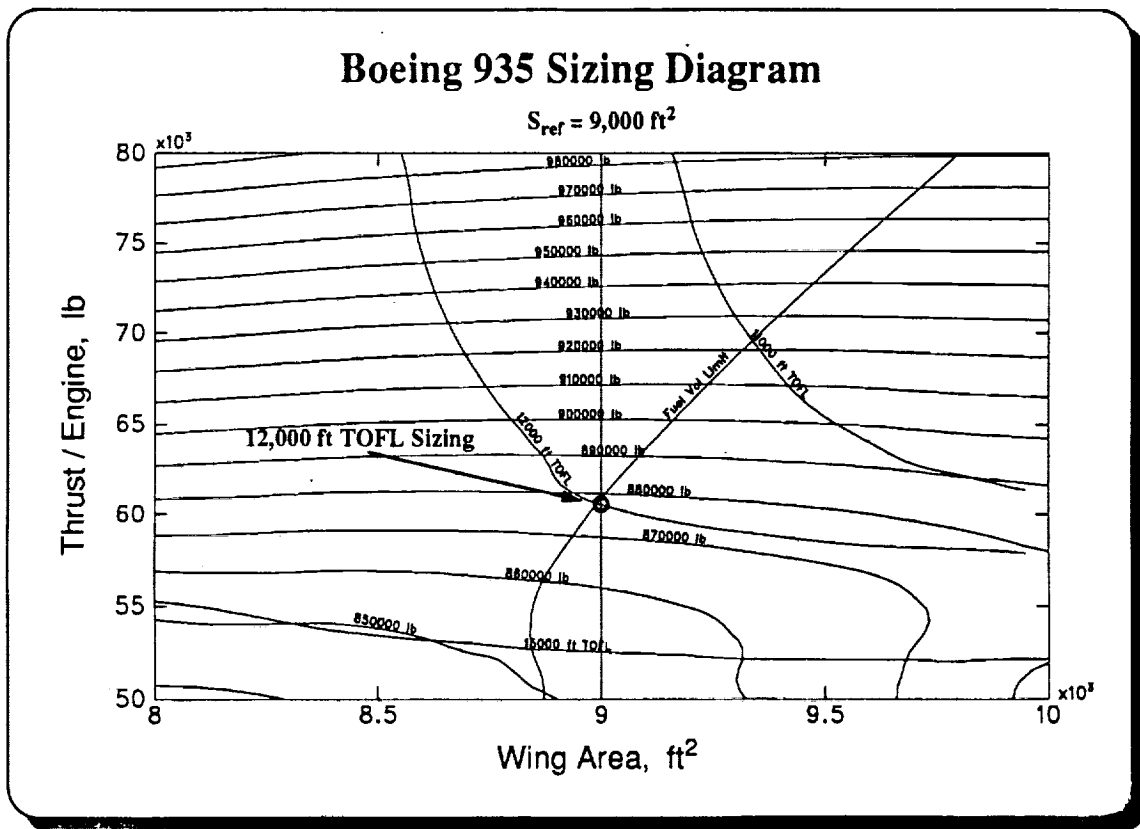
Shown below is a sizing diagram for the Ames Model 2 configuration. The Ames model 2 is an arrow-wing configuration with four underwing engines and an aft mounted tail. The reference wing area is $11,590 \text{ ft}^2$, shown as the vertical line on the diagram, which is close to the $11,690 \text{ ft}^2$ calculated planform area. The Ames Model 2 was designed to cruise at a low-boom Mach number of 2.0 overland and Mach 2.4 overwater. The configuration was designed with the same engine concept as the Ames Model 1, and the year 2005 MFTF engine nacelles are again relocated 5 ft forward. This replacement of the original nacelles yields an increase in wave drag of 1.5 counts and 0.7 counts at the cruise Mach numbers of 2.0 and 2.4, respectively. The maximum lift-to-drag ratio at an altitude at 40,000 ft is 8.4 at Mach 2.4 and 8.5 at Mach 2.0. As illustrated in the diagram below, the vehicle can be sized at the intersection of the design wing reference area and the 11,000 ft TOFL constraint line with a thrust per engine of approximately 80,000 lb. This sizing results in a TOGW of 1,013,600 lb and burns 473,500 lb of fuel for the mission. Sizing on the 12,000 ft TOFL constraint line requires 70,250 lb of thrust per engine. This vehicle has an estimated TOGW of 960,900 lb and burns 446,100 lb of fuel. The configuration that results from the thrust-to-weight ratio equal to 0.25 sizing requires only 57,200 lb of thrust and weighs 915,100 lb at takeoff with a fuel burn of 430,600 lb, but has a TOFL of 15,500 ft. The configuration has more than adequate internal volume to carry 309 passengers for all of the above sizings.



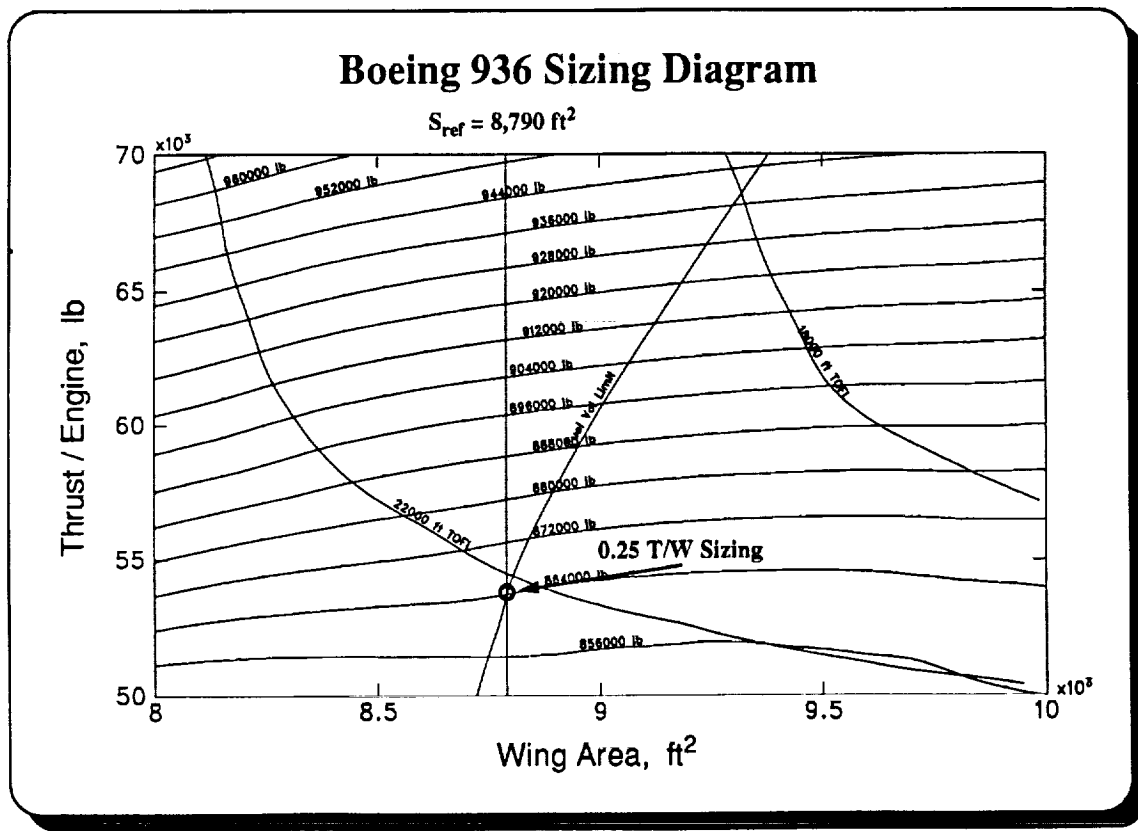
A sizing diagram for the Ames Model 3 low-boom HSCT configuration is illustrated below. This single lifting surface configuration has a reference wing area of 10,040 ft², indicated by a vertical line on the diagram. The calculated planform area is 10,580 ft². The concept was designed for low-boom cruise at Mach 1.7 overland, and Mach 2.4 overwater. The configuration features some rather complex and pronounced shaping of the fuselage immediately aft of the wing for sonic-boom signature tailoring; however, the incorporation of the much larger year 2005 MFTF engine nacelles 5 ft forward of the original nacelle positioning would almost certainly compromise the function of this shaping. The larger MFTF nacelles increased the configuration's wave drag by 2.3 counts at Mach 1.7 and 3.2 counts at Mach 2.4. This results in a maximum lift-to-drag ratio of 9.6 and 8.9 at Mach numbers 1.7 and 2.4, respectively. Having a low aspect ratio, highly-swept wing, but lacking a horizontal tail or canard to function as a trimming surface, the configuration is hampered by a low-speed lift deficit. As a result, the configuration cannot meet the desired takeoff field length requirements at any engine size for the design wing area and mission. When sized to a thrust-to-weight ratio of 0.25, the vehicle has a TOGW of approximately 925,200 lb at an engine size of 57,900 lb thrust per engine. This vehicle sizing point is indicated on the diagram below; and at this size, the vehicle consumes 452,600 lb of mission trip fuel. The configuration as analyzed has internal volume adequate for 309 passengers and 512,000 lb of fuel for trip fuel and reserves. The estimated TOFL for the configuration is over 20,000 ft.



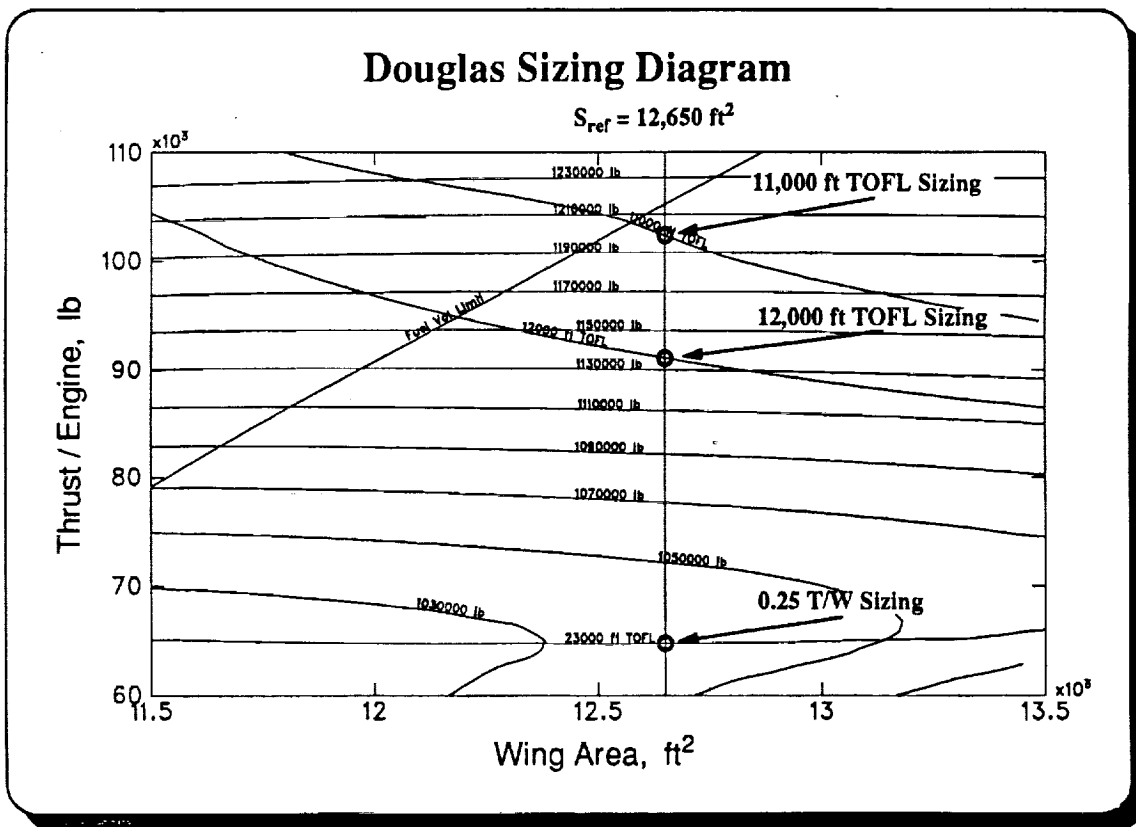
Shown below is the sizing diagram for Boeing's model 935 configuration. The 935 has an arrow wing with aft mounted horizontal tail configuration layout. The reference wing area of $9,000 \text{ ft}^2$ for this design is represented by the vertical line on the sizing diagram. Calculated planform area for this concept differs significantly at $9,710 \text{ ft}^2$. The original Boeing 935 nacelles are within 0.01 ft of the year 2005 MFTF engine nacelle length and, therefore, the original nacelle longitudinal location is easily preserved. However, the replacement nacelles are lowered 0.3 ft to allow for the increased diameter of the MFTF nacelles. The replacement of the original propulsion system engine nacelles results in a wave drag increase of 2.0 counts at Mach 2.4 and 3.2 counts at the low-boom cruise Mach number of 1.7, resulting in maximum lift-to-drag ratios at 40,000 ft of 8.9 and 9.6, respectively. As shown in the diagram below, the 11,000 ft TOFL constraint line nearly asymptotes the designed wing area and does not allow for a reasonably sized vehicle. However, as marked by the sizing point, the 12,000 ft TOFL constraint can be met for a thrust level of 60,700 lb per engine at the design wing area. This vehicle sizing results in a TOGW of 876,700 lb and a mission fuel burn of 417,300 lb. The estimated passenger load for this vehicle is 300, and the required fuel volume with reserves is 476,100 lb. For the thrust-to-weight ratio equal to 0.25 sizing, the thrust level drops to 53,300 lb per engine for a resultant TOGW of 853,900 lb. This lighter vehicle requires 10,000 lb less fuel capacity which allows 2 more passengers on board, and has an estimated 14,500 ft TOFL.



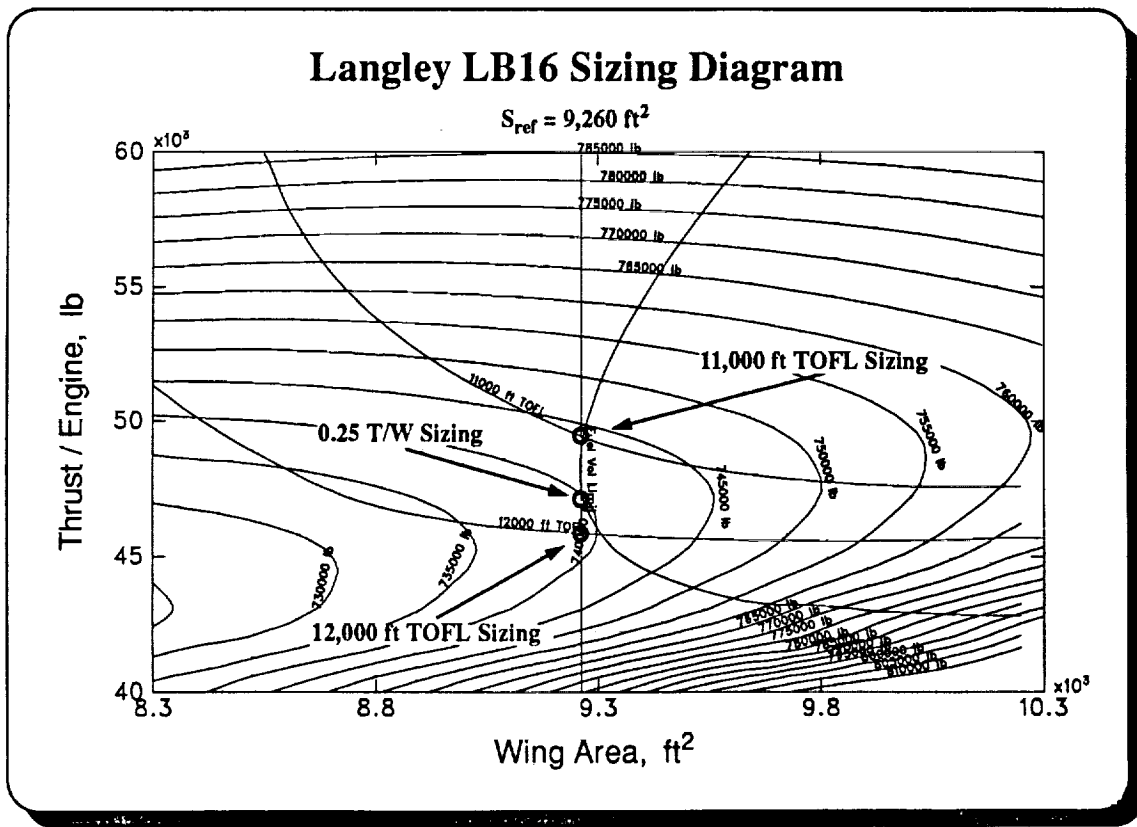
The sizing diagram for the Boeing 936 low-boom concept is presented below. The 936 configuration layout is similar to the Boeing 935, but has higher inboard and outboard wing sweep, less span, and a lower wing reference area of 8,790 ft². The calculated planform area is 9,340 ft². As with the 935 design, the variation between the original and replacement engine nacelles is small. As a result, the longitudinal position is preserved, and the nacelles are again lowered 0.3 ft. The larger year 2005 MFTF engine nacelles cause a wave drag increase of 1.9 counts at Mach 2.4 and 3.1 counts at the reduced boom cruise Mach number of 1.7 providing maximum lift-to-drag ratios at 40,000 ft of 8.7 and 9.0, respectively. The sizing point shown on the diagram is for the thrust-to-weight ratio equal to 0.25 sizing. This sizing yields a calculated TOGW of 864,300 lb for a thrust level of 54,000 lb per engine. Fuel burn for the mission is 422,200 lb; required fuel volume, 481,000 lb; and passenger load, 303. The TOFL for this vehicle would be over 22,000 ft. Sizing for an 11,000 ft or 12,000 ft TOFL could not be achieved for the design wing area. This model has an efficient high-speed planform; however, the low-speed performance is poor. The estimated low-speed $C_{L\alpha}$ is 0.033, which when combined with the relatively small wing area for this type of vehicle, results in poor takeoff performance.



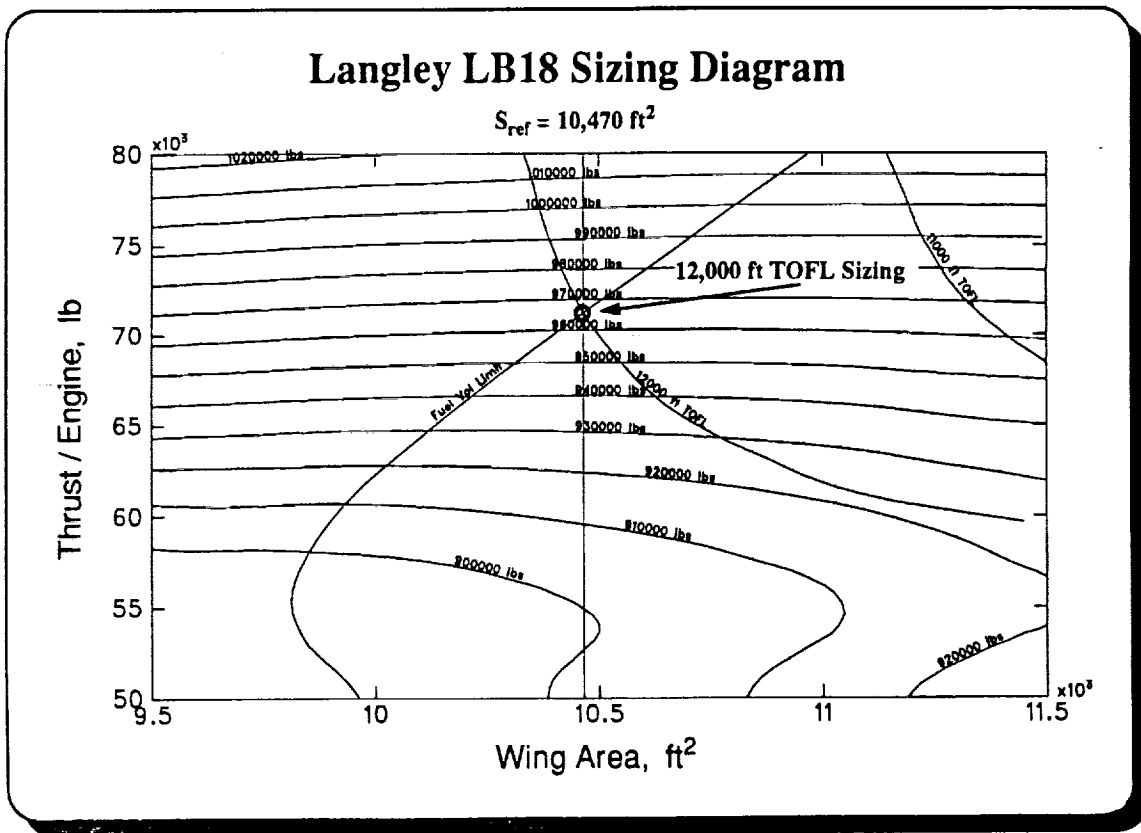
Shown below is the sizing diagram for the Douglas Mach 2.4/1.8 low-boom concept. The Douglas design layout is unique with a bow canard containing a forward-facing flap for sonic-boom shaping. The Douglas-calculated wing reference area of 12,650 ft² (the vertical line on the sizing diagram) correlates well to the 12,710 ft² calculated platform area. The original lateral and longitudinal nacelle placement locations are preserved even though the original Douglas nacelles are nearly 12 ft shorter than the replacement year 2005 MFTF engine nacelles. However, the MFTF nacelles are raised by 0.2 ft to account for the difference in engine diameters. The longer MFTF nacelles cause a significant wave drag increase of 6.0 counts at Mach 1.8, and 4.0 counts at Mach 2.4. The maximum lift-to-drag ratio at 40,000 ft is 9.8 and 8.7 for Mach numbers 1.8 and 2.4, respectively. As seen in the diagram below, the 11,000 ft TOFL constraint line can be met for a thrust of 102,100 lb per engine which results in a 1,197,400 lb vehicle TOGW which includes 573,300 lb of trip fuel. For the 12,000 ft TOFL sizing, the thrust per engine is 91,300 lb, and the resultant TOGW and fuel burn are 1,137,800 lb and 541,000 lb, respectively. When this configuration is sized to have a thrust-to-weight ratio of 0.25, the thrust per engine level drops to 64,700 lb with a TOGW of 1,034,700 lb and fuel consumption of just over 500,000 lb. For this case, the estimated TOFL is 23,000 ft. The Douglas design is the largest configuration in this study and easily carries 309 passengers for all sizings. In fact, this study's first-order passenger count estimation indicates that the Douglas-reported value of 300 passengers (ref. 5) is very conservative. Since the current method correlates well with the reported Boeing passenger count numbers (ref. 4), a fundamental difference between the companies' passenger estimation methods may exist.



A sizing diagram for the Langley LB16 low-boom configuration is shown below. This single lifting surface configuration with four wing-mounted engines has a reference wing area of $9,260 \text{ ft}^2$, nearly equal to the calculated planform area of $9,280 \text{ ft}^2$. This vehicle was designed to carry 250 passengers at a low-boom Mach number of 1.6 overland and Mach 2.0 overwater. Therefore, the results for this configuration are that of a Mach 2.0 overwater mission, and may be difficult to compare to the other Mach 2.4 configuration results. The year 2005 MFTF engine nacelles are over 15 ft longer than the original turbine-bypass engine nacelles and are, therefore, relocated 9.6 ft forward to prevent an excessive nacelle overhang. Smaller position changes were also required in the lateral and vertical planes. This significant nacelle relocation would likely negate the sonic-boom shaping of the vehicle. An increase in wave drag of 1.8 counts and 4.0 counts at the cruise Mach numbers of 2.0 and 1.6, respectively, results from the installation of the larger MFTF nacelles. The maximum lift-to-drag ratios at an altitude of 40,000 ft are 10.8 at Mach 1.6 and 10.0 at Mach 2.0. As illustrated on the diagram below, the vehicle satisfies the 11,000 ft TOFL constraint for 49,400 lb of thrust per engine resulting in a TOGW of 743,100 lb. The 12,000 ft TOFL vehicle sizes at a thrust per engine level of 45,800 lb resulting in a TOGW of 738,800 lb. At a thrust-to-weight ratio of 0.25, the Langley LB16 sizes at a per engine thrust of 46,200 lb corresponding to a TOGW of 738,700 lb. The estimated TOFL for this sizing is 11,845 ft. The approximate 357,000 lb fuel burn varies relatively little between these sizings providing the same 252 passenger count and 405,000 lb total fuel volume requirement for each vehicle.



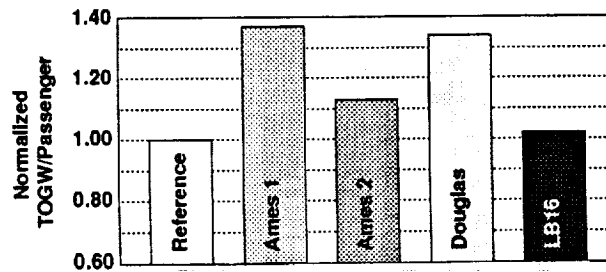
The sizing diagram for the last low-boom configuration to be presented, Langley's LB18, is shown below. The wing reference area is $10,470 \text{ ft}^2$, nearly identical to the $10,500 \text{ ft}^2$ calculated planform area. The aft-fuselage nacelle placement for this single lifting surface configuration prohibits any favorable nacelle interference lift contributions, and fuselage structural penalties are incurred. The magnitude of the weight penalties assessed for this unconventional nacelle placement may be over- or underestimated, which could cause a relative difference to the other configuration analyses. Because of the nacelle locations on the aft fuselage, the original longitudinal positions of the nacelles are easily maintained for the year 2005 MFTF engine nacelles. The lateral and vertical position of the MFTF nacelles are changed only slightly to allow for the relative diameter difference. Replacing the original propulsion system engine nacelles results in a significant wave drag increase of 5.0 counts at Mach 2.4 and 9.7 counts at the reduced boom cruise Mach number of 1.8 with resulting maximum lift-to-drag ratios of 8.7 and 9.2, respectively. The trailing-edge flaps for this design cannot be fully utilized for low-speed lift augmentation (because of little trim authority) which contributes to its inability to meet an 11,000 ft TOFL at its design wing area. However, the 12,000 ft TOFL constraint may be met for 71,400 lb of thrust per engine with a fuel consumption of 464,800 lb resulting in a TOGW of 966,600 lb. The 530,700 lb fuel volume requirement of this case allows for the transport of only 252 passengers. When sized to a thrust-to-weight ratio of 0.25, the thrust per engine drops to 56,800 lb resulting in a 908,600 lb TOGW and a 440,500 lb fuel burn. This significantly down-sized vehicle requires 31,000 lb less fuel volume which allows for 8 additional passengers and has an estimated 13,500 ft TOFL.



Summary characteristics are tabulated below for the configurations which could meet an 11,000 ft balanced TOFL requirement while carrying maximum passenger loads of up to 309. The reference configuration is allowed to size at its optimum wing area while the low-boom configurations are at their originally reported reference area as shown on the previously presented sizing diagrams. The wing area given below, however, is not the configuration's reference area, but the consistently calculated planform area, allowing for a meaningful comparison of actual concept size. For each sized configuration the overwater maximum lift-to-drag ratio at 40,000 ft, takeoff gross weight, passenger count, block time, and final engine thrust are shown. Since the TOGWs are difficult to compare for varying passenger loads, the TOGW divided by the number of passengers is presented. Finally, this ratio is normalized to the reference configuration and presented graphically to provide one possible rating of the configurations for which the percent difference is easily identifiable. The weight penalty per passenger for the low-boom configurations is seen to vary from 2 percent for the Langley LB16 design to over 30 percent for the Ames Model 1 and Douglas concepts. Though the weight penalty per passenger is small for the Langley LB16 configuration, it operates overwater at Mach 2.0 and incurs a block time penalty which does not enter into the presented normalized rating. Other ratings could be used which include block time and, therefore, penalize the reference and LB16 designs relative to the other low-boom designs.

11,000 ft TOFL Constrained Sizings

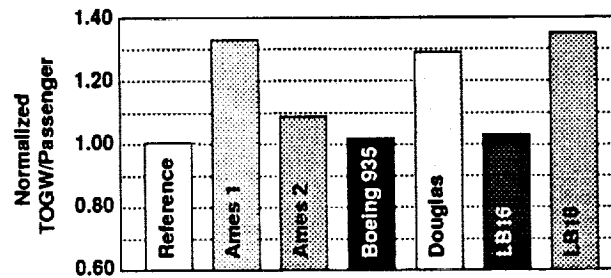
Configuration Identification	Wing Area (ft ²)	L/D Max Overwater	TOGW (lb)	Pass #	Block Time (hr)	Thrust per Engine (lb)	TOGW / Pass #	Normalized Rating
Reference	9,760	7.9	895,600	309	5.74	57,500	2,898	1.00
Ames Model 1	10,600	8.1	1,032,400	260	4.49	107,400	3,971	1.37
Ames Model 2	11,690	8.4	1,013,600	309	4.43	80,000	3,280	1.13
Douglas	12,710	8.7	1,197,400	309	4.55	102,100	3,875	1.34
Langley LB16	9,280	10.0	743,100	252	5.26	49,400	2,949	1.02



It is thought that the 11,000 ft TOFL constraint may be too severe at the elevated TOGWs which result in part from replacing the original configurations' propulsion systems. Therefore, the TOFL constraint is relaxed to 12,000 ft for the table of sized configuration characteristics presented below. The tabulated and graphed parameters are identical to the ones shown on the previous page. As for the 11,000 ft TOFL sizings, the percent range of weight penalty per passenger varies from 2 to over 30 percent. The Boeing 935 design is the most efficiently rated low-boom design, closely followed by the Langley LB16. In addition, the Ames Model 2 has less than a 10 percent penalty. Two of the three low-boom configurations showing the greatest penalty, the Douglas and Langley LB18 designs, incurred the largest wave drag increase resulting from the incorporation of the year 2005 MFTF engine nacelles. This partially accounts for their relatively poor performance levels. The poor performance of the Ames Model 1 may be attributable to the inefficiencies associated with a trijet configuration layout that is constrained by takeoff performance characteristics.

12,000 ft TOFL Constrained Sizings

Configuration Identification	Wing Area (ft ²)	L/D Max Overwater	TOGW (lb)	Pass #	Block Time (hr)	Thrust per Engine (lb)	TOGW / Pass #	Normalized Rating
Reference	9,200	7.9	881,000	309	5.72	55,500	2,851	1.00
Ames Model 1	10,600	8.1	999,500	264	4.52	95,000	3,786	1.33
Ames Model 2	11,690	8.4	960,900	309	4.45	70,300	3,110	1.09
Boeing 935	9,710	8.9	876,700	300	4.66	60,700	2,922	1.02
Douglas	12,710	8.7	1,137,800	309	4.57	91,300	3,682	1.29
Langley LB16	9,280	10.0	738,800	252	5.28	45,800	2,932	1.03
Langley LB18	10,500	8.7	966,600	252	4.58	71,400	3,836	1.35



As mentioned previously, a 0.25 thrust-to-weight ratio sizing is presented for each design to allow for a relative comparison of the low-boom configurations independent of their takeoff characteristics. These arbitrary sizings do not represent closed vehicles. Therefore, the normalized ratings are not presented for this sizing method and care should be exercised when comparing the numbers below. As expected, all of the low-boom designs exhibit better supersonic-cruise aerodynamics than the reference configuration because of their aggressive arrow wing planforms. However, the combination of higher empty weights and poorer low-speed performance combine to totally negate this supersonic aerodynamic advantage when TOGW per passenger is considered. The effect of the reference configuration flying at only 0.9 Mach number overland is clearly seen in increased block time. The reference configuration arrives at the airport a full hour after most Mach 2.4 overwater low-boom configurations, and even arrives 25 minutes after the Mach 2.0 Langley LB16. Thus, a significant advantage in block time is achieved for even small percentages of low-boom supersonic overland flight.

Thrust-to-Weight Ratio = 0.25 Sizings

Configuration Identification	Wing Area (ft ²)	L/D Max Overwater	TOGW (lb)	Pass #	Block Time (hr)	Thrust per Engine (lb)	TOFL (ft)	TOGW / Pass #
Reference	8,300	7.9	873,000	309	5.69	54,600	13,500	2,825
Ames Model 1	10,600	8.1	988,200	263	4.57	82,200	15,100	3,757
Ames Model 2	11,690	8.4	915,100	309	4.52	57,200	15,500	2,961
Ames Model 3	10,580	8.9	925,200	309	4.71	57,900	20,100	2,994
Boeing 935	9,710	8.9	853,900	302	4.69	53,300	14,500	2,827
Boeing 936	9,340	8.7	864,300	303	4.69	54,000	22,200	2,852
Douglas	12,710	8.7	1,034,700	309	4.69	64,700	23,000	3,349
Langley LB16	9,280	10.0	738,700	252	5.28	46,200	11,800	2,931
Langley LB18	10,500	8.7	908,600	260	4.67	56,800	13,500	3,495

A consistent performance analysis of eight low-boom configurations and a reference configuration has been completed. The reference and low-boom configurations were designed with vastly differing propulsion systems. Therefore, all of the concepts' engines were replaced with a single representative year 2005 EIS MFTF engine to ensure a consistent evaluation. This propulsion system raised the absolute TOGW values for all of the configurations slightly, but the relative difference between the TOGW numbers is thought reliable. The normalized TOGW per passenger rating of the analyzed configurations indicates that selected low-boom concepts have made significant progress towards achieving the performance level of non-boom constrained designs. However, the TOGWs of the low-boom configurations are heavier than assumed during the original design process. At the TOGWs calculated in this study, another design cycle would be required to ensure successful low-boom shaping. During the next design cycle, careful attention should be given to the low-speed high-lift arena to prevent large TOGW penalties due to poor low speed aerodynamics. The design cycles required to close the gap between the assumed TOGWs of the initial low-boom design process and the final calculated TOGWs of this study emphasize the importance of a coordinated systems analysis during sonic-boom design studies. Mission parameters, technology assumptions, and analysis methodologies should be agreed upon for future design efforts. Additionally, it was observed that supersonic overland flight offers large block time (and, therefore, economic) advantages even when the assumed overland cruise segment is a small percentage of the overall mission.

Conclusions

- ❖ Selected low-boom designs achieved a TOGW per passenger only slightly higher than the reference configuration. However, the low-boom TOGWs are heavier than originally assumed and the configurations would require an additional design cycle to ensure successful low-boom shaping.
- ❖ Most highly-swept low-boom planforms are challenged in the high-lift, low-speed regime.
- ❖ Supersonic flight overland offers significant block time (and, therefore, economic) advantages.

Lessons Learned

These results emphasize the importance of a coordinated systems analysis during sonic-boom design studies. Mission parameters, technology assumptions, and methodologies should be agreed upon for future design efforts.

References

1. Goodsell, Aga M.; Lee, Christopher A.; and Hicks, Raymond M.: *Use of CFD in the Design of Low Sonic Boom Aircraft*. NASA CP 10133, 1993.
2. Cliff, Susan E.: *On the Design and Analysis of Low Sonic Boom Configurations*. NASA CP 10133, 1993.
3. Cheung, Samson: *Design Process of Ames Wind-Tunnel Model 3*. NASA CP 10133, 1993.
4. Haglund, George T.: *Low Sonic Boom Studies at Boeing*. NASA CP 10133, 1993.
5. Morgenstern, John M.: *Low Sonic Boom Design and Performance of a Mach 2.4/1.8 Overland High Speed Civil Transport*. NASA CP 3173, 1992.
6. Baize, Daniel G.; and Coen, Peter G.: *A Mach 2.0 / 1.6 Low Sonic Boom High-Speed Civil Transport Concept*. NASA CP 10133, 1993.
7. Mack, Robert J.: *Low-Boom Aircraft Concept with Aft-Fuselage-Mounted Engine Nacelles*. NASA CP 10133, 1993.
8. Plencner, Robert M.; and Snyder, Christopher A.: *NNEP89 - The Navy/NASA Engine Program (NNEP89) - A User's Manual*. NASA TM -105186, 1991.
9. Fenbert, James W.; Ozoroski, L. P.; Geiselhart, K. A.; Shields, E. W.; and McElroy, M. O.: *Concept Development of a Mach 2.4 High-Speed Civil Transport*. NASA/TP-1999-209694, 1999.
10. Sommer, Simon C.; and Short, Barbara J.: *Free-Flight Measurement for Turbulent-Boundary-layer Skin Friction in the Presence of Severe Aerodynamic Heating at Mach Numbers From 2.8 to 7.0*. NACA TN 3391, 1955.
11. Harris, Roy V., Jr.: *An Analysis and Correlation of Aircraft Wave Drag*. NASA TM X-947, 1964.
12. Carlson, Harry W.; and Darden, Christine M.: *Validation of a Pair of Computer Codes for Estimation and Optimization of Subsonic Aerodynamic Performance of Simple Hinged-Flap Systems for Thin Swept Wings*. NASA TP 2828, 1988.

References, cont.

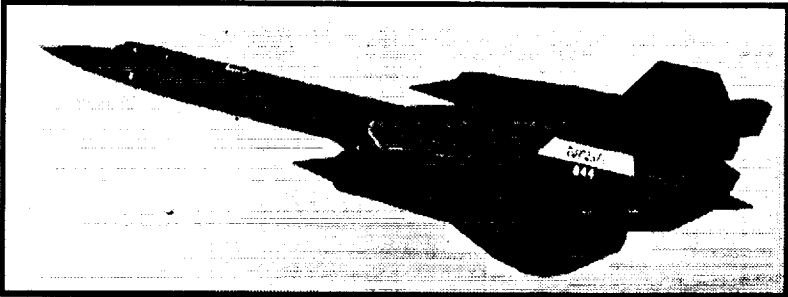
13. Carlson, Harry W.; and Mann, Michael J.: *A Survey and Analysis of Research on Supersonic Drag-due-to-lift Minimization with Recommendations for Wing Design*. NASA TP 3202, 1992.
14. Bonner, E.; Clever, W.; and Dunn, K.: *Aerodynamic Preliminary Analysis System II, Part I- Theory*. 1988.
15. Middleton, W. D.; Lundry, J. L.; Coleman, R. G.: *A Computational System for Aerodynamic Design and Analysis of Supersonic Aircraft. Part 1 -- General Description and Theoretical Development*. NASA CR 3351, 1980.
16. Middleton, W. D.; Lundry, J. L.; Coleman, R. G.: *A Computational System for Aerodynamic Design and Analysis of Supersonic Aircraft. Part 2 -- User's Manual*. NASA CR 3352, 1980.
17. Carlson, Harry W.; Darden, Christine M.; and Mann, Michael J.: *Validation of a Computer Code for Analysis of Subsonic Aerodynamic Performance of Wings With Flaps in Combination With a Canard or Horizontal Tail and an Application to Optimization*. NASA TP 2961, 1990.
18. McCullers, L. A.: *Aircraft Configuration Optimization Including Optimized Flight Profiles. Recent Experiences in Multidisciplinary Analysis and Optimization*. Jaroslaw Sobieski, compiler, NASA CP-2327, Part 1, 1984, pp. 395-412.
19. Killian, M. J.: *IDAS Configuration Definition Module User's Manual (CDM)*. NA-82-467 (Tasks II.D and III.D of Contract F33615-80-C-3012), Volume II, Rockwell International, 1992.

Airplane design studies have developed configuration concepts that may produce lower sonic boom annoyance levels (Ref. 1). Since lower noise designs differ significantly from other HSCT designs, it is necessary to accurately assess their potential before HSCT final configuration decisions are made. Flight tests to demonstrate lower noise design capability by modifying an existing airframe have been proposed for the Mach 3 SR-71 reconnaissance airplane (Ref. 2, 3).

To support the modified SR-71 proposal, baseline in-flight measurements were made of the unmodified aircraft. These measurements of SR-71 near-field sonic boom signatures were obtained by an F-16XL probe airplane at flightpath separation distances ranging from approximately 740 to 40 ft. This paper discusses the methods used to gather and analyze the flight data, and makes comparisons of these flight data with CFD results from Douglas Aircraft Corporation and NASA Langley Research Center. The CFD solutions were obtained for the near-field flow about the SR-71, and then propagated to the flight test measurement location using the program MDBOOM (Ref. 4).

The CFD and MDBOOM data from Douglas Aircraft Corporation in this paper are covered by limited exclusive rights data provisions.

**Measurement of the Basic SR-71
Airplane Near-Field Signature**




**Edward A. Haering, Jr.
Stephen A. Whitmore
L. J. Ehernberger**

**NASA Dryden Flight Research Center
Edwards, California**

**1994 Sonic Boom Workshop
NASA Langley Research Center
June 1-3, 1994**

**DRYDEN
FLIGHT
RESEARCH
CENTER**



The objectives for this flight test are given below. Validation of (present) state-of-the-art design techniques requires closer vertical separations or higher Mach numbers than used for previous experiments (Ref. 5, 6, 7). The SR-71 experiment was conducted to obtain data at distances comparable with those for near-field signatures measured in wind tunnels and at distances near the domain of current CFD solutions at distances approaching 1/3 body length.

Previous in-flight signature measurement has been accomplished by Mullens (Ref. 5), Smith (Ref. 6) and Maglieri et al. (Ref. 7). The Mullens data were 85 to 1770 ft below and 100 to 1420 ft to the side of an F-100 airplane at a Mach number of 1.05. A B-58 bomber airplane was the boom generator for the Smith and the Maglieri investigations. Smith includes data for the F-100 and F-104 airplanes at Mach 1.2 as well as for the B-58 at Mach 1.3 to 1.8 using lateral separation distances from 120 to 425 ft. The investigation was conducted to determine the near-field flow patterns for assessing the danger involved in close-formation flying. Maglieri's data were obtained at distances from 4600 to 9100 ft below and from 1300 to 2000 ft above and below the B-58 operating at Mach numbers between 1.42 and 1.69. Emphasis was on obtaining data to assess lift-volume interaction effects on the near field signature of a delta wing bomber. For all these experiments, the data are either too low in Mach number, not below the generating aircraft, or too far away for the present needs.

D
R
Y
D
E
N

F
L
I
G
H
T


R
E
S
E
A
R
C
H

C
E
N
T
E
R

OBJECTIVES AND BACKGROUND

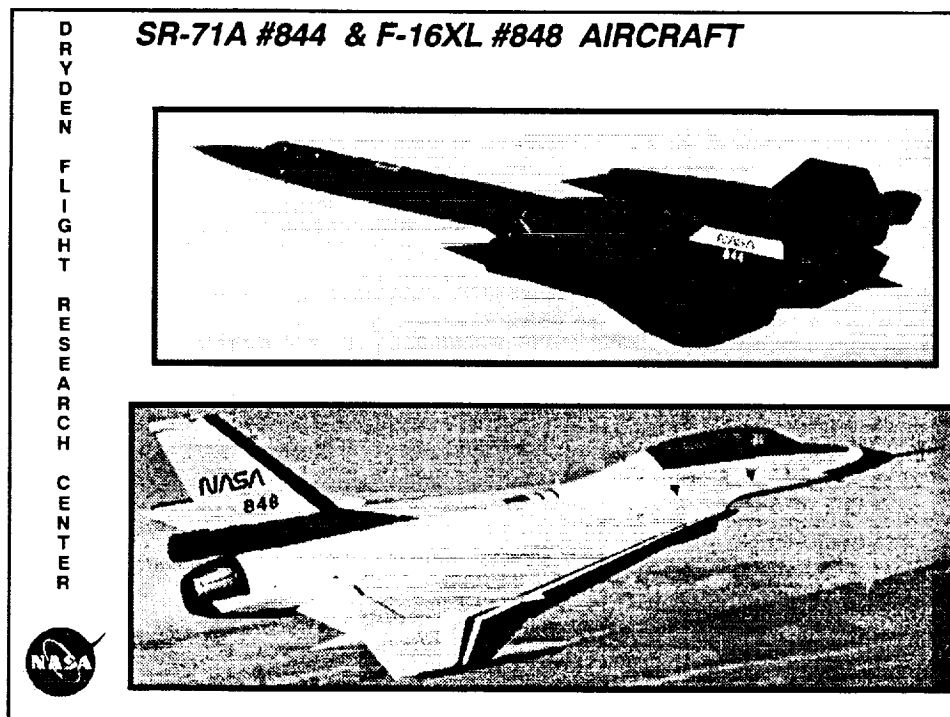
- Determine if near-field measurements possible (as close as 1/3 body length)
- Obtain flight data for CFD / wind tunnel validation
- Obtain baseline data for low boom SR-71 modification
- Study propagation of sonic booms through the atmosphere
- Background: previous work too slow, not below, or too far away

<u>Conductor</u>	<u>Aircraft</u>	<u>Mach</u>	<u>Distance and Position</u>
- Mullens, 1956	F-100	1.05	85'-1770' below 100'-1420' to side
- Smith, 1960	B-58, F-100, F-104	1.2-1.8	120'-425' to side
- Maglieri, 1963	B-58	1.42-1.69	1300'-9100' below 1700'-2000' above



The sonic-boom generator aircraft was an SR-71A, the same airplane proposed for the modified SR-71A experiment. The SR-71A is a delta-wing aircraft designed and built by Lockheed, capable of cruising at Mach 3.2. The aircraft is 107.4 ft (32.73 m) long, has a wing span of 55.6 ft (16.94 m), and is 18.5 ft (5.63 m) high (ground to the top of the rudders when parked). Gross takeoff weight is about 140,000 lb (52253.83 kg), including a fuel weight of 80,000 lb (29859.33 kg). The SR-71A used for this sonic boom experiment is NASA 844, military serial 64-17980, and was manufactured in July 1967 (Ref. 8).

An F-16XL was used to probe the shock signatures of the SR-71A. Two F-16XL aircraft were built by General Dynamics Corp. as prototypes for a derivative fighter evaluation program conducted by the Air Force between 1982 and 1985. The aircraft were developed from basic F-16 airframes. The most notable difference is the delta (cranked arrow) wing, which gives the aircraft a greater range because of increased fuel capacity in the wing tanks and a larger load capability because of increased wing area. The number 2 aircraft, tail number 848, was used in this flight test. The aircraft has a two-seat cockpit, and has a length of 54.2 ft (16.52 m), a wingspan of 34.3 ft (10.45 m), and a height at the vertical tail of 17.7 ft (5.39 m). Its maximum gross weight is 48,000 lb (17915.60 kg) (Ref. 9). Note the conventional flight test noseboom that was used to measure the sonic boom overpressures.




The flight test maneuver description for this experiment is outlined below. For safety, probings were ordered starting with the greatest separation and progressively flying closer. Because of the shock angle of 34° at Mach 1.8, the F-16XL never was directly below the SR-71, even though the flight path of the F-16XL was directly below the SR-71. For the SR-71 to hold this Mach number and altitude, the right engine was in afterburner and the left engine was in military power, resulting in about 1.5° angle of sideslip. Both inlets were started and had nearly identical airflow and engine rpm. The planned data were obtained with the SR-71 in straight and level flight.

The aircraft did have to turn around to remain in the proper airspace. Probes were continued during these turns for practice and additional data, although these data require extra effort for analysis. Turning at constant altitude results in elevated g 's and increased angle of attack. Additional CFD solutions at these elevated angles of attack have not yet been generated. The airdata systems of the two aircraft have not been calibrated at these higher angles of attack. INS errors increase during elevated g 's. The data analysis is also complicated by the nonsteady wind component present in a turn.

According to the pilot of the F-16XL, "The probe aircraft could be repeatedly flown in and out of shocks generated by the SR-71. The shocks were well defined with little additional turbulence. The work load was normal for close formation. The easiest way to determine if the F-16XL was ahead of the (tail) shock was loss of engine noise."

D R Y D E N F L I G H T R E S E A R C H C E N T E R	FLIGHT TEST MANEUVER DESCRIPTION
	• Maneuver sequence
	- SR-71 maintains Mach 1.8, altitude 48,000 ft
	- F-16XL positions at desired distance below, and more than (1.5 x distance below) behind SR-71: now behind tail shock
	- F-16XL accelerates while maintaining altitude separation
	- After clearly ahead of bow shock, F-16XL drops back
	• Because of shock angle, F-16XL is never directly below SR-71
	• F-16XL always has visual contact with SR-71; SR-71 cannot see F-16XL
	• For data in turns, F-16XL remains in vertical body plane of SR-71
	• Pilot comments: safe, work load not excessive, can see shocks



On July 28, 1993, the SR-71 #844 was used to generate sonic booms at a nominal flight condition of Mach 1.8 and 48,000 ft altitude. A total of 22 distinct near field probes were made with the F-16 XL #848, with flightpath separation distances of 40 to 740 ft. These data are summarized at the end of the paper.

No modifications were done to either aircraft and existing instrumentation and resources were used, as listed below. Ground-based radar data gave aircraft separation information, the F-16XL noseboom gave overpressure information, and other aircraft sensors and an atmospheric analysis (Ref. 10) for the flight day were used for the data analysis.

Trajectory reconstruction was used to determine the reference noseboom pressures that would have been measured in the absence of the SR-71. These pressures were then subtracted from the actual pressures to give the overpressures caused by the shocks from the SR-71. The F-16XL pneumatic airdata system has very long lines and large volume, which caused large lag and attenuation for the static pressure measurement and moderate lag and minimal attenuation for the total pressure measurement. These lag-and-attenuation effects were removed by deconvolution, which will be discussed on the next page.

D
R
Y
D
E
N

F
L
I
G
H
T

R
E
S
E
A
R
C
H

C
E
N
T
E
R

EXPERIMENT METHOD

- A total of 22 near field probes of SR-71A made with F-16XL on one flight, 7/28/93
- Separation distances of 40 to 740 ft
- Conventional flight-test instrumentation used:
 - Ground-based radar used for vehicle separation data
 - Noseboom airdata probe on both aircraft
 - INS on both aircraft
 - Atmospheric analysis
- Variation of F-16XL noseboom pressures yields shock measurements
 - Reference pressures determined from trajectory reconstruction
 - Pneumatic lag and attenuation effects removed by deconvolution




The flight data analysis consists of pressure and position determination. The pressure analysis is discussed first. The F-16XL pitot-static pneumatic effects are removed by deconvolution. A series of step-input responses were obtained during ground tests of the airdata system, and a second-order model was fit to these data to give the natural frequency and damping ratio. These values were then extrapolated to the pressure and temperature of the flight condition. The second-order model was then used to amplify and phase shift the data to recover the original pressure time histories at the noseboom orifice location.

The reference pressures are determined as shown below. The first and last few seconds in a signature time history are chosen so they are clearly outside the influence of the SR-71 shocks. It is assumed that the vertical velocity from radar will give a true indication of F-16XL pressure altitude rate as if the SR-71 were not there. The difference between geometric altitude and pressure altitude in the absence of the SR-71 is assumed constant for the entire maneuver. The INS and radar velocity components of each aircraft exhibited differences of up to 50 ft/sec. Both aircraft use the same model of INS. Most of the time these differences could be explained by INS heading discrepancies of 0.4° on the SR-71, and 1.6° on the F-16XL; however, the INS has better dynamic velocity data than the radar. The INS velocities were generally used for the F-16XL data analysis, and constant wind values were chosen to match reference and measured airspeeds at the beginning and end of the signatures. Ambient temperature was determined from the atmospheric analysis, as the SR-71 temperature sensor was inoperative. Each assumption and measurement error adds to the reference pressure error. Because the reference total pressure has more assumptions and measurements than the reference static pressure, the reference static pressure always has less error than the reference total pressure.

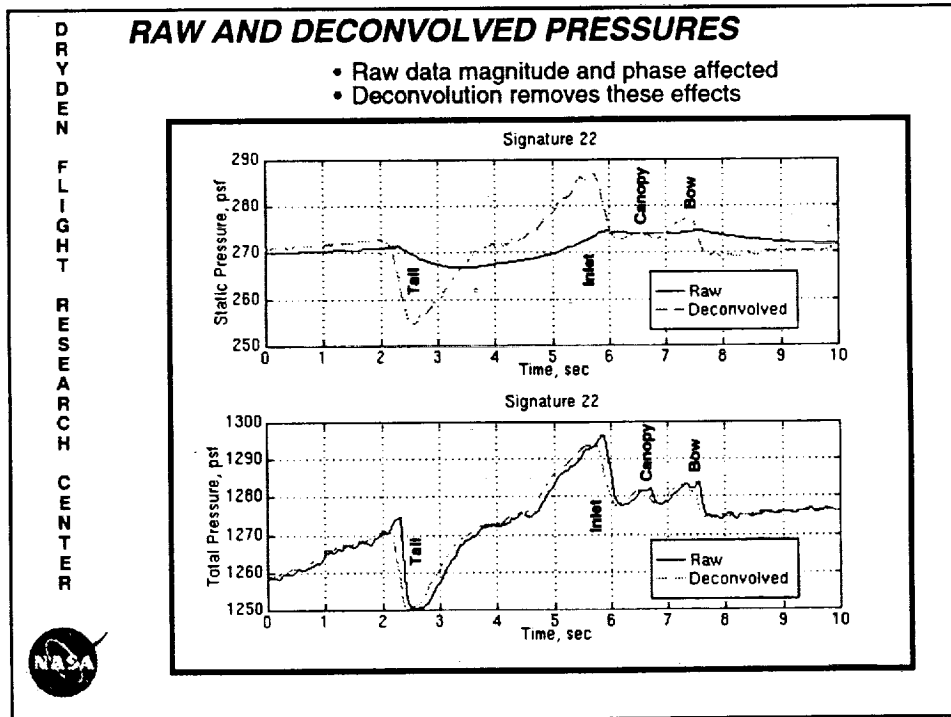
The overpressures from the static pressure and total pressure measurements are determined separately, although the total pressure reference uses the static pressure reference. Good agreement between the two gives confidence of the quality of the analysis.

Relative aircraft position is determined by ground-based radar, as outlined below. Poor data quality is readily apparent for low radar elevation angles and very close aircraft. A few minutes of air-to-air video show good agreement with radar data at moderate elevation angles and moderate aircraft separations. Further comments on radar data errors will be discussed later.

D R Y D E N F L I G H T R E S E A R C H C E N T E R	FLIGHT DATA ANALYSIS
	<ul style="list-style-type: none"> • F-16XL pitot-static pneumatic effects removed <ul style="list-style-type: none"> - Step response of F-16XL pitot-static system measured on ground - 2nd order model fit to data - Frequency and damping extrapolated to flight conditions - Deconvolution applied: lag and attenuation removed
	<ul style="list-style-type: none"> • Reference pressures determined from trajectory reconstruction <ul style="list-style-type: none"> - Radar altitude and atmospheric data give reference Ps - INS / radar velocities and winds give reference airspeed - Reference airspeed and ambient temperature give reference Mach - Reference Mach and reference Ps give reference Pt
	<ul style="list-style-type: none"> • Overpressure is deconvolved pressure minus reference pressure <ul style="list-style-type: none"> - Overpressures from Ps and Pt are separately determined
	<ul style="list-style-type: none"> • SR-71 - F-16XL relative position determined <ul style="list-style-type: none"> - Radar positions subtracted for relative position - Coordinates are in SR-71 stability axes with origin at SR-71 nose-tip - Data below 10° elevation of low quality - Data when aircraft very close is poor because of multipath - Nearly colocated ground-based radars minimize refraction errors
	

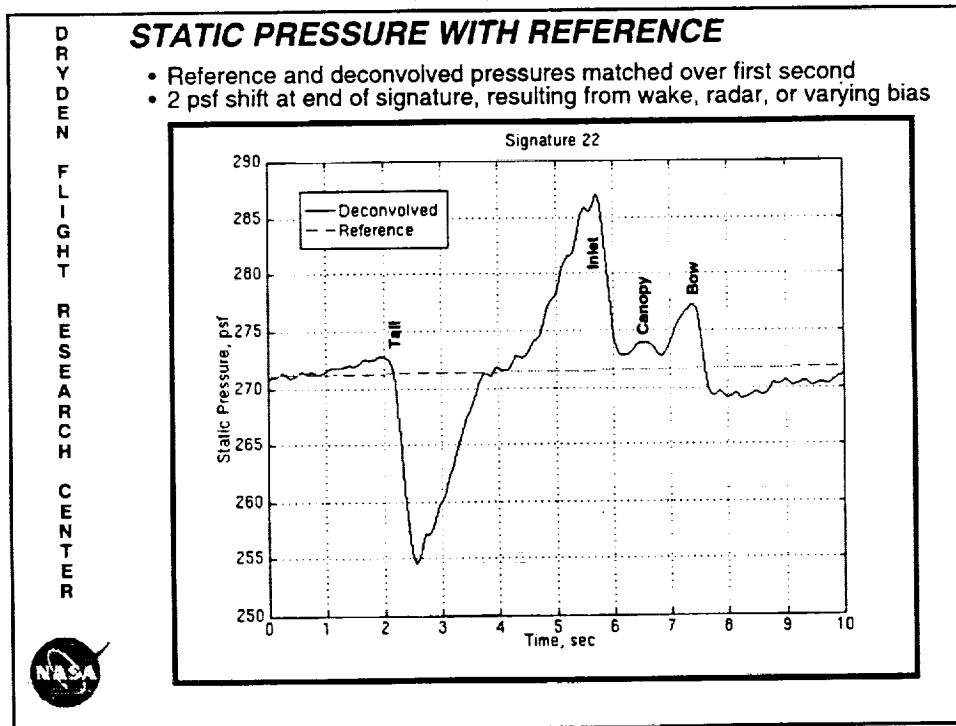
Data from signature 22 will now be shown in detail to illustrate the steps taken in the flight data analysis. This signature was measured from the back to the front of the SR-71. Time histories of raw and deconvolved static and total pressure are shown below. The shock waves generated by the aircraft tail, inlet, canopy, and bow are labeled. The raw static pressure has been greatly attenuated and lagged by the pneumatics of the static pressure line. The raw total pressure is slightly lagged and has slightly higher amplitudes than the deconvolved total pressure. This is because of resonance in the total pressure line of the airdata system.

After the measured pressures have been corrected by deconvolution, the reference pressures need to be determined. These reference pressures are the pressures that the F-16XL would experience in the absence of the SR-71. First, the reference static pressure is calculated as shown on the next page.



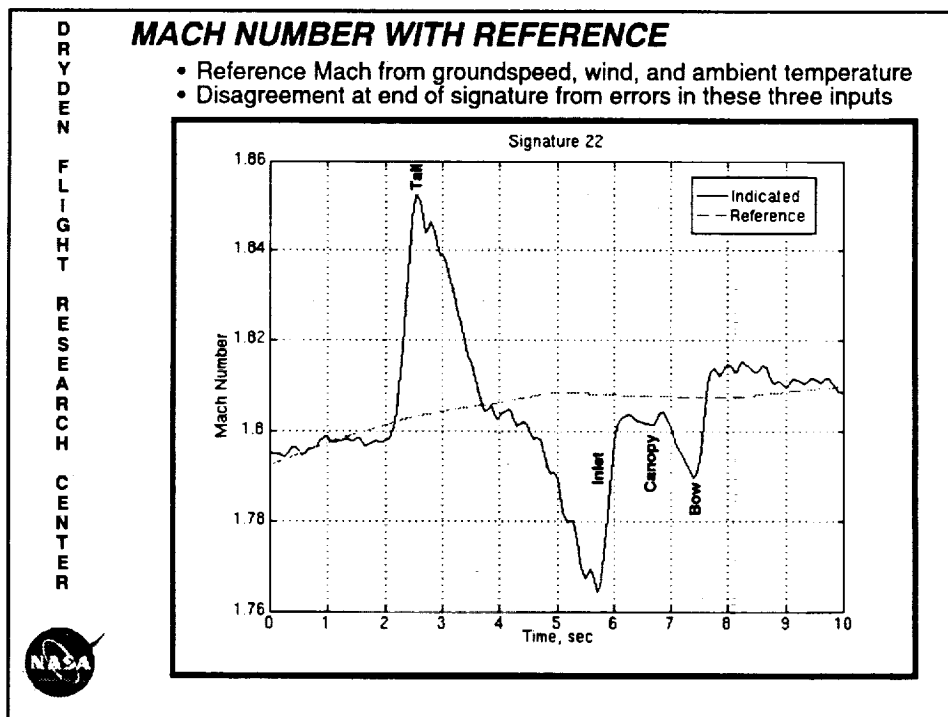
Shown here are the time histories of deconvolved and reference static pressure. Deconvolved static pressure is converted into indicated pressure altitude. The mean difference between geometric altitude from the radar and indicated pressure altitude for the first 20 data points (one second of the time history) is used as a bias to the geometric altitude to give reference pressure altitude from the radar data. Therefore, the two curves below agree very well by definition for the first second of time. The agreement is worse after about 7.6 sec, which is forward of the bow shock. This 2 psf shift may be because of the influence of the wake, or accumulated errors in the radar data, or an altitude bias that is not constant.

The difference between the two curves below is the sonic boom overpressure as measured by static pressure. This will be plotted later after the overpressure measured by total pressure analysis is illustrated.

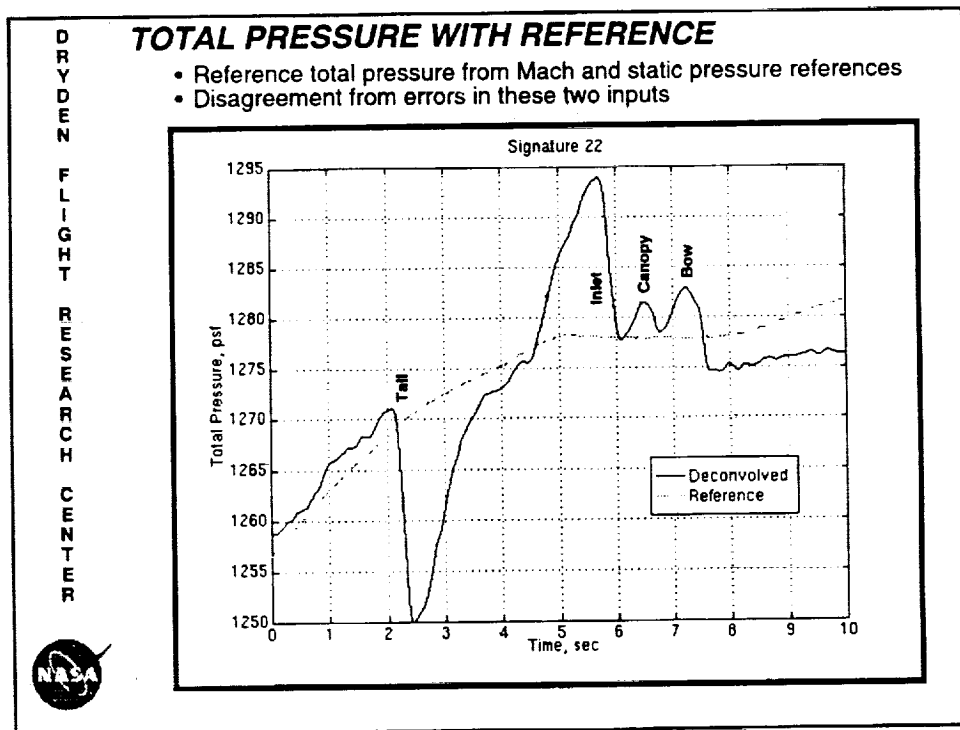


Total pressure is affected by the pressure altitude and Mach number of the aircraft. The reference pressure altitude was determined as described on the previous page. Reference Mach number is determined from Earth-relative velocity from INS or radar, the wind vector, and the ambient temperature. As discussed earlier both the INS and radar velocities have some discrepancies. The INS velocities were generally used with a constant wind value that matched indicated and reference airspeeds outside the influence of the SR-71 shocks. Ambient temperature from the atmospheric analysis was used as discussed earlier. Below is the time history of indicated and reference Mach number for signature 22. Again there is good agreement aft of the tail shock and worse agreement forward of the bow shock. The error in reference Mach number forward of the bow shock could be because of INS velocity errors, an unsteady wind, and an unsteady ambient temperature.

Now that the reference static pressure and reference Mach number are known, the reference total pressure can be determined.



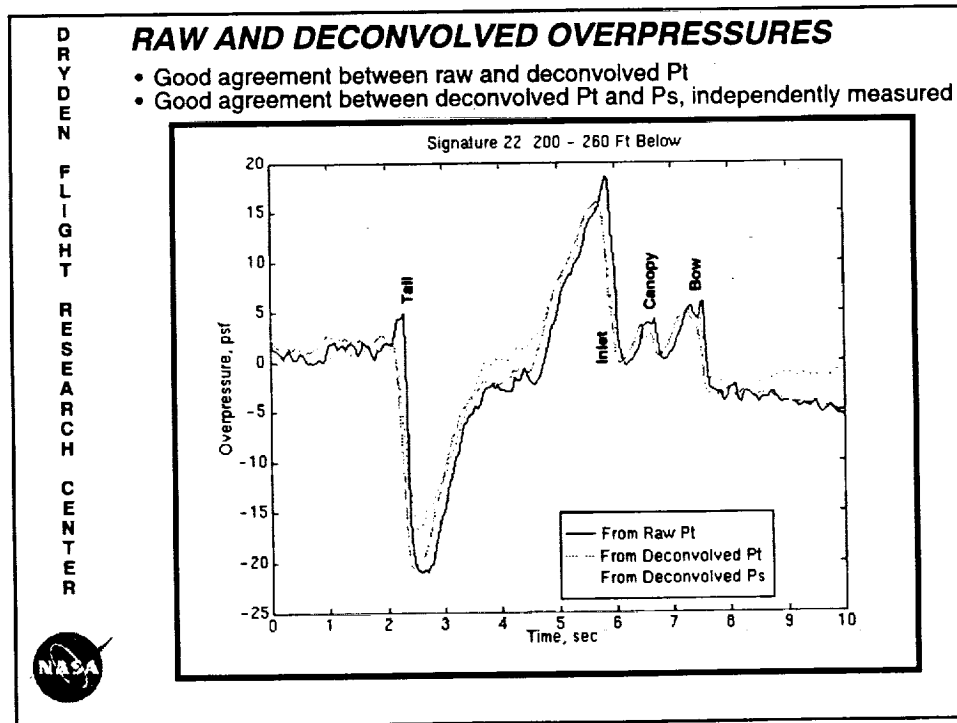
The time history of deconvolved total pressure and reference total pressure is given below. The errors in the reference static pressure and the reference Mach number both contribute to give the disagreement between the deconvolved and reference total pressure curves aft of the tail shock and forward of the bow shock. The difference of these two curves is the sonic-boom overpressure as measured by total pressure.



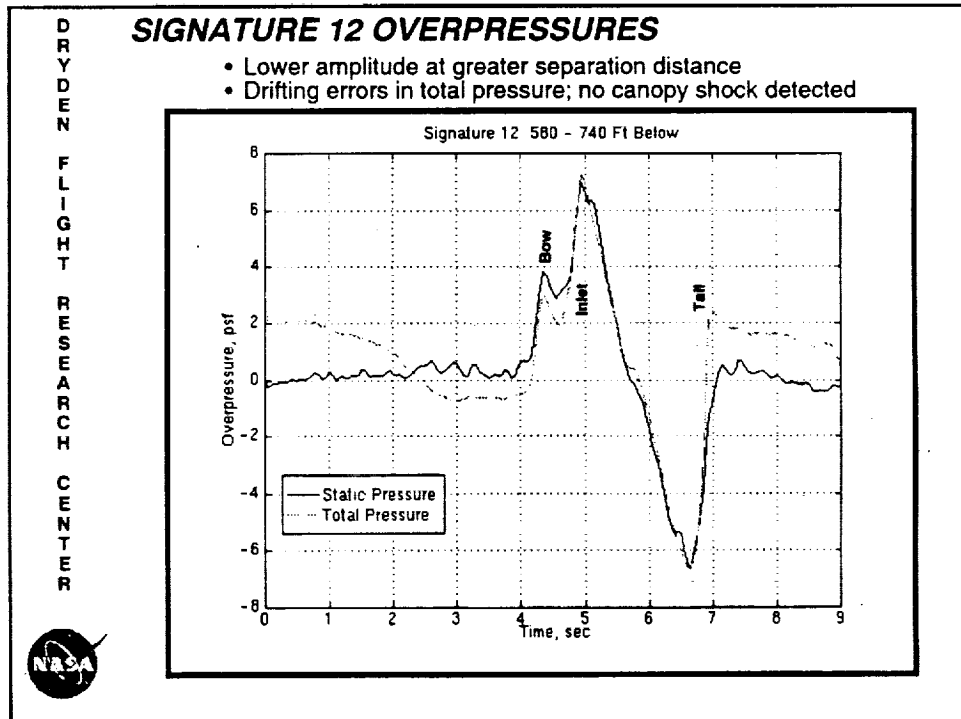
The overpressures can now be plotted from both total pressure, Pt, and static pressure, Ps. For comparison purposes, the overpressure using raw total pressure is also shown in the plot below.

Since the total pressure line does not have a large volume, large lag and attenuation are not expected. This is confirmed by the good agreement of the raw and deconvolved total pressure overpressures; only a slight resonance and lag are evident in the raw data. There is also good agreement between the overpressures from deconvolved total and static pressure, which are independently measured. This is illustrated in the following plots of overpressures from this and other signatures, which give confidence in the deconvolution analysis method used.

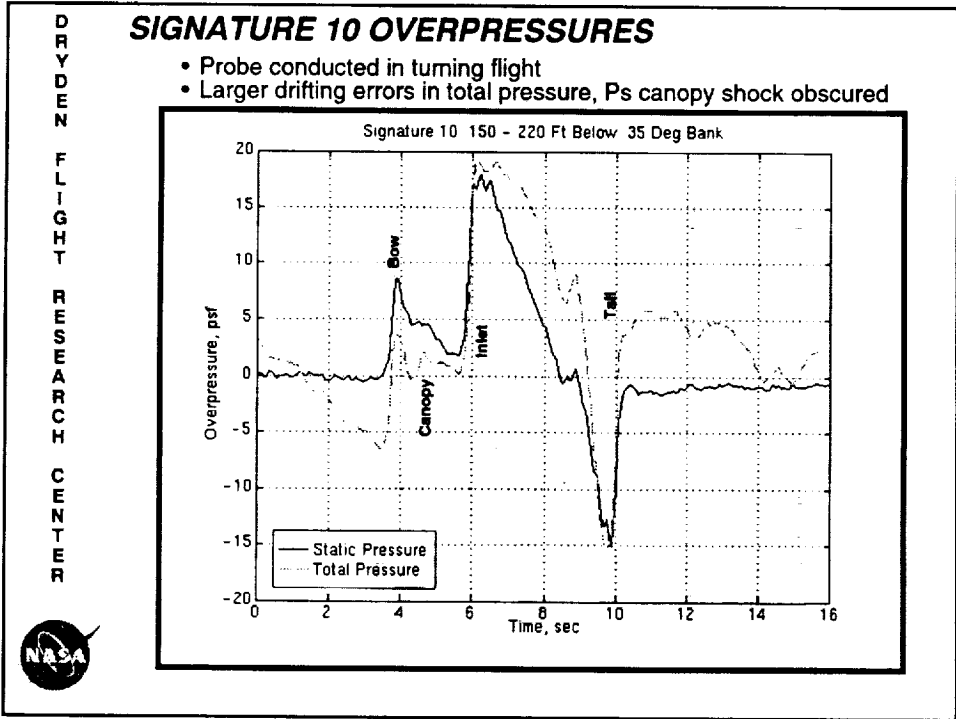
Signature 22 is measured from 200 to 260 ft below the flightpath of the SR-71. The F-16XL made this probe at a relatively fast overtake speed, so there was less time for its trajectory to be influenced by the shocks of the SR-71. Notice that the maximum and minimum overpressures at this separation are about ± 15 psf.



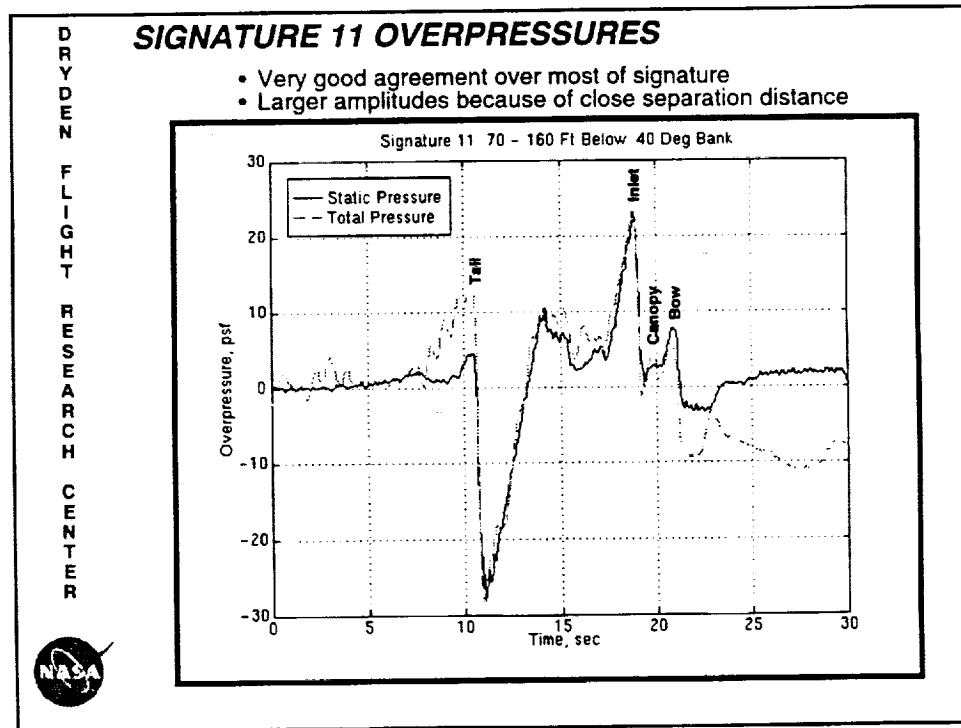
Here in signature 12 the amplitude of the overpressure is about 7 psf. This is much lower than for signature 22 because the separation between aircraft is about three times as large. The probe was from front to back, and this signature does not have a defined canopy shock. This may be because of the relatively fast overtake rate during the probing, because the update rate of the pressure transducers is only about 0.05 sec. The overpressure from total pressure has a drifting error as much as 2 psf.



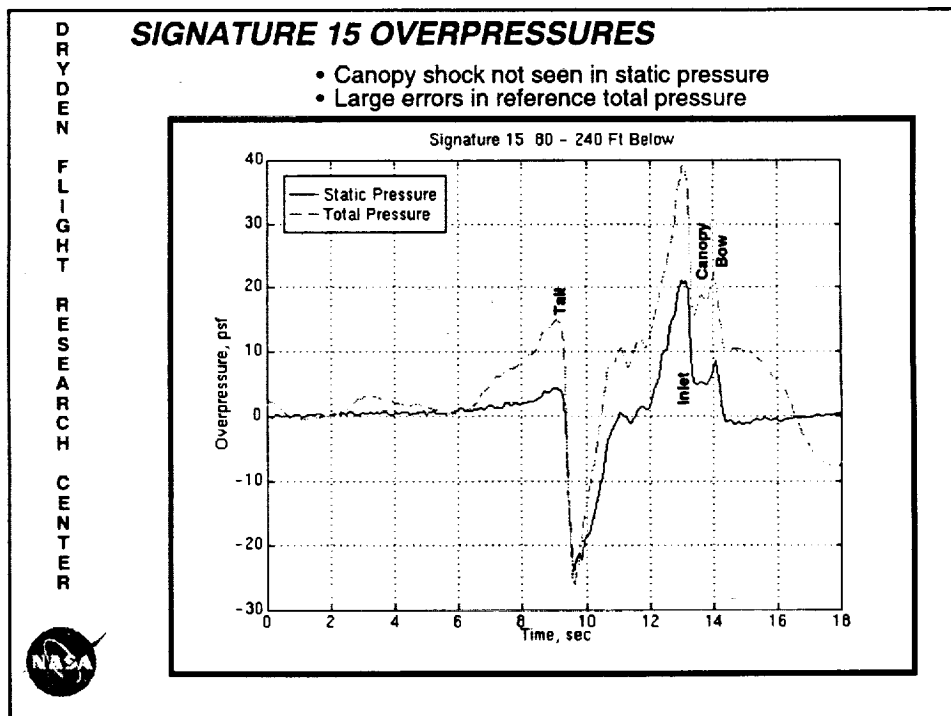
Signature 10 shows overpressures in a 35° bank turn, probed from front to back. The canopy shock can be seen in the total pressure data, but is obscured in the static pressure data. The total pressure reference here is worse than that seen in the previous plots, possibly because of the effect of elevated g's on the INS data and assuming steady winds over a longer time interval.



Signature 11 was also taken in a turn probed back to front. It shows very good agreement between total and static pressure, except for a small region aft of the tail shock and forward of the bow shock. The larger amplitudes correspond to the close flightpath separation distance of 70 to 160 ft.

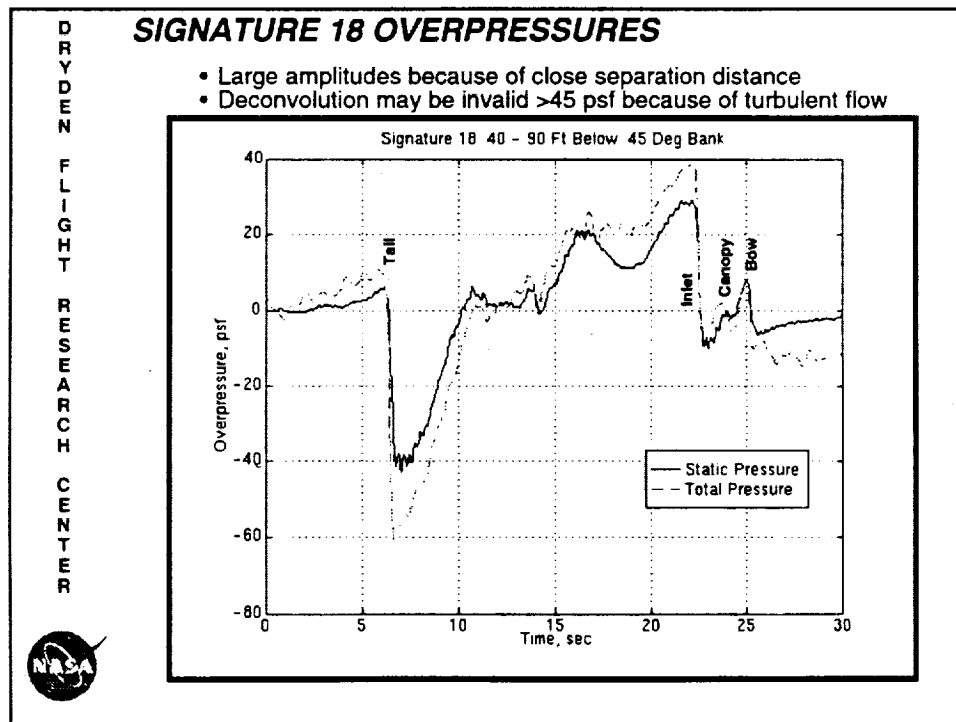


Signature 15 was probed from back to front while flightpath separation varied from 80 to 240 ft. The canopy shock is not seen in the overpressure from static pressure, and there are large errors in the reference total pressure. The static pressure measurement may have been too greatly attenuated for deconvolution to extract the canopy shock. The reference total pressure calculation may have suffered from the aircraft just completing a turn. The overpressure measured from static pressure is still a valid signature, even if some of the fine structure is lost.



The closest probing occurred on signature 18, back to front, with a flightpath separation of 40 to 90 ft. These data were also taken in banked flight. There is a large disagreement between the total and static pressure overpressures at the tail shock and bow shock, which may be explained by limitations of the deconvolution scheme. The second-order model that the pneumatic pitot-static system is assumed to have is only valid for laminar flow through the system. For the altitude and Mach number of the F-16XL, both the total and static pressure lines will experience turbulent flow with pressure spikes greater than about 45 psf. Therefore the deconvolution method is not expected to work for shocks that approach 45 psf overpressure. Of course, some of the disagreement can also be because of reference total pressure errors.

The overpressures for these six signatures have been plotted as a function of time. If the data are plotted as a function of longitudinal distance from the SR-71, they can be compared to data computed from CFD. For the flight to CFD data comparisons, only the overpressure from static pressure flight data will be shown, as it has less errors in its reference. One reason for presenting these overpressure data in the time domain is that it is generally easier to see the features than data plotted as a function of longitudinal distance along the signature. This is because of errors in the radar position data that will be discussed shortly.



The results of the flight data analysis are outlined below. In spite of the fact that the instrumentation was not optimum for sonic boom measurement and some sensors had significant problems, the techniques of deconvolution and trajectory reconstruction were able to extract very good near-field sonic boom data from the static pressure measurements. Although some of the overpressures measured from total pressure had significant biases, the general shape of the signature and the intensity of the shocks could still be seen.

D
R
Y
D
E
N

F
L
I
G
H
T

R
E
S
E
A
R
C
H

C
E
N
T
E
R

FLIGHT DATA RESULTS

- All 22 signatures analyzed
- Total pressure
 - Good response
 - Some slowly drifting biases remain after trajectory reconstruction
- Static pressure
 - Large pneumatic lag
 - Deconvolution successfully removes pneumatic effects for $\Delta P < 45$ psf
 - Easier trajectory reconstruction task to remove altitude effects
- Shock strengths from independent static and total pressures agree well
- Signatures show structure from various aircraft components
- Signatures decrease in amplitude and increase in length with increasing separation
- Radar data still have some unexplained biases



CFD data from Douglas Aircraft Corporation and the NASA Langley Vehicle Integration Branch were provided with the properties listed below. These data give pressures on a cylindrical surface around the SR-71, with a radius of 28 percent of aircraft length from Douglas and one-third of aircraft length from Langley. This distance is closer than any probing by the F-16XL. The program MDBOOM (Ref. 4) was modified to propagate the CFD cylinder data to the probing location. These modifications do not affect the propagation algorithms.

MDBOOM normally outputs a time history of overpressures for a series of points in space as the aircraft flies past. MDBOOM was modified to accept the vertical and lateral separation flight data between the SR-71 and F-16XL as inputs for these series of points. The zero time point nearly corresponds to the bow shock. The time of the overpressure was multiplied by the true airspeed of the SR-71 to give overpressure as a function of longitudinal distance from the bow shock. The bow shock was then assumed to occur on the analytic Mach cone emanating from the nose of the SR-71, to give overpressure as a function of longitudinal distance from the nose of the SR-71 for comparison to the flight data. These MDBOOM overpressures are a more sparse data set in distance than the flight data, so the nearest MDBOOM data point to the flight location was used to compare to the flight measured overpressure. Interpolation of the MDBOOM data was specifically avoided to get the correct peak pressures. This results in some stair-step patterns in the data.

There are several errors and limitations with MDBOOM and the radar data that is used in MDBOOM. MDBOOM cannot currently handle more than two shocks coalescing at a time. This prevented the analysis of all 22 signatures. The bow shock of the MDBOOM overpressure not being located at the zero time point of the time history causes a slight shift in the position of the shocks. The largest errors are problems with the radar data that are used as inputs to MDBOOM. Large biases in the radar flight separation data exist for some signatures. This is determined by the indicated location of the bow shock being several hundreds of feet different from that expected from the analytical Mach cone from the nose of the SR-71. These biases are unexplained at this time. These biases were applied to the flight data before input into MDBOOM. For the closest separations the radar separation data are very erratic, probably because of multipath errors of the radar.

D
R
Y
D
E
N


F
L
I
G
H
T

R
E
S
E
A
R
C
H

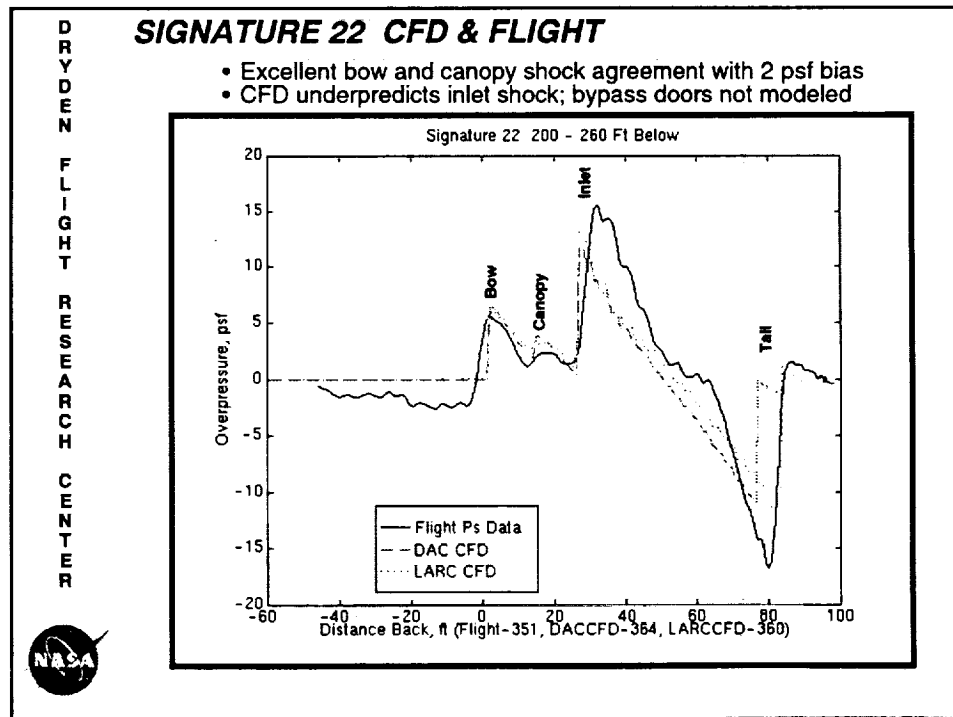
C
E
N
T
E
R

CFD TO FLIGHT DATA COMPARISONS

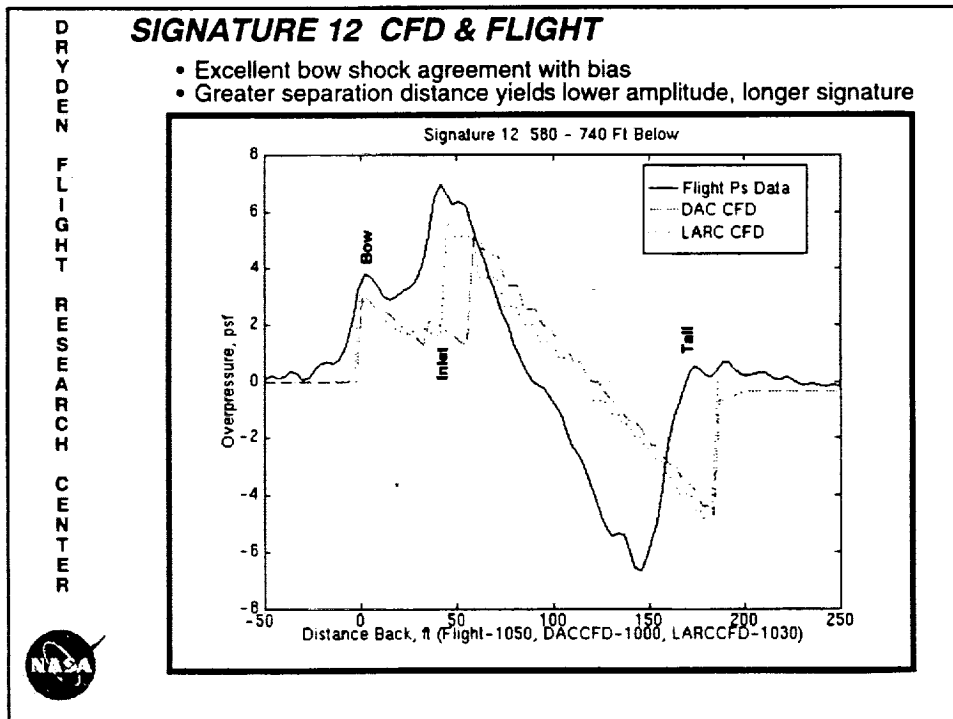
- CFD solution cylinders provided by DAC and LARC
 - Both solutions
 - Mach = 1.8, Pressure Altitude = 48,188', alpha = 3.5°
 - Lateral symmetry
 - Modeling effort concentrated forward of inlet
 - Douglas Aircraft Company
 - SCRAM code
 - R/L = 0.28
 - Langley Vehicle Integration Branch
 - USM3D / VGRID3D unstructured grid
 - R/L = 1/3
- MDBOOM used to propagate solutions.
 - Program modified to generate solutions at flight locations
 - Assume that CFD bow-shock occurs on Mach cone from nose
 - Cannot handle three shocks coalescing simultaneously
- CFD and flight overpressures plotted as a function of distance



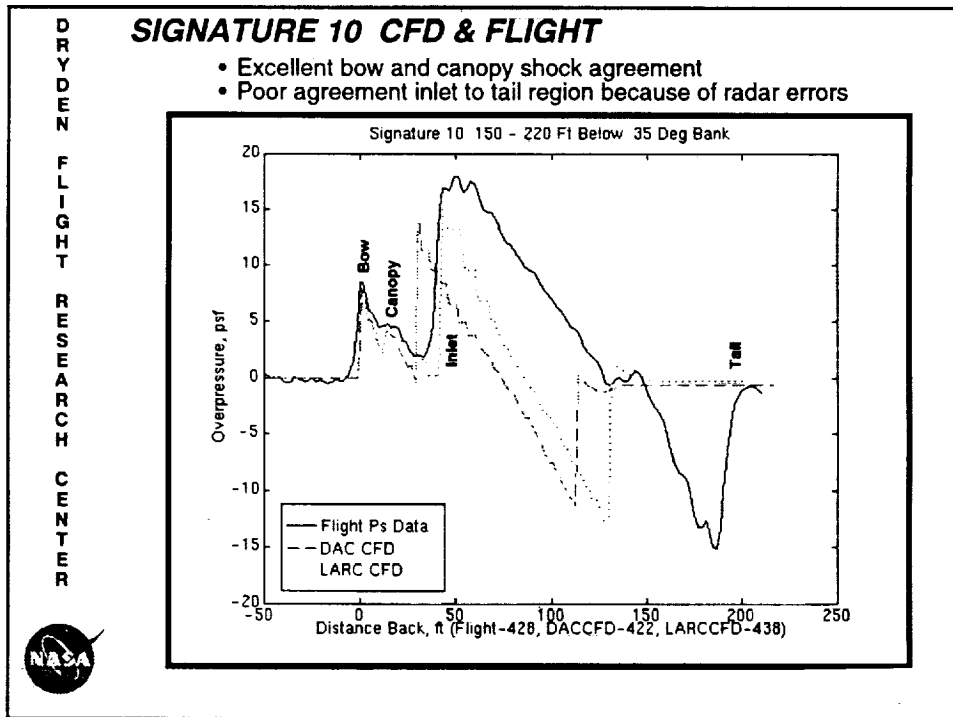
Overpressures from CFD and flight for signature 22 are plotted as a function of distance back from the bow shock. The distances that the bow shock is from the nose of the SR-71 at this separation are given in the abscissa label next to each of the three labels. As discussed on the previous page these distances are not equal. The length of the signature is about 80 ft, which is less than the SR-71 length, because the F-16XL flightpath was inclined to the flightpath of the SR-71. The overpressure from CFD is zero forward of the bow shock, as compared with -2 psf for the flight data. If the flight data were biased up 2 psf, the CFD and flight data for the bow and canopy shocks would give excellent agreement. The CFD data underpredict the inlet shock strength, but this is to be expected because the CFD does not model the bypass doors on the engines. The Douglas and Langley CFD results are very similar from the bow shock to the inlet shock, with diverging results towards the tail. Because the CFD work was concentrated forward of the inlet for a sonic-boom modification experiment (Ref. 2, 3), less effort was put into the CFD grid aft of the inlet, and engine bypass doors were not modeled.



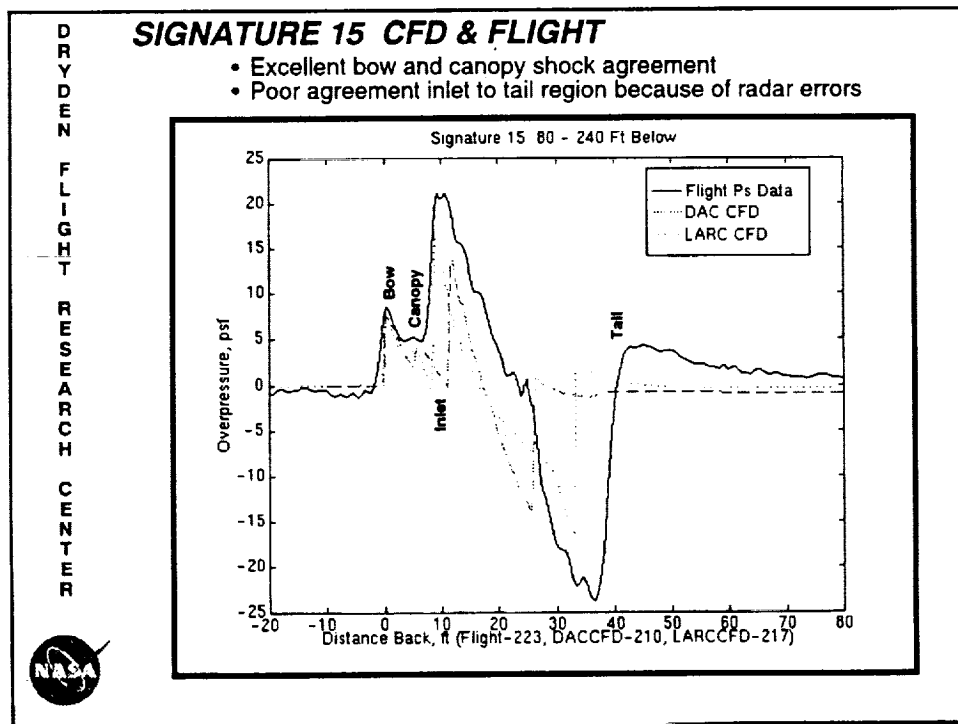
Signature 12 also shows very good agreement between CFD and flight data on the bow shock after the flight data bias is considered. As stated on the time history of signature 12 earlier, the canopy shock is missing from the static pressure data. This signature has about three times the separation distance that signature 22 has, and so it has smaller overpressures and a longer signature length. These are normal features of the signature aging process.




Excellent agreement is shown for the bow and canopy shocks for signature 10, with quite poor agreement in distance in the tail shock region. The poor agreement in the tail area is because of radar errors in longitudinal position. Since these data are from a turn, the angle of attack of the SR-71 is about 5.2° as compared with the CFD solutions calculated at 3.5° .



Signature 15 shows very good agreement between CFD and flight data for the bow and canopy shocks. The inlet and tail shock location differ for all three data sets. The F-16XL started the probe from behind at the 80-ft flightpath separation, then diving to 240 ft flightpath separation while moving forward through the SR-71 shocks. The radar data may be inaccurate at the close separation while probing the tail region. The diving motion shortens the apparent signature length.



The CFD-to-flight-data comparison results are outlined below. It is important to remember that the good agreement achieved is between flight data and CFD that have been propagated 40 to 740 ft through the atmosphere using the MDBOOM program.

D R Y D E N F L I G H T R E S E A R C H C E N T E R	CFD TO FLIGHT DATA RESULTS
	• Very good agreement for bow and canopy shock strength and position
	• CFD underpredicts inlet shock because of limited CFD engine detail
	• Poor agreement in tail region where CFD effort not concentrated
	• CFD from Douglas Aircraft Corp. and NASA Langley give very comparable results
	• Need to fix MDBOOM infinite loop to analyze remaining signatures
	• Cause for large biases in radar separation distance as yet unknown
• Ability of CFD and MDBOOM to predict near field overpressures gives confidence to use it as a design tool	
	

For future experiments of this nature the following recommendations for enhancements are made in the figure below. To determine accurate relative position, the differential GPS option is currently available at NASA Dryden. The other options have not yet been developed at NASA Dryden.

D R Y D E N F L I G H T R E S E A R C H C E N T E R	ENHANCEMENTS FOR FUTURE EXPERIMENT
	• Noseboom specifically for shock wave probing
	• Pneumatic system with high rate, low lag, low attenuation
	• Airdata calibration of SR-71 will enhance quality of trajectory reconstruction
	• GPS velocities will minimize INS/radar velocity errors
	• Better relative position determination
	– Differential GPS (3-5 m accuracy)
	-- No 10° elevation limit, 100 nmi range of each ground station
	– Carrier phase or pseudolite technology
	-- Centimeter accuracy may be possible
-- Relative attitude determination may be possible	
– Optical methods	
-- Laser rangefinder	
-- Air-to-air video and image processing	



The general conclusions address each of the objectives for this flight experiment. Referring back to the objectives of the experiment, (1) near-field measurements as close as 40 ft were demonstrated and enhancements were identified, (2) flight data were compared with CFD with very good agreement forward of the inlet, (3) baseline data of an unmodified SR-71 were provided for a modified SR-71 experiment (Ref. 2, 3) and confidence was gained of its success, and (4) this data can be used for analyses of sonic-boom propagation through the atmosphere to 740 ft and has good agreement with MDBOOM.

D
R
Y
D
E
N

F
L
I
G
H
T

R
E
S
E
A
R
C
H

C
E
N
T
E
R

CONCLUSIONS

- Near-field measurements as close as 40 ft demonstrated; enhancements identified
- CFD compared with flight data: very good agreement forward of inlet
- Confidence gained in CFD tools for SR-71 lower noise design based on baseline SR-71 CFD – flight data comparison
- Near-field flight data gathered for propagation studies; good agreement with MDBOOM



REFERENCES

1. Various Authors, High-Speed Research: Sonic Boom Volume II, NASA CP-10133, May, 1993.
2. Morganstern, John M., Bruns, Dave B., and Camacho, Peter P.: SR-71A Reduced Sonic Boom Modification Design. Presented at the NASA High Speed Research Program Sonic Boom Workshop, Hampton, VA, June 1994.
3. Lux, David, Ehernberger, L.J., Moes, Tim, Haering, Edward A., Jr.: Description of the Low-Boom SR-71 Modified Signature Demonstration Program. Presented at the NASA High Speed Research Program Sonic Boom Workshop, Hampton, VA, June 1994.
4. Plotkin, Kenneth J., "Calculation of Sonic Boom From Numerical Flowfield Solutions: MDBOOM Version 2.2", Wyle Research Report WR 92-14, July 1992.
5. Mullens, Marshall E., "A Flight Test Investigation of the Sonic Boom", AFFTC-TN-56-20, Air Res. and Dev. Command, U.S. Air Force, May 1956.
6. Smith, Harriet J., *Experimental and Calculated Flow Fields Produced by Airplanes Flying at Supersonic Speeds*, NASA TN D-621, Nov. 1960.
7. Maglieri, Domenic J., Ritchie, Virgil S., Bryant, John F. Jr., *In-Flight Shock-Wave Pressure Measurements Above and Below a Bomber Airplane at Mach Numbers from 1.42 to 1.69*, NASA TN D-1968, Oct. 1963.
8. SR-71 Blackbird Fact Sheet, World Wide Web,
http://www.dfrf.nasa.gov/Dryden/FactSheets/SR_71FACTS.html
9. F-16XL Fact Sheet, World Wide Web,
http://www.dfrf.nasa.gov/Dryden/FactSheets/F_16XLFACTS.html
10. Ehernberger, L.J., Haering, Edward A., Jr., Lockhart, Mary G., and Teets, Edward H., "Atmospheric Analysis for Airdata Calibration on Research Aircraft," AIAA-92-0293, Jan. 1992.

FLIGHT DATA SUMMARY

This is a summary of all 22 signatures. The start and stop times of the signatures are in Pacific daylight time. The F-16XL refueled at a tanker between signatures 11 and 12. The parameters are

- Radar elevation - radar elevation, deg, minimum, mean, and maximum
- Distance below - distance that the F-16XL is below the SR-71, in the vertical plane of the SR-71, ft, minimum, mean, and maximum
- Phi - angle off directly below, as viewed from behind, positive toward the right, deg, minimum, mean, and maximum
- F-16XL bank angle - roll attitude of the F-16XL, deg, minimum, mean, and maximum
- SR-71 bank angle - roll attitude of the SR-71, deg, minimum, mean, and maximum
- Overpressure - overpressure from static pressure, psf, minimum and maximum
- Probe region - direction and region of probe, ~ denotes difficult to tell
- SR mean gross wgt. - mean gross weight of the SR-71, lb, from the Mission Recorder System, (MRS)
- SR mean alpha - mean SR-71 fuselage reference angle of attack, deg, from MRS
- SR mean pr. alt. - mean SR-71 pressure altitude, ft, from MRS
- SR mean Mach # - mean SR-71 Mach number, from MRS

Data enclosed in a heavy border are of questionable quality or off-nominal condition, such as resulting from low radar elevation angle, high bank angle, incomplete probing, or off Mach number.

#	start time	end time	radar elevation			distance below			phi			F-16XL		SR-71			Overpressure		probe region	SR mean gross wgt	SR mean alpha	SR mean pr alt	SR mean Mach #	
			min	mean	max	min	mean	max	min	mean	max	min	max	min	mean	max	min	max						
1	10:34:50	10:35:12	8.5	8.9	9.4	76	158	193	-10	5	59	-8	8	23	2	9	23	-27	11.1	tail only	107687	4.8	48467	1.665
2	10:35:12	10:35:42	7.4	8	8.5	8	76	132	-7	49	86	-12	-1	11	1	3	7	-10	12.8	~back to front	107244	4.7	48440	1.664
3	10:35:42	10:36:18	6.4	6.9	7.5	85	163	271	-24	-7	39	-41	-9	13	-15	-8	7	-21	22.7	~front to back	106887	4.7	48487	1.702
4	10:37:11	10:37:30	5.2	5.2	5.3	123	185	233	-14	11	22	40	48	51	46	48	49	-15	17.1	back to front	106467	6.2	48088	1.636
5	10:37:40	10:37:55	5.1	5.2	5.2	202	317	447	-22	-10	5	-3	19	46	7	20	43	-14	13.9	front to back	106229	5.1	47825	1.601
6	10:41:30	10:42:00	9.1	9.2	9.4	162	175	197	-5	2	11	-42	-34	-27	-37	-32	-26	-20	10.3	tail only	103479	4.9	49150	1.822
7a	10:42:00	10:42:32	9.4	9.7	10	161	185	205	-10	-1	10	-54	-41	-33	-42	-40	-33	-18	17.4	~back to front	103081	5.3	48997	1.815
9	10:42:32	10:42:45	10	10	11	154	187	223	-3	2	5	-47	-42	-35	-41	-39	-35	-0.4	20.8	front only	102786	5.3	48714	1.808
10	10:42:47	10:43:03	11	11	12	153	193	218	-1	3	7	-43	-35	-31	-37	-35	-32	-15	17.9	front to back	102452	5.2	48655	1.806
11	10:43:30	10:44:00	14	16	19	73	171	677	-57	-19	0	-86	-50	-39	-43	-40	-37	-26	23.2	back to front	101649	5.3	48968	1.786
tanker																								
12	11:05:50	11:06:16	33	35	36	584	694	737	6	7	7	-4	-1	1	0	1	2	-6.6	7	front to back	88120	3.7	47977	1.802
13	11:06:40	11:07:05	18	21	25	153	321	505	16	22	28	13	35	44	24	38	43	-8.6	3.2	tail only	88024	4.2	48154	1.796
14	11:07:33	11:08:05	11	12	13	110	133	167	5	13	22	34	39	42	40	42	44	-20	8.4	tail only	87370	4.4	47890	1.798
15	11:08:25	11:08:45	9	9.4	9.8	76	140	243	-23	-11	2	-5	11	34	0	13	35	-24	21.1	back to front	87139	3.7	47873	1.835
15b	11:08:50	11:08:59	8.6	8.7	8.9	172	191	206	2	22	29	-31	-19	0	-11	-10	-9	-13	12	front to back	86985	3.7	47955	1.809
16	11:09:10	11:09:51	6.9	7.5	8.2	47	87	145	-14	0	16	-16	-5	5	-11	-3	5	-34	12.2	tail only	86602	3.7	48378	1.775
17	11:09:54	11:10:34	5.9	6.3	6.8	19	93	168	-2	25	12	36	51	17	39	51	-41	37.8	back to front	86121	4.3	48664	1.755	
17b	11:10:33	11:10:50	5.7	5.8	5.9	-17	169	286	-98	15	32	42	48	51	48	49	51	-20	19.6	front to back	85819	4.7	48529	1.767
18	11:15:50	11:16:20	13	15	17	34	56	88	-24	-15	-5	-50	-45	-38	-47	-44	-41	-43	29.1	back to front	82553	4.3	48599	1.812
19	11:16:37	11:16:50	20	21	23	153	197	231	-5	-1	4	-45	-19	-4	-35	-17	-3	-17	18.3	front to back	82122	3.8	48485	1.819
20 21	11:17:02	11:17:52	24	26	26	94	126	197	-18	-10	-4	-16	-4	3	-8	-3	3	-30	35.8	back-front-back	81718	3.5	48731	1.797
22	11:17:54	11:18:04	22	23	23	204	233	264	-8	-7	-6	-6	-2	1	-2	-1	-1	-17	15.5	back to front	81504	3.5	48675	1.805

This page intentionally left blank.

SR-71A REDUCED SONIC BOOM MODIFICATION DESIGN

John M. Morgenstern, David B. Bruns, and Peter P. Camacho
McDonnell Douglas Aerospace-West
Long Beach, CA 90846

INTRODUCTION

The adverse impact of sonic booms stems from the loudness and startle they produce. It is desirable, for future generation supersonic transport studies, to develop technology for reduced sonic boom environmental impact and possibly enhance operational economics. Previous sonic boom reduction studies developed sonic boom waveform shaping as a method for reducing loudness. The shape of the waveform is altered by tailoring the distribution of lift and volume of the vehicle, generating a waveform shape that does not evolve into an 'N' wave when it reaches the ground. Waveform shaping has been validated in wind tunnel tests, demonstrating that waveform shaping can be achieved up to several body lengths from a vehicle in a uniform atmosphere. Sonic boom propagation theory has been developed to predict how the sonic boom waveform evolves as it travels to the ground in the real atmosphere, without winds, atmospheric turbulence, or finite rise time calculation. This propagation theory has been validated for 'N' wave sonic booms under calm atmospheric conditions, and predicts the mean loudness well for the more random waveforms obtained under unsteady atmospheric conditions.

An investigation was undertaken by McDonnell Douglas, under NASA funding, to determine if a flight experiment could be developed to: demonstrate the propagation of shaped sonic boom waveforms through a real atmosphere, and obtain an indication of the effects of turbulence on sonic boom shaping. This investigation led to the conclusion that an SR-71A was a suitable vehicle for further waveform shaping studies. A very rough analysis developed a preliminary modification, consisting of only volume additions, that appeared to make the experiment feasible. More detailed studies were then undertaken to validate methods and refine the design.

In-flight data was obtained for the unmodified SR-71A to validate sonic boom predictions in the near-field of the SR-71A. An F-16XL flew several passes 100 to 500 feet under the SR-71A to measure the SR-71A waveform pressure distribution at the design condition of Mach 1.8. McDonnell Douglas Euler CFD calculations linked with propagation codes predicted the pressures under the SR-71A. The CFD propagation method was then used for modification design analysis and the shape of the modification was finalized through an iterative design approach.

Sonic boom annoyance, along with engine emissions and airport noise, is one of the three major environmental challenges facing the next supersonic transport. Studies have indicated that shaping offers the best chance for reducing the annoyance that characterizes the sonic boom noise problem. The technology of sonic boom shaping has been demonstrated in wind tunnel tests and methods for propagating the waveforms to the ground have been validated with 'N-wave' signatures. The propagation of shaped waveforms has never been demonstrated, and recently even the rate of shock coalescence has come into question as new, non-linear propagation methods are showing differences with linear theory. In April 1992, a separate study on Flight Research Requirements, reference 1, was undertaken to determine where flight testing could enhance NASA's High Speed Research (HSR) program. An investigation was undertaken by McDonnell Douglas, under NASA funding, to determine if a flight experiment could be developed to: demonstrate the propagation of shaped sonic boom waveforms through a real atmosphere, and obtain an indication of the effects of turbulence on sonic boom shaping. That study recommended more detailed study of the SR-71A as the best aircraft to modify for sonic boom shaping demonstration. To validate shaped sonic boom technology, the following objectives need to be addressed.

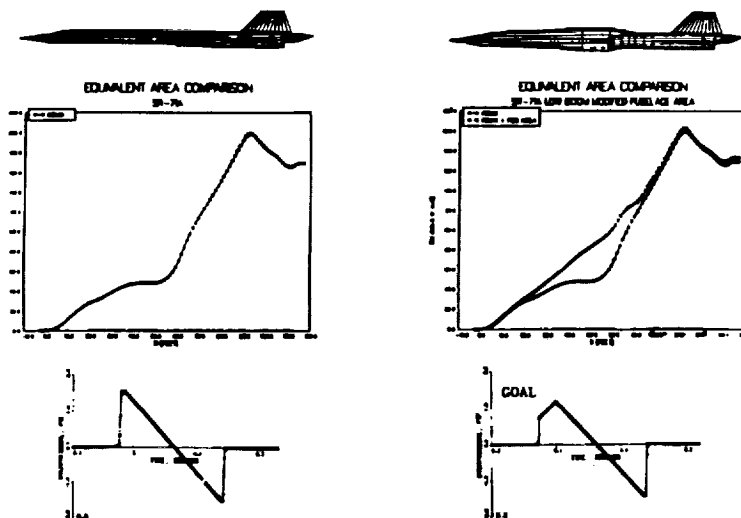
OBJECTIVES

- 1) Demonstrate propagation of shaped waveform.
- 2) Provide an indication of turbulence effects on a shaped waveform.
- 3) Provide experimental data for developing theoretical models for propagation through atmosphere.
- 4) Validate design methods for sonic boom loudness reduction.

The Flight Research Requirements study included a very rough analysis of what it would take to modify an SR-71A for a shaped sonic boom waveform. The linear analysis below gives an approximation of what a shaped waveform modification might look like. Its analysis is based on linear design methods, including the far-field wave drag method. Volume has been added to the vehicle starting just behind the nose with a large peak area just ahead of the engines. This modification was reviewed by NASA and some preliminary design work of the modification was done indicating that it seemed feasible. More detailed studies followed under NASA contract NAS1-19345 task order.

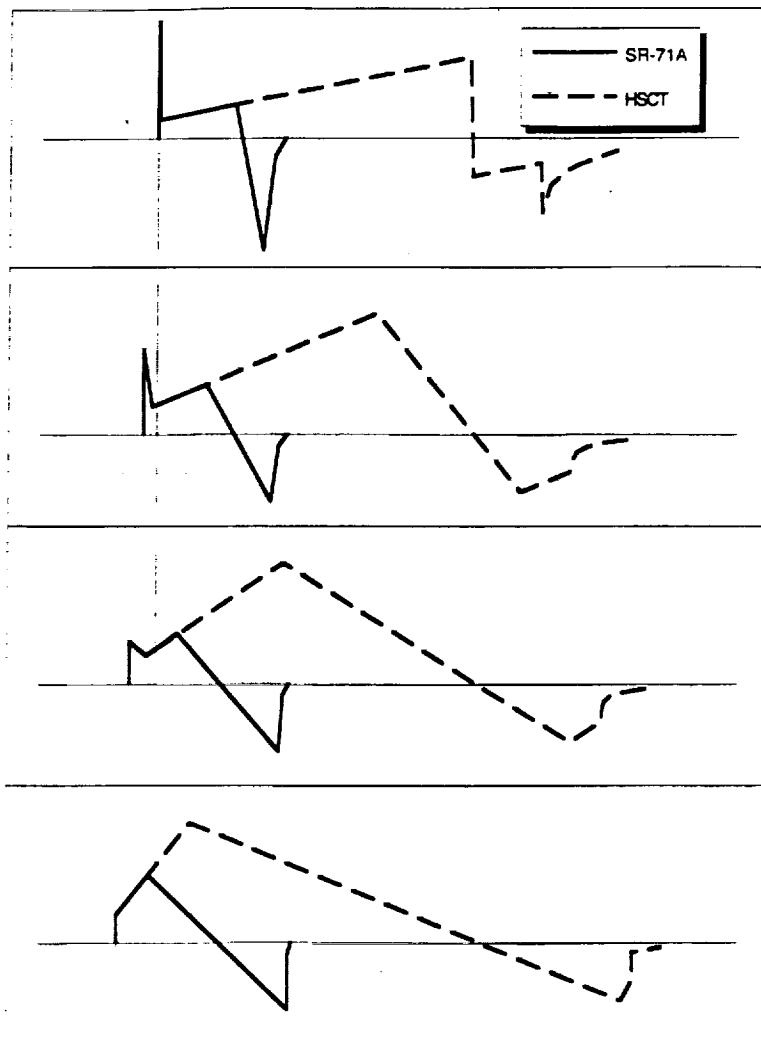
SR-71A PRELIMINARY ANALYSIS

Mach = 1.8 h = 48,000 ft.



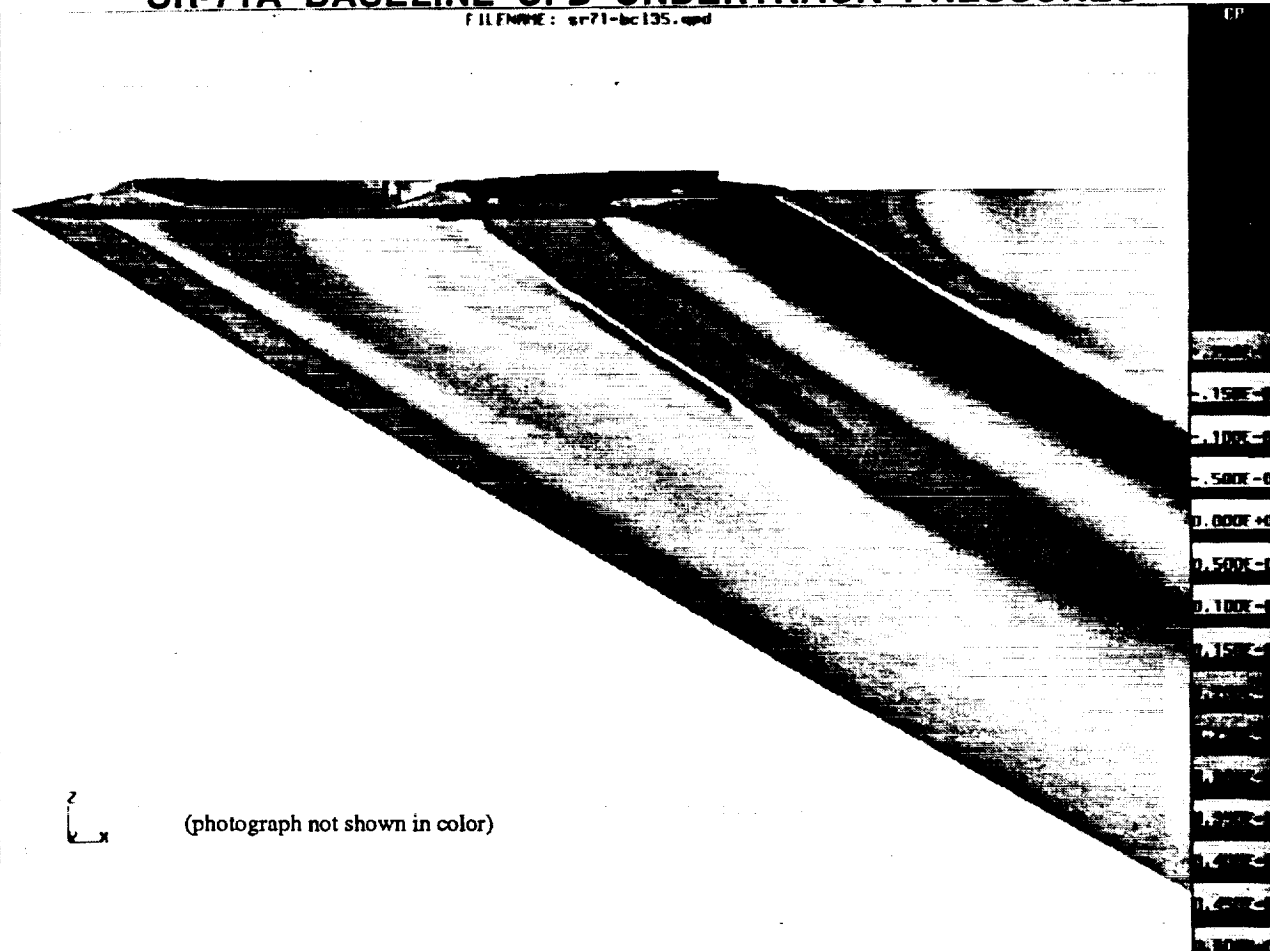
The SR-71A proposed design uses design conditions similar to most High-Speed Civil Transport (HSCT) low boom designs. Below is a comparison between an HSCT low boom design and the modified SR-71A. The SR-71A can generate the same pressure disturbance but the length of the disturbance is shorter. So there are no scaling issues between the SR-71 test and proposed HSCT Low Boom designs, only a shorter shaped portion of the signature. Also, there has been no attempt to shape the aft portion of the SR-71A signature because its shaping was not considered necessary to meet the preceding objectives and the large modifications that would be necessary to achieve a shaped aft waveform.

SR-71A AND HSCT WAVEFORM COMPARISON



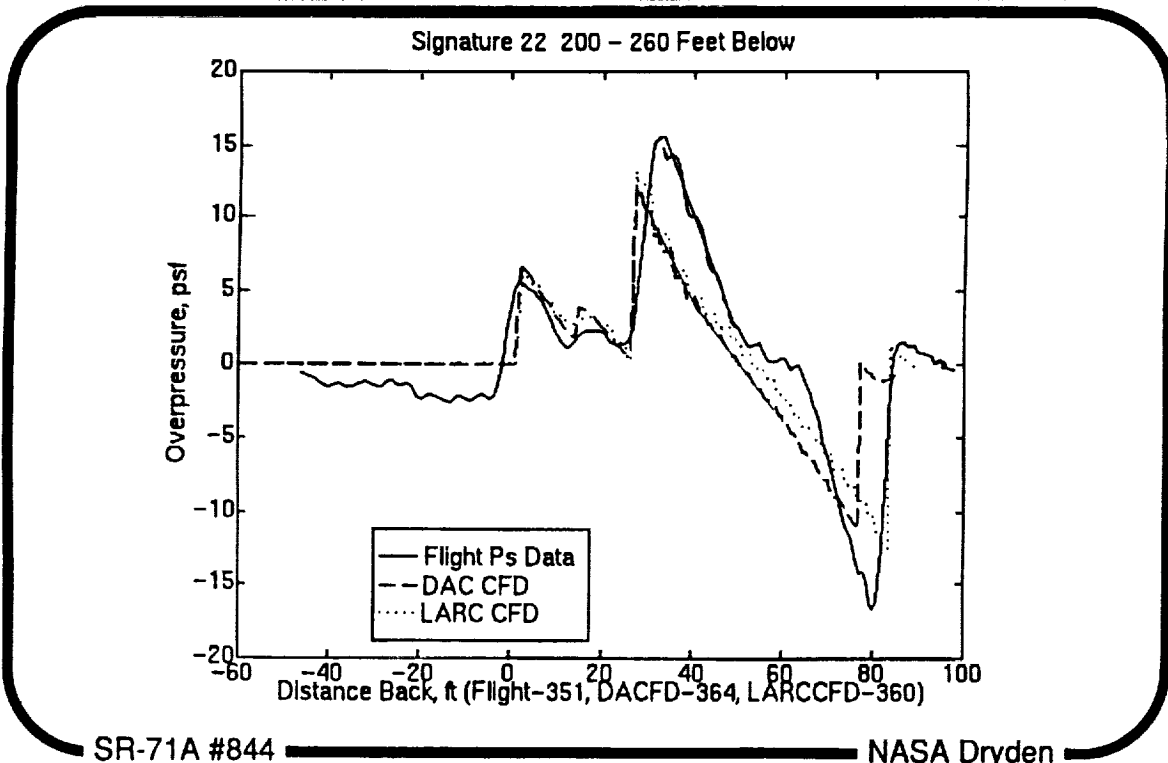
Computational Fluid Dynamics (CFD) was employed using the McDonnell Douglas SCRAM Euler solver. Wind tunnel tests and other design work have highlighted inaccuracies of linear, far-field design methods. Specifically, large volume bumps in the vicinity of other large surfaces behave differently than the transparent assumptions used by far-field theory. For example, a nacelle mounted right on the wing lower surface creates a strong shock that is reflected by the wing so that the nacelle on wing produces 2 strong shocks underneath and none above, instead of the single strong shock that an isolated nacelle would produce. Another example of this is the SR-71 canopy shock being reflected by the chine. Since the chine does not extend out far spanwise, only some of the shock is reflected; the rest travels around the chine before it can propagate downward causing it to be farther behind the front shock underneath the vehicle than with linear theory. This can be seen in the figure by tracing from the canopy at the Mach angle--the trace falls in the green region well ahead of the actual canopy seen as the yellow-orange following the green. Some of the canopy shock is reflected upward by the chine, so while the linear, far-field theory predicts that the canopy shock is the same strength as the front shock, the CFD predicts a shock of half the strength.

SR-71A BASELINE CFD UNDERTRACK PRESSURES



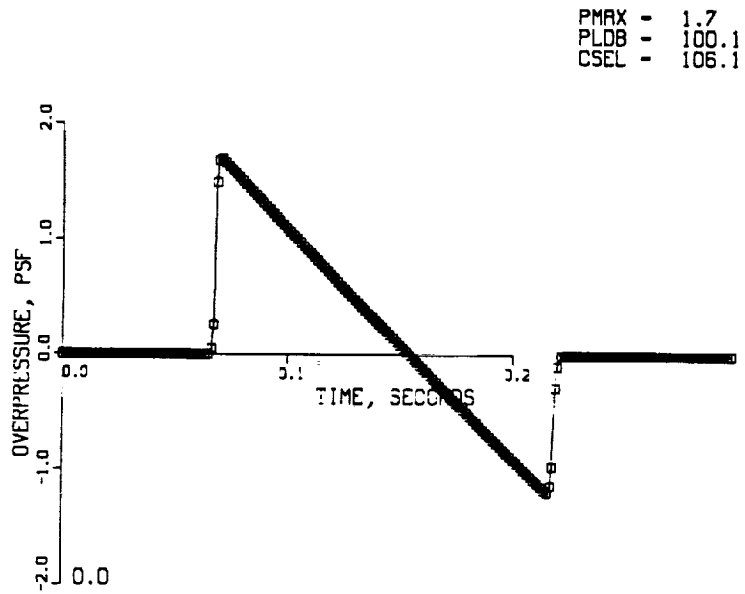
To validate the CFD method, a flight experiment was performed at the NASA Dryden Flight Research Center, Edwards A.F.B., reference 2 (located in these proceedings). An F-16XL flew under the SR-71A at the low boom design conditions: Mach 1.8 and alpha of 3.5 degrees (45,400 to 50,000 feet). The corrected pressure measurements are compared with CFD predictions from NASA LaRC and McDonnell Douglas, which were propagated to the flight trajectory from near-field pressure cylinders using the MDBOOM-Cylinder method described and validated in reference 3, and validated for a full configuration in reference 4. (In short, this method takes close-in near-field CFD data, where accuracy is best, and mathematically eliminates the near-field diffraction that typically takes from 2 to 6 body lengths to completely disappear. It then propagates by the typical modified-linear Thomas method.) The predictions show excellent agreement except for 2 places: the nacelle shock is 20% under predicted and the aft shock levels are also off (the DAC CFD aft shock position matches the LaRC position in later, smoother grids). These findings were somewhat expected because the inlet and nozzle operating conditions were not fully modeled, including a significant amount of inlet bypass bleed dumped from the forward bypass doors and the nozzle and ejector settings. To avoid the complication of trying to model inlet bleed, an increase in the nacelle shock strength was added to the near-field data that makes the flight data and predictions align at the measuring point. Differences in the aft shock do not affect the front shock shaping area so no corrections to the aft shock were made.

 **SIGNATURE 22 CFD & FLIGHT** 



The predicted ground waveform, with the increased nacelle shock, is shown below.

SR-71A BASELINE GROUND WAVEFORM



The first design iteration was based on linear theory analysis and a SEEB (reference 5) design goal, to get started quickly with existing methods. The geometry, in green, was generated at the Mach angle on UNIGRAPHICS using a specified area distribution and engineering judgement for how to place it. The red areas denote landing gear doors, navigation, refueling, and parachute deployment areas that we avoided in making the modifications.

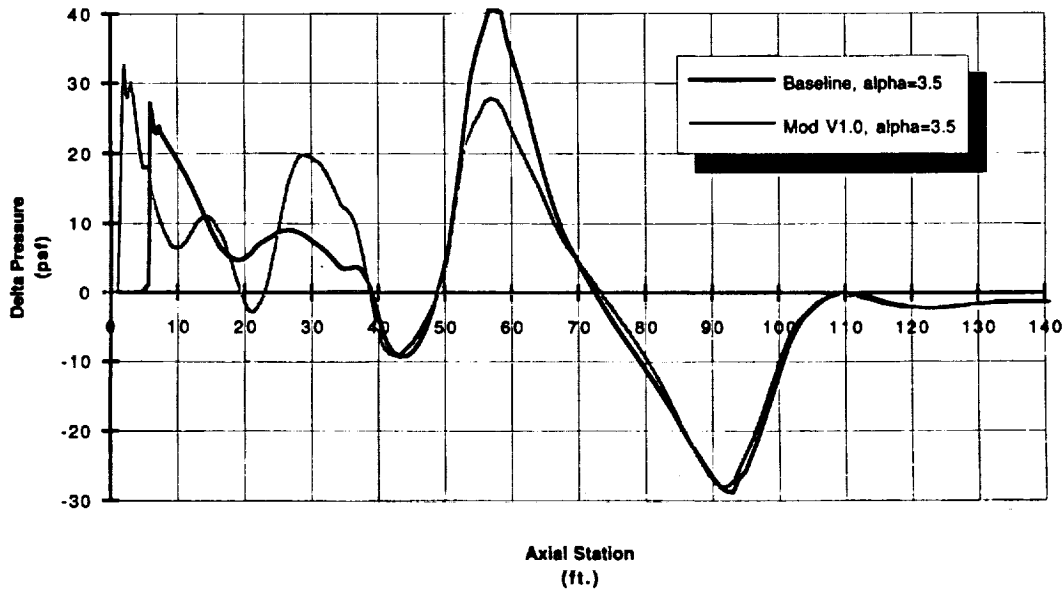
SR-71A MOD V1.0



(photograph not shown in color)

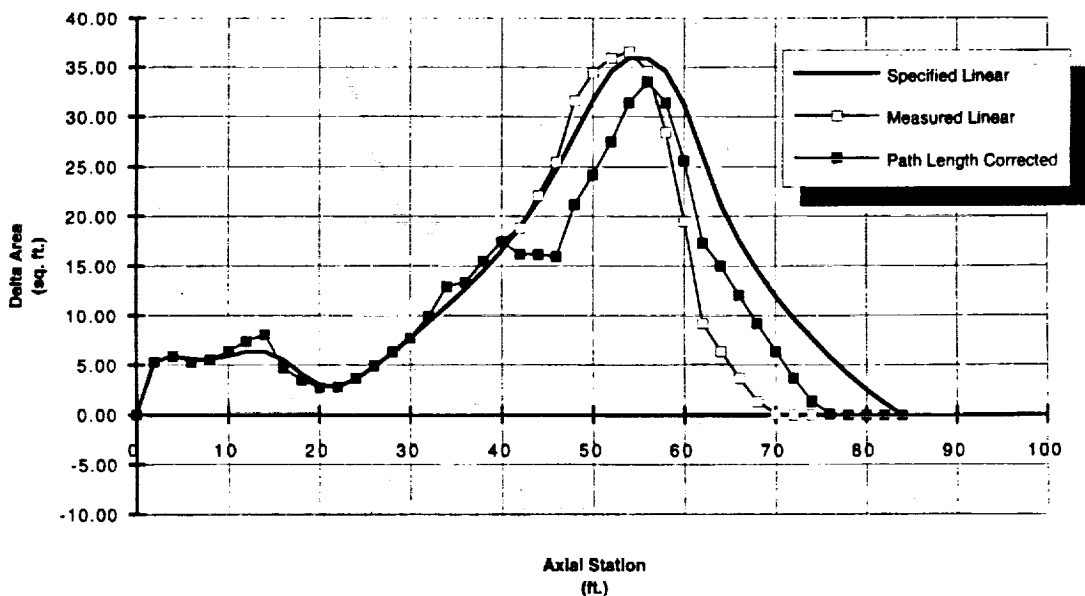
After generating Mod V1.0 based on linear methods, it was analyzed using an Euler CFD solver. The figure below shows the diffraction corrected pressures comparison with the baseline very close to the vehicles. While the diffraction has not disappeared at this point, this form is necessary for redesign to be sure that the proper waveform is achieved after diffraction effects subside. The Mod V1.0 pressure distribution shows a front spike and following pressures averaging a ramp but with large under and over shoots of the average.

**SR-71 Area Modification Effect
Version 1.0, R = 416**



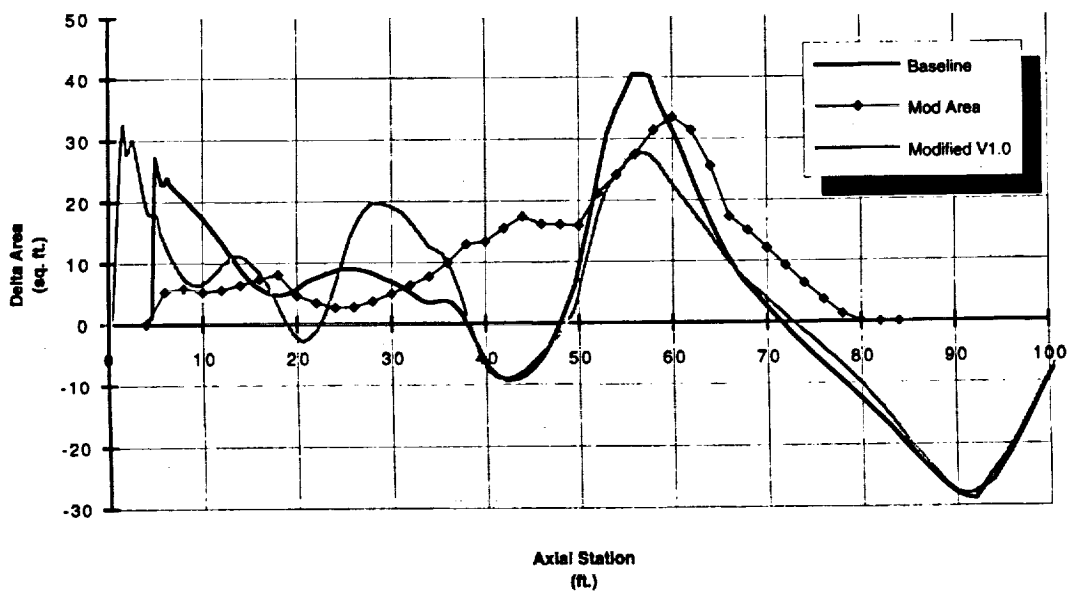
Looking back at the area modification in more detail revealed three reasons for over and under shoots: some coarseness in the area tolerance, a mis-match in the position of the upper mod and the location of its pressure influence after traveling around the chine (just like the canopy shock mentioned earlier), and a failure of linear theory to account for the aging of the nacelle shocks and the modification expansion which shift relative to one another before they travel far enough to begin interacting and canceling. The first two reasons are corrected in the figure below by creating a new "corrected" area distribution with more accuracy and a shift in the upper surface mod location to account for the increased propagation path length.

**SR-71 Area Modifications
Version 1**



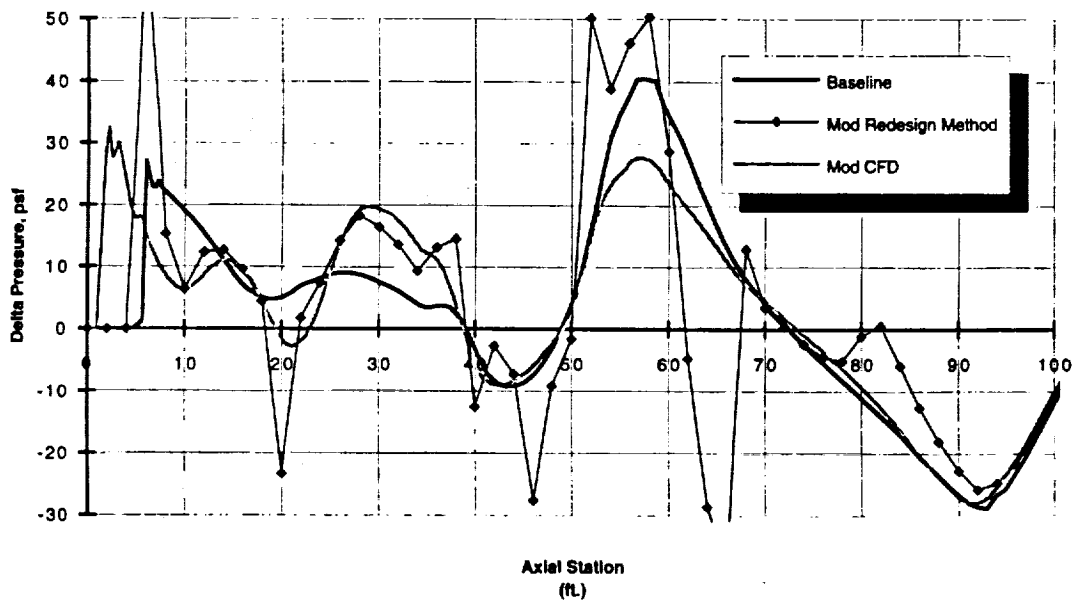
The modification area distribution then has to be carefully matched in location relative to the pressures. This is difficult to determine exactly since the pressures age (move) as they propagate.

SR-71 Area Modification Effect Version 1.0

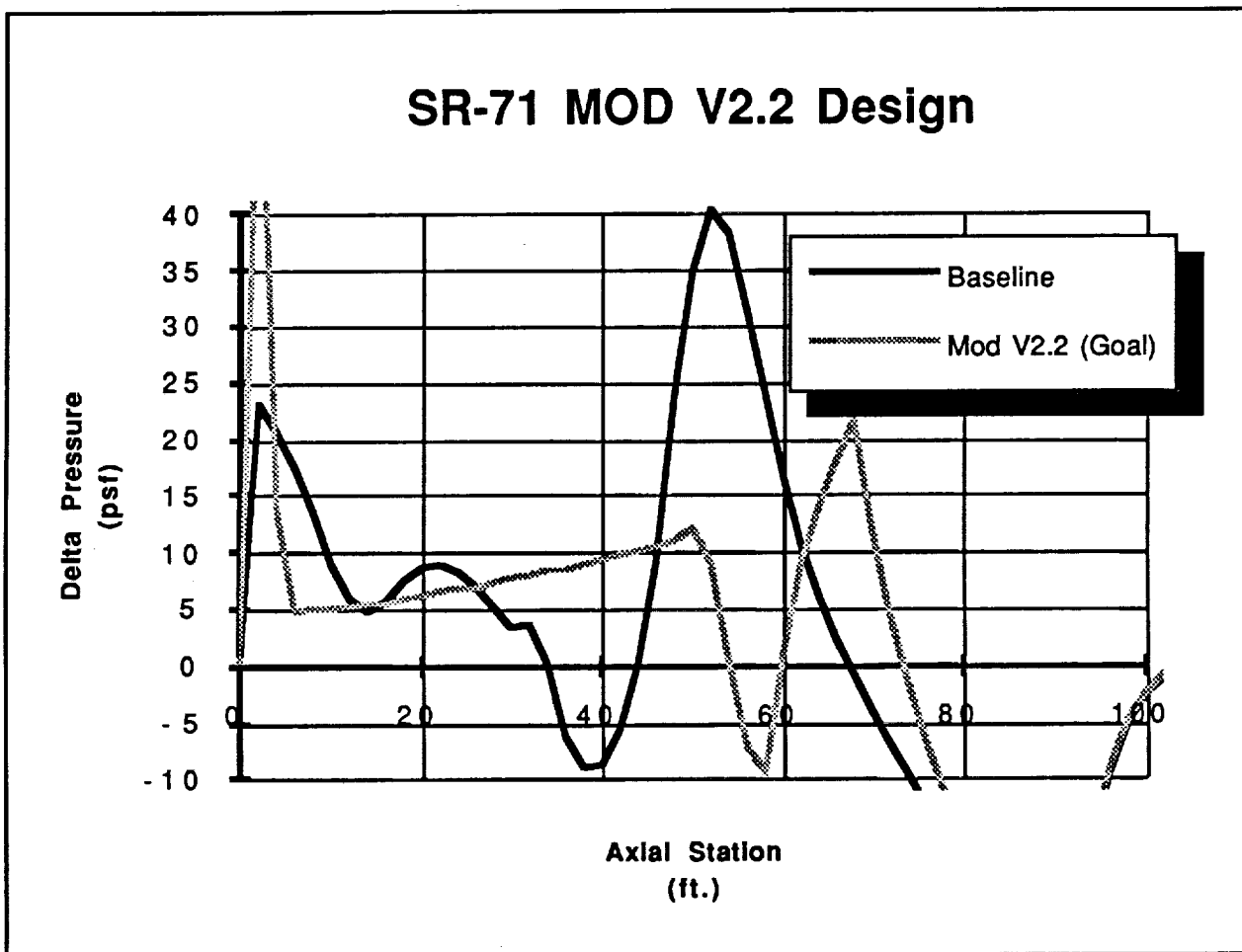


The objective at this point was to use the higher accuracy of CFD to do the design of the low boom modification. The key to implementing such a method was to get a very close-in pressure prediction where a minimum of aging has occurred and somehow eliminate the close-in diffraction that distorts the pressures in the near-field. This is provided by the aforementioned MDBOOM-Cylinder method. With such a baseline pressure prediction, linear theory can be used to apply changes in pressure to the baseline based on the modification area. This approach was implemented in a spreadsheet where the modification area can be changed until the desired diffraction-free pressure distribution is reached. To validate this redesign method before putting it into use, it was applied to the baseline using the Mod V1.0 area distribution and compared with the Mod V1.0 CFD analysis in the figure below. There are lots of spikes with the redesign method that would disappear or interact and cancel if the aging could be modelled; so the match is actually considered validating.

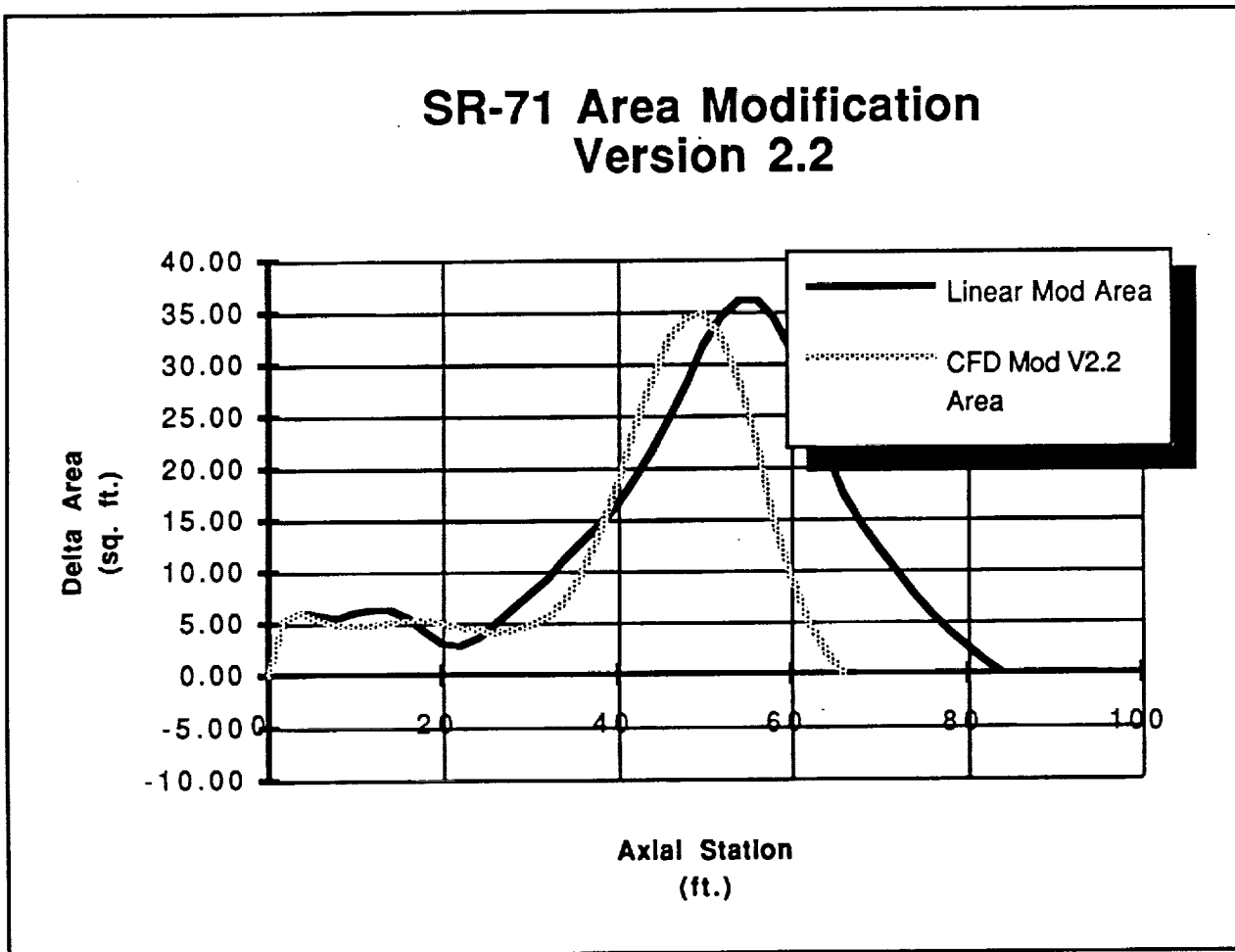
SR-71 Area Modification Effect Redesign Method Validation



This is the Mod V2.2 design which actually is designed to cancel out the stronger in-flight measured nacelle shock with a negative pressure spike of the corresponding size.

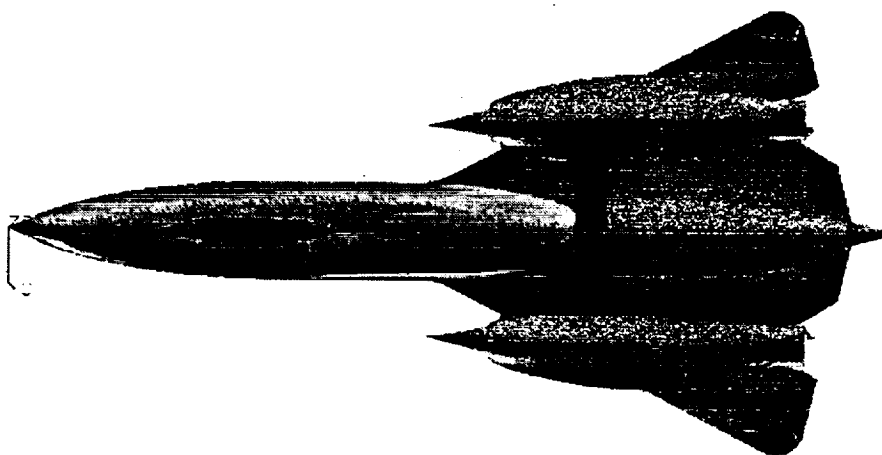
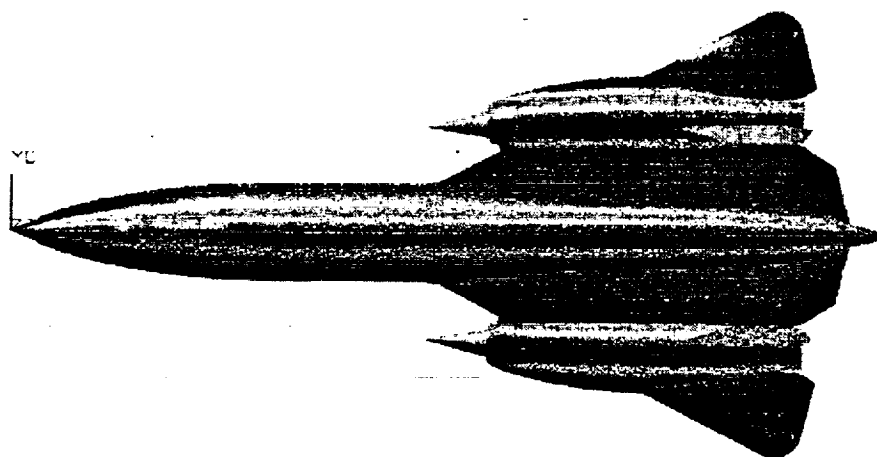


Notice that the Mod V2.2 area differs mainly from the linear design in that the area is smoother around the canopy and that the expansion to cancel out the nacelle shock is moved forward to account for the nacelle shock aging forward.



The modification area V2.2, in green, was held to the exact specified area distribution tolerance (+/-0.05 sq. ft. which is +/- 0.5 psf).

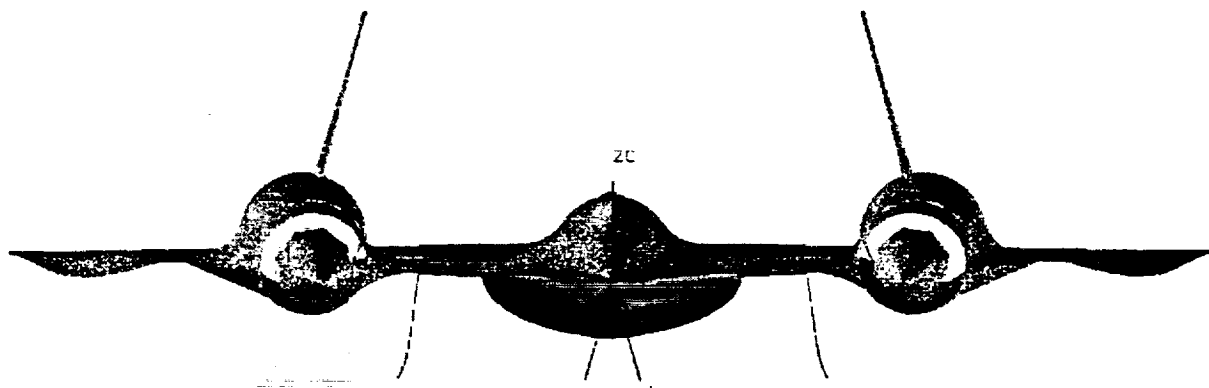
SR-71A MOD V2.2 VIEW



(photograph not shown in color)

The modification area was applied only to the lower surface to eliminate the path length issue and simplify the modification.

SR-71A MOD V2.2 VIEW



FEPO_1714.7 MOD

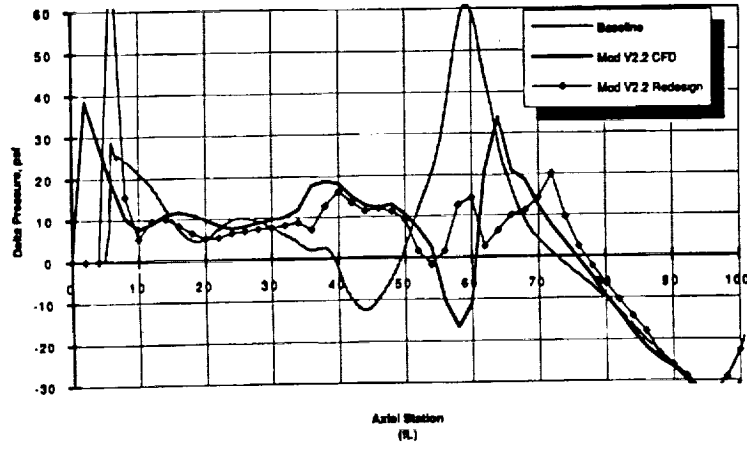


(photograph not shown in color)

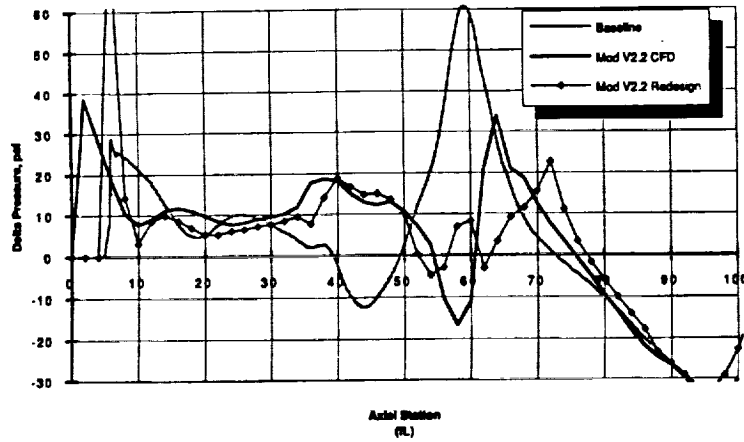
SR-71A MOD V2.2 CFD UNDERTRACK PRESSURES

The one strong effect left out of this redesign is that the changes in area also cause changes in lift, which affect the pressure distribution. Since the modification is now only on the lower surface, changes in volume that cause increases in pressure probably also cause increases in lift. This in effect means that the volume is more "effective" so the constant in the area changes could be changed to allow for a better correlation on the next iteration. The baseline 8.8 case was run with increased values of 10 and 11.2. 11.2 was chosen as the best.

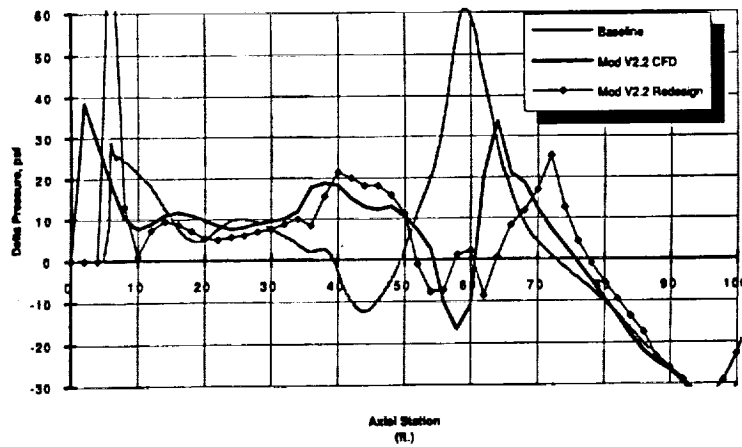
8.8 SR-71A Redesign Method Validation



10 SR-71A Redesign Method Validation



11.2 SR-71A Redesign Method Validation



CONCLUSION

In conclusion, a method for efficiently incorporating CFD into the sonic boom reduction design process has been refined and applied to an SR-71A. The design process works on complex configurations and the spreadsheet based redesign has a fast turn around time (hours to a couple days) but the overall process time is dominated by the CFD analysis (weeks to months). It is hoped that the final design will be flight tested to meet the four objectives required for sonic boom reduction technology validation.

REFERENCES

1. **High Speed Research System Study Flight Research Requirements.** Douglas Aircraft Co., NASA CRAD-9103-TR-8509, August 1992 (LER Restricted).
2. Edward A. Haering, Jr.; Stephen A. Whitmore, and L. J. Ehernberger: **Measurement of the Basic SR-71 Airplane Near Field Signature.** High Speed Research: Sonic Boom, NASA/CP-1999-209699, 1999.
3. Page, J. A. and Plotkin, K. J.: **An Efficient Method for Incorporating Computational Fluid Dynamics into Sonic Boom Prediction.** AIAA-91-3275, September 23-25, 1991.
4. Camacho, Peter: **CFD Analysis of the MDC Mach 2.4/1.8 Low Boom Wind Tunnel Model.** High Speed Research: Sonic Boom, Vol. 2; NASA CP-10133; May 12-14, 1993.
5. Darden, Christine M.: **Sonic Boom Minimization with Nose-Bluntness Relaxation.** NASA TP-1348, January 1979.

This page intentionally left blank.

**CFD PREDICTIONS OF SONIC-BOOM CHARACTERISTICS FOR
UNMODIFIED AND MODIFIED SR-71 CONFIGURATIONS**

Kamran Fouladi

Lockheed Engineering & Sciences Co.

Hampton, VA

Shaped sonic-boom signatures refer to signatures that look something other than the typical N-waves. The potential benefits of shaped signatures for supersonic aircraft have been discussed in ref. 1. Shaped sonic-boom signatures such as “flat-top,” “ramp-type,” or “hybrid-type” waveforms have been shown to reduce the subjective loudness without requiring reductions in overpressure peaks (ref. 2). The shaping of sonic-boom signatures requires increasing the shock rise time and changes in frequency spectra. So far, a flat-top waveform was shown to be achievable in wind tunnels (ref. 3); however, the influence of long propagation distance and real atmosphere on shaped signatures should be addressed using flight tests. Several techniques for establishing the persistence of shaped signatures were identified and listed in ref. 4.

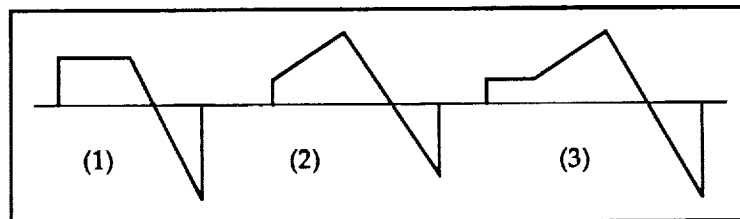
BACKGROUND

- * SHAPED SIGNATURES (NON N-WAVE) HAVE HIGHER SHOCK RISE TIME AND DIFFERENT FREQUENCY SPECTRA THAN N-WAVE SIGNATURES
- * SHAPED SIGNATURES SHOWN TO REDUCE SUBJECTIVE LOUDNESS
- * EXAMPLES OF VARIOUS SHAPED SIGNATURES WAVEFORMS ARE:

(1) FLAT-TOP

(2) RAMP

(3) HYBRID



- * A “FLAT-TOP” WAVEFORM HAS BEEN ACHIEVED IN WIND-TUNNEL TESTS
- * NECESSARY TO ESTABLISH THE PERSISTENCE OF SHAPED SIGNATURES THROUGH REAL ATMOSPHERE

Two different approaches have been proposed for sonic-boom minimization flight tests. The first approach, proposed by Eagle Aerospace (ref. 4), is for a flight test using a modified BQM-34 "FIREBEE" remotely piloted vehicle. The 30-foot long FIREBEE has a steady state flight condition at the Mach number and altitude of interest, and it can be recovered by helicopter from the water. As an alternative approach, a modified SR-71 vehicle has been proposed by the McDonnell Douglas Corporation (ref. 5). Benefits of the SR-71 include its variable geometry supersonic inlets, small cockpit bulge, higher Mach number capabilities, slender design, and longer length (105 foot). The present investigation addresses the sonic-boom analysis for the second vehicle.

PROPOSED SHAPED SIGNATURE PERSISTENCE FLIGHT TESTS

TWO ALTERNATIVE FLIGHT TESTS HAVE BEEN CONSIDERED TO ESTABLISH
PROPAGATION AND PERSISTENCE OF SHAPED SIGNATURES

- * MODIFIED BQM-34 "FIREBEE" REMOTELY PILOTED VEHICLE
- * MODIFIED SR-71 AIRCRAFT

The objective of the current investigation is to assess the feasibility of a modified SR-71 configuration, with McDonnell Douglas-designed fuselage modifications, intended to produce shaped sonic-boom signatures on the ground. The present study describes the use of a higher-order computational fluid dynamics (CFD) method to predict the sonic-boom characteristics for both unmodified and modified SR-71 configurations. An Euler unstructured grid methodology is used to predict the near-field, three-dimensional pressure patterns generated by both SR-71 models. The computed near-field pressure signatures are extrapolated to specified distances below the aircraft down to impingement on the ground using the code MDBOOM (ref. 6). Comparisons of the near-field pressure signatures with available flight-test data are presented in the current paper.

OBJECTIVE

ASSESS THE FEASIBILITY OF AN SR-71 CONFIGURATION MODIFIED TO
PRODUCE SHAPED GROUND SIGNATURES USING A HIGHER-ORDER CFD
METHOD



UNMODIFIED SR-71 CONFIGURATION,

$M_{\infty} = 1.8$; $\alpha = 3.5$ DEG.



SR-71 CONFIGURATION WITH McDONNELL DOUGLAS-MODIFIED FUSELAGE

$M_{\infty} = 1.8$; $\alpha = 3.9$ DEG.

In the present study, a fast and efficient algorithm based on an unstructured grid is used to predict near-field signatures of the SR-71 configurations. As a first step and prior to surface and volume grid generation, a geometrical representation of the configuration is prepared using points, curves, and patches as input to GridTool (ref. 7), an interactive surface representation code.

Grid generation and flow solver application are the next steps in the procedure to predict near-field signatures. The USM3D/VGRID3D (refs. 8 and 9) unstructured grid generation and flow solver scheme has been used and validated for sonic-boom analysis applications (refs. 10 and 11). This scheme allows greater geometrical flexibility for simulation of flows past complicated configurations such as the SR-71, and it also requires less effort in grid generation compared to structured grids (ref. 11).

MDBOOM, an extrapolation code (ref. 6), is the final step in predicting a mid-field or ground signature procedure. MDBOOM is used to post-process the three-dimensional flow solution to obtain pressure signatures at various distances below the aircraft down to the ground.

NUMERICAL SCHEME

- * UNSTRUCTURED GRID SCHEME IS USED FOR SONIC-BOOM ANALYSES DUE TO ITS
 - (1) GEOMETRICAL FLEXIBILITY
 - (2) DECREASED EFFORT IN GRID GENERATION (COMPARED TO STRUCTURED GRIDS)

- * THE PRESENT SCHEME IS MADE UP OF FOUR CODES:
 - (1) GRIDTOOL - INTERACTIVE GRAPHICAL PROGRAM FOR SURFACE REPRESENTATION FOR INPUT TO GRID GENERATION
 - (2) VGRID3D - SURFACE AND VOLUME GRID GENERATOR
 - (3) USM3D - THREE-DIMENSIONAL EULER FLOW SOLVER
 - (4) MDBOOM - PROPAGATION PROGRAM

Computer Aided Design (CAD) programs typically represent the surfaces of aerodynamic configurations with a set of parametric surfaces such as NonUniform Rational B-Splines (NURBS). CFD surface grids can then be generated on the NURBS surfaces. GridTool program (ref. 7), an interactive and graphical program, allows the grid generation program to accomplish this task by approximating the NURBS surfaces with a smaller number of bi-linear patches.

The grid generation code VGRID3D (Ref. 9) is used to generate the three-dimensional unstructured tetrahedral inviscid grid. VGRID3D is based on an advancing front technique. The advantage of this technique over other unstructured grid-generation techniques, such as Voronoi/Delaunay, is that it does not require separate library modules to distribute grid points throughout the domain.

The combination of GridTool and VGRID3D has greatly simplified the task of grid generation for complex configurations. Using this combination, a three-dimensional grid can be generated in a few weeks for a complex configuration such as the SR-71, and in a matter of days for a simple wing-body configuration.

GRID GENERATION

GRIDTOOL:

- * WORKS WITH OUTPUT FROM CAD PROGRAMS (NURBS, IGES FORMAT)
- * APPROXIMATES NURBS SURFACES BY A FEW SMALLER BI-LINEAR PATCHES
- * GRAPHICAL AND INTERACTIVE

VGRID3D:

- * BASED ON FRONT ADVANCING TECHNIQUE
- * SMOOTH GRID DISTRIBUTION WITH STRUCTURED BACKGROUND GRID
- * GRID RESTARTING AND LOCAL REMESHING

USM3D is a NASA-Langley developed finite volume, upwind code which solves Euler equations on unstructured tetrahedral meshes (ref. 8). In this flow solver, spatial discretization is accomplished by cell-centered finite-volume formulations, and Roe's flux difference splitting is used to compute the fluxes across cell faces. Higher-order accuracy is achieved by fast multidimensional linear reconstruction algorithms. Solutions are advanced by a 3-stage Runge-Kutta time-stepping technique. Residual smoothing and local time stepping are used for convergence acceleration.

MDBOOM (ref. 6) is a propagation code which computes sonic-boom characteristics of a supersonic aircraft in a horizontally stratified atmosphere. The overpressure ratios computed using USM3D and interpolated on the surface of a cylinder with a specified radius and azimuth can be directly input to MDBOOM. MDBOOM allows the cylinder to have small radii since it uses a matching technique based on an acoustic multipole formulation and accounts for diffraction effects in the flow field near the aircraft. This feature allows for flow-field solutions to be calculated at distances practical for CFD schemes.

FLOW SOLUTION

FLOW SOLVER USM3D:

- * SOLVES 3-D EULER EQUATIONS ON UNSTRUCTURED TETRAHEDRAL CELLS
- * CELL-CENTERED, FINITE VOLUME SPATIAL DISCRETIZATION
- * ROE'S FLUX -DIFFERENCE SPLITTING
- * 3-STAGE RUNGA-KUTTA TIME INTEGRATION

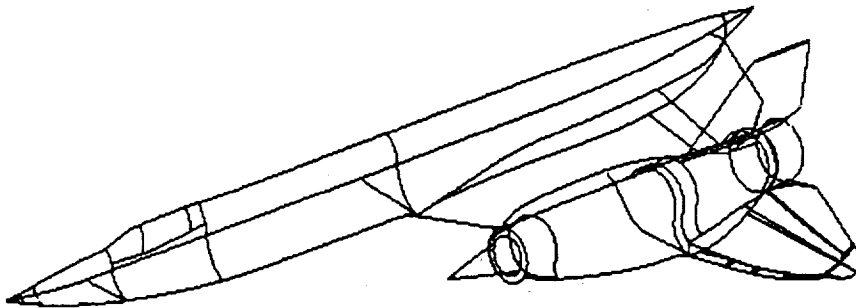
PROPAGATION CODE MDBOOM:

- * COMPUTES SONIC-BOOM CHARACTERISTICS IN STRATIFIED ATMOSPHERE
- * BASED ON ACOUSTIC MULTIPOLE FORMULATION TO ACCOUNT FOR DIFFRACTION
- * UTILIZES FLOW SOLUTION FROM CFD CALCULATIONS

Various issues of importance in grid generation codes such as the grid spacing parameters, the background grid, and nodal and linear sources in the background grid were detailed in refs. 9, 10, and 11 and are not discussed here for the sake of brevity. The background grid for each SR-71 configuration includes 28 linear source elements on the aircraft and 16 nodal source elements for the outer boundaries. All source elements have directional intensities for better control of grid-point distribution on components of the configuration.

Due to complexity of the configuration, the surface geometry of the unmodified SR-71 was approximated, using GridTool, with 75 bi-linear patches. The number of bi-linear patches for the modified SR-71 configuration was increased to 112 to ensure geometrical integrity of the changes. The surface patches of the unmodified SR-71 configuration are shown below.

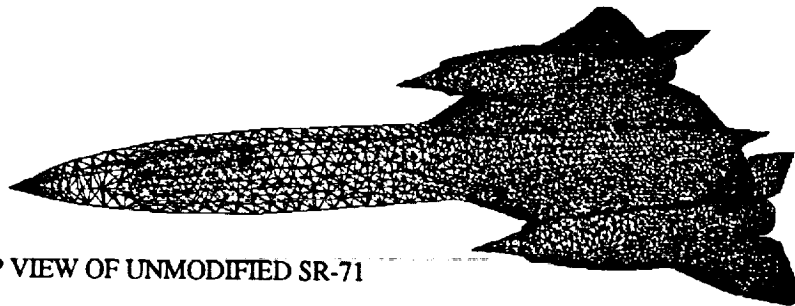
SURFACES PATCHES REPRESENTING SR-71



A set of unstructured grids with varying grid resolution was generated for the unmodified SR-71 to obtain a grid-independent solution. The finest grid consisted of 152,255 grid points and 844,344 grid cells. The finest grid generated for the modified SR-71 configuration consisted of 165,246 grid points and 918,867 grid cells. The surface grid of the unmodified SR-71 configuration is shown below. Only the results for the finest grids are presented in this study.

USM3D has a computational speed of about 17.5 μ -sec/cell/iteration and a required memory of 45 words/cell. For the present computation, this translates to approximately 38 and 41.5 megawords of core memory for the unmodified and modified SR-71 configurations, respectively. The converged solution for cases in the present calculation was obtained in approximately 6 hours of CPU time on the CRAY-YMP at the NASA Langley Research Center.

SURFACE GRID REPRESENTATIONS FOR BOTH SR-71 CONFIGURATIONS



TOP VIEW OF UNMODIFIED SR-71

152,255 NODES - 844,344 CELLS

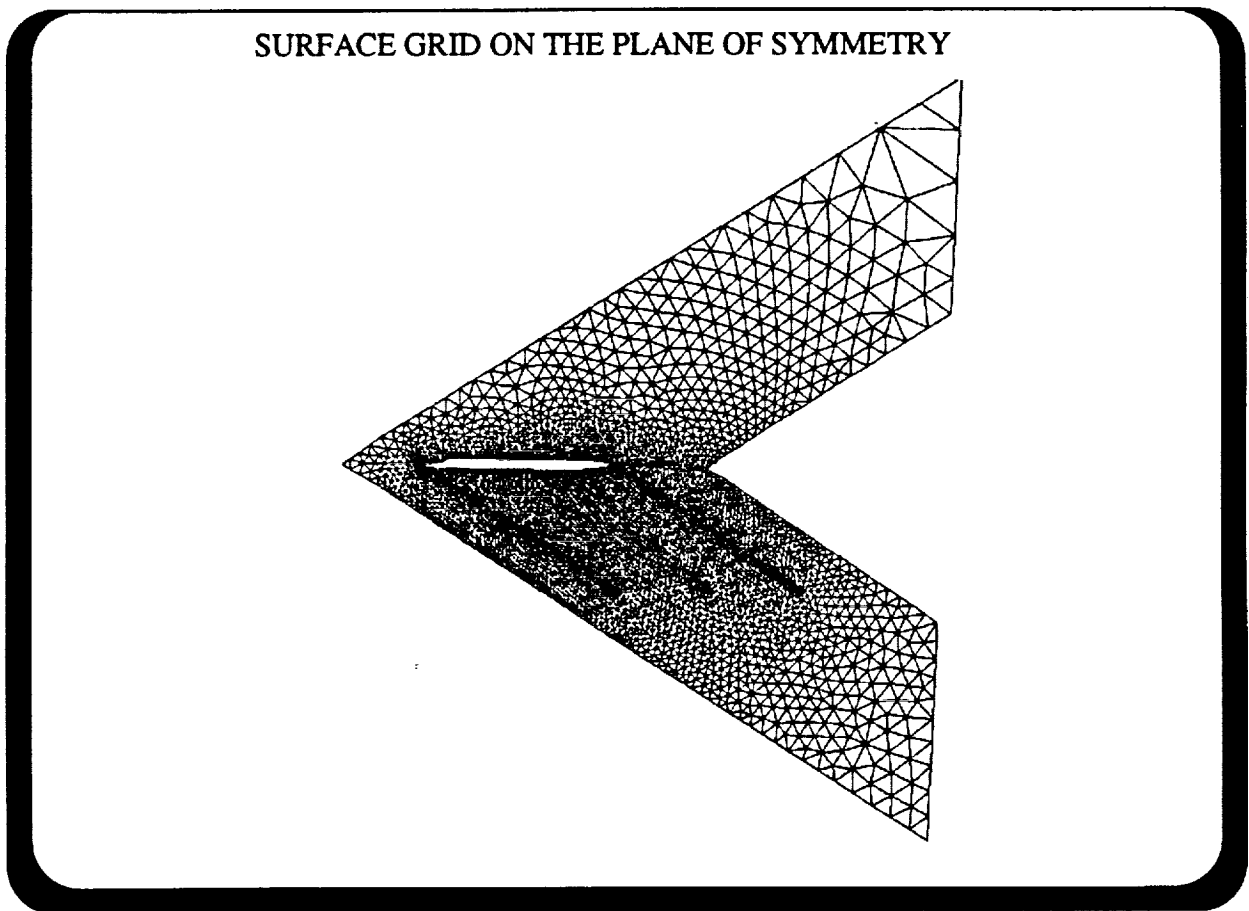


SIDE VIEW OF MODIFIED SR-71

165,246 NODES - 918,867 CELLS

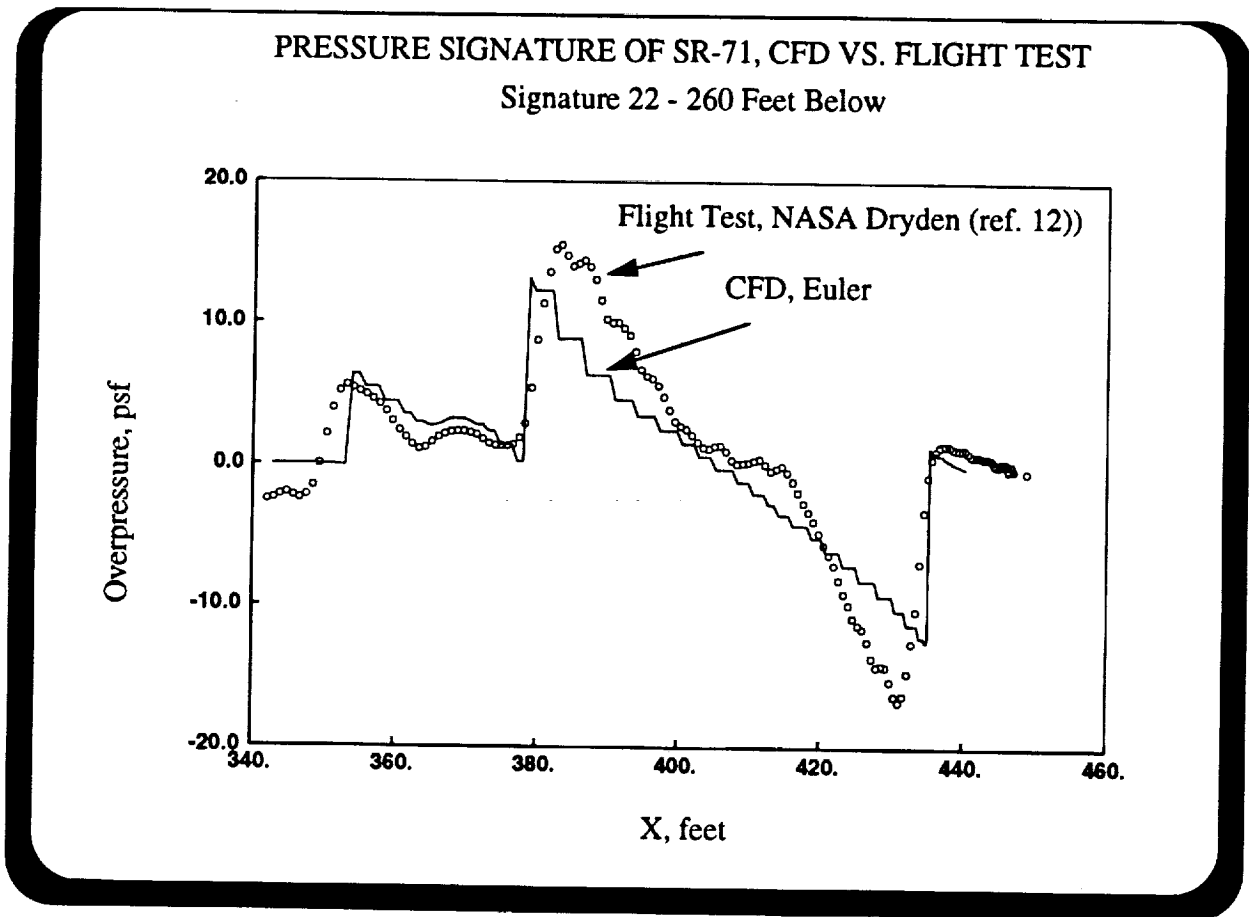
It has been shown that supersonic configurations may generate significant off-ground-track sonic-boom levels in comparison with the level on the ground track. It is, therefore, important to maintain sufficient grid resolution off the plane of symmetry. Hence, integration of "sonic-boom grid topology" with the current scheme may be required for accurate prediction of off-centerline pressure signatures (refs. 10,11).

The sonic-boom grid topology mimics the method of characteristics. The upstream and downstream boundaries both flare out at the Mach angle of the free-stream Mach number. Therefore, the wave characteristics emanating from the configuration are contained between the two boundaries and grid resolution can be greatly increased. This type of grid is ideal for off-centerline pressure signature prediction since the grid clustering can be extended in the lateral direction. The shape of the computational domain results in a savings in grid points which should make up for the increase in the number of grid points due to this clustering. The surface grid on the plane of symmetry for the unmodified SR-71 configuration is shown below.

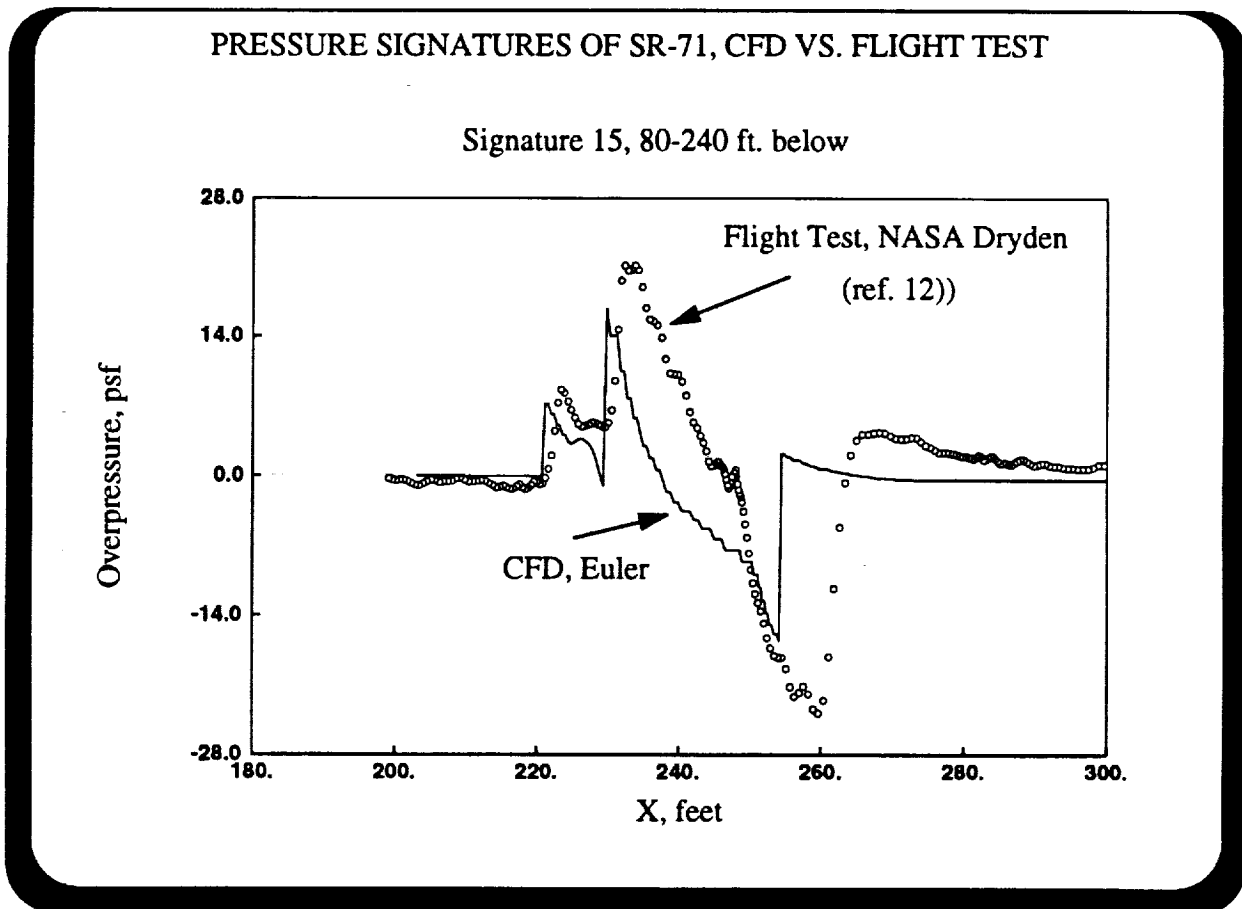


A comparison of flight-test data (ref. 12), signature 22, and computationally obtained pressure signatures are presented below for the unmodified SR-71 configuration. To obtain the computed pressure signature, the overpressure ratios on the surface of a cylinder with a radius of 35 feet (one third of the aircraft length) are extracted from the three-dimensional solution. MDBOOM is then used to propagate the computed data to locations where pressure data are recorded in the flight test.

The comparison of the trends of the two signatures indicates good agreement, particularly in the first half. The pressure peak in the inlet region is, however, underpredicted in the computed signature. This may be due to the lack of modeling of some features such as bypass doors on the engine in the CFD computations.

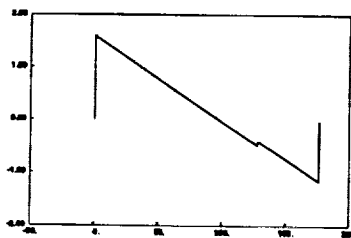


A comparison of computed signatures with flight-test signature 15 is shown below. Good agreement is shown between the computed signature and the flight test signature in the bow and the canopy region; however, the inlet shock is underpredicted. For signature 15, as the probe aircraft moved from the rear to the front of the SR-71 aircraft, the separation distance between the two aircraft varied between 80 feet below in the tail region to 240 feet below in the front half. The close separation between the two aircraft in the tail region may have introduced inaccuracies in the radar data, which is used to measure the separation distances. The poor agreement between the flight-test data and the computed signature in the tail region may be due to this inaccuracy since the computed signature would not be propagated to the correct locations.

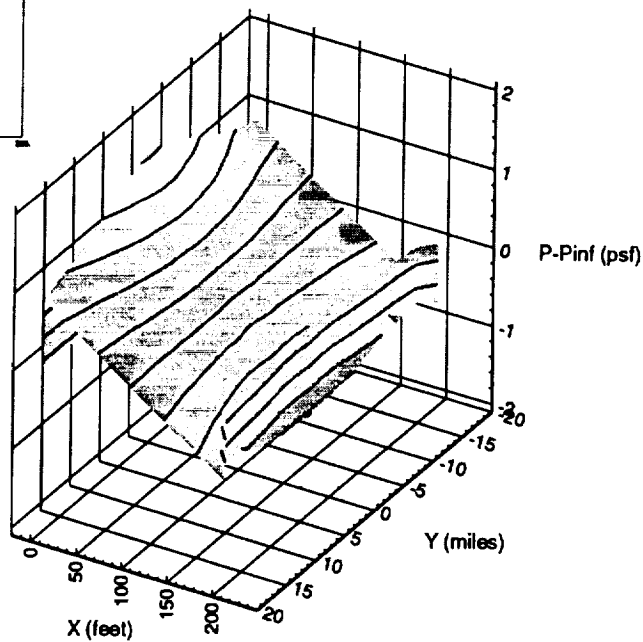


Ground signatures of the unmodified SR-71 can be illustrated with a pressure carpet plot generated by the aircraft. The ground carpet plot shown below depicts the pressure signatures versus flight path axis (X) as well as the lateral distance to the side of the flight path (Y). Also shown is the ground-pressure signature at the centerline. As expected, the shape of the ground pressure signature at a given lateral distance is a typical N-wave. The carpet plot indicates a significant variation in the pressure pattern in the lateral direction up to approximately 18.2 miles with the largest overpressure peaks occurring at the centerline and attenuating laterally.

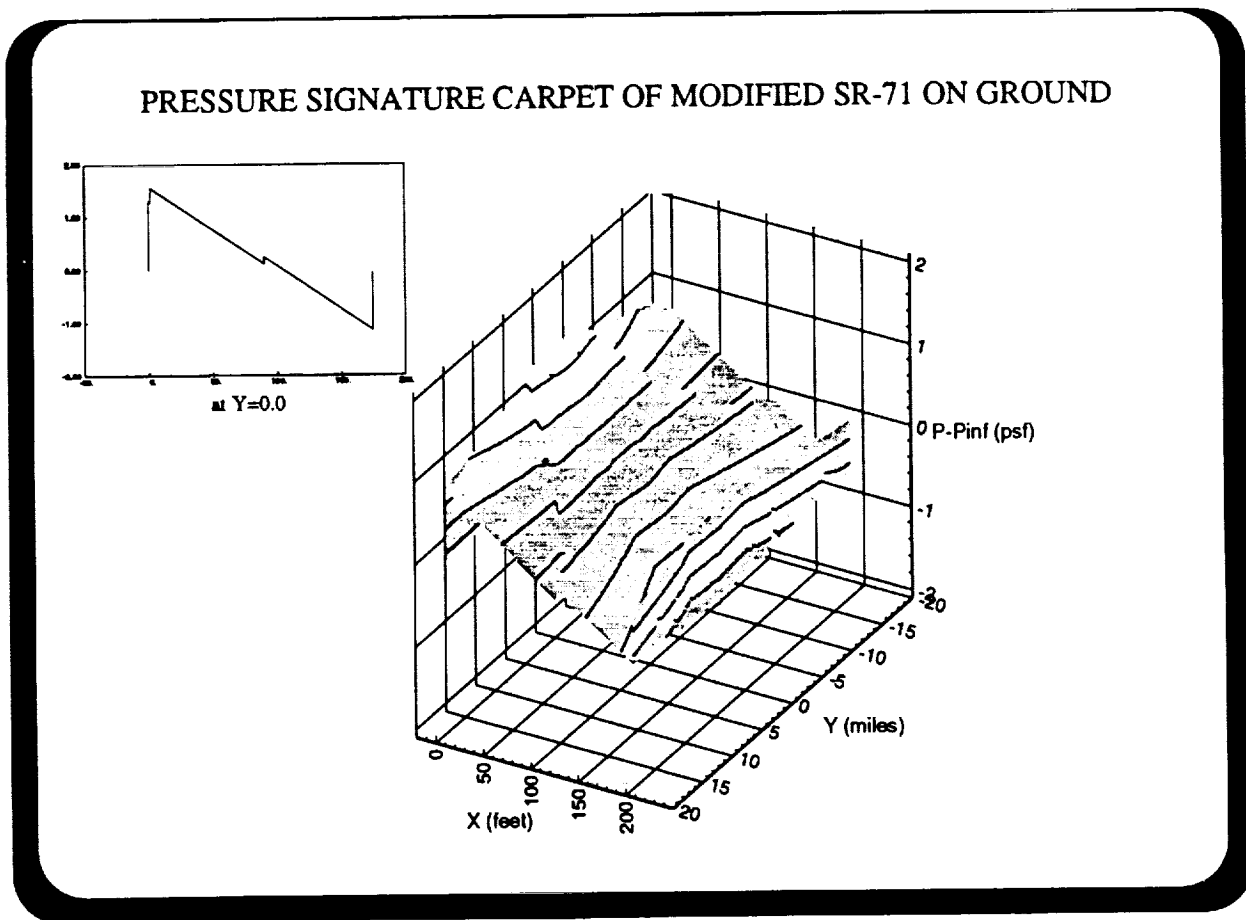
PRESSURE SIGNATURE CARPET OF UNMODIFIED SR-71 ON GROUND



at Y=0.0

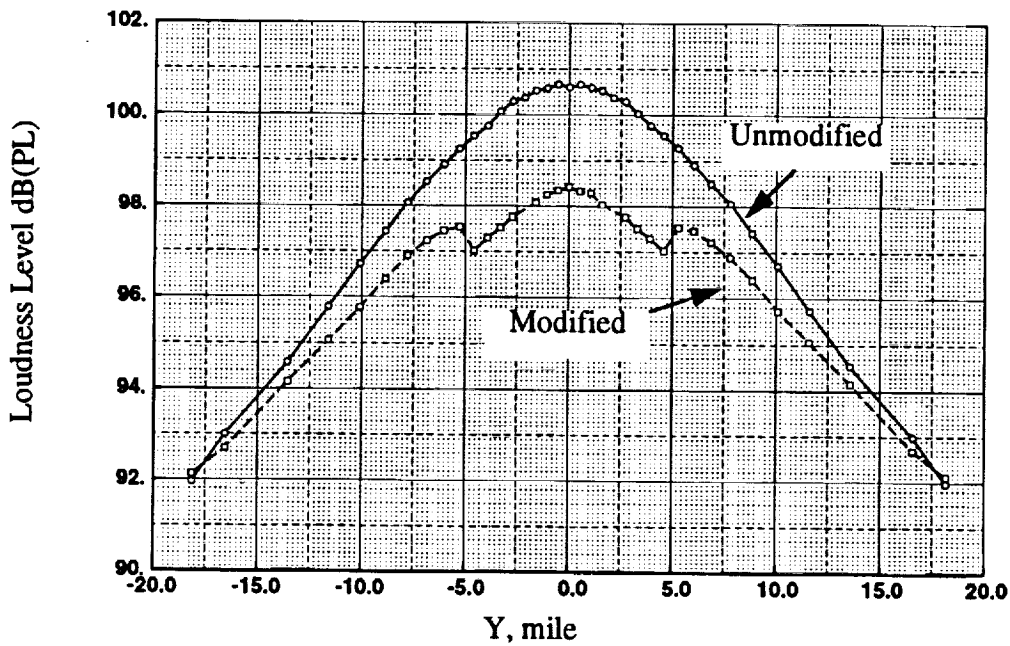


The ground-pressure carpet plot of the modified SR-71 and its centerline ground-pressure signature are shown below. The carpet plot for this configuration also indicates a significant variation in the pressure pattern in the lateral direction up to approximately 18.2 miles. Similar to the unmodified configuration, the highest signature overpressures are located on and near the centerline with the ground signatures close to the flight path indicating a subtle double shock overpressure peak in the nose region. Though this is not the intended signature shape, the present analysis shows that shapes other than N-waves may persist to the ground.



The differences in the sonic-boom characteristics of the two SR-71 models are highlighted in the plot shown below. The variation of loudness levels versus lateral distances to the side of the flight path (Y) was calculated using the procedure developed by Shepherd and Sullivan (ref. 13). A shock rise time of 3 milliseconds per 1 psf of shock was used to calculate rise time for both configurations. The computed noise loudness level for the modified SR-71 is predicted to be consistently lower than the unmodified configuration. The major differences between the loudness patterns for both configurations lie in the region near the flight path up to Y=5.0 miles.

LOUDNESS LEVELS ON AND OFF-FLIGHT PATH FOR BOTH SR-71 CONFIGURATIONS



An Euler unstructured grid methodology has been used to analyze the sonic-boom characteristics of an unmodified SR-71 aircraft and a modified SR-71 with a Douglas-designed fuselage modification intended to produce shaped sonic-boom signatures. The predicted near-field pressure signatures of the unmodified configuration were compared with the flight-test data. The results indicate very good agreement in the front half of the signatures and in overall trends. The pressure peaks due to the inlet, however, were underpredicted in the computed signatures. Non N-wave signatures with double shock overpressure peaks in the nose region were predicted for the modified configuration, which resulted in lower noise loudness level near the flight path.

CONCLUDING REMARKS

- * SONIC BOOM ANALYSES OF BOTH UNMODIFIED AND MODIFIED SR-71 CONFIGURATIONS WERE PERFORMED USING AN UNSTRUCTURED GRID SCHEME
- * GOOD CORRELATIONS WERE OBTAINED BETWEEN THE COMPUTED RESULTS AND AVAILABLE FLIGHT-TEST DATA FOR UNMODIFIED SR-71
- * COMPUTED SIGNATURES UNDERPREDICTED THE INLET SHOCKS
- * MODIFIED SR-71 CONFIGURATION PRODUCED NON N-WAVE PRESSURE SIGNATURE ON THE GROUND

ACKNOWLEDGMENT

This work is supported under NASA Contract No. NAS1-19000. The technical monitor is C. M. Darden. The author would like to thank J. Samareh-Abolhassani and N. T. Frink for their help and expertise. The author also wishes to acknowledge the helpful conversations with S. Pirzadeh.

REFERENCES

1. Niedzwiecki, A.; and Ribner, H. S.: Subjective Loudness and Annoyance of Filtered N-Wave Sonic Booms, *J. Acoustic Soc. America*, Vol. 6, No. 3, 1974.
2. Leatherwood, J. D.; and Sullivan, B. M.: Subjective Loudness Response to Simulated Sonic Booms, *High-Speed Research: Sonic-Boom Workshop*, NASA CP 3172, Vol. 1, 1992.
3. Siclari, M. J.; and Darden, C. M.: CFD Predictions of the Near-Field Sonic-Boom Environment for Two Low-Boom HSCT configurations, *AIAA Paper No. 91-1631*, June 1991.
4. Maglieri, D. J.; Sothcott, V. E.; Keefer, T. N.; and Bobbitt, P. J.: Overview of Feasibility Study on Conducting Overflight Measurements of Shaped Sonic-Boom Signatures Using RPV's, *First Annual High-Speed Research Workshop*, NASA CP 10087, 1992.
5. Morgenstern, J.: SR-71 A Low Boom Modification and Flight Test Plan, *High-Speed Research: Sonic Boom Workshop*, NASA CP 10133, Vol. II, 1993.
6. Plotkin, Kenneth, J.: Calculation of Sonic Boom From Numerical Flow Field Solutions: MDBOOM Version 2.2, *Wyle Research Report WR 92-14*, July 1992.
7. Samareh-Abolhassani, J.: Triangulation of NURBS Surfaces, *Numerical Grid Generation in Computational Fluid Dynamics and Related Fields*, ed. Weatherhill, N.P., et.al., Pineridge Press, pp. 377-388, 1994.
8. Frink, N.; Parikh, P.; and Pirzadeh, S.: A Fast Upwind Solver for the Euler Equations on Three-Dimensional Unstructured Meshes, *AIAA Paper No. 91-0102*, January 1991.
9. Pirzadeh, S.: Recent Progress in Unstructured Grid Generation, *AIAA Paper No. 92-0445*, 1992.
10. Fouladi, K.: Unstructured Grids for Sonic-Boom Analysis Applications, *AIAA Paper No. 2929*, 1993.
11. Fouladi, K.: Assessment of a New Unstructured Grid Scheme for Sonic-Boom Analysis Applications, *High-Speed Research: Sonic Boom*, NASA CP 10133, Vol. II, 1993.
12. Haering, E.; Witmore, S.; and Ehrenberger L.: Measurement of the Basic SR-71 Airplane Near-Field Signature, *High-Speed Research: 1994 Sonic-Boom Workshop*. NASA/CP-1999-209699, 1999.
13. Shepherd, K.; and Sullivan B.: A Loudness Calculation Procedure Applied to Shaped Sonic Booms, *NASA TP-3134*, November 1991.

This page intentionally left blank.

Low-Boom SR-71 Modified Signature Demonstration Program

David Lux, L. J. Ehernberger,
Timothy R. Moes, and Edward A. Haering

NASA Dryden Flight Research Center
Edwards CA 93523-0273

Abstract

A flight program using the SR-71 airplane to validate sonic boom technologies for High-Speed Commercial Transport (HSCT) operation and potentially for low- or softened-boom design configurations is described. This program employs a shaped signature modification to the SR-71 airplane which is designed to demonstrate computational fluid dynamics (CFD) design technology at a full-scale HSCT operating condition of Mach 1.8 at 48,000 feet altitude. Test plans call for measurements in the near-field, at intermediate propagation altitudes, and through the more turbulent boundary layer near the Earth surface. The shaped signature modification to the airplane is comprised of added cross-section areas on the underside of the airplane forward of the wing and engine nacelles. Because the flight demonstration does not approach maximum SR-71 altitude or Mach number, the airplane provides more than adequate performance and maneuver margins for safe operation of the modified airplane. Probe airplane measurements in the near-field will use fast response pressure sensors. Far-field and ground-based boom measurements will use high response microphones or conventional sonic boom field recorders. Scope of the planned demonstration flights also includes ground level measurements during conditions which cause minimal signature distortion and conditions which cause high distortion of the signature.

Outline

- **Introduction**
- **Justification**
- **Flight test objectives**
- **Demonstration test approach**
- **Modified signature flight test plan**
- **Measurement requirements**
- **Discussion**
- **Summary**

INTRODUCTION

Air traffic-routing plans for large supersonic passenger aircraft consider that ground level sonic boom strength may be too large to allow regular flight routes over populated areas. Thus, supersonic routes used by the Concorde and those envisioned for second-generation "High-Speed Commercial Transport" (HSCT) aircraft are essentially restricted to over-water segments. This restriction extends the travel time required for many city pairs and thereby reduces the utilization (mileage) rate for each airframe. Intercontinental service to inland cities would be faster and the overall return on airframe investment would be greater if supersonic speeds could be used on overland routes. However, supersonic operation over most populated areas is not likely to be allowed for current baseline HSCT designs because they would produce boom over pressures on the order of 3.0 pounds per square foot (psf) at cruise (Mach 2.4) and somewhat higher in the Mach 1.2 to 1.4 region during the accelerating climb and decelerating descent. To alleviate this problem, recent airplane design studies developed configuration concepts that could be used to reduce boom annoyance levels (refs. 1 and 2). These modifications of the configuration cross-section area and lift distributions would reduce the initial overpressure rise. The resulting shock pattern at ground level would not be as large and sharp as the N-wave usually produced at the ground by aircraft at high cruise altitudes.

Flight tests to demonstrate low-boom design capability by modifying existing airframes have been proposed for the BQM-34E remotely piloted vehicle (RPV, the "Firebee," Teledyne Ryan Aeronautical Co., San Diego, CA, refs. 3 and 4) and the manned Mach 3 SR-71 (Lockheed Corporation, Burbank CA) reconnaissance airplane (refs. 5 and 6). An important reason for testing the viability of low-boom design concepts is provided by route performance trade studies (ref. 7) which indicate that reduced boom configurations using a cruise Mach number of 1.8 for sensitive overland corridors and 2.0 over oceanic routes would reduce travel time for many city pairs and increase airframe utilization rates relative to conventional configurations using 0.9 Mach overland and 2.4 Mach over oceanic route segments. Moreover, the ability to serve additional cities would improve the return on fixed investment costs by increasing the production run. Thus, successful demonstration of the computational fluid dynamics (CFD) technology to predict the near-field boom signature and to design supersonic configurations which produce low-annoyance boom signatures at ground level could allow expansion of supersonic HSCT flight to a number of additional overland route segments. Since low-boom characteristics require major differences in airframe configuration, accurate assessment of their potential is important before HSCT pre-production design specifications are finalized.

Introduction

- **Demonstrate low-boom, shaped signature technology in flight**
- **Acquire in situ, near-field signature measurements to validate low-boom design technology**
- **Examine signature formation and initial coalescence characteristics**
- **Evaluate state-of-the-art computation tools for sonic boom propagation**
- **Document sonic boom distortion caused by Earth turbulent boundary-layer effects for shaped and N-wave signatures under quiet and turbulent conditions**

JUSTIFICATION

Unique merits of the plan to demonstrate low (or reduced) boom design technology with the SR-71 include the (1) large, essentially full-scale HSCT capability for the signature modification evaluation, (2) demonstration test condition would be at a realistic flight altitude and Mach number for HSCT cruise, (3) test altitude permits propagation evaluation over a conservatively long propagation path to the ground, (4) measurements at intermediate altitudes would scale directly to the actual HSCT operating condition, (5) SR-71 performance margins can support a wide range of experimental modifications and aerodynamic conditions within the HSCT altitude envelope. The plan incorporates measurements of near-field signature formation, coalescence, aging over long propagation paths and turbulent distortions through the ground layer. These measurements will serve to assess CFD near-field prediction, establish the capability for state-of-the-art propagation codes and illustrate the effects of Earth turbulent boundary-layer and signature shape. As such, the design technology enabled by the SR-71 demonstration will support sonic boom impact assessment for standard planforms as well as for low-boom configurations. It will substantiate, and most likely improve, the technologies needed to address boom sensitivity concerns for both overland and over-water routes. The primary driver in the choice between reduced boom and conventional HSCT configurations is likely to be future national and international standards for maximum over-pressure metrics and exposure rates over various population zones and natural habitats. Hence, the ability to formulate recommendations and negotiate favorable route agreements will hinge on expert first-hand skills in the sonic boom technical areas.

Significant resources in research program dollars, intellectual effort, CFD development and wind-tunnel testing have been directed at improving traditional boom prediction tools during recent years (ref. 2). State-of-the-art improvements for boom propagation prediction appear to center on rise time as influenced by oxygen and nitrogen molecular absorption. Sound attenuation by water vapor is also indicated by some investigators. Turbulence effects have been explored experimentally using shocks produced by sparks in the laboratory and by using parameterized boundary-layer characterization with previous field study data. Adequate field data for empirical validation of these new refinements in boom signature propagation and boundary-layer distortion have not been acquired for their use in the significant decision-making processes that face the HSCT.

Delay of the real atmosphere experience at HSCT flight conditions, which brings the above refinements to maturity, increases program risk and cost penalties. Outside interests (other agencies, other countries and environmental groups) will continue to periodically bring confrontation on sonic boom issues to the table. If the High Speed Research (HSR) Program is ready with mature, demonstrated boom technology, the program risks attending these confrontations will be minimized. If test and demonstration of the boom technology elements are delayed, the costs needed to maintain the current technological position on the learning curve will increase, or capabilities for accomplishment at a later date will decrease. Decreased capability could result from human and technical attrition because of several factors. First, inadequate career phasing can fail to provide the needed expert personnel. Second, in the face of pressing decision-making situations, the lack of adequate expertise easily leads to over-reaching assumptions, or perhaps worse yet, to technical apathy and misdirected attention. The element of human attrition is particularly critical for several reasons. Sonic boom technologies span several areas of expertise. Personnel retention is difficult since levels of program support vacillate from "some" to "nearly none". Present capabilities rely strongly on empirical experience and "engineering art" as practiced by only a few experts. New theoretical formulations are not quickly validated in flight nor rapidly assimilated as permanently established engineering practices.

JUSTIFICATION (cont'd)

A large part of the existing national ability can be attributed to NASA HSR Program efforts at Langley Research Center, Hampton, Virginia. These efforts have brought together broad interdisciplinary expertise from government, industry and academia. Note that these disciplinary areas are thinly staffed and, that historically, industry has not internally maintained more than one or two of the requisite skills in any given corporate entity at any given time. Continuation of the national team activity is the least costly way to provide the critical expertise necessary to deal with future challenges to supersonic fleet operations.

Sonic boom technology is and will continue to be a competitive element for national and international acceptance of supersonic passenger aircraft design and operation. Low-boom concept technologies could be established as a potential HSCT enhancement factor for overland route segments. Moreover, the U.S. sonic boom technical ability will be one of the HSCT make-or-break issues for environmental review of routes over water and sparsely populated areas.

Justification

- **Reduced boom overland flight segments will increase HSCT utilization rate and airframe production run.**
- **Flight-demonstrated technology will be applicable to soften boom strength for conventional Mach 2.4 HSCT planforms.**
- **Critical expertise in sonic boom technologies cultivated from the 1960's to 1990's can be sustained for application during the HSCT era - 2000 to 2020.**

FLIGHT TEST OBJECTIVES

The modified signature demonstration using the SR-71 will address four goals:

1. Demonstrate a shaped sonic boom waveform (non N-wave signature) at the ground.
2. Validate the CFD code capabilities for design of shaped near-field sonic boom signatures.
3. Evaluate the abilities of state-of-the-art tools to predict shaped signature propagation from cruise altitude to mid- and low-altitudes.
4. Obtain empirical data for shaped signature (non N-wave) propagation through the Earth boundary layer under quiet (stable, low wind) and turbulent (convective, windy) conditions.

The ultimate test of low-boom design technology is for the sonic boom waveform generated by the test airplane at HSCT cruise conditions to reach ground level without coalescing into the classic N-wave form with its large, strong, sharp rise to maximum overpressure at the leading-edge. Instead, it is desired that the shaped signature would reach ground level with a smaller leading-edge pressure rise followed by a gradual pressure rise ramp, or a "flat-top" segment, before producing the maximum boom overpressure. Such shaping of the boom decreases the annoyance to humans and the startle effect on other animals. The SR-71 flight capability provides an especially conservative demonstration of low-boom technology because it can reach HSCT flight conditions. Its relatively shorter length (approximately 100 feet vs. 300 feet for the HSCT) gives a longer propagation in terms of altitude-to-fuselage-length (h/l) scaling units. The SR-71 bow to inlet distance allows the shaped signature to have a ramp with the rate of pressure increase representative of that desired for the full-scale HSCT (ref. 6).

Near-field validation of CFD code design ability requires in situ measurement of the sonic boom overpressure signature that is close to the generating aircraft (approximately 100 feet). Evaluation of signature propagation tools requires in situ measurement in the near-field (roughly 100 to 1000 feet) below the generating aircraft and at mid- and low-altitudes to examine coalescence, signature aging caused by molecular absorption of acoustic energy, and distortion caused by atmospheric perturbations.

Flight Test Objectives

- **Demonstrate shaped boom waveform at ground level**
- **Validate CFD design codes with in situ near-field measurements**
- **Evaluate propagation codes and coalescence behavior**
- **Observe boundary-layer induced distortions for N- and non N-wave signatures**

DEMONSTRATION TEST APPROACH

The three main areas of the low-boom demonstration program include design and fabrication, flight test operations, and sonic boom measurements and data analysis. Industry, NASA, and the science community will conduct the program.

A modification to the cross-sectional area of the SR-71 forebody is being designed by industry (ref. 6). The design uses CFD in an iterative process. Area is added to achieve a desired signature shape. Then, the resulting local aerodynamics and near-field signature shape are evaluated. The primary flight condition for design of a low-boom HSCT is taken to be Mach 1.8 at 48,000 feet pressure altitude. Interest also exists in boom softening for a conventional HSCT planform at a cruise speed of Mach 2.4. However, additional fabrication costs are entailed for demonstration at the higher Mach number. Thus, this paper emphasizes the Mach 1.8 low-boom demonstration.

The SR-71 airplane manufacturer completed structural design for the low-boom modification using preliminary loft lines. Final design, fabrication, and installation will allow functional access to the service bays, operation of the landing gear, and removal of the modification to return the aircraft to its original flight configuration.

Flight test responsibilities center on the NASA Dryden Flight Research Center where the SR-71 is presently operating. These responsibilities include flight safety and flight readiness reviews, flight test engineering, aircrew preparations, and data acquisition. The CFD analysis of the final low-boom modification design will be accomplished independently by industry, NASA Langley Research Center, and NASA Ames Research Center. Aerodynamic margins will be examined on the basis of CFD results and flight simulation. If any performance or safety concerns are identified, wind-tunnel tests using a model of the modified SR-71 will be conducted. Data analysis and evaluation will be shared with HSR Program participants in industry, academia, and NASA.

Demonstration Test Approach

- **Modification loft design and CFD aeroloads conducted by Douglas**
- **Structural aircraft modification design conducted by Lockheed**
- **Low-boom modification fabrication and installation by Lockheed**
- **Research flights using modified SR-71, probe aircraft, and ground measurements at Dryden**
- **Data analysis by HSR Contractors, Langley, Ames, and Dryden**

MODIFIED SIGNATURE FLIGHT TEST PLAN

Flight operations will involve the modified SR-71 airplane, instrumented probe airplane, and safety chase. The SR-71 will generate the modified sonic boom signature in steady flight at Mach 1.8 and 48,000 feet similar to the previous flight tests (ref. 8). The instrumented near-field probe airplane will probe forward from a position behind and below the SR-71. The probe airplane can keep the SR-71 in view, even as the SR-71 bow shock is crossed. This is possible since the bow shock cone sweeps backward from the airplane to allow a longitudinal gap between the probe airplane nose below and the SR-71 tail above. Next, the probe airplane will drop back and reposition itself for another pass. During near-field signature sampling, the relative speed between the aircraft is expected to range up to 25 fps. Significantly higher rates would be expected to increase the time needed to reposition as well as decrease safety margins. Plans call for 12 good near-field probes: 3 each at altitude separations of 100, 200, 500, and 1000 feet below the SR-71.

Ground-based signature measurements will be accomplished by overflying an array of sonic boom recorders. To cover the signature variations caused by naturally unsteady atmospheric conditions, six passes are planned for calm or low-signature-distortion conditions which are most likely during morning hours. Another six passes are planned for conditions when the typical N-wave signatures would be more strongly distorted by atmospheric turbulence and winds. An additional six passes are anticipated for "off-design" test points at other Mach-altitude combinations. Supporting measurements will include rawinsonde measurement of the atmospheric wind, temperature, and humidity profiles from Edwards AFB, California, near the flight time. Detailed atmospheric boundary-layer characteristics at the sonic boom array will be measured by tethered sonde and ground-based acoustic probes (SODAR) to document wind and temperature profiles and fluctuations in the boundary layer.

Signature measurements during propagation at middle and low altitudes above the Earth turbulent boundary layer will be obtained with subsonic platforms using sonic boom recorders or microphones with equivalent dynamic characteristics.

Modified Signature Flight Test Plan

- **SR-71 maintains Mach 1.8 and constant altitude**
- **Probe airplane positions below and aft, then moves forward**
- **Probe airplane passes bow shock, drops back and repeats**
- **Both aircraft use differential Global Positioning System (GPS)**
- **Signature measured with short-coupled, high-response total and static pressure sensors**
- **Mid-field, far-field, and ground signatures measured with boom recorders, microphones, or narrow range differential pressure sensors**

MEASUREMENT REQUIREMENTS

Near the signature-generating airplane, the overpressures are relatively large and decrease rapidly with distance as the Mach cone propagates away. Therefore, to validate computed pressure fields near the airplane, adequate precision must be used for the in situ pressure measurements and the distance between the generator and the probe aircraft. A table of measurement quality goals is given below.

In the near-field region of interest, the maximum overpressure ranges from approximately 20 percent to less than 2 percent of the flight altitude ambient pressure. In terms of operational absolute pressure transducers used for pressure altitude, these overpressures become 2 to 0.2 percent of the full-scale range. Thus, the goal for overpressure accuracy of 5 percent calls for sensor stability and resolution reaching 0.01 percent of transducer full scale. Measurement risk will be reduced by implementing high-response probes for static and total pressure. In addition, absolute pressure transducers may be augmented with differential transducers referenced to nominal pressure reservoirs for increased resolution and redundancy. Relative aircraft positions will be obtained with differential GPS on each airplane (ref. 8). Precision ground-based tracking radar will provide backup data for each airplane.

Measurement Requirements

<u>Parameter</u>	<u>Tolerance</u>
SR-71 test condition, Mach number	0.05
SR-71 test point pressure altitude, ft	150
Relative separation distance, percent	5
Overpressure accuracy, percent	5
Minimum damping ratio	0.7
Minimum natural frequency, Hz	50
Minimum sample rate, sps	100

DISCUSSION

The proposed modified SR-71 sonic boom flight test program represents a highly comprehensive demonstration of sonic boom technologies. This program presents the first opportunity to explore the propagation of shaped signatures with in situ data documentation in the airplane near field, at mid-field, through the Earth boundary layer, and at ground level. These near-field data will validate wind-tunnel and CFD techniques. These techniques are the primary tools for HSCT evaluation during the airplane design stage. Wind-tunnel measurements and CFD data are restricted to flow near the body of the aircraft because of practical limitations in wind-tunnel dimensions and CFD grid point density (or computational cost). Thus, the near-field, in-flight data will validate assumptions used to bridge the gap between local aerodynamics and specification of initial conditions for boom propagation codes. Signature measurements at middle and ground levels will provide data for evaluation of boom propagation code abilities to account for atmospheric absorption and rise time characteristics which impact annoyance statistics. Demonstrated skill in the state-of-the-art for these technologies is crucial to low-boom design decisions and vital to environmental impact clearance for conventional HSCT platforms.

Flight operations planning and safety reviews will thoroughly consider impacts of the modification on aircraft structural integrity, performance, and flight control. Structural design of the cross-sectional area modification for the Mach 1.8 test point has been approached using a safety factor of 2.25. Aerodynamics results from a preliminary design indicate minimal change in pitching moment. Final design CFD will be confirmed independently by analysis codes at NASA Langley Research Center and NASA Ames Research Center. The resulting aerodynamic characteristics will be used in the flight simulator to examine airworthiness of the modification. Any performance factors or stability and control anomalies with the potential to compromise flight safety will be evaluated using further CFD and wind-tunnel tests.

Discussion

- **Proposed SR-71 modified boom signature demonstration would validate design and propagation technologies for application to the HSCT.**
- **Go-ahead for the SR-71 modification was deferred because of budget decreases and ongoing design rework.**
- **Current emphasis is redirected toward signature coalescence and propagation issues.**

DISCUSSION (cont'd)

A final design for the SR-71 modified boom signature demonstration has not been completed. Budget reductions and program redirection indicate that a go-ahead is not imminent. In the interim, independent approaches to low-boom CFD design are emerging (ref. 9). These approaches may provide additional confirmation of or optimization to the proposed SR-71 modification.

Sonic boom flight research and field study needs can be grouped into four phenomenological areas: (1) the local boom signature aerodynamic formation processes within approximately three body lengths or six span distances below the airplane, (2) the signature feature coalescence region in which higher pressure shock zones overtake lower pressure zones, (3) molecular interactions which exert frequency dependent acoustic absorption, and (4) focusing and distortion caused by maneuvers and atmospheric perturbations. A major thrust of the proposed SR-71 modified signature demonstration addresses the ability of CFD techniques to account for signature formation during the design phase of an aircraft. Some discrepancies between CFD, analytical methods and wind tunnel test data in this region are not adequately understood. Because of programmatic constraints, attention to these areas may be deferred in favor of field measurements to examine the coalescence phenomena which result in the N-wave signature shape. Initial suggestions for signature coalescence flight test points are listed below.

Recommended Coalescence Test Point Objectives

- **Measure signature at 4 separations from near-field to N-wave formation**
- **Accomplish for three Mach numbers between 1.2 and 2.4**
- **Emphasize lightweight, high dynamic pressure, low altitude conditions**
- **Spot-check heavy high altitude conditions at two Mach numbers**
- **Spot-check signature coalescence above the airplane at two Mach numbers and two separations**

SUMMARY

Sonic boom technologies are a critical element in the United States High-Speed Civil Transport (HSCT) efforts. In fact, these technologies could easily be make or break factors with respect to such issues as (1) environmental acceptance for over water and overland routes, (2) precise discrimination between boom strength from U.S. HSCT designs and those of competing countries, (3) realistic negotiations of specific routes and supersonic approach corridor distances, and (4) assessment of domestic and foreign low-boom design proposals. The proposed SR-71 modified boom demonstration offers a timely opportunity to ascertain whether state-of-the-art technologies for computational fluid dynamics (CFD) design techniques and boom propagation prediction codes can move from the drawing board to practice in full-scale flight.

At HSCT altitudes and Mach numbers, the SR-71 has a broad flight envelope. At given altitudes, its speed range extends a full Mach number. At fixed Mach numbers, its altitude envelope is approximately 20,000 feet thick. This envelope provides a broad capability for the safe conduct of flight experiments that entail additional weight and drag. Other test bed vehicles either lack in size, speed range, and reliability or use mixed compression inlets which can not represent anticipated HSCT configurations as well as does the SR-71 (at Mach numbers from 1.6 to 3.0). Similar capability is not anticipated in future aircraft or in HSCT prototypes because of their requirement for increased mission optimization.

The SR-71 ability to flight test design techniques, propagation prediction codes and signature distortion all together in the real atmosphere at essentially full-scale HSCT conditions represents a highly cost-effective and timely use of program resources.

Remarks

- **SR-71 is the most "*experimenter friendly*" test bed for Mach numbers between 1.8 and 2.4 anticipated to be available over the next 20 years**
 - Payload margin
 - Flight endurance
 - Speed altitude envelope
- **HSCT prototype financial commitment requires demonstrated technology maturity**
- **Partial or fragmented sonic boom expertise could very likely be an "*HSCT Show Stopper*" in the environmental-political arena**

REFERENCES

1. Haglund, George T., "Low Sonic Boom Studies at Boeing," High-Speed Research: Sonic Boom, NASA CP-10133, vol. II, 1994, pp. 81-94.
2. Darden, Christine M., Powell, Clemans A., Hayes, Wallace D., George, Albert R., and Pierce, Allan D.: *Status of Sonic Boom Methodology and Understanding*, NASA CP-3027, 1988.
3. Darden, Christine M. and Needleman, Kathy E., "Assessment of the BQM 34-E "Firebee" as a Test Vehicle for Sonic Boom Minimization," High-Speed Research: Sonic Boom, NASA CP-10133, vol. II, 1994., pp. 417 -448.
4. Maglieri, Domenic J.; Sothcott, Victor E.; and Keefer, Thomas N.: Feasibility Study on Conducting Overflight Measurements of Shaped Sonic-Boom Signatures Using the Firebee BQM 34-E RPV. NASA CR-1879715, 1993
5. Morgenstern, John, SR-71A Low Boom Modification and Flight Test Plan. High-Speed Research Sonic Boom, NASA CP-10133, vol. II, 1994 pp. 399-415.
6. Morgenstern, John M., Bruns, Dave B., and Camacho, Peter P., SR-71 Reduced Sonic Boom Modification Design, NASA/CP-1999-209699, 1999.
7. Metwally, Munir, "Economic Benefits of Supersonic Overland Operation," NASA CP-3173, vol. 2, 1992.
8. Haering, Edward A., Whitmore, Stephen A., and Ehernberger, L. J., "Measurement of the SR-71 Airplane Near Field Signature," NASA/CP-1999-209699, 1999.
9. Siclari, Michaiel J., "The Analysis and Design of Low Boom Configurations Using CFD and Numerical Optimization Techniques," NASA/CP-1999-209699, 1999.

IN-FLIGHT TECHNIQUE FOR ACQUIRING MID- AND FAR-FIELD SONIC BOOM SIGNATURES

Eugene G. Stansbery
NASA Johnson Space Center
Houston, TX

Daniel G. Baize
NASA Langley Research Center
Hampton, VA

and
Domenic J. Maglieri
Eagle Aerospace, Inc., Aeronautics Division
Hampton, VA

ABSTRACT

Flight test experiments have been conducted to establish the feasibility of obtaining sonic boom signature measurements below a supersonic aircraft using the NASA Portable Automatic Triggering System (PATS) mounted in the USMC Pioneer Unmanned Aerial Vehicle (UAV). This study forms a part of the NASA sonic boom minimization activities, specifically the demonstration of persistence of modified boom signatures to very large distances in a real atmosphere. The basic objective of the measurement effort was to obtain a qualitative view of the sonic boom signature in terms of its shape, number of shocks, their locations, and their relative strength. Results suggest that the technique may very well provide quantitative information relative to mid-field and far-field boom signatures. The purpose of this presentation is to describe the arrangement and operation of this in-flight system and to present the resulting sonic boom measurements.

Adaption and modification of two PATS to the UAV payload section are described and include transducer location, mounting arrangement, and recording system isolation. Ground static runup, takeoff and landing, and cruise flight checkouts regarding UAV propeller and flow noise on the PATS automated triggering system and recording mode are discussed. For the proof-of-concept tests, the PATS instrumented UAV was flown under radar control in steady-level flight at the altitude of 8700 feet MSL and at a cruise speed of about 60 knots. The USN F-4N sonic boom generating aircraft was vectored over the UAV on reciprocal headings at altitudes of about 11,000 feet MSL and 13,000 feet MSL at about Mach 1.15. Sonic boom signatures were acquired on both PATS for all six supersonic passes. Although the UAV propeller noise is clearly evident in all the measurements, the F-4 boom signature is clearly distinguishable and is typically N-wave in character with sharply rising shock fronts and with a mid-shock associated with the inlet-wing juncture.

Consideration is being given to adapting the PATS/UAV measurements technique to the NASA Learjet to determine feasibility of acquiring in-flight boom signatures in the altitude range of 10,000 feet to 40,000 feet.

An outline of the presentation is given in Chart 1. First, some background material will be provided and includes a description of various means/techniques used to acquire and define the shock flow-field about an aircraft in supersonic flight, a discussion on the application of in-flight supersonic flow field data in providing considerable insight into the sonic boom phenomena, and a summary of the existing data base. Next to follow is a discussion of the manner in which the Portable Automatic Triggering Systems (PATS) were adapted to the Unmanned Aerial Vehicle (UAV) and the checkout procedures involved to assess their performance during ground static and flight operations prior to the sonic boom measurement phase. A description of the sonic boom measurement phase of the program will then be covered and includes the flight test setup and measured results. The presentation will also provide a brief discussion of the potential application of this in-flight measurement technique to other subsonic vehicles having greater attitude capability than the UAV. Finally, the results of this experimental in-flight sonic boom measurement program will be summarized.

OUTLINE OF PRESENTATION

- BACKGROUND
 - methods used to define flow field
 - application of results
 - existing data base
- ADAPTATION AND CHECKOUT OF PATS/UAV
- FLIGHT TEST SETUP/RESULTS
- POTENTIAL APPLICATIONS
- SUMMARY REMARKS

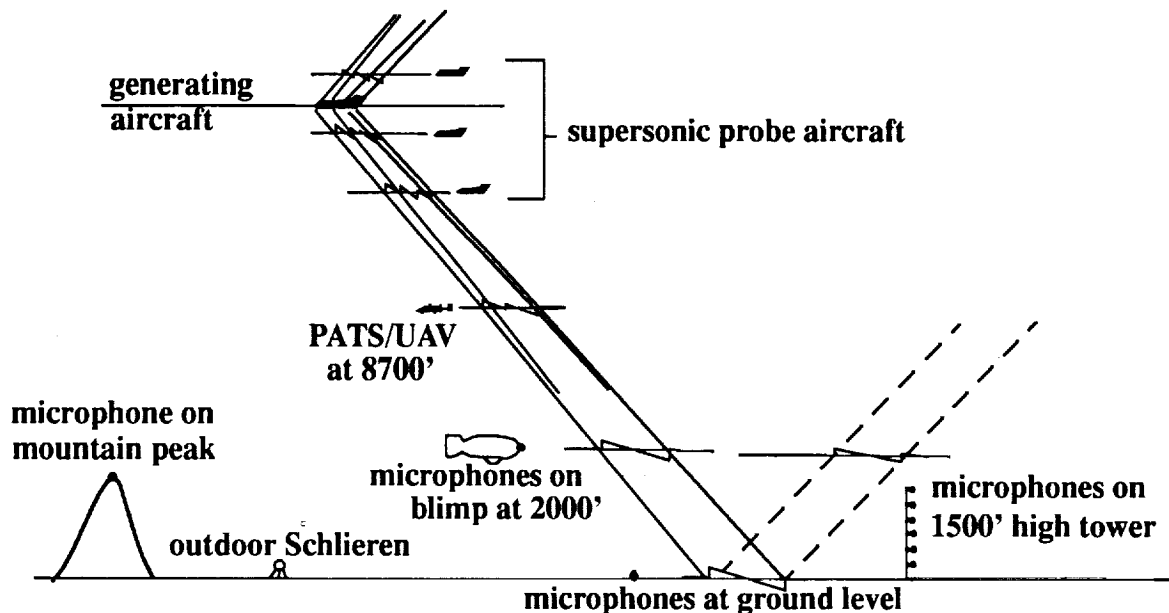
An indication of the various methods used to describe the shock flow-field about an aircraft in supersonic flight is schematically illustrated in Chart 2. These methods include probe flights with instrumented supersonic aircraft, measurements taken with transducers located on high mountains, on blimps hovering high above the ground surface, on relatively high fixed towers, at ground level, the recently developed ground-based "outdoor Schlieren" photography method, and the present in-flight PATS/UAV airborne measurement method.

Probing the near and mid flow-field of the shock generating aircraft, by means of an instrumented aircraft passing or being passed at positions above, to the side, and below has been the most utilized technique and provides the clearest detail as to the complex nature of the shock flow-field near the aircraft.

Some boom measurements have been made on high mountains, but little, if any, data are available in the literature. Sonic boom signatures have been measured by means of balloon-borne and tower-mounted microphones and provide considerable information on signature distortion due to turbulence in the first few thousand feet of the earth's boundary layer, ground reflection coefficients, and information regarding the extremities of shock waves for flight operations at Mach cutoff and at the lateral cutoff. Ground level measurements make up the majority of the sonic boom data base.

The ground-based outdoor Schlieren method described in an earlier paper presented at this Workshop (ref. 1) and PATS/UAV airborne in-flight technique described in this paper are both recent and innovative approaches to defining the aircraft's supersonic flow-field.

METHODS OF DEFINING SHOCK FLOW FIELD ABOUT AN AIRCRAFT IN SUPERSONIC FLIGHT



Application of the in-flight supersonic flow field data acquired through any of the various methods/techniques just discussed is paramount to the design of an HSCT having a minimized boom waveform (Chart 3). A description of the supersonic shock flow-field will provide information on the number, location, and strength of the shocks contained in the flow-field and can also show how many aircraft body lengths (h/l) it takes for these shocks to coalesce into a far-field N-wave. Qualitative and quantitative information of this nature provides a means of validating the present CFD prediction codes out to much larger distances than are attainable in wind tunnels using small models. This insight then allows for a more accurate means of determining when the flow field about the aircraft has reached an equivalent body state where the sonic boom propagation codes can be properly applied and the correctly predicted pressure signatures at ground level can be established.

Measurement techniques, such as the outdoor Schlieren photography, also provide insight into the persistence of a sonic boom signature shock structure as it moves from locations very near the aircraft to many body lengths away as the local shocks age and coalesce. The present PATS/UAV airborne measurement technique may also provide a source of information on atmospheric turbulence as it relates to signature distortions and shock rise times. Better definition of the influence of O_2 , N_2 , and RH (relative humidity) on shock smoothing (rise time) could also surface. Finally, many of the shock flow-field observation techniques, especially the Schlieren photography and PATS/UAV airborne systems would provide a data base regarding the initial conditions of the secondary (over-the-top) sonic boom.

APPLICATION OF IN-FLIGHT SUPERSONIC FLOW-FIELD DATA

- Establishes number, location, strength of shocks
- Describes shock wave coalescence
- Validates prediction methods
- Provides insight into waveform persistence/aging
- Source of information on turbulence scale/waveform shape/shock rise time
- Define O_2 , N_2 , RH influence on shock rise time
- Describe initial conditions of secondary booms

A brief summary of the in-flight supersonic flow-field data base that has been gathered over almost four decades in regards to the sonic boom phenomena, is given in Chart 4. Information listed in the table includes the test aircraft, location of the flow field observation about the aircraft, number of body lengths (h/l) from the test aircraft, the technique utilized, type results acquired, the time period of the observations, and the publication source.

An examination of the information contained in Chart 4 indicates that the present sonic boom flow field data base is a result of ten (10) experiments involving nine (9) different aircraft which include the F-100, F-104, B-58, F-106, XB-70, F-18, SR-71, T-38 and F-4. The majority of flow field experiments have been conducted using supersonic aircraft with instrumented probes and flying below the test aircraft at distances of from 0.4 to 95 body lengths, and also above and to the side of the test aircraft from 1 to 33 body lengths away (refs. 1, 2, 3, 4, 5 and 6).

Airborne measurements using transducers carried aloft on a blimp (ref. 7) and stationary transducers located on a very high tower (refs. 8-11) have provided very useful information but are usually confined to far-field N-wave type signatures.

The two most recent developments in flow-field definition techniques that can be used to describe the nature of the shock flow-field about an aircraft, indicated by the three check (✓) marks on Chart 4, are the ground-based outdoor Schlieren and the airborne PATS/UAV system, both of which are discussed in the present workshop.

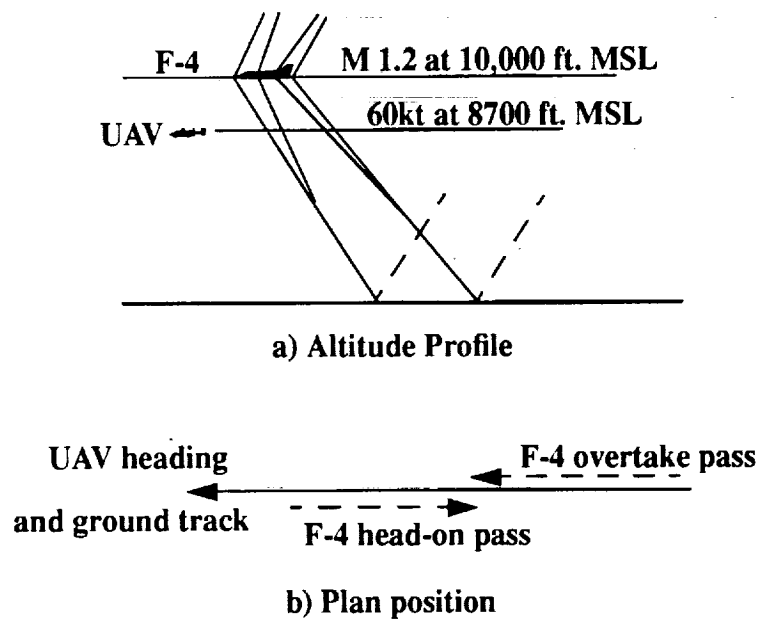
IN-FLIGHT SUPERSONIC FLOW-FIELD DATA BASE

Test Aircraft	Observation Location	Separation Distance h/l	Method/Technique	Data/Format	Date	Report/Source
F-100	below side	2-41 2-33	supersonic probe aircraft	pressure signatures	1956	AFFTC-TN-56-20
F-100 F-104 B-58	side side side	4-8 3-8 1-2	supersonic probe aircraft	pressure signatures	1960	NASA TN D-621
B-58	above below	17-20 14-95	supersonic probe aircraft	pressure signatures	1963	NASA TN D-1968
F-106	below	600	Blimp with airborne microphone	pressure signatures	1963	NASA SP-147
XB-70	above below	11 11-27	supersonic probe aircraft	pressure signature	1966	NSBEO 1-67
F-104	below	600	1500 high BREN tower w/ microphones	pressure signatures	1970	NASA SP-255 NASA CR 2167 NASA CR 2417
SR-71	below	0.4-7	supersonic probe aircraft	pressure signatures	1993	present workshop
✓ T-38	above	0-2	outdoor Schlieren	photographs	1994	present workshop
✓ F-18	above below	0-4 0-59	outdoor Schlieren	photographs	1994	present workshop
✓ F-4	below	38-86	airborne PATS/UAV	pressure signatures	1994	present workshop

The PATS/UAV measurement concept came about during the planning phase of a proposed sonic boom flight test program aimed at demonstrating the persistence of shaped sonic boom signatures to very large distances ($h/l \sim 300$) using the Teledyne Ryan BQM 34-E supersonic RPV (refs. 12 and 13). Predictions of the modified waveform produced by the alteration of the basic BQM 34-E area development were strongly influenced by the assumptions made regarding inlet shock/spillage. Thus, the need for a remotely activated airborne measurement platform was identified - one that would provide at least a qualitative measure of the modified signature and, in particular, the inlet shock in the mid-field of the BQM 34-E. Since the BQM 34-E is a remotely piloted vehicle (RPV) it was apparent that any airborne sonic boom signature measurement would have to be acquired using an unmanned and remotely operated system.

The nominal flight plan arrangement for proving the PATS/UAV airborne measurement system using a USN F-4N aircraft, which is 58.3 feet long, as the generating aircraft is shown in Chart 5. Two parameters were to be satisfied on the planned flight tests, the UAV would be flown in the altitude range planned for the BQM 34-E (8700 ft.) and the F-4 would be flown in a clean configuration at altitudes of 10,000 feet and 12,000 feet so that sonic boom signatures with Δp levels of about 10 psf and 5 psf, respectively, would be experienced by the UAV, the same as would be experienced in the BQM 34-E tests. The PATS/UAV system would fly at constant speed altitude-heading out over the water and the F-4 would make supersonic passes on the same and reciprocal headings (overtaking and head-on). Mach/altitude conditions would be attained about 4 n.mi. prior to being overhead of the UAV. Precision radar tracking was provided on both vehicles.

F-4/UAV NOMINAL FLIGHT PLAN ARRANGEMENT

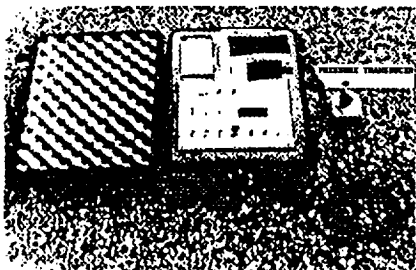


Proposing the PATS as the in-flight measurement system to be flown on the UAV was logical and practical because of its remote digital-self triggering, self powered capability and its relatively low weight and compact size. The PATS was developed by NASA JSC in 1983 for the purpose of providing an unmanned and self triggering digital system to record sonic boom signatures from Space Shuttle operations (ref. 14). A photograph of this system, along with a wiring schematic listing of its general characteristics, a listing of key specifications, and a sample of a measured boom signature, is given in Chart 6. The performance of this system has been directly compared during sonic boom field tests (refs. 15 and 16) with the formerly deployed NASA analog systems and the current USAF Boom Event Analyzer and Recorder System (BEARS).

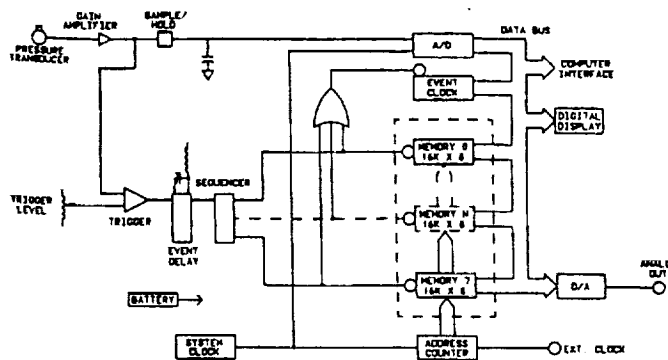
The frequency capability of the pressure transducer is from DC to 10 kHz. Each of the 8 memory banks stores 16,000 digital samples at a rate of approximately 8,000 samples/second or about 2 seconds of data. The highest resolved frequency is therefore about 4 kHz. The low frequency response of the unit is set by an RC circuit and is approximately 0.3 Hz. The maximum overpressure recordable is set by the gain of the signal conditioning amplifier and for the PATS/UAV application, Unit 1 was set at ± 23 psf and Unit 2 was set at ± 13 psf. The measured F-4 boom signature, shown in the lower part of Chart 7, is associated with the field flight calibration tests of reference 15 and is for steady-level flight at $M = 1.15$ at 6,000 feet AGL.

The PATS triggers on pressure levels that exceed an adjustable pressure threshold and remains above the threshold for a minimum duration that is also set by an RC circuit.

CHARACTERISTICS OF PORTABLE AUTOMATIC TRIGGERING SYSTEM (PATS)



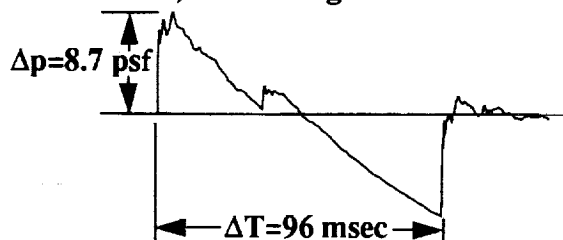
a) Photograph of Standard PATS



b) Block Diagram of PATS

- unit weight..... 15 lbs.
- frequency response..... 0.3 Hz to 4 KHz
- memory banks 8
- Δp range 0.1 to 13 psf

c) Typical Specifications



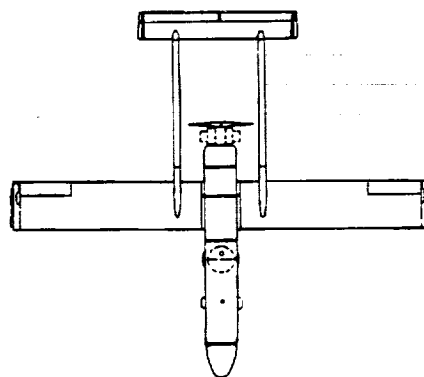
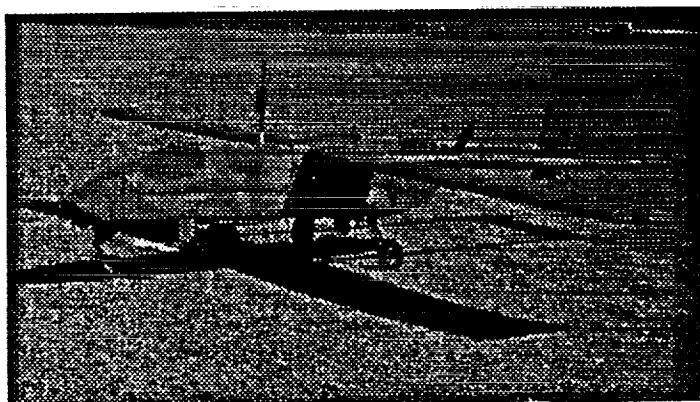
d) Measured F-4 Signature at Ground Level (M = 1.15 at 6000 ft. AGL)

The Pioneer UAV is built by Pioneer UAV Inc. (PUI), a joint venture composed of AAI and Israeli Aerospace Industries (IAI). Pioneer is presently flown by the U. S. Marine Corps, U. S. Army, and U. S. Navy, and is utilized to carry a wide variety of electronic, electro-optical and infrared airborne sensors (ref. 17). A photograph of the UAV, a two-view schematic and some general characteristics, are provided in Chart 7. The Pioneer is a high winged, twin tail boom, pusher propeller driven vehicle, 14-feet in length and having a 17-foot wing span. It is powered by a Sachs SF-350 horizontally opposed, twin-cylinder, two-stroke engine which produces 26 1/2 hp and drives a 29 inch diameter two-blade, 18 degree, fixed pitch pusher propeller. Maximum design gross take-off weight is 452 pounds and the wing loading is 19 lbs/ft². Payload carrying capacity is approximately 70 pounds with a full fuel load, and the electrical system can supply 275 W to power the payload. The payload compartment is approximately 3.6 cu feet in volume. Pioneer has a flight ceiling of 15,000 feet, a mission radius of 100 n.mi., a 4-5 hour endurance, and cruises at 60-65 knots.

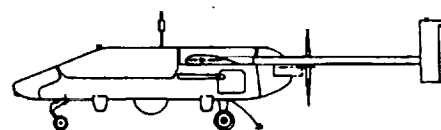
An onboard auto-pilot allows for platform stability and ease of control through all phases of flight. The GCS-2000 Ground Control Station operates and controls the UAV and its payloads, and receives, computes, and displays real time data from the UAV. Real time optical or IR video imagery of the target area is also transmitted to the GCS via an automatic tracking and communications station which utilizes a jam resistant, semi-secure two-way data link to transmit and receive UAV/GCS information. The system requires a four man crew (Internal Pilot, External Pilot, Payload Operator, and Crew Chief) to operate.

The Pioneer UAV system utilized for the present studies was provided by the Naval Air Warfare Center, Weapons Division, Point Mugu, and was operated by the Fleet Assistance Support Team (FAST), Marine Aviation Detachment, China Lake, Point Mugu Support Office.

CHARACTERISTICS OF PIONEER UNMANNED AERIAL VEHICLE (UAV)



maximum gross weight.....	452 lbs.
payload.....	70 lbs.
length.....	14 ft.
wingspan.....	17 ft.
cruise speed.....	60 kts.
maximum altitude.....	15,000 ft.



A number of major concerns arose regarding the adaptation of the PATS to the UAV and these are listed in Chart 8. One of the first concerns was the nature of the boom signature that would result because of the 60 kt cruise speed of the UAV. Another concern regarding the PATS/UAV arrangement had to do with the PATS trigger level settings. More specifically, would the noise levels associated with the UAV propulsion system and/or the aerodynamic flow during cruise flight or acceleration loads due to turbulence, runway roughness, or landing impact, cause the PATS to trigger (turn on) and, thus, use up all 8 memory banks before the boom signatures were recorded? Even though the PATS circuitry is designed to ignore the signals produced by the propeller, which are of very short duration, it was not known what influence the propeller noise would have on the recorded sonic boom signature. Possible triggering of the PATS due to landing impact would occur after completion of the mission, and thus, would be of no concern.

Additionally, the influence of electronic interference from the UAV systems, the C-band beacon, or the IFF-strobe light signal was unknown. Transducer location was of great importance. Since the sonic boom generating aircraft would overfly the UAV, the PATS transducer would be flush-mounted and located on its upper surfaces on an area as remote as possible from the propulsion system and in as "clean" an airflow as possible.

The availability of an "up-link" channel on the UAV was very significant since it permitted the "clearing" of all eight RAM memory banks of the PATS just prior to the sonic boom passes. Finally, the USMC concern for the response of the UAV to high level sonic boom overpressures was satisfied based upon the results of flight tests regarding the response of two general aviation airplanes exposed to intense boom while on the ground and in flight (ref. 18).

MAJOR CONCERNS ON ADAPTING PATS TO UAV

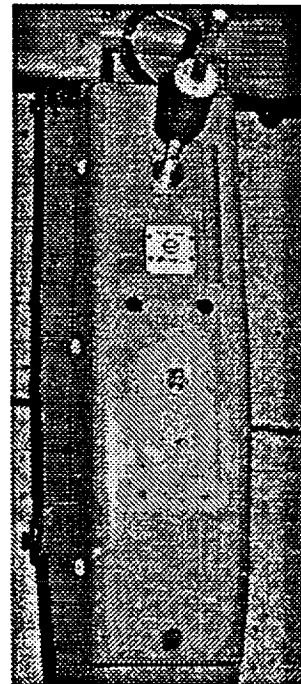
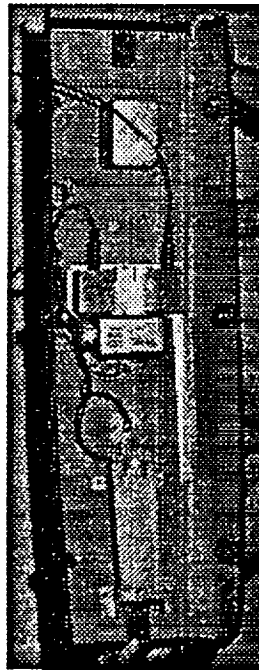
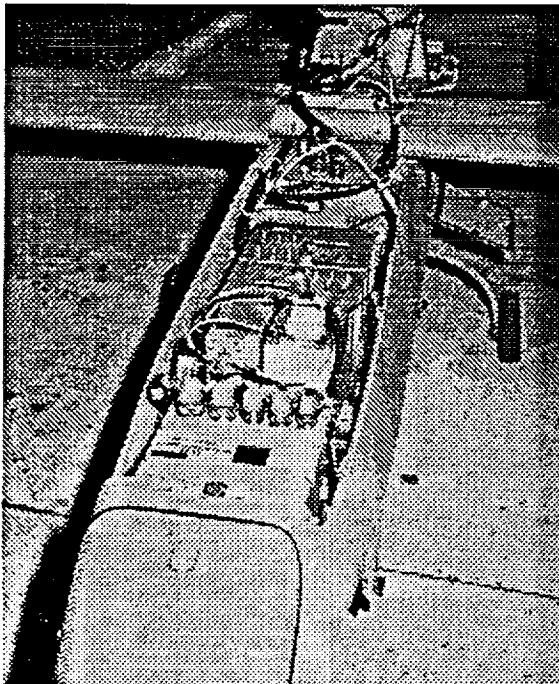
- Signature quality/moving platform
- System trigger level/propulsion and flow noise/accelerations
- Electronic interference (beacon, IFF, strobe)
- Transducer location
- Availability of "up-link" channel
- Response of UAV to sonic boom loading

The manner in which the PATS system was mounted on the UAV can be illustrated with the aid of Chart 9. In order to provide for redundancy and also allow for a range of pre-set triggering levels, two of the PATS were adapted to the UAV payload compartment. A re-packaging of the PATS from the normal "suitcase" arrangement was required in order to fit two systems into the allowable payload space and these were mounted on a base plate that was shock-mounted to the UAV airframe.

Locating the PATS electronic package within the UAV was not a problem from a space-payload limit viewpoint. Arrangement of the pressure transducer in a side-by-side flush-mounting scheme allowed for easy access to calibration and the "soft" mounting to the large section of the payload canopy cover. The transducers were recessed approximately 1/8 inch from the canopy surface to avoid generation of additional flow noise and to ensure that ram air pressure would not produce false triggering.

Two minor problems were encountered. The IFF (identify friend or foe) transducer produced R-F interference, to which the piezo-resistive pressure transducers are sensitive. To help alleviate this problem, the IFF antenna was moved from the top to the bottom of the UAV. The second problem was that the transducer housings were originally mounted in contact with the high voltage (HV) power supply for the UAV strobe light and a little rubber insulation solved this problem.

PHOTOGRAPHS OF PATS/UAV INSTALLATION



Three vehicle operational modes were considered in assessing the PATS/UAV functional compatibility and these included ground static, taxi, and flight tests. Specific concerns related to each of these three modes of operation are listed in Chart 10.

Propeller and engine noise are common to ground run-up, taxiing, and flight operations, but have varying characteristics. During the static ground run-up and systems checkout, propeller RPM is increased to near the maximum of 7500 rpm as compared to the cruise mode setting of about 6600 rpm. As such, a range of noise levels will be experienced. The propeller noise radiation patterns are also altered from static to flight by vehicle forward velocity effects and changes in inflow to the pusher propeller, and by the presence of the fuselage-wing arrangement, which will also alter the noise levels. Electronic emission concerns are also common to all three checkout modes, and include those resulting from the UAV control system, communication links, C-band beacon, strobe light, and IFF system.

The influence of vehicle acceleration levels ("g" loads) associated with runway roughness on taxiing, in-flight turbulence during cruise flight, and impact on landing on the PATS trigger level setting were not expected to pose a problem. Even though some landing impacts did trigger the PATS, the event always occurred after the test data was acquired. Ambient pressure changes associated with the 8700 foot flight altitude were not expected to influence the PATS modified piezo-resistive pressure transducer measurement results.

Pressure fluctuations associated with the airflow across the flush-mounted PATS transducers were thought to pose the most serious threat to the in-flight measurement technique regarding trigger level and boom signature definition. Results from the PATS/UAV static, taxi, and flight operational checkouts indicated that trigger level settings of from 0.5 psf to 2 psf would ensure that the F-4 sonic booms would be captured.

PATS/UAV CHECKOUT MODES

- **Ground Static Tests**
 - propeller/engine noise
 - electronic emissions

- **Taxi Tests**
 - propeller/engine noise
 - runway roughness
 - RF interference

- **Flight Tests**
 - airflow/propeller/engine noise
 - turbulence
 - RF interference
 - pressure/temperature change
 - landing impact

A tabulation of the F-4 sonic boom flights on which sonic boom signatures were measured, using the PATS/UAV airborne measurement platform, is given in Chart 11. Two F-4 sorties were made over a 2-day period consisting of four alternating passes on the first day and two alternating pass on the second day. Passes were accomplished in the late morning time period about every 5 minutes on the first day and about every 10 minutes on the second day.

The nominal flight conditions were for the UAV to fly a constant heading of 230° out to sea at 8700 feet altitude and at a cruise speed of 60 knots. Supersonic passes of the F-4 were to be flown at about M = 1.10 to 1.2 at altitudes of from about 11,000 feet to about 14,000 feet with the aircraft being on conditions at least 4 miles prior to passing over the UAV. The F-4 would perform the first pass overtaking the UAV from the rear on the same 230° heading. After passing overhead of the UAV, the F-4 would then make another supersonic pass from a head-on approach to the UAV, once again being on Mach-altitude 4 miles prior to passing overhead of the UAV. Mild to moderate turbulence was reported at the UAV flight altitude with crosswinds of from about 25-40 knots.

Examination of Chart 11 indicates that the flight altitudes of the F-4 were slightly higher (by about 1000 feet) than planned, resulting in larger separation distances. Note that the separation distances varied from 2200 feet to 5000 feet and headings varied from 32° to 233°, resulting in lateral offset distances at the 2 n.mi. steady point prior to overhead of from 10 feet to 6500 feet.

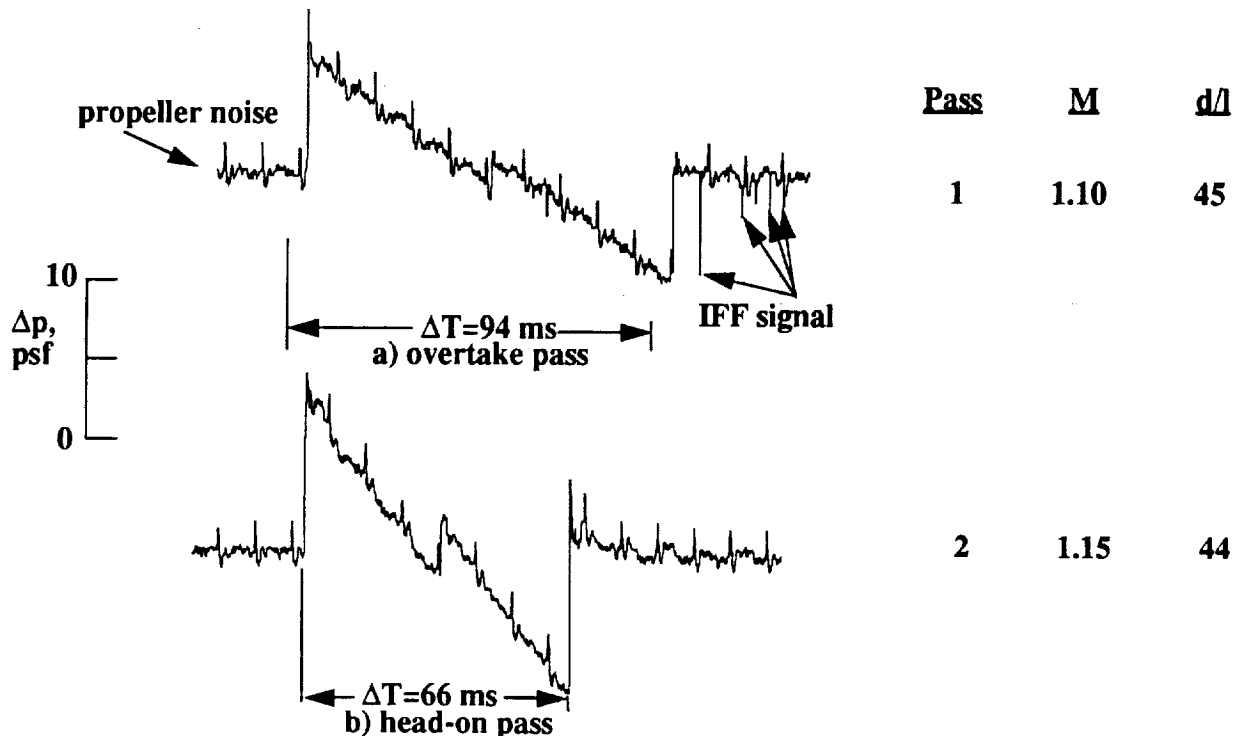
TABULATION OF F-4 SONIC BOOM FLIGHT OVER PATS/UAV AIRBORNE MEASUREMENT PLATFORM							
Date	F-4					Separation from UAV	
	Pass No.	Weight lbs.	Mach Number	Altitude, ft.	Heading, deg	Δh ft.	Δ offset ft.
1/9/94	1	40400	1.10	11,300	233	2600	550
	2	39200	1.15	10,900	59	2200	1350
	3	36900	1.20	13,700	228	5000	10
	4	34900	1.20	13,200	32	4500	6500
1/10/94	5	39800	1.12	11,900	230	3200	320
	6	37000	1.13	11,800	48	3100	900

Two measured sonic boom signatures recorded on the PATS Unit 2 from passes 1 and 2 are presented in Chart 12. The signature for Pass 1 is from the F-4 approaching the UAV from the rear and overtaking it, and the signature associated with Pass 2 is from the F-4 head-on pass to the UAV. On passes 1 and 2, the F-4 was at Mach numbers of about 1.10 and 1.15 and altitudes of 11,300 feet and 10,700 MSL, respectively. Slant range separation distances from the F-4 to the UAV, in terms of aircraft lengths (d/l) are 45 and 44, respectively, for passes 1 and 2.

For both measurements, the F-4 waveforms are quite distinguishable as sonic boom signatures that have relatively rapid rising shocks at the bow and tail, and also a mid-shock which results from the aircraft's inlet-wing juncture. Boom shock overpressure levels, Δp , of about 8 psf and 10 psf were observed. Also expected, and evident, is the difference in signature period ΔT between the rearward approaching and head-on passes, Pass 1 having a slightly longer, and Pass 2 a slightly shorter, ΔT than would be measured with a stationary platform. This time difference is, of course, related to the relative velocity between the F-4 and UAV.

Another signal is quite dominant throughout each of the boom signatures and represents a periodic frequency of about 110 Hz (6600 rpm) which is the frequency associated with the propeller rotational speed during cruise flight of the UAV. Although the amplitude of the propeller signal is greater than the PATS 0.5 psf threshold level setting, it did not trigger the PATS because of their short durations. The PATS was triggered by the onset of boom signature which it retained, along with the propeller noise signals which it sensed prior to, during, and after the boom event. Note also the presence of the IFF signal following the boom event.

IN-FLIGHT F-4 SONIC BOOM SIGNATURES MEASURED WITH PATS/UAV AIRBORNE SYSTEM

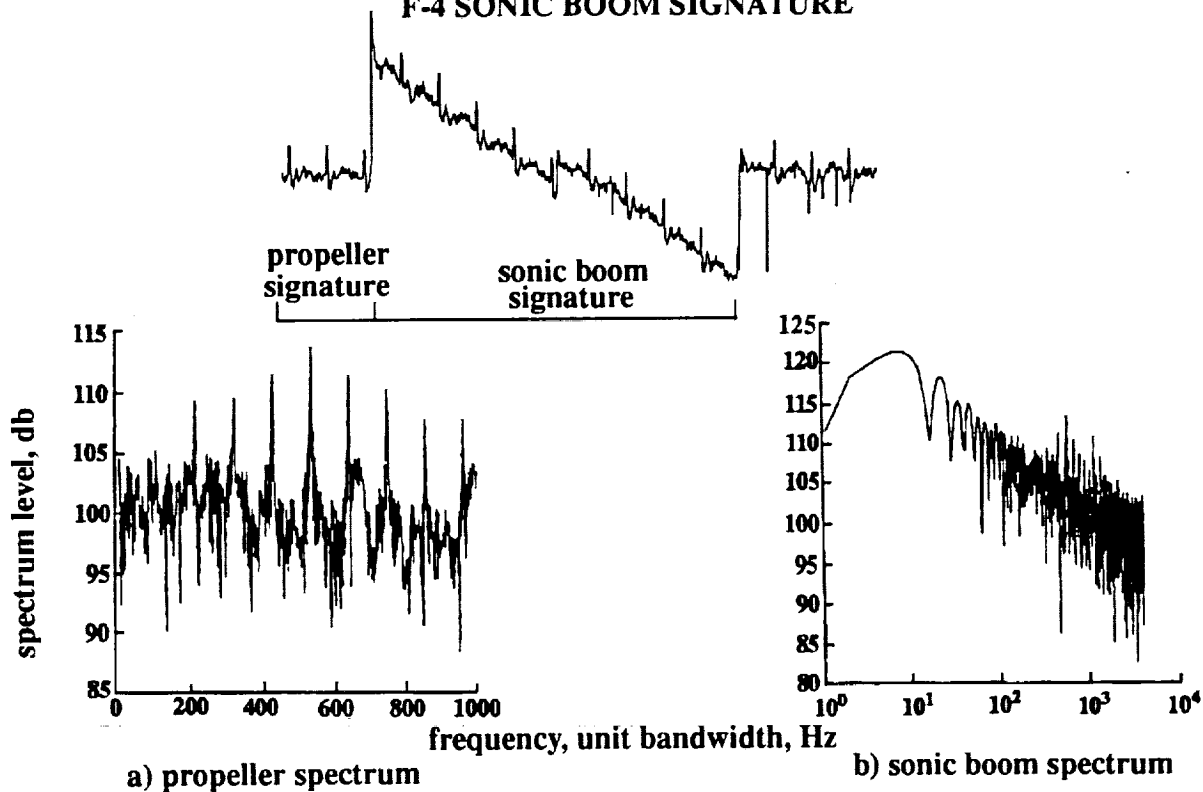


“Clean-up” of the measured F-4 sonic boom signatures requires a knowledge of the frequency content of the waveform. Each of the measured F-4 signatures was analyzed using a Fast Fourier Transform technique and the results are typical of those shown on Chart 13. At the top of the Chart is shown the measured boom signature from PATS Unit 2 for Pass 1. Two portions of the signature are noted, the propeller noise recorded prior to the onset of the bow shock, and the actual sonic boom signature involving the piece of the time history just prior to and after the bow and tail shocks. The corresponding frequency spectra are illustrated at the bottom of the chart.

The propeller noise spectrum indicates dominant frequencies at not only multiples of the fundamental blade passage frequency of about 220 Hz (two-bladed propeller at rotational frequency of 110 Hz), but also at each individual blade passage frequency and their harmonics. This is due to the geometry of the wing and tail boom arrangement with respect to the propeller center of rotation resulting in variations in inflow to the propeller disk and non uniform loading on each blade, and the location/arrangement of the flush mounted pressure transducers.

The sonic boom signature spectrum is typical of that expected for the near N-wave shape with the peak occurring at a frequency about equal to the reciprocal of the waveform period and decaying at about 6 dB per octave. Note, however, that from about 110 Hz on, the influence of the UAV propeller noise becomes quite evident.

FREQUENCY SPECTRA ASSOCIATED WITH MEASURED F-4 SONIC BOOM SIGNATURE

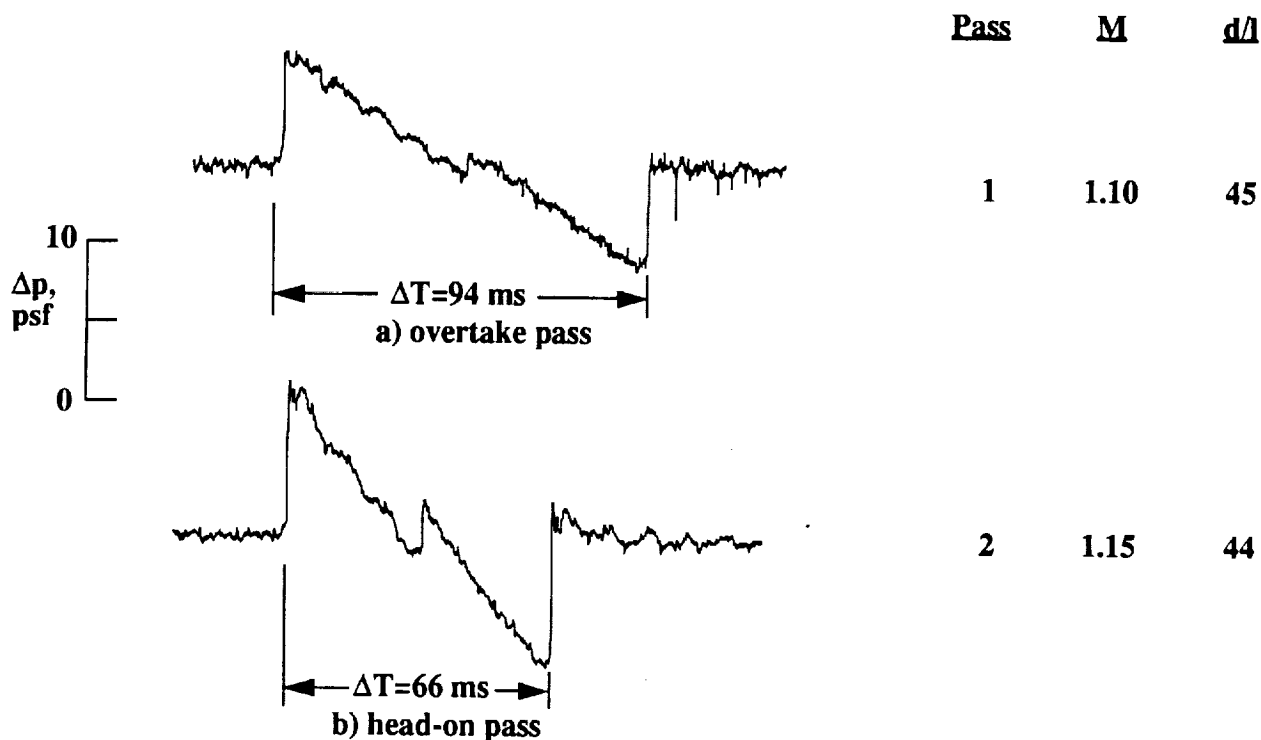


Filtering of the F-4 signatures was accomplished using a spectrum clean-up method. A fast Fourier Transform (FFT) was performed on the first 2048 points of the pressure record which contained only propeller noise. Similarly, a 2048 point FFT was performed on the portion of the record which contained the sonic boom. The amplitudes of the noise spectrum were subtracted from the amplitudes of the signal plus noise spectrum while maintaining the phase of the signal plus noise spectrum. The inverse FFT of the resulting spectrum produced the filtered time history illustrated in Chart 14.

It can be noted that although the two signatures are not entirely clean and still show traces of both propeller and IFF signals, there is a considerable improvement over their original state (see Chart 12). Complete elimination of the propeller and IFF noise signals is not possible for a number of reasons. First, although the propeller pulses are uniformly repeated, they contain considerable broadband noise due to inflow variations and geometry asymmetries. Second, IFF signals occur at random intervals (it was agreed that for future measurements, the IFF could be deactivated during the time the sonic boom measurement is being acquired). Finally, the PATS units were not provided with an anti-aliasing filter, and thus, spurious signals will be inherent to the system when performing the signature clean-up.

The two filtered sonic boom signatures shown in Chart 14, which are typical of all the signatures measured by both PATS units and for all six (6) passes, provide qualitative and possibly quantitative information relative to shock number, locations, strength, rise time, and waveform character.

IN-FLIGHT F-4 FILTERED SONIC BOOM SIGNATURES MEASURED WITH PATS/UAV AIRBORNE SYSTEM

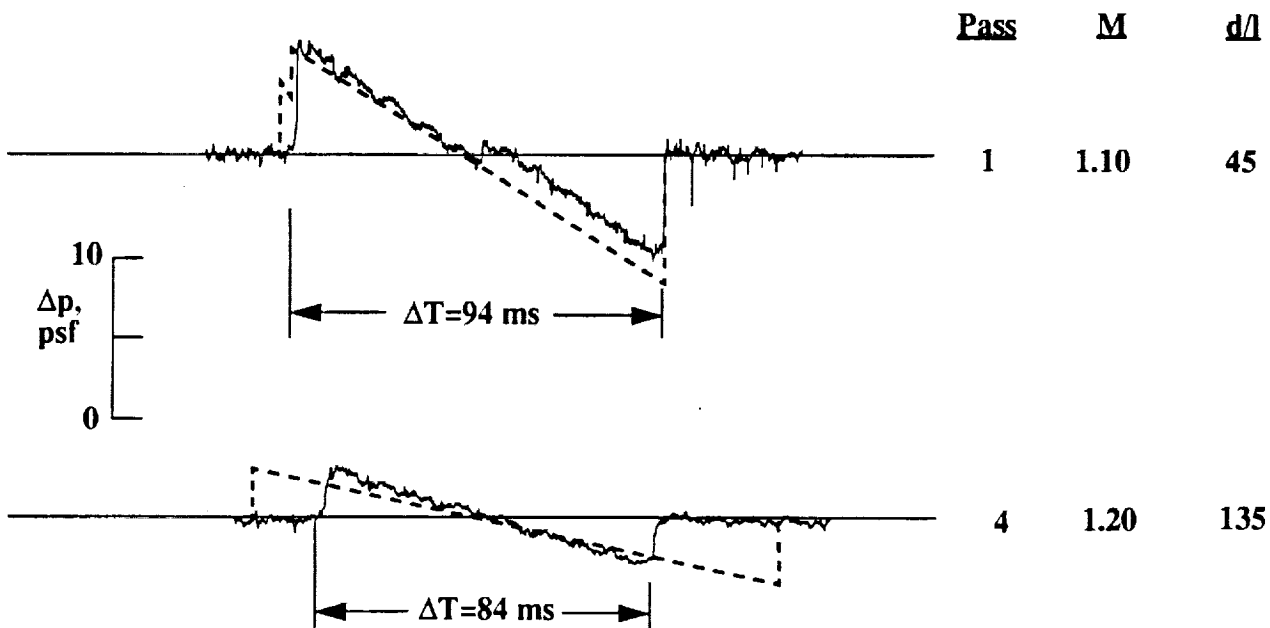


A comparison of the in-flight measured and predicted F-4 sonic boom signatures is given in Chart 15. The measured signatures are from the PATS Unit 2 for Pass 1 and Pass 4 of the F-4 over the PATS/UAV airborne platform at Mach numbers of 1.10 and 1.2, respectively. Note that on Pass 1, the PATS/UAV measurement position was about 45 body lengths (d/l) below and to the left of the F-4 passing overhead ($\Delta h = 2600$ feet, Δ offset = 550 feet). For Pass 4, the PATS/UAV was about 135 body lengths (d/l) below and to the left of the F-4 passing overhead ($\Delta h = 4500$ feet, Δ offset = 6500 feet). Pass 1, an overtaking pass from the rear, is not quite an N-wave and contains the inlet-wing mid-shock even at 45 body lengths. Pass 4, a head-on pass, produced an N-wave which would be expected because of the larger distance involved and the large lateral displacement from the overhead position ($d/l = 135$).

The predicted signatures, shown by the dashed lines, are based on the NASA Langley Sonic Boom Prediction Program (refs. 19 and 20). On Pass 1, the predicted signature confirms the existence of a mid-shock, but indicates it has propagated more towards the bow shock. On Pass 4, an N-wave is predicted to exist. Good comparison is noted between the measured and predicted bow shock overpressures on both passes (6.8 psf versus 6.4, and 3.2 psf versus 3.4, respectively).

Good correlation between predicted and measured signature period was not expected because the UAV is a moving platform. However, for Pass 1 (overtake pass) the calculated (stationary) signature period should be shorter than the measured period. The large discrepancy in calculated and measured signature period for Pass 4 is expected because the measured signature is from a head-on pass.

COMPARISON OF IN-FLIGHT MEASURED AND PREDICTED F-4 SONIC BOOM SIGNATURE



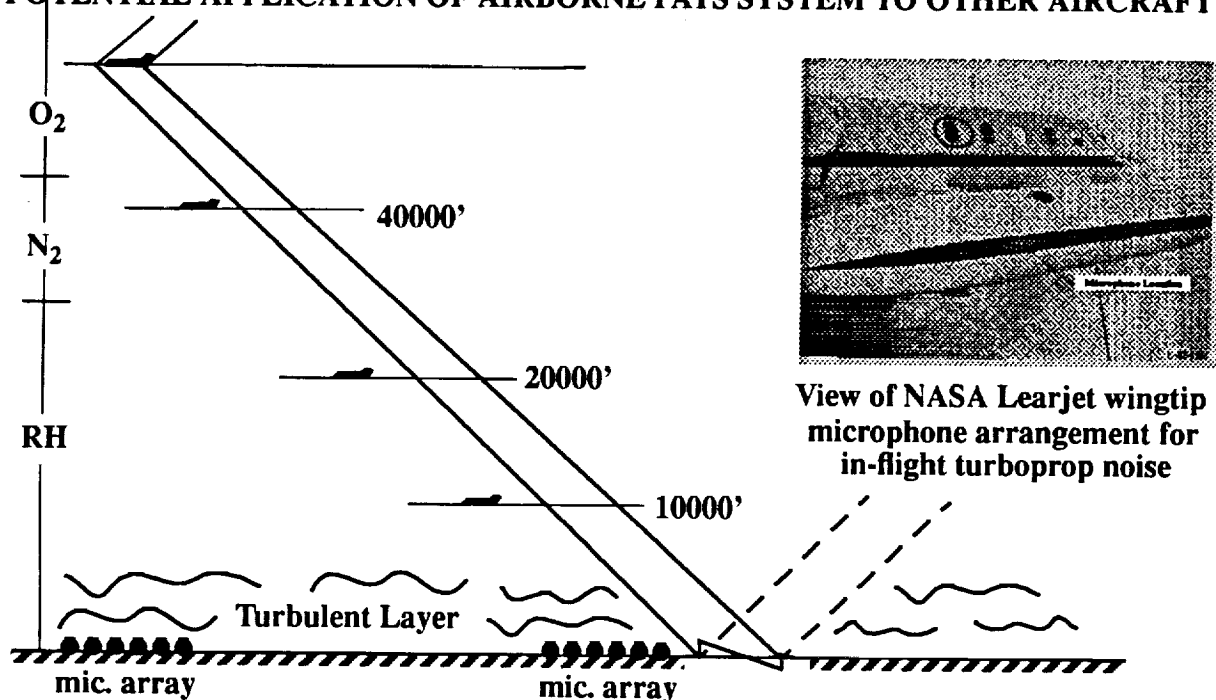
Based upon the results of this flight experiment, it is believed that the PATS sonic boom measurement system could be applied to other airborne platforms, especially those that have higher altitude capabilities than the Pioneer UAV (15,000 feet). Probing the shock flow-field of supersonic aircraft at higher altitudes would provide an opportunity to examine the influence of different portions of the atmosphere on the boom signature as it propagates downward to the ground and back upwards, as illustrated in Chart 16.

It has been shown, for example (ref. 21), that oxygen (O_2), nitrogen (N_2) and relative humidity (RH) influence shock rise time. Since O_2 , N_2 , and RH influence depends upon certain altitude regimes, in-flight measurements at specific altitudes would provide a measure of the influence of each of these parameters on the boom rise time.

Information that relates to the initial conditions of the ground reflected signature (soon to become an over-the-top or secondary boom) would depend upon its intensity and the PATS capability to trigger and record these upward propagating signatures.

An unmanned airborne system that would have high altitude potential at relatively low speed would be most desirable. However, a higher subsonic speed aircraft, such as the NASA Learjet, which has been used to acquire in-flight measurements of a turboprop (ref. 22), may also be suitable. This latter application would also allow for on-board operations and observations with a minimum influence of propulsion noise contamination. The potential effect of high speed flow noise is expected to be minimal but would have to be established.

POTENTIAL APPLICATION OF AIRBORNE PATS SYSTEM TO OTHER AIRCRAFT



An in-flight technique for acquiring mid- and far-field sonic boom signatures has been described. This airborne measurement platform consists of the adaptation of the NASA-JSC Portable Automatic Triggering System (PATS), and digital remote and self triggering sonic boom measurement unit, to USMC Pioneer Unmanned Aerial Vehicle (UAV). The PATS/UAV system has been checked out in the ground static, taxi, takeoff-landing, and cruise modes to assure that the system is able to provide for a qualitative measurement of a sonic boom signature that would not be hampered as a result of the vehicle propulsion system noise, in-flight flow noise, accelerations due to rough air, runway roughness, landing impact, and electronic disturbances from onboard equipment.

Six supersonic passes at about $M = 1.15$ and 12,000 MSL were made under radar controlled conditions over the PATS/UAV quasi-stationary airborne measurement platform flying at 60 knots at 8700 MSL. Sonic boom signatures were recorded on all six passes and on both PATS units. The signatures, although heavily influenced by the UAV propeller noise, provide a very clear indication of the number, location, and strength of the shocks. As expected, signature period varied somewhat depending upon whether the supersonic pass overtook the UAV from the rear or head-on.

Post filtering of these signatures was quite successful at minimizing the influence of propeller noise interference such that qualitative information regarding waveform variability and shock rise time variation is possible. Adaptation of the PATS to other aircraft having greater altitude capability could provide a means of acquiring boom signature at higher altitudes in that part of the atmosphere where shock rise times are influenced by N_2 , O_2 , and RH effects. The PATS airborne measurement technique could also lend considerable definition to the initial phase of the over-the-top (secondary) boom phenomena.

SUMMARY REMARKS

- Described in-flight technique for acquiring mid- and far-field sonic boom signatures
- Technique utilizes NASA PATS on USMC UAV
- PATS/UAV system checkout in static and flight operations
- Measured F-4 mid-field sonic boom signatures
- Quantified number, location, and strength of shocks
- Signature period varies depending upon closure rate
- Post filtering of signature reduced propeller noise contamination
- Signatures provide qualitative insight on waveform distortion and shock rise time variations
- PATS could be adapted to other subsonic aircraft
 - higher altitudes
 - effects of O_2 , N_2 , RH
 - establish initial conditions for "over-the-top" booms

1. Weinstein, Leonard: An Optical Technique for Examining Aircraft Shock Wave Structures in Flight. NASA Paper, NASA High Speed Research Program Sonic Boom Workshop, June 1-3, 1994.
2. Mullens, Marshall E.: A Flight Test Investigation of the Sonic Boom. AFFTC TN 56-20, Air Res. and Dev. Command, U. S. Air Force, May 1956.
3. Smith, Harriet J.: Experimental and Calculated Flow Fields Produced by Airplanes Flying at Supersonic Speeds. NASA TN D-621, 1960.
4. Maglieri, Domenic J.; Ritchie, Virgil S.; and Bryant, John F., Jr.: In-Flight Shock Wave Pressure Measurements Above and Below a Bomber Airplane at Mach Numbers from 1.42 to 1.69. NASA TN D-1968, October 1963.
5. Maglieri, D. J.; Huckel, V.; Henderson, H. R., and Putman, T.: Preliminary Results of XB-70 Sonic Boom Field Tests During National Sonic Boom Evaluation Program. NSBEO 1-67, pp. C-II to C-II-17, July 28, 1967.
6. Haering, Edward A., Jr.; Whitmore, Stephen A.; and Ehernberger, L. J.: Measurement of the Basic SR-71 Airplane Near Field Signature. NASA High Speed Research Program Sonic Boom Workshop, NASA/CP-1999-209699, 1999.
7. Maglieri, Domenic J.: Sonic Boom Flight Research - Some Effect of Airplane Operations and the Atmosphere on Sonic Boom Signatures. NASA SP 147, pp. 25-48, April 12, 1967.
8. Maglieri, Domenic J.; Hilton, David A.; Huckel, Vera; and Henderson, Herbert R.: Measurements of Sonic Boom Signatures From Flight at Cutoff Mach Number. NASA SP-255, pp. 243-254, October 1970.
9. Hubbard, Harvey H.; Maglieri, Domenic J.; and Huckel, Vera: Variability of Sonic Boom Signatures With Emphasis on the Extremities of the Ground Exposure Patterns, NASA SP-255, pp. 351-359, October 1970.
10. Haglund, George T.; and Kane, Edward J.: Flight Test Measurements and Analysis of Sonic Boom Phenomena Near the Shock Wave Extremity. NASA CR 2167, February 1973.
11. Haglund, George T.; and Kane, Edward J.: Analysis of Sonic Boom Measurements Near Shock Wave Extremities for Flight Near Mach 1.0 and for Airplane Accelerations. NASA CR-2417, July 1974.
12. Darden, Christine M.; and Needleman, Kathy E.: Assessment of the BQM 34-E "Firebee" as a Test Vehicle for Sonic Boom Minimization. NASA Conference Publication 10133, pp. 417-448, May 1993.

13. Maglieri, Domenic J.; Sothcott, Victor E.; Keefer, Thomas N.: Feasibility Study of Conducting Overflight Measurements of Shaped Sonic-Boom Signatures Using the Firebee BQM-34E RPV. NASA CR-189715, 1993.
14. Stansbery, E. G.; and Stanley, J. F.: Descent Sonic Boom Measurements for STS-26, Including a Mach 23 Measurement, JSC-23579, April 1989.
15. Lee, Robert A.: Air Force Boom Event Analyzer Records (BEAR): Comparison with NASA Boom Measurement System, USAF AAMRL-TR 88-039, 1988.
16. Lee, R. A.; and Downing, J. M.: Sonic Booms Produced by United States Air Force and United States Navy Aircraft: Measured Data, AL-TR-1991-0099, Wright Patterson AFB, Ohio, December 1990.
17. Munson, Kenneth: World Unmanned Aircraft, AMRAeS, ARHistS, ISBN 07106 0401 7, pp. 58-59.
18. Maglieri, Domenic J.; and Morris, Garland J.: Measurements of the Response of Two Light Airplanes to Sonic Booms. NASA TN D-1941, August 1963.
19. Hayes, Wallace D.; Haefeli, Rudolph C.; and Kulstrud, H. E.: Sonic Boom Propagation in a Stratified Atmosphere, With Computer Program. NASA CR-1299, 1969.
20. Thomas, Charles L.: Extrapolation of Sonic Boom Pressure Signatures by the Waveform Parameter Method. NASA TN D-6832, 1972.
21. Pierce, Allan D.: Progress in Modeling Atmospheric Propagation of Sonic Booms. NASA Conference Publication 10132, May 12-14, 1993.
22. Balombin, Joseph R.; and Loeffler, Irvin J.: Farfield In-flight Measurements of High-Speed Turboprop Noise, NASA TM 83327.

PROGRESS IN SONIC-BOOM UNDERSTANDING: LESSONS LEARNED AND NEXT STEPS

Christine M. Darden
NASA Langley Research Center

ABSTRACT

In January 1988, representatives from NASA, NOAA, academia, and industry gathered at the NASA Langley Research Center to assess the status of understanding of the sonic boom which accompanies supersonic flight. As a result of that meeting, a research program on sonic boom within the NASA High-Speed Research (HSR) Program was implemented. This paper discusses the elements of the sonic-boom program, progress which has been made since 1988, and the current change in direction for the Sonic-Boom Element of the NASA HSR Program.

INTRODUCTION

NASA's HSR Program was initiated in 1990 with two phases planned. Phase I, to run from 1990-1995, was to focus on environmental concerns of a commercial supersonic aircraft, and Phase II, to run from 1994-2001, was to focus on technologies which were needed in order to develop an economically viable vehicle. Strategies used in planning the direction of the Program were an outgrowth of a Sonic-Boom Workshop held at NASA Langley in January 1988. At that meeting, representatives from NASA, other government agencies, industry, and academia--many of whom had worked in the sonic-boom research during the 1960's and early 1970's--gathered to assess the state of knowledge of sonic boom, and to suggest the direction that a focused research effort should take. The results of that Workshop¹ outlined the following areas for future research efforts: primary carpet width, carpet edge phenomena, secondary carpet, focused boom (the exact caustic solution), sonic-boom predictions at Mach numbers above 3, the effect of atmospheric phenomena on sonic-boom parameters, the definition of an appropriate sonic-boom metric, the ability to theoretically predict that metric, and the design of viable low-boom designs.

Though the High-Speed Civil Transport (HSCT) feasibility studies originally considered Mach numbers from 2 to 25, initial studies showed that productivity gains dropped significantly beyond Mach 4. By 1989, the upper limit of consideration for the HSCT Mach number had become 3. Because Mach numbers above 3 were no longer in consideration, there has been no emphasis placed on sonic-boom predictions at the higher Mach numbers. In 1992, an HSR programmatic decision was made to establish 2.4 as the design Mach number.

THE SONIC-BOOM PROGRAM

The organization of the HSR Sonic-Boom Element relied heavily on recommendations from the 1988 Workshop. Participants of that Workshop were aware of the tremendous progress made in sonic-boom prediction and minimization during the 1960's and early 1970's, but they were also aware that a solution was still not available. Though the ideal situation would have been to first decide whether any level of sonic boom was acceptable, schedules and constraints within the HSR Program prohibited this linear approach to the sonic-boom problem. The recommendation from the Workshop was to proceed concurrently with the three areas shown in Fig. 1. It was determined that the most pressing question to be answered was "could an HSCT designed to begin operation around the year 2005 be configured so that it would be permitted to fly overland supersonically?"

In order to answer that question, not only was information on the waveform generated at the aircraft necessary, but also the impact of the atmosphere on the waveform as it propagated, the metric of the waveform which best correlated with its annoyance, and a prediction of how the waveform was perceived by those on the ground. To pursue these answers, the acceptability studies and the atmospheric propagation studies, which included the elements listed in Fig. 1, were managed by the Acoustics Division at NASA Langley Research Center, and the Configuration Design and Operation studies were managed by the Advanced Vehicles Division. Since 1988, configuration work has also been done at NASA Ames Research Center and, through contracts and university grants, at Boeing Commercial Airplanes, Douglas Aircraft, Grumman Aerospace, Pennsylvania State University, the University of Texas at Austin, the University of Mississippi, and Virginia Polytechnic Institute and State University. To promote communication and coordination across the different study areas, Sonic-Boom Workshops have been held in 1992, 1993, and 1994.

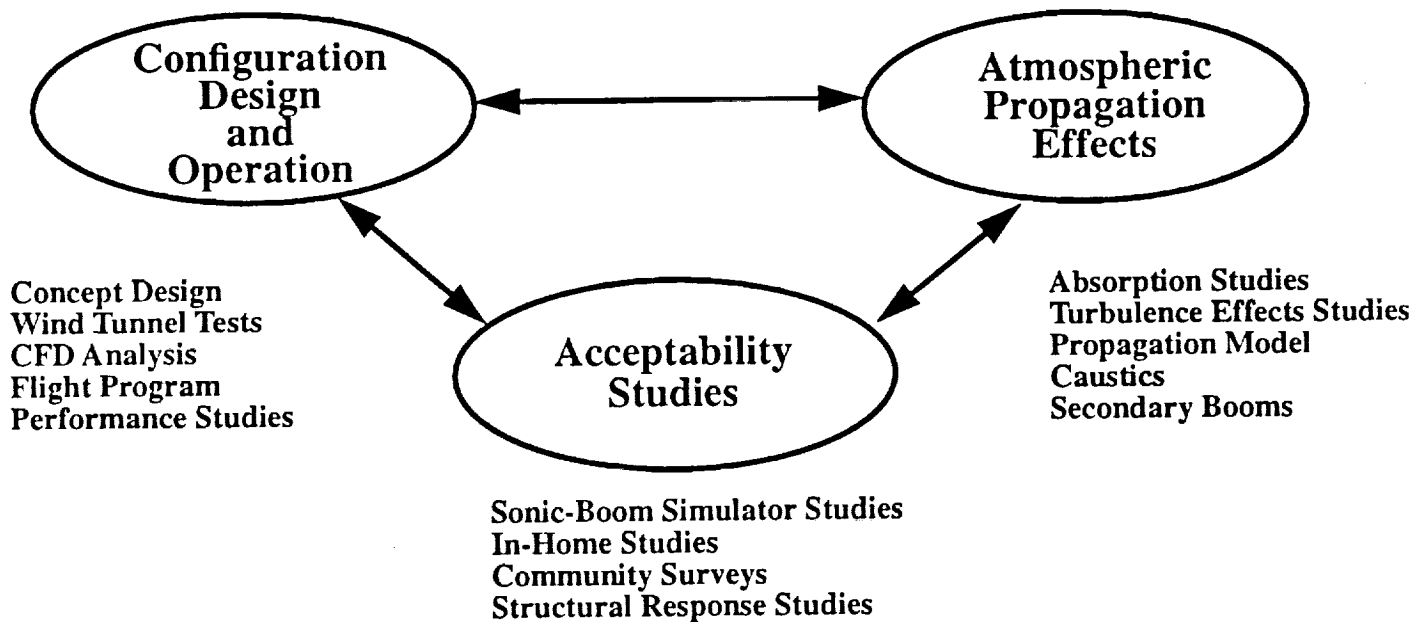


Figure 1. Sonic-Boom Program

ECONOMIC BENEFIT OF SUPERSONIC CORRIDORS

The economics of a future HSCT depends largely on the number of global routes serviceable by such an airplane, and thus the number of airplane units sold. The larger the number of units, the smaller the portion of developmental cost to be borne by each unit. It is through a potential increase in routes, and thus units, that overland supersonic flight offers great potential to the economic viability of a future supersonic transport.

Discussions of unlimited overland supersonic flight were held initially in the HSR Program and economic studies performed by Douglas Aircraft indicated that with that possibility, an airplane could have up to a 17 percent performance penalty (compared to a baseline concept which cruises subsonically overland) and still be economically competitive--because of the increased number of routes, and therefore, airplane units which would be needed. With time, the realization that unlimited overland supersonic flight was highly improbable led to the consideration of several strategically located remote overland corridors. Fig. 2 shows results of a study² performed by Douglas Aircraft on the scenario of 15 supersonic corridors around the globe.

Beginning with 932 city pairs, routes were eliminated from possible HSCT service if they failed to meet the criteria listed in the box shown in Figure 2. Assuming subsonic overland flight, only those routes which were mainly overwater, and of a given range and frequency were retained. With that criteria, only 287 routes of the original 932 remained. With the scenario of overland supersonic corridors, 103 of the eliminated routes were reclaimed as serviceable by an HSCT. The increase in routes would mean a viable market for an additional 570 airplanes.

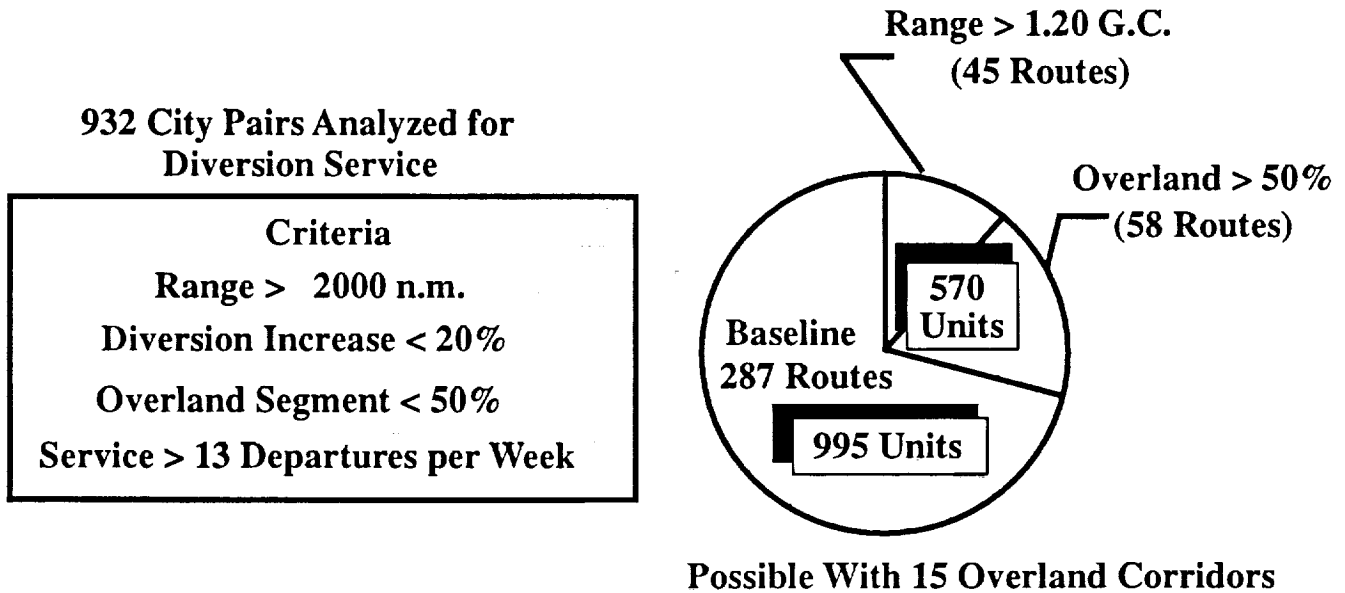


Figure 2. Economic benefit of Supersonic Corridors.

PROGRESS IN ANALYSIS AND METHODS

During sonic-boom research in the 1960's and early 1970's, Whitham Theory and modified linear theory methods became the standards for use in predicting the sonic boom of airplane configurations. Because most of these highly-loaded, winged configurations generated N-waves within a few body lengths of the airplane, and because comparisons with ground-measured N-waves gave good agreement, these methods were considered to be adequate for sonic-boom analysis in the mid- and far-field. Advances in low-boom design methods and tunnel-testing techniques uncovered weaknesses in the application of Whitham Theory or in the modified linear methods used during the application of Whitham theory.

When the work of McLean³, Jones⁴, Seebass⁵, and George⁶ indicated that the generation of non-N-waves was possible at the ground, control of the growth in volume and lift of the configuration--and therefore accuracy in predictions---became critical. Wind-tunnel test results⁷ in the late 1970's, which essentially validated sonic-boom minimization theory at Mach 1.5, proved to be inconclusive at Mach 2.7. At that time, discrepancies were attributed to boundary-layer displacement thicknesses, but experimental results in 1990⁸ and 1994 indicate that linear theory lifting methods used with the Whitham Theory to design the 1979 models gave inadequate lift predictions at Mach 2.7. Modifications have been made to the lifting-codes to correct these deficiencies.⁹

An unexpected strong shock from the flow-through nacelles on the Mach 2 and Mach 3 low-boom designs tested in 1990 illustrated the incorrect use of Whitham Theory in analyzing these discontinuous surfaces beneath the wing/body configuration. A fix to this problem was recommended in Ref. 10, where the addition of Whitham F-Functions, and not areas, was applicable to these discontinuous surfaces.

Tremendous advances in supercomputers, gridding schemes, and computational algorithms have allowed computational fluid dynamics (CFD) to become a new tool in the prediction of near-field sonic-boom signatures. Validation of these methods continues as their results are integrated into sonic-boom design programs. With the increased use of CFD methods and larger wind-tunnel models, however, a need for three-dimensional extrapolation methods which are valid from approximately one-half body length to at least 10 body lengths has surfaced. Work is currently being pursued in this area.

- Improved F-Function analysis and design methods to predict inlet shocks**
- Increased use of CFD for design and analysis of near-field signatures**
- Increased use of non-linear corrections to modify linear theory methods**
- Progress in developing intermediate propagation methods**

Figure 3. Progress in Analysis and Methods

COMPUTATIONAL GRID MODIFICATIONS

Powerful, nonlinear CFD methods have been applied to sonic-boom predictions for the first time within the current HSR Program. Additionally, because the traditionally-used Whitham Theory is valid only at mid- to far-field distances, CFD methods are the only means of generating a near-field signature--one which can be compared directly with wind-tunnel data, and one in which signature features can be directly correlated with configuration features.

References 11-13 discuss the application of full potential methods, marching Euler methods, relaxation methods, and thin-layer Navier-Stokes methods for sonic-boom predictions. One difficulty encountered in the application of CFD methods for sonic-boom prediction has been that of generating an accurate flow-field some distance from the body. At Mach 2.0, to generate the signature at one body-length away from the body, calculations must be made approximately two body-lengths downstream. This is almost impossible for many relaxation methods because of the grid density and time required. For marching methods, the fidelity of the shocks is lost because of the grid spreading which has occurred at this distance. Fig. 4 illustrates an example of one topology change made to the grid for a sonic-boom calculation. Because the grid is retained between two Mach angles which capture the region of flow disturbance, the spreading of the grid is reduced, and thus flow fidelity is retained to a larger distance in a radial direction. Work continues on the development of three-dimensional Method-of-Characteristics (MOC) codes which could match CFD methods in the near field, and yet propagate accurately and more rapidly in a radial direction.

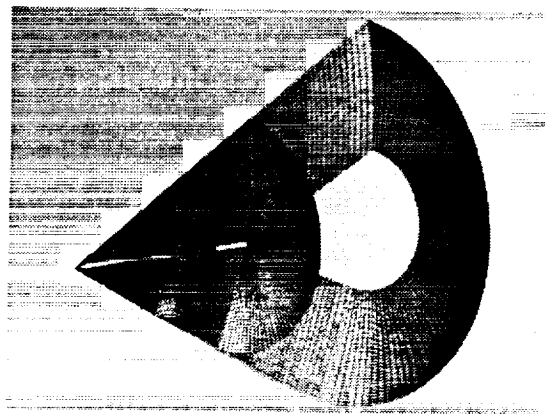


Figure 4. Computational grid modifications.

PROGRESS IN DESIGN OF LOW-BOOM CONCEPTS

Prior to the current HSR program, the most recent effort in low-boom design was reported in Ref. 7. In that effort, three wing-body designs were built and tested---one at Mach 1.5 and two at Mach 2.7. The minimization theories were considered validated at Mach 1.5, and the results were mixed for Mach 2.7. With those designs, no effort was made to produce a real airplane with real airplane constraints. The initial low-boom design efforts within the HSR program resulted in Mach 2 and Mach 3 twisted wing-body-nacelle concepts--the Mach 2 designed to produce a flat-top signature, and the Mach 3, a ramp-type signature. Though these designs had more characteristics of real airplanes, no systems or performance trade studies were attempted. It was during the test of these concepts that the error in nacelle-integration methods (from a sonic-boom view) was realized. For the Mach 2 model without nacelles, the minimization theory was validated, but results for the Mach 3 model were different than predicted.

The next iteration of low-boom design (beginning in 1991) had as major objectives, the correct integration of the nacelles (shocks), and the improved performance of the concepts (when compared to the program baseline configuration). During this iteration, concepts were designed by Boeing, Douglas, NASA Ames and NASA Langley--with varying levels of systems integration during the design. The Vehicle Integration Branch at NASA Langley accepted the task of performing a consistent systems analysis of these concepts so that an assessment of their performance could be made.

- **Validated sonic-boom minimization theories for cambered wing-body**
- **Included flow-through nacelles on sonic-boom models**
- **Designed low-boom concepts using iterative CFD methods**
- **Successfully embedded nacelle shock in signature expansion**
- **Improved performance characteristics of low-boom designs and analysis shows weights within 2 to 3% of baseline**
- **Performed systems study on all low-boom designs**

Figure 5. Progress in design of low-boom concepts.

BOOM-SHAPING DESIGN CYCLES

During Phase I of the HSR Program, improvements have been made in generating conceptual designs in which low-boom design concepts and performance goals have been combined. Difficulties have arisen, however, because of changing program guidelines in the midst of design cycles, and because of concurrent methods development and design.

The sizes of the first two low-boomwind-tunnel models within the current program were 12-inches in length---more than twice as long as any previous sonic-boom model---to allow more fidelity in the model design and construction. This length, however, created a situation in the NASA Langley Unitary Plan Wind Tunnel (4' x 4') in which measurements could be made no further than 2 to 2.3 body lengths away (depending on the Mach number). Extrapolation of signatures measured at this distance with 2-D extrapolation methods created debate within the sonic-boom community because of beliefs that significant 3-D effects were not included in the results. When the 1990-built Mach 2 & Mach 3 concepts were tested in the larger Ames 9x7 Unitary Wind Tunnel, it was found that the integral model sting was too short and that the signature was contaminated by shocks from the model support system.

A second difficulty within the current design cycle has been caused by programmatic decisions. In sonic-boom minimization based on the Seebass-George technique, the vehicle Mach number, weight, length, and altitude are initial parameters. After several of the low-boom designs had been defined assuming a different overwater cruise Mach number, a programmatic decision was made that the cruise Mach number for the HSCT would be 2.4. An additional change which occurred within Langley was the mandated use in mid-1993 of a different and more realistic engine cycle. This introduced a tremendous change in the weight of the concepts. While most of the low-boom concepts were able to adapt to the Mach number change, the designs in this cycle were not redone to accommodate the larger and less advanced engines.

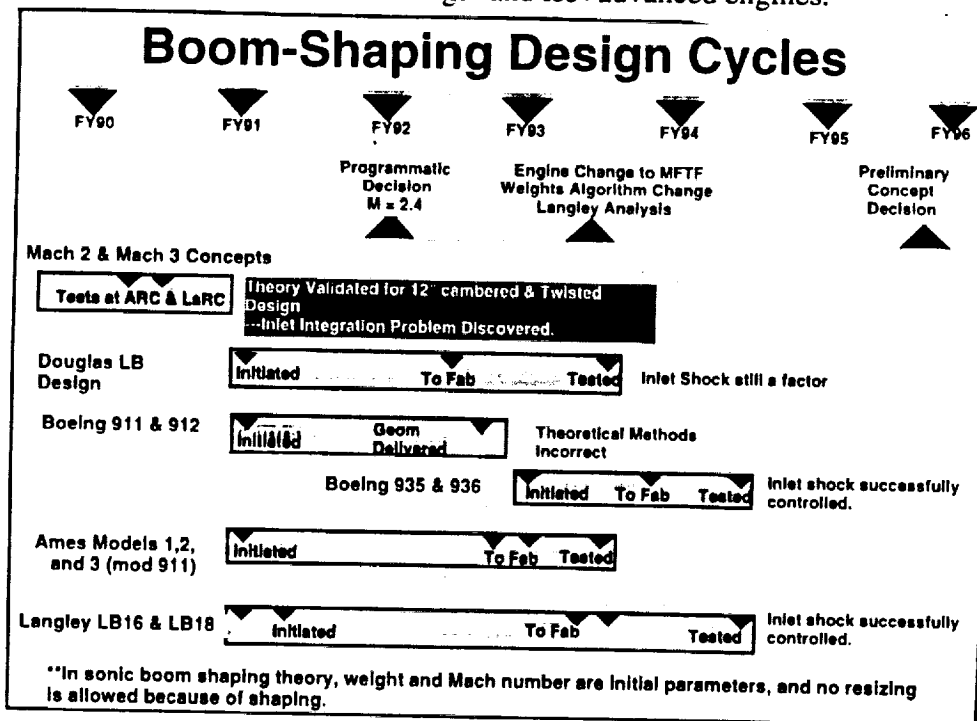


Figure 6. - Boom-Shaping design cycles.

HISTORY OF LOW-SONIC BOOM DESIGN EXPERIMENTAL PROGRAMS

The chart shown in Fig. 7 gives an overview of the experimental programs conducted with sonic-boom models during the past 15 years. It shows the year of the test, the models tested, their characteristics, the purpose of the test and the major findings.

Though the 1994 results indicate that a ramp signature was successfully achieved for the first time, the slope of that ramp is higher than theoretically predicted. Hypotheses about why this has occurred vary. One speculation is that the shock-advance rate in the uniform-atmosphere wind-tunnel is much higher than in a variable-density real atmosphere, and thus extrapolation is begun with a signature which is more-highly developed than it would be in flight. A second hypothesis is that the modified linear theory methods used for most of the designs do not properly locate some of the shock and expansion disturbances and thus, some cancellations planned in the design are not occurring. The third hypothesis is that the flow has not become axisymmetric at the 2.3 body-length measurement and that the missing three-dimensional effects could cause further moderation of the steepening shocks.

To test the third hypothesis, a test is being pursued in the much-larger Arnold Engineering Development Corporation (AEDC) 16S Supersonic Tunnel at Tullahoma, TN. Within this 16-foot cross-section facility, and using a longer integral sting on the low-boom concept, a fully developed signature should be measured at from 5 to 7 body lengths, and the signature development question resolved.

Test Year	1979	1990	1993	1994
Models	Mach 1.5 W/B - N (V) Mach 2.7 W / B - N (V) Mach 2.7 W / B - N (PI)	Mach 2 W / B/ N - N(V) Flat Sig Mach 3 W/B/N - N (V) Ramp Sig	Ames Model 1 Ames Model 2 Mach 2 Low-Boom Cr. Douglas Mach 1.8 Low-Boom Cr.	LB 16 1.6 / 2.0 LB - 18 1.8 / 2.4 B - 935 1.7 / 2.4
Characteristics	Flat Wing Target - Flat-Top Sigs 5° Models	Camber & Twist Flow-Through Nacelles 12 - Inch Models	Two lifting surfaces Use of CFD to design Ames models for multi-shock signatures.	Designed using Whitham Theory with F-Function Addition to place Nacelle Shocks System study performed
Purpose	Validation of Minimization Theory	Theory Validation for more sophisticated model and different signature	Use of CFD to properly account for lift, interference lift, and nacelle shock.	Validation of Nacelle Placement Method. Validation of Ramp or Hybrid-Type Sig.
Findings	1.5 Model Validated 2.7 Model found to have pressure growth larger than expected. Attributed to inadequacies of Linear Theory Lift Predictions	Theory did not account for nacelle shock. Discontinuity nullifies applicability of area addition. Mach 2 - Validated without nacelles. Mach 3 - Not validated without nacelles.	Successful in generating multi-shock designs with CFD. Impact of nacelle placement is mixed.	-Shocks from nacelles used in design are successfully embedded in expansion. -Ramp signature achieved though steeper than predicted. -Attributed to possible misalignment of influences, 3-D , and/or uniform atm eff.

Figure 7. History of low sonic-boom design experimental programs.

NASA AMES WING-CANARD, (MODEL 2)

While low-boom designs were being pursued at NASA Langley, Boeing, and Douglas using the more traditional Seebass-George minimization theory, researchers at NASA Ames pursued the use of CFD methodology¹⁴ to generate multi-shock signatures on the ground rather than flat-top or ramp signatures. Shown in Fig. 8 is an example of one of the models designed by that process. Also shown in Fig. 8 is a signature measured in the NASA Ames 9x7 Unitary Wind Tunnel at a normal force coefficient of 0.068 and at an h/l of 1.16. The figure inset at the lower right of Fig. 8 shows wind-tunnel measurements which have been extrapolated to the ground. In this case, the measurements were at C_N 's of 0.068, 0.094, and 0.114. $C_N(\text{Des})$, based on the projected weight of the model, was 0.08.

From these results, one might conclude that at a $C_N = 0.08$, a multi-shock signature would be successfully generated at ground level with this concept. There is discussion within the sonic-boom community that multi-shock signatures such as these may be more stable than the ramp type when propagating through a real atmosphere. Calculated loudness of these signatures, and their simulation within the NASA Langley Sonic-Boom Simulator demonstrate that these multi-shock signatures present a viable alternative to strictly shaped flat-top or ramp signatures.

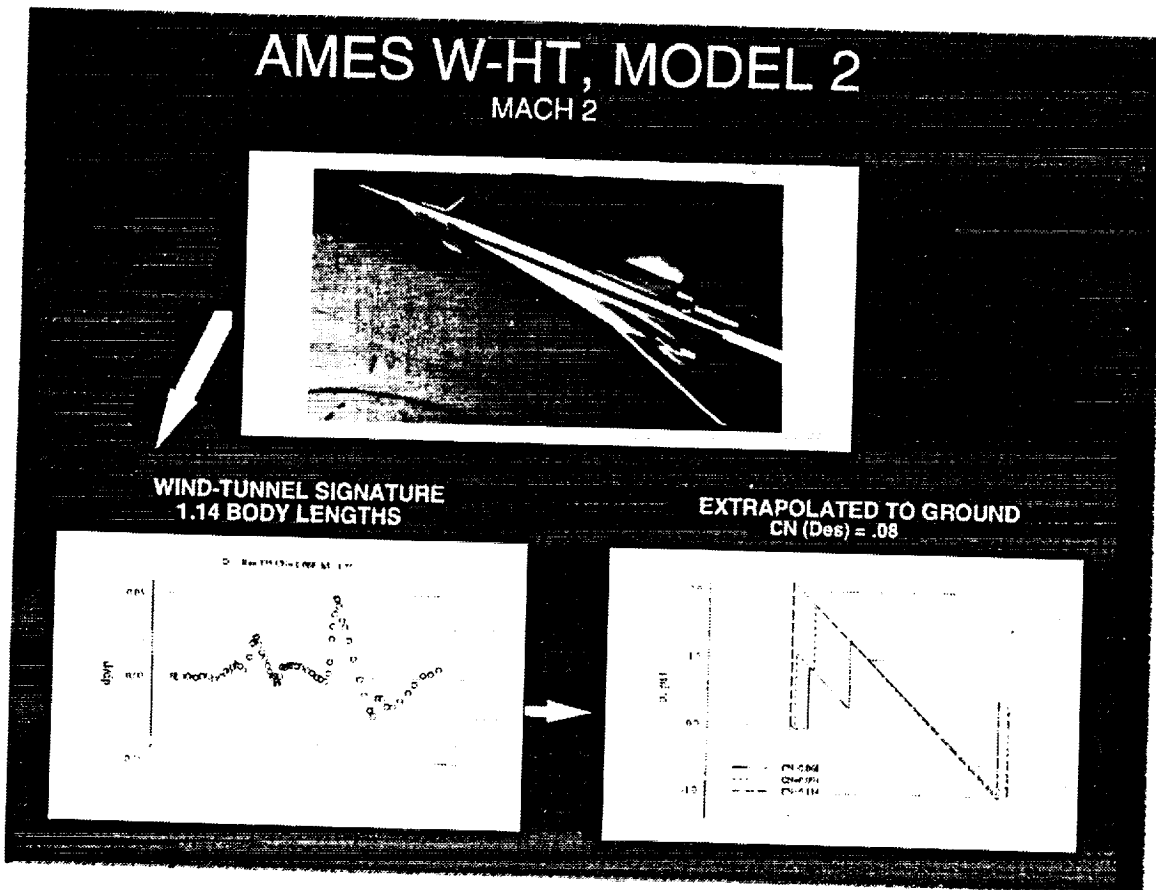


Figure 8. - Ames W-C; Model 2

LANGLEY LB-16 LOW-BOOM DESIGN

Shown in Fig. 9 is the NASA Langley-designed LB-16 low-boom concept. Also shown is the theoretical ground signature predicted using the Whitham Theory with Modified Linear Theory analysis methods. To the right of the model photograph is the signature measured in the wind tunnel at 2.3 body lengths away from the model. The extrapolation of the measured tunnel signature to the ground using the axisymmetric extrapolation method of Ref. 15 is shown in the bottom right of the figure. Note that while an N-wave is not predicted at the ground, the signature has a steeper pressure slope and higher pressure levels than those predicted by theory. While the calculated 98 PLdB loudness of the extrapolated signature is only 1.6 PLdB higher than the 96.4 PLdB of the predicted signature, reasons for the slope and pressure differences should be pursued—especially since the steep signature is more likely to fold over into an N-wave if disturbed by turbulence in the atmosphere.

Sonic-boom wind-tunnel tests conducted in 1993 and 1994 were the first in which signatures generated by full wing-body-nacelle concepts at cruise attitude have been extrapolated to produce non-N-wave-type signatures at ground level. As stated previously, however, investigations continue to discover the reason for discrepancies in the predicted and extrapolated wind-tunnel results.

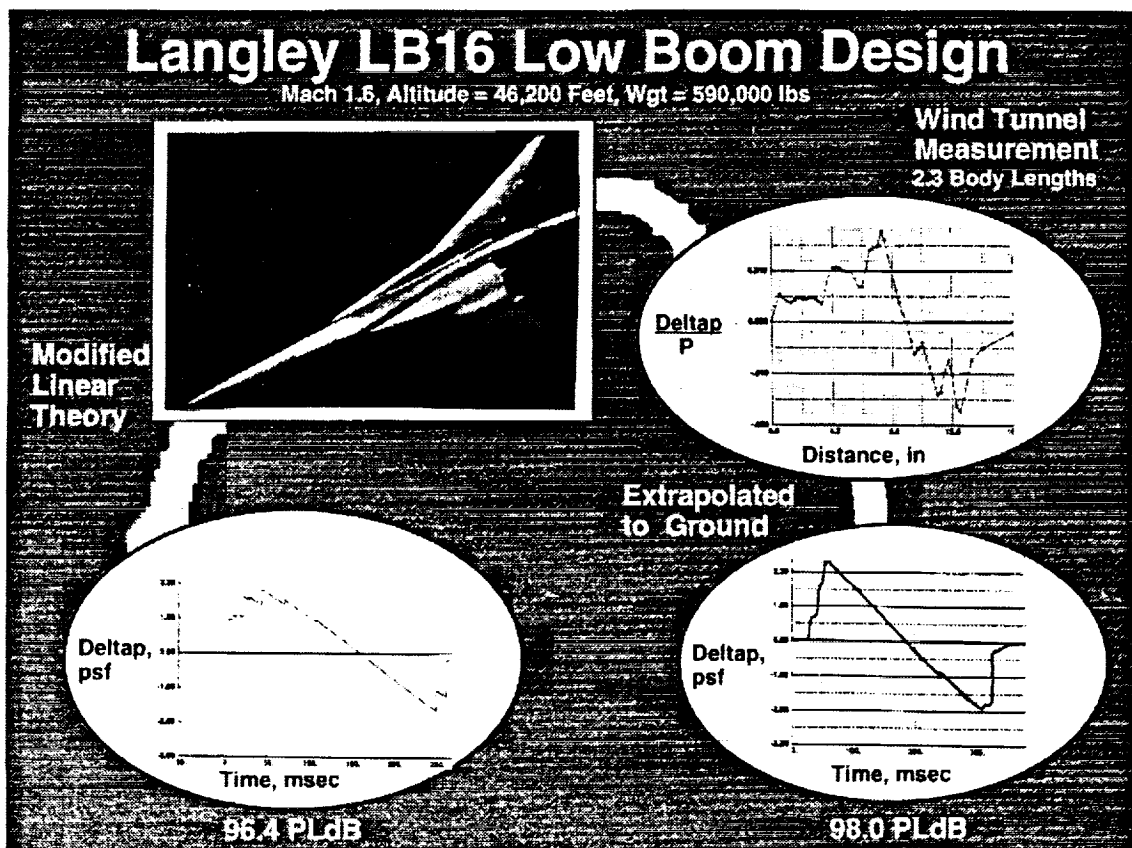


Figure 9. - Langley LB16 low boom design.

IMPACT OF NACELLES ON SONIC-BOOM SIGNATURES

Shortcomings in the method for the sonic-boom integration of engine nacelles were outlined in reference 10 where a modification to the previous method for designing low-boom concepts was discussed. This modified methodology was applied to the designs of two wind-tunnel models so that the modified methodology could be validated. On one model, the LB-16, the engine nacelles were mounted, as usual, under the wings. In this position, *both nacelle-volume and nacelle-wing interference-lift disturbances* would be generated. The other model, the LB-18, had the nacelles mounted behind the wing on the aft fuselage. This insured that *only nacelle-volume disturbances* would be generated. The design of the LB-16 and LB-18 concepts were described in the proceedings of the 1993 and 1994 Sonic-Boom Workshops.

Wind-tunnel signatures obtained from the LB-18 wind-tunnel model are presented on page 59 of these proceedings¹. No nacelle shocks (from either the small or the large nacelles) were observed in the LB-18 pressure signatures, two of which are repeated in figure 10(a), with the model at one-half the cruise C_L .

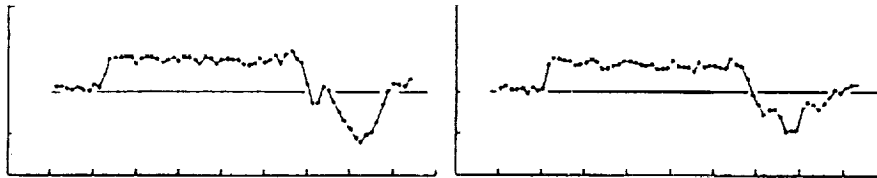


Figure 10(a). LB-18 pressure signatures. $M = 1.8$, $h = 24$ in., $C_L = 0.5 C_{L,Cruise}$.
Large nacelles (left), small nacelles (right).

It was concluded from these test results that *the modified engine-nacelle-integration methodology had worked for nacelle-volume effects*.

Pressure signatures generated by the other low-sonic-boom wind-tunnel model, the LB-16, are shown in figure 10(b).

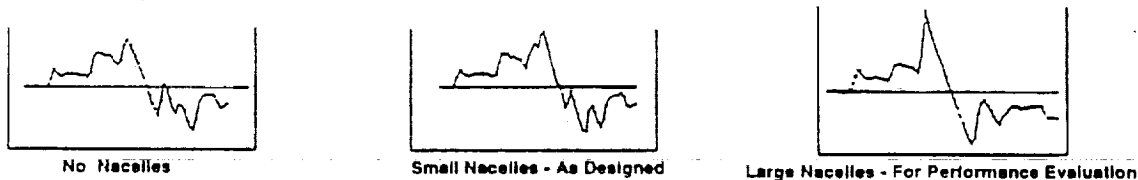


Figure 10(b) LB-16 pressure signatures. $M = 1.6$, $h = 20$ in., $C_L = C_{L,Cruise}$

These measured pressure signatures have wing and nacelle shocks that were not predicted during the design process. The nacelle shocks could have appeared because: (1) the nacelle-volume contribution was under-predicted, or (2) the interference-lift contribution was under-predicted. It was also possible that (3) the nacelles could not be mounted far enough aft due to lack of adequate available wing structure. In view of the LB-18 results, (1) does not seem likely, but (2) and/or (3) might be the cause(s). It is clear that the modified nacelle-integration methodology worked *for nacelle-volume effects*; it remains to be demonstrated that it can be made to work for *both nacelle-volume and nacelle-wing interference-lift effects* when the nacelles are conventionally mounted under the aircraft's wing.

¹"Wind-Tunnel Overpressure Signatures From a Low-Boom HST Concept With Aft-Fuselage-Mounted Engines"
by Robert J. Mack

PERFORMANCE COMPARISONS EARLY IN LOW-BOOM DESIGN WORK

As an example of the progress made in the low-boom design effort, Fig. 11 shows a comparison of the L/D Max for a Langley in-house aerodynamic Mach 2 cruise design with that of the Mach 2.0 low-boom validation concept tested in 1990, and two of the interim concepts of the latest low-boom design cycle. Initially, the measure of success within the low-boom design cycle was to achieve cruise L/D 's which were comparable with those of the aerodynamic designs. There was very little effort expended to improve the performance of the Mach 2 1990 minimization validation design. With the succeeding cycle, however, performance became a major criteria and it was quickly found that the cruise L/D 's of the highly-swept, low-boom concepts was often better than that of the baseline. It was then determined that weight, and not cruise L/D should be used as a measure of comparison for these concepts. Because of their high wing sweep, low-speed performance penalties were increased and higher structural weights were estimated for the low-boom designs--generally making them heavier than their non-low-boom constrained counterparts.

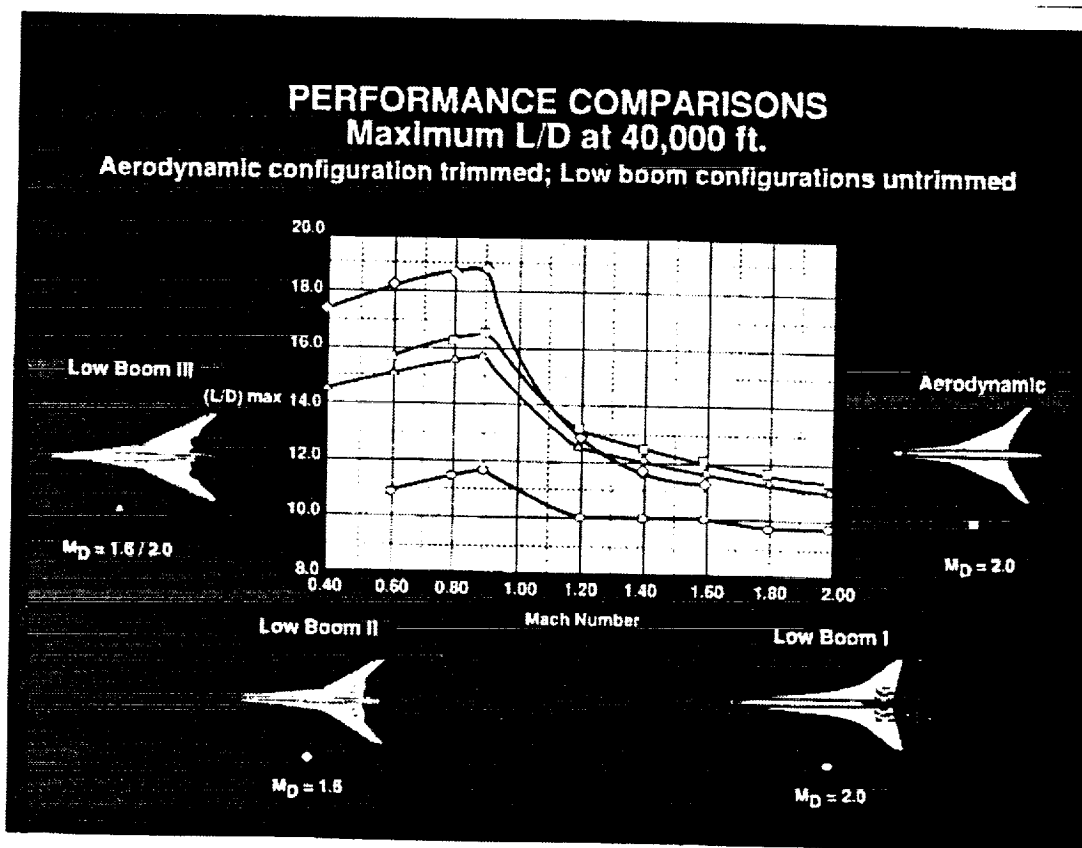


Figure 11. - Performance comparisons early in low-boom design work.

PERFORMANCE COMPARISONS OF 2ND ITERATION LOW-BOOM DESIGNS

Initially after testing the Mach 2 and Mach 3 validation models, researchers at Boeing Commercial Airplanes, Douglas Aircraft, NASA Ames, and NASA Langley became involved in low-boom design. Design procedures involved several different methods---varying from the use of Seebass-George Minimization Concepts, based on the Whitham Theory, to total use of nonlinear CFD methods. Because there were different levels of systems analysis which accompanied these designs, and because the impact of sonic-boom reduction techniques on the mission performance is a critical measure of success, the decision was made to conduct a consistent analysis of mission performance on all of the low-boom designs.¹⁶ A critical decision was made early in the systems analysis process to use an engine concept which was the leading contender in a concurrent HSR engine- downselect exercise. A 0.4-bypass mixed-flow turbofan engine concept provided to NASA Langley by the NASA Lewis Research Center was chosen. While changing the engines on all of the concepts introduced error (large for some concepts and smaller for others), the difficulty of assessing weight differences using several different engine cycles which had several different technology level assumptions was perceived to introduce an even greater complexity into interpreting the results. Because several concepts had different passenger loads, the results shown in Fig.12 are in gross weight per passenger normalized to a reference baseline which had an identical analysis with the same engine. The LB-16 shown here has a cruise Mach number of 2 while all of the other concepts would cruise at the program baseline of Mach 2.4.

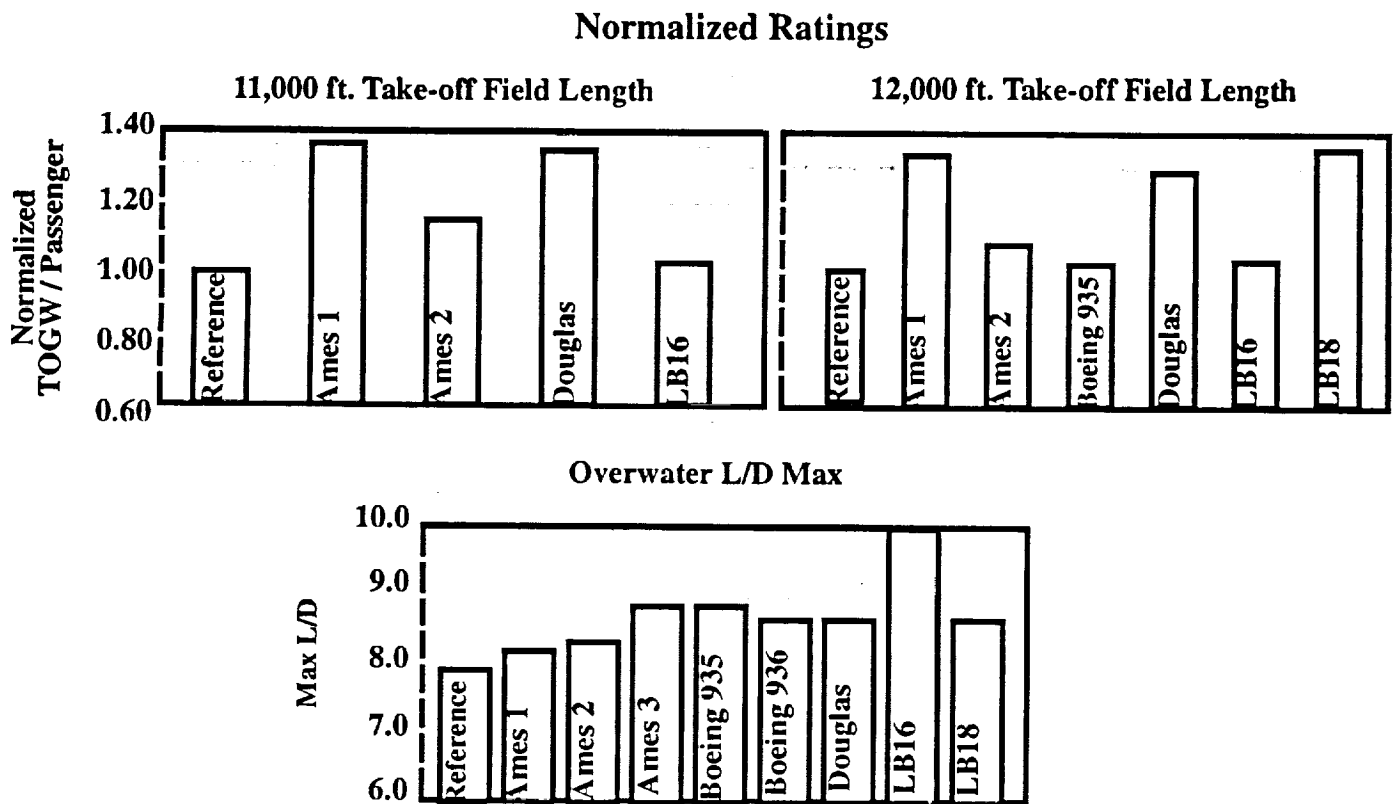


Figure 12. - Performance comparisons of 2nd iteration low-boom designs.

PROGRESS IN PROPAGATION AND ATMOSPHERIC EFFECTS

Work in the atmospheric-effects portion of the sonic-boom program has concentrated on the incorporation of atmospheric-absorption effects and turbulence effects into sonic-boom propagation codes which traditionally have only accounted for nonlinear steepening (Refs.15,17). In order to have a well-documented set of experimental measurements in which temperature and winds were measured at several altitudes and correlated with sonic-boom measurements, a sonic-boom flight test was conducted at White Sands Missile Range in New Mexico in August 1992.¹⁸ This test piggy-backed on a NATO-sponsored noise measurement test in which extensive weather measurements were made.

Several researchers¹⁹⁻²¹ have worked independently to develop methods for incorporating molecular relaxation into sonic-boom signature results. Initial results indicate that if signature shock levels can be lowered through minimization procedures, the atmospheric molecular relaxation will have an even greater effect in rounding the signature than for the traditionally larger N-wave signatures. Atmospheric-turbulence modeling and signature propagation through turbulence are also being pursued. Efforts continue in the correlation of theoretical predictions of sonic-boom pressure signatures and measured flight data. Because the results vary, a probability distribution of expected signature levels and frequencies would be the ultimate outcome of research in this area.

In 1994, an in-flight Schlieren system²² was developed at NASA Langley. The system was validated with a photograph of a NASA T-38 trainer aircraft which was at a distance of approximately 5 miles. Individual shocks could be seen emanating from the nose, canopy, and wing of the aircraft. It is hoped that with improvements to this technique, several thousand feet of the propagating shock patterns can be observed. This technique, along with a planned flight of the NASA SR-71 with several in-flight signature measurements,²³ will be used to assess the signature coalescence rate which is predicted currently with propagation codes.

- White Sands Flight Tests for correlation of signatures with weather**
- Theoretical absorption methods developed**
- Progress in propagation through turbulence**
- In-flight Schlieren**
- Progress in planning flight to validate coalescence rate**

Figure 13. - Progress in propagation and atmospheric effects.

EFFECT OF TURBULENCE ON RISE TIME OF T-38 SIGNATURES

The sonic-boom flight tests described in Ref. 18 were held over a two-week period in August, 1991, at the White Sands Missile Range in New Mexico. Thirty supersonic passes were flown with a T-38 aircraft, 21 with an F-15, and six with an F-111. The measuring array consisted of 16 Boom Event Analyzer Recorder (BEAR) units²⁴ arranged in a linear array with a 200 ft distance between each recorder. Flights were made in the early morning to have data in which low turbulence levels were expected and in the mid-afternoon when the desert-like conditions often generate high turbulence levels. Because rise time is a significant factor in determining the disturbance of a sonic-boom signature, there is interest in being able to correlate rise time with turbulence levels.

Shown in Fig. 14 are histograms of rise times (measured from 10 percent to 90 percent of maximum pressure for the initial shock) for the signatures measured using the T-38 aircraft. This aircraft has a nominal sonic boom of approximately 0.8 psf. for the test conditions. Though the number of measurements taken during low levels of turbulence is much higher, some trends can be extrapolated from the results shown. The mean rise time of 4.8 ms during low turbulence is much lower than the rise time measured from the signatures taken during moderate levels of turbulence. These results tend to corroborate theoretical results which indicate that both molecular relaxation and turbulence lengthen the rise time of the bow shock.

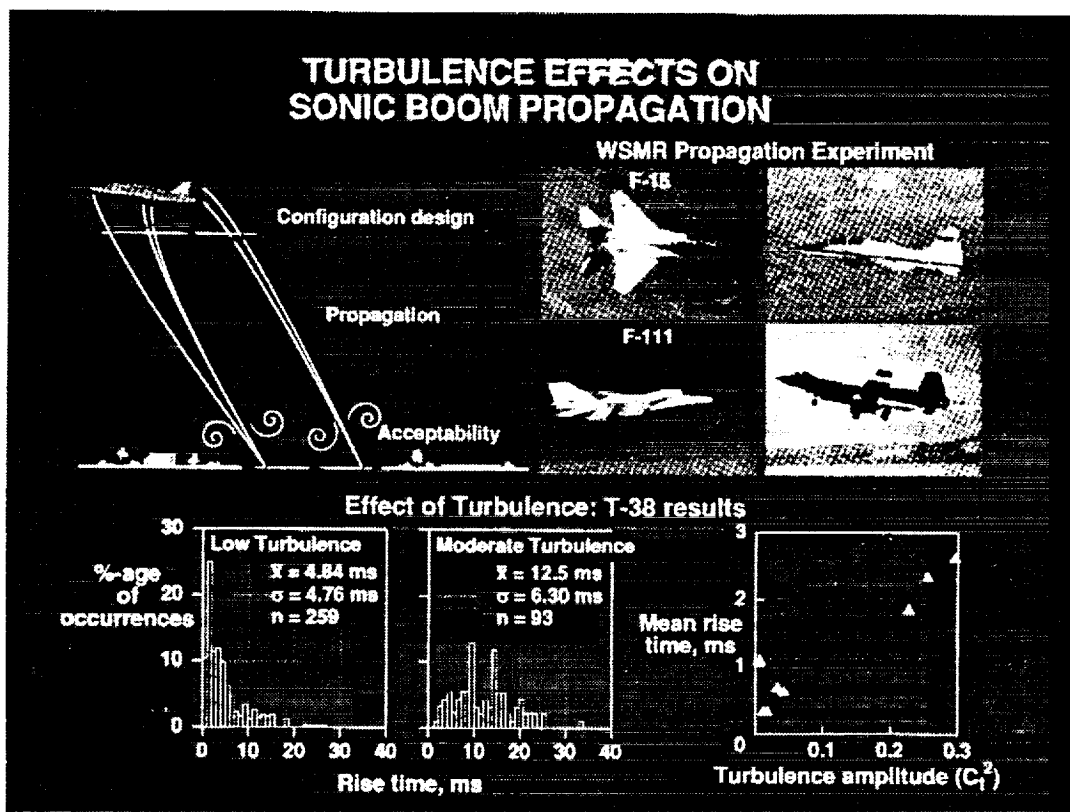


Figure 14. - Effect of turbulence on rise time of T-38 signatures.

CALCULATED LOUDNESS OF EXPERIMENTAL SIGNATURES

The loudness of the experimentally measured T-38 signatures was calculated according to the method described in Ref. 25, and histograms for those values are shown in Fig. 15. Because of the trend in rise time shown in Fig. 14, one may have expected the loudness levels to be lower during the low-turbulence conditions. In actuality, the loudness levels are nearly the same at both conditions--and in fact slightly higher during the low turbulence. Not shown in these results is the histogram for pressure levels. While loudness goes down with shock rise time, it increases with increasing shock pressure. During increased turbulence levels, the rise time of the bow shock increased, but the maximum pressure levels also increased, resulting in a net effect of very little change in overall loudness. Because the number of signatures at the moderate turbulence levels is much lower than at the low levels, there should be additional confirmation of these results.

Progress has been made in developing the theoretical models needed to include the effects of molecular relaxation and atmospheric turbulence on sonic-boom signatures. An algorithm which combines all effects and predicts the statistical variation of the loudness of a given pressure signature does not yet exist, but it is believed that such a method will be available within the next year.

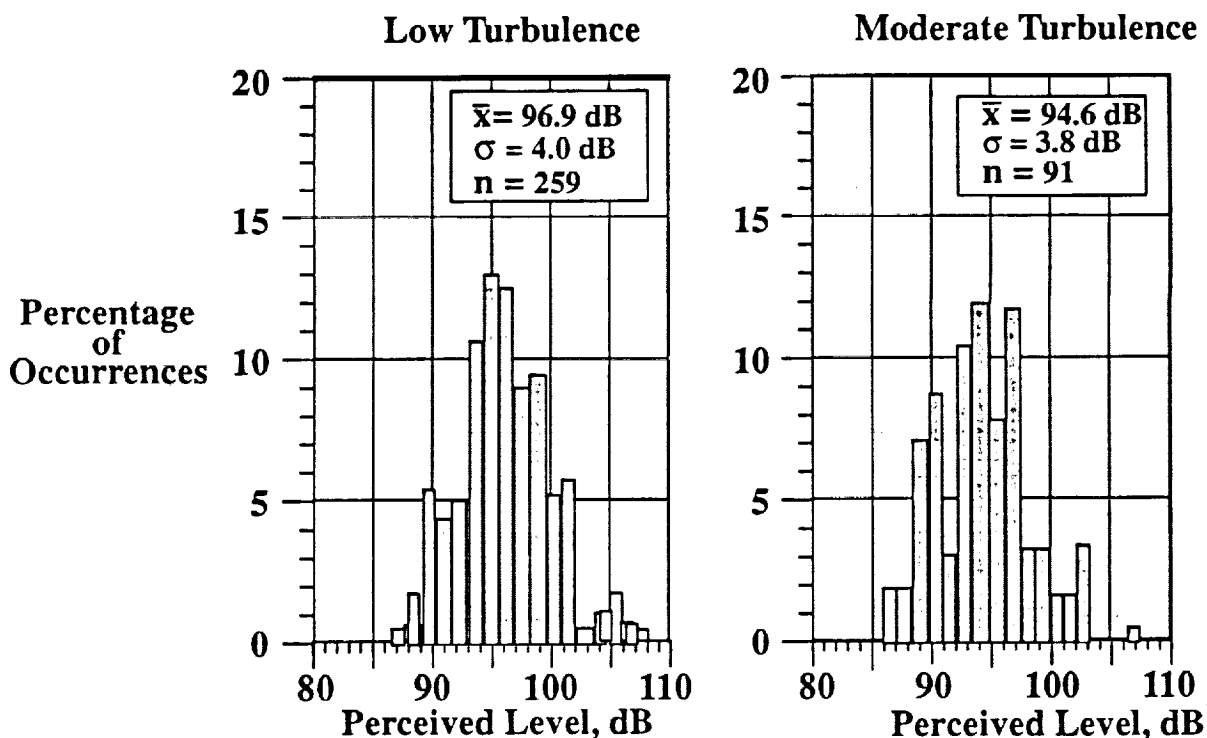


Figure 15. Calculated loudness of experimental signatures.

PROGRESS IN ACCEPTABILITY STUDIES

During sonic boom research in the 1960's and early 1970's, sonic booms were generally characterized by the overpressure of the bow shock, or Δp . As work in sonic-boom shaping increased, it was realized that signatures which resulted from a "shaped" aircraft were often characterized by several embedded shocks. The character of these signatures could not be described by Δp of the bow shock only, and thus some other metric for describing sonic-boom levels was needed. Perceived Loudness, dB, (PLdB) a metric based on an approach developed by Johnson and Robinson²⁶ and which uses the Stevens' Mark VII loudness method,²⁷ showed high correlation with sonic-boom disturbance levels during experimental tests. It was decided that this metric should be used within the program for describing sonic-boom outdoor disturbances.

This metric was employed to report results of tests in a sonic-boom simulator²⁸⁻²⁹ and in private homes,³⁰ and to report results of community surveys³¹ conducted in areas which are used for military operational flights and which are subjected to periodic sonic booms. Refs. 32-34 report results of studies done to evaluate subjective responses of persons inside houses and buildings. These results include the effects of loudness attenuation due to transmission through walls, but they also include the effects of vibration and rattle which are more bothersome indoors.

Metric defined

Simulator booth constructed and tests conducted to determine:

- most favorable shape for outdoor signature**
- effects of asymmetry on loudness**
- effect of measuring on ground rather than at ear**

In-home studies conducted

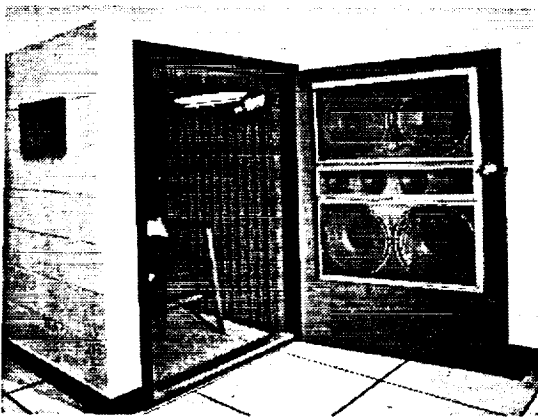
Community response studies conducted

Figure 16. Progress in Acceptability Studies.

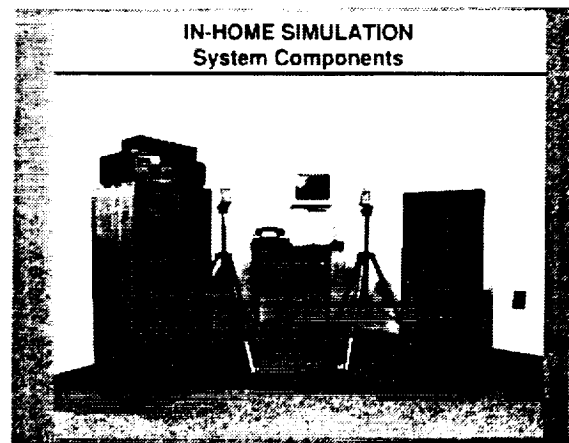
SONIC-BOOM SIMULATOR SYSTEMS

Shown in Fig. 17 are two of the sonic-boom simulator systems developed to conduct tests on human acceptability of sonic booms. The sonic-boom simulator booth at NASA Langley,²⁹ shown in Fig.17(a), is a human-rated system consisting of a computer-driven sound system contained within a rigid-walled booth in order that low-frequency sound components can be duplicated. Both ideal and measured sonic-boom signatures can be duplicated in this system which requires that the signals be predistorted. Rise times of up to 5 milliseconds and maximum pressures up to 4 psf can be duplicated. Tests on signature shapes, duration, and asymmetry have been conducted in this booth with human subjects responding subjectively on their level of disturbance.

In order to test individual respondents in a more realistic environment, several in-home systems such as that shown in Fig.17(b) were developed. This computer-driven, compact disk system³⁰ played random sonic booms throughout the day and respondent reactions were gathered each evening on the computer which was delivered as a part of the system. Independent measurements of the loudnesses within the home were made. Only subjects within the home a large portion of the day were used in the test program. Detailed results of this study are reported in Ref. 30.



(a) Sonic Boom Simulator



(b) In-Home Sonic-Boom System

Figure 17. - Sonic-Boom Simulator Systems.

INDOOR SIMULATION AND COMMUNITY SURVEYS

Within the sonic-boom community there is continuing debate on some aspects of sonic-boom minimization. Previous studies have shown that outdoor annoyance of sonic boom is most highly correlated with shock levels within the signature, particularly the bow-shock level. Indoors, however, the highest correlation of annoyance has been reported with maximum overpressure level--not necessarily at the shocks. In minimization studies, shock levels are generally reduced at the expense of maximum overpressure levels. Theoretical studies on indoor responses to sonic booms are included in Refs. 32-33. To gather additional information on indoor disturbance, the Georgia Tech Simulation Facility shown in Fig. 18 was planned and constructed. A detailed description of this facility and initial results of studies are included in Ref. 34. Because of funding cuts within the HSR program, studies in this facility beyond the initial phase were abandoned.

The most realistic data used to construct a Dosage-Response Chart for sonic-boom responses are felt to be gathered from persons living in communities which have been subjected to sonic-boom exposures. Military operational areas within the western portion of the United States offer such possibilities. Because the U.S. Air Force often monitors the sonic booms in operational areas exposed to supersonic flights, an initial survey was conducted within the operational area of Nellis Air Force Base in Nevada and further surveys are planned near Edwards Air Force Base in the Mojave Desert in California during FY-95.

INDOOR SONIC BOOM SIMULATION FACILITY
Georgia Tech Research Institute

Special low frequency acoustic drivers developed; 3Hz - 30 Hz, 30Hz - 300Hz

Real houses to create indoor acoustic effects

- High frequency attenuation
- Rattles and vibrations
- Room reverberation

Planned research

- Indoor/outdoor annoyance
- Comparison with other noise sources
- Building response

USAF/NASA SONIC BOOM STUDY

Nellis range:

- Tactical Air Command supersonic operations
- >1000 sonic booms per year
- 0 - 3 p.s.f.
- Impacted population ~ 5000

USAF:

- Sonic boom exposure prediction model
- Model validation
 - Aircraft tracking
 - Sonic boom measurements (40 stations, 6 months)

NASA:

- Community response survey

Nevada

Nellis Range

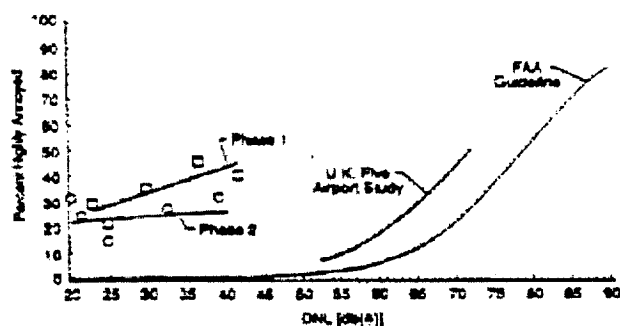
Las Vegas

Figure 18. - Indoor simulation and community surveys.

NELLIS SURVEY RESULTS

Initial results of the Nellis survey are reported in Ref. 31 and shown in Fig. 19. In this figure, loudness is plotted in DNL, a metric which incorporates the effects of repeated sonic booms, and the effects of sonic booms occurring at times other than during the daylight hours. Included on the chart for reference are the percentages of persons predicted to be highly annoyed based on studies done by CHABA (Committee on Hearing and Bioacoustics of NRC) and airport noise studies. The Nellis Survey studies (completed in two phases) indicate that people are much more annoyed by the sonic booms than was predicted by either of the other studies. Because of the significant difference in predicted and actual response, surveys are planned at Edwards Air Force Base to corroborate these results. In the interim, these results have had a significant impact on HSR planning.

Results shown in Fig. 19 indicate that there is little possibility of overland supersonic flight of an HSCT. Because of these results, the sonic-boom program has been critically reviewed and a program redirection has been undertaken. Emphasis will now be placed on assessing the impact on marine life and wild birds of 500+ HSCTs crossing the oceans daily. As this assessment is being made, studies on "softening" the sonic boom of the HSR baseline concepts will continue.



- BOOM MONITORING AT 3 LOCATIONS, 2-7 MONTHS PRIOR TO INTERVIEWS
- 0.1 - 0.9 BOOMS / DAY, AVERAGE DELTAP 0.5 - 2.0 PSF, MAX DELTAP 8 PSF
- 526 INTERVIEWS IN 3 COMMUNITIES-(100% RESPONSE RATE)

PRELIMINARY RESULTS INDICATE:

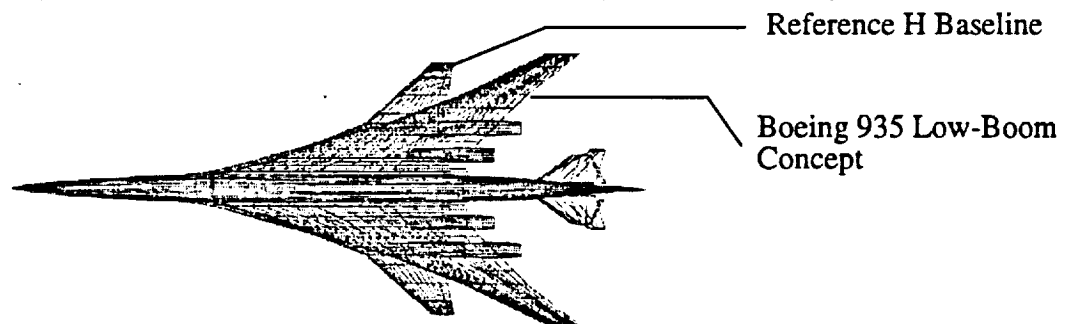
- RESIDENTS ARE MORE ANNOYED BY SONIC BOOM THAN OTHER COMMUNITY NOISE
- RESIDENTS ARE MORE ANNOYED BY SONIC BOOMS THAN PREDICTED BY THE NRC-CHABA

Figure 19. - Nellis survey results.

LESSONS LEARNED

Several difficulties have manifested themselves during Phase I of the HSR sonic-boom program, especially within the configuration design component. Whereas the acceptability studies and the propagation studies have been managed within one Langley organization (with contracts and grants), the design work has been conducted at two NASA centers, and at two major airframers. While outstanding progress in design work has been reported, there were difficulties encountered when different methods were used. This may be an unavoidable difficulty when methods are being developed concurrently with design studies. More communication between designers, and earlier exchange of concepts may have avoided some of the difficulties encountered, especially within the milestone-driven atmosphere of the HSR program.

A very important lesson learned during the low-boom design studies has been the importance of concurrent system studies so that sonic-boom designs do not deviate from the missions expected within the program. In addition to the Nellis response results, a major factor in the redirection of the program was the belief that the long lifting lengths and high notch ratios of the low-boom designs (see comparison of low-boom concept with baseline) would have unacceptable aeroelastic effects and poor low-speed behavior in addition to unacceptable weights. Early interaction between structural experts and sonic-boom experts is needed to prevent unacceptable designs.



HSR Baseline compared to Low-Boom Concept

TEAMING AND STRONG COORDINATION NEEDED IN APPROACH AND METHODS

- Poor communication resulted in false directions
- Competition rather than cooperation in some instances has slowed progress

ADAPTATION TO CHANGING TARGETS AND GUIDELINES NECESSARY

- Project guidelines, engines, etc. continue to change
- Project atmosphere makes adherence to milestones important

CONTINUOUS SYSTEM STUDIES DURING DESIGN PHASE CRITICAL

- Tremendous energies and time spent in defining concepts consistently
- Extreme performance deviations attack credibility of low-boom concepts

Figure 20. Lessons Learned.

FUTURE DIRECTIONS OF SONIC-BOOM RESEARCH

Because the official position of the HSR program is now that supersonic flight will occur only over water, any emphasis on low-boom designs will be eliminated. The progress which has been made during Phase I in this area will be documented and work stopped. Studies, using many of the same shaping principles, will be conducted to determine whether the sonic-boom levels of the program baseline configuration can be reduced. The importance of the baseline softening studies cannot be determined until the impact of sonic booms on marine mammals can be more accurately assessed.

In addition to the softening studies, algorithms which predict ground locations impacted by supersonic flight will be developed and assessed. Ground disturbances are caused by the primary sonic-boom carpet, secondary booms (reflected sonic booms), and focused booms (enhanced booms due to accelerations or maneuvers). Any deviations from optimum flight profiles which may be necessary to alter ground disturbances due to the sonic boom will be assessed.

Because prediction methods depend on propagation codes which predict the coalescence of shock waves, a flight test using an unmodified SR-71 is being planned in which currently used propagation codes can be validated. In-flight measurements are planned so that non-N-wave signatures can be measured as wave coalescence is assessed.

Finally, studies which will determine whether sonic booms impact the mating habits, migratory patterns, or cause any deviation in the natural patterns of marine mammals will be initiated.

Low-boom design work has been cancelled.

Flights of either modified FIREBEE or SR-71 cancelled

Directions during next year will include:

- Boom-softening studies on HSR baseline concepts
- Increased emphasis on predicting ground impact area due to primary boom, secondary booms, and focused booms
- Studies of altered flight operations to minimize ground impact
- Possible wind-tunnel entry in AEDC 16S Tunnel to answer 3-D propagation question
- Flight test of unmodified SR-71 to validate shock coalescence rate of propagation methods
- Initial studies of sonic-boom impact on marine life.

Figure 21. Future directions of sonic boom research.

REFERENCES

1. Darden, Christine M.; Powell, Clemans A.; Hayes, Wallace D.; George, Albert R.; and Pierce, Allan D.: Status of Sonic-Boom Methodology and Understanding, NASA CP-3027, June 1989.
2. Metwally, Munir: Economic Benefits of Supersonic Overland Operation, NASA CP-3173. October 1992, pp. 1-13.
3. McLean, F. W.: Some Asymptotic Effects on Sonic Booms of Large Airplanes." NASA TN D-28777, 1965.
4. Jones, L. B.: "Lower Bounds for Sonic Bangs in the Far Field." *Aeronautical Quarterly*, Vol. XVIII, pt. 1, Feb. 1967, pp. 1-21.
5. Seebass, R.: "Minimum Sonic-Boom Shock Strengths and Overpressures." *Nature*, Vol. 221, Feb. 1969, pp. 651-653.
6. George, A. R.: "Lower Bounds for Sonic Booms in the Mid-Field." *AIAA Journal*, Vol. 7, Aug. 1969, pp. 1542-1545.
7. Mack, R. J.; and Darden, C. M.: A Wind-Tunnel Investigation of a Sonic-Boom Minimization Concept. NASA TP-1421, 1979.
8. Darden, Christine M.; Mack, Robert J.; Needleman, Kathy E.; Baize, Daniel G.; Coen, Peter G.; Barger, Raymond L.; Melson, N. Duane; Adams, Mary S.; Shields, Elwood W.; and McGraw, Marvin E.: Design and Analysis of Low-Boom Concepts at Langley Research Center. Vol. III, Proceedings, First Annual High-Speed Research Workshop, May 14-16, 1991, Williamsburg, VA, pp. 1-25.
9. Carlson, Harry W.; and Mack, Robert J.: Estimation of Wing Nonlinear Aerodynamic Characteristics at Supersonic Speeds. NASA TP-1718, 1980.
10. Mack, Robert J.: Some Considerations on the Integration of Engine Nacelles into Low-Boom Aircraft Concepts. NASA CP-3173, Oct. 1992, pp. 221-236.
11. Siclari, M. J.: Sonic Boom Predictions Using a Modified Euler Code. Vol. III, Proceedings, First Annual High-Speed Research Workshop, May 14-16, 1991, Williamsburg, VA.
12. Cliff, Susan E.: Computational/Experimental Analysis of Three Low Sonic-Boom Configurations with Design Modifications. NASA CP-3173, Oct. 1992, pp. 89-117.
13. Edwards, T.; Hicks, R.; Cheung, S.; Cliff, S.; Madson, M.; and Mendoza, J.: Sonic Boom Prediction and Minimization Using Computational Fluid Dynamics. Vol. III, First Annual High-Speed Research Workshop, May 14-16, 1991, Williamsburg, VA.
14. Cliff, Susan E.; Baker, Timothy J.; and Hicks, Raymond M.: Design and Computational / Experimental Analysis of Low Sonic-Boom Configurations. NASA HSR Sonic-Boom Workshop, NASA/CP-1999-209699, 1999.
15. Thomas, Charles L.: Extrapolation of Sonic-Boom Pressure Signatures by the Waveform Parameter Method. NASA TN D-6832, 1972.
16. Baize, Daniel G.; McElroy, Marcus O.; Fenbert, James W.; Coen, Peter G.; Ozoroski, Lori P.; Needleman, Kathy E.; Domack, Chris S.; and Geiselhart, Karl A.: A Performance Assessment of Eight Low-Boom High-Speed Civil Transport Concepts. NASA HSR Sonic-Boom Workshop, NASA/CP-1999-209699, 1999.
17. Hayes, Wallace D.; Haefeli, Rudolph C.; and Kulsrud, H. E.: Sonic Boom Propagation in a Stratified Atmosphere with Computer Program. NASA CR-1299, 1969.
18. Willshire, William L., Jr.; and DeVilbiss, David W.: Preliminary Results from the White Sands Missile Range Sonic-Boom Propagation Experiment. NASA CP-3172, Oct. 1992, pp.137.

19. Pierce, Allan D.; and Sparrow, Victor W.: Relaxation and Turbulence Effects on Sonic-Boom Signatures, Vol. III, Proceedings, 1st Annual HSR Workshop, May 14-16, 1992, Williamsburg, VA.
20. Plotkin, Kenneth J.: The Effect of Turbulence and Molecular Relaxation on Sonic-Boom Signatures, Vol. III, Proceedings 1st Annual HSR Workshop, May 14-16, 1992, Williamsburg, VA.
21. Yao, Lixin; Bass, Henry E.; Raspet, Richard; and McBride, Walton E.: Statistical and Numerical Study of the Relation Between Weather and Sonic-Boom Characteristics, Vol. III, Proceedings 1st Annual HSR Workshop, May 14-16, 1992, Williamsburg, VA.
22. Weinstein, Leonard: An Optical Technique for Examining Aircraft Shock-Wave Structures in Flight, NASA HSR Sonic-Boom Workshop, NASA CP-3279, 1994.
23. Haering, Edward A. Jr.; Whitmore, Stephen A.; and Ehernberger, L.J.: Measurement of the Basic SR-71 Airplane Near-Field Signature, NASA HSR Sonic-Boom Workshop, NASA/CP-1999-209699, 1999.
24. Lee, Robert A.; Mazurek, Doug; Price, Dale; Crabill, Monty; and Palmer, Barbara: Boom Event Analyzer Recorder (BEAR): System Description. AAMRL-TR-89-035 (AD-A218 048), August 1989.
25. Shepherd, Kevin P.; Sullivan, Brenda M.; Leatherwood, Jack; and McCurdy, David: Sonic Boom Acceptability Studies, Vol. IV, Proceedings 1st Annual HSR Workshop, May 14-16, 1991, Williamsburg, VA.
26. Johnson, D. R., and Robinson, D. W.: "The Subjective Evaluation of Sonic Bangs," *Acustica*, 18(5) 1967.
27. Stevens, S. S.: "Perceived Level of Noise by Mark VII and Decibels (E)," *Journal of the Acoustical Society of America*, 51 (2), pp. 575-601 (1972).
28. Leatherwood, Jack D.; Shepherd, Kevin P.; and Sullivan, Brenda M.: A new Simulator for Assessing Subjective Effects of Sonic Booms. NASA TM-104150, September 1991.
29. Leatherwood, Jack; and Sullivan, Brenda M.: Subjective Loudness Response to Simulated Sonic Booms. NASA CP-3172, Oct. 1992, pp. 151.
30. McCurdy, David A.; and Brown, Sherilyn A.: An In-Home Study of Subjective Response to Simulated Sonic Booms. NASA HSR Sonic-Boom Workshop, NASA CP-3279, 1994.
31. Fields, James, M.; Moulton, Carey; Baumgartner, Robert M.; and Imm-Thomas, Jeff: Resident's Reactions to Long-Term Sonic-Boom Exposure: Preliminary Results, NASA HSR Sonic-Boom Workshop, NASA CP-3279, 1994.
32. Brown, David; and Sutherland, Louis: Sonic-Boom Outdoor-to-Indoor Response to Minimized Sonic Booms, Vol. IV, Proceedings 1st Annual HSR Workshop, May 14-16, 1991, Williamsburg, VA.
33. Sutherland, L. C.; and Czech, J.: Evaluation of Human Response to Structural Vibration Induced by Sonic Boom, NASA CP-3172, Oct. 1992, pp. 171.
34. Ahuja, Krish K.: Georgia Tech Sonic-Boom Simulator. Vol. IV, Proceedings 1st Annual HSR Workshop, May 14-16, 1991, Williamsburg, VA.

PARTICIPANTS*

Dr. Richard Antcliff
Mail Stop 235A
NASA Langley Research Center
Hampton, VA 23681-0001
Ph.: 804-864-4606
FAX: 804-864-8315
E-Mail: R.R.ANTCLIFF@LARC.NASA.GOV

Mr. Daniel G. Baize
Mail Stop 412
NASA Langley Research Center
Hampton, VA 23681-0001
Ph.: 804-864-1071
FAX: 804-864-3553
E-Mail: D.G.BAIZE@LARC.NASA.GOV

Dr. Timothy J. Baker
Room D309
Dept. of Mechanical & Aeronautical Engineering
Olden Street, Engineering Quadrangle
Princeton University
Princeton, NJ 08544-5263
Ph.: 609-258-5205
FAX: 609-258-1939
E-Mail: BAKER@COUGARXP.PRINCETON.EDU

Dr. Richard Barnwell
Mail Stop 119
NASA Langley Research Center
Hampton, VA 23681-0001
Ph.: 804-864-4129
FAX: 804-864-8852
E-Mail:
RICHARD_BARNWELL@HSR.LARC.NASA.GOV

Mr. David T. Blackstock
Applied Research Laboratories
University of Texas at Austin
P.O. Box 8029
Austin, TX 78713-8029
Ph.: 512-835-3374
FAX: 512-835-3259
E-Mail: DTB@MCL.CC.UTEXAS.EDU

Mr. Percy J. Bobbitt
Eagle Aerospace, Inc.
Tower Box 77
2101 Executive Drive
Hampton, VA 23666
Ph.: 804-827-1100
FAX: 804-827-1106
E-Mail: BOBBITT@EAGLE.COM

Ms. Sherilyn A. Brown
Mail Stop 463
NASA Langley Research Center
Hampton, VA 23681-0001
Ph.: 804-864-3593
FAX: 804-864-8823
E-Mail: S.A.BROWN@LARC.NASA.GOV

Mr. David B. Bruns
Mail Stop 35-59
McDonnell Douglas Aerospace—West
3855 Lakewood Blvd.
Long Beach, CA 90846
Ph.: 310-593-8312
FAX: 310-982-7787
E-Mail:
C372746%DVSS.DECNET@LBGWY.MDC.COM

Mr. Peter P. Camacho
Mail Code 35-59
McDonnell Douglas Aerospace—West
3855 Lakewood Blvd.
Long Beach, CA 90846
Ph.: 310-593-7012
FAX: 310-982-7787
E-Mail: camacho@mdta.mdc.com (lower case)

Mr. Frank W. Cazier, Jr.
Mail Stop 462
NASA Langley Research Center
Hampton, VA 23681-0001
Ph.: 804-864-2860
FAX: 804-864-7687
E-Mail: F.W.CAZIER@LARC.NASA.GOV

Mr. Joseph R. Chambers
Mail Stop 246A
NASA Langley Research Center
Hampton, VA 23681-0001
Ph.: 804-864-6399
FAX: 804-864-6135
E-Mail: J.R.CHAMBERS@LARC.NASA.GOV

Professor Hsien K. Cheng
Dept. of Aerospace Engineering
University of Southern California
Los Angeles, CA 90089-1191
Ph.: 213-740-5365
FAX: 213-740-7774
E-Mail: CHENG@SPOCK.USC.EDU

*Attendance at the Configuration Design, Analysis, and Design sessions was restricted to U.S. citizen and permanent resident participants funded from and working in the sonic boom element of the High Speed Research Program. Therefore, some of the above participants were allowed to only attend the unrestricted Atmospheric Propagation and Acceptability Studies sessions.

Dr. Samson H. Cheung
MCAT Institute
Mail Stop 258-1
NASA Ames Research Center
Moffett Field, CA 94035-1000
Ph.: 415-604-4462
FAX: 415-604-4377
E-Mail: CHEUNG@NAS.NASA.GOV

Mr. Robin O. Cleveland
Applied Research Laboratories
The University of Texas at Austin
P.O. Box 8029
Austin, TX 78713-8029
Ph.: 512-835-3032
FAX: 512-835-3259
E-Mail: ROBIN@CCWF.CC.UTEXAS.EDU

Ms. Susan E. Cliff
Mail Stop 227-2
NASA Ames Research Center
Moffett Field, CA 94035-1000
Ph.: 415-604-3907
FAX: 415-604-4357
E-Mail: CLIFF@RA-IRIS.ARC.NASA.GOV

Ms. Brenda Cook
USAF HQ ACC/CEVA
Langley AFB, VA 23665-2769
Ph.: 804-764-3056/3328
FAX: 804-764-5363
E-Mail: COOKB@CEMAIL.ACC.AF.MIL

Dr. Christine M. Darden
Mail Stop 412
NASA Langley Research Center
Hampton, VA 23681-0001
Ph.: 804-864-5258
FAX: 804-864-3553
E-Mail: CMDARD@AVDOO.LARC.NASA.GOV

Ms. Latoya Deans
Mail Stop 412
NASA Langley Research Center
Hampton, VA 23681-0001
Ph.: 804-864-5258
FAX: N/A
E-Mail: N/A

Dr. J. Micah Downing
USAF AL/OEBN
2610 Seventh Street
Wright-Patterson AFB, OH 45433-7901
Ph.: 513-255-3664
FAX: 513-476-7680
E-Mail:
JMD%OSPNEY@EAGLEB.AAMRL.WPAFB.AF.MIL

Mr. L. J. Ehemberger
Aerodynamics Branch
Mail Stop D-2033
P.O. Box 273
NASA Dryden Flight Research Center
Edwards, CA 93523-0273
Ph.: 805-258-3699
FAX: 805-258-2842
E-Mail: EHRE@CS1.DFRF.NASA.GOV

Dr. Sanford Fidell
BBN Systems and Technologies
21120 Vanowen Street
Canoga Park, CA 91303
Ph.: 818-226-0323
FAX: 818-716-8377
E-Mail: FIDELL@BBN.COM

Dr. James M. Fields
Consultant in Acoustics
10407 Royal Road
Silver Spring, MD 20903-1112
Ph.: 301-439-4356 / 202-512-9796
FAX: 301-439-4356
E-Mail: JFIELDS@CAP.GWU.EDU

Dr. Kamran Fouladi
Lockheed Engineering & Sciences Co.
Mail Stop 412
NASA Langley Research Center
Hampton, VA 23681-0001
Ph.: 804-864-5993
FAX: 804-864-3553
E-Mail: FOULADI@AVD00.LARC.NASA.GOV

Mr. Edward A. Haering, Jr.
Aerodynamics Branch
Mail Stop D-2033
P.O. Box 273
NASA Dryden Flight Research Center
Edwards, CA 93523-0273
Ph.: 805-258-3696
FAX: 805-258-2842
E-Mail: HAERING@CS1.DFRF.NASA.GOV

Mr. George T. Haglund
Mail Stop 6H-FK
Boeing Commercial Airplane Group
P.O. Box 3707
Seattle, WA 98124-2207
Ph.: 206-965-3773
FAX: 206-234-4543
E-Mail: N/A

Mr. Jerry N. Hefner
Mail Stop 462
NASA Langley Research Center
Hampton, VA 23681-0001
Ph.: 804-864-3640
FAX: 804-864-7687
E-Mail: J.N.HEFNER@LARC.NASA.GOV

Mr. R. David Hilliard
Wyle Laboratories
Mail Stop 239
NASA Langley Research Center
Hampton, VA 23681-0001
Ph.: 804-865-0000, X234
FAX: 804-865-8116
E-Mail: N/A

Mr. Harvey H. Hubbard
Mail Stop 463
NASA Langley Research Center
Hampton, VA 23681-0001
Ph.: 804-864-3610
FAX: 804-864-8823
E-Mail: N/A

Mr. Joseph Laiosa
1111 Stewart Avenue
Mail Stop C50-05
Grumman Aircraft Corporation
Bethpage, NY 11793-3582
Ph.: 516-575-0900
FAX: 516-575-1968
E-Mail: LAIOSA@GRUMMAN.COM

Dr. Jack D. Leatherwood
Mail Stop 463
NASA Langley Research Center
Hampton, VA 23681-0001
Ph.: 804-864-3591
FAX: 804-864-8823
E-Mail: J.D.LEATHERWOOD@LARC.NASA.GOV

Mr. Bart Lipkens
MacroSonix
1054 Technology Park Dr.
Glen Allen, VA 23060
Ph.: 804-262-3700
FAX: 804-266-4627
E-Mail: N/A

Mr. David P. Lux
Aerospace Projects/SR-71 Project
Mail Stop D-2071
P.O. Box 273
NASA Dryden Flight Research Center
Edwards, CA 93523-0273
Ph.: 805-258-3026
FAX: 805-258-2134
E-Mail: DAVE_LUX@QMGATE.DFRF.NASA.GOV

Mr. Robert J. Mack
Mail Stop 412
NASA Langley Research Center
Hampton, VA 23681-0001
Ph.: 804-864-5988
FAX: 804-864-3553
E-Mail: R.J.MACK@LARC.NASA.GOV

Dr. Lucio Maestrello
Mail Stop 463
NASA Langley Research Center
Hampton, VA 23681-0001
Ph.: 804-864-1067
FAX: 804-864-8823
E-Mail: N/A

Mr. Domenic J. Maglieri
Eagle Engineering, Inc.
Tower Box 77
2101 Executive Drive
Hampton, VA 23666
Ph.: 804-827-1100
FAX: 804-827-1106
E-Mail: VSOTI@EAGLE.COM

Mr. Gerry L. McAninch
Mail Stop 460
NASA Langley Research Center
Hampton, VA 23681-0001
Ph.: 804-864-5269
FAX: 804-864-8290
E-Mail: G.L.MCANINCH@LARC.NASA.GOV

Mr. David A. McCurdy
Mail Stop 463
NASA Langley Research Center
Hampton, VA 23681-0001
Ph.: 804-864-3596
FAX: 804-864-8823
E-Mail: D.A.MCCURDY@LARC.NASA.GOV

Mr. John M. Morgenstern
Mail Code 35-59
McDonnell Douglas Aerospace—West
3855 Lakewood Blvd.
Long Beach, CA 90846
Ph.: 310-593-7012
FAX: 310-982-7787
E-Mail: DBRUNS@MDTA.MDC.COM

Mr. Alan K. Mortlock
Mail Code 35-29
McDonnell Douglas Aerospace—West
3855 Lakewood Blvd.
Long Beach, CA 90846
Ph.: 310-593-3937
FAX: 310-982-7787
E-Mail: N/A

Ms. Kathy E. Needleman
Lockheed Engineering & Sciences Co.
Mail Stop 412
NASA Langley Research Center
Hampton, VA 23681-0001
Ph.: 804-864-5987
FAX: 804-864-3553
E-Mail: K.E.NEEDLEMAN@LARC.NASA.GOV

Professor Allan D. Pierce
Dept. of Aerospace & Mechanical Engineering
Boston University
110 Cummington Street
Boston, MA 02215
Ph.: 617-353-4841
FAX: 617-353-5760/5866
E-Mail: ADP@BUENGA.BU.EDU

Dr. Kenneth J. Plotkin
Suite 701
Wyle Laboratories
2001 Jefferson Davis Highway
Arlington, VA 22202
Ph.: 703-415-4550
FAX: 703-415-4556
E-Mail: KPLOTKIN@ACCESS.DIGEX.NET

Mr. Joe W. Posey
Mail Stop 460
NASA Langley Research Center
Hampton, VA 23681-0001
Ph.: 804-864-7686
FAX: 804-864-8290
E-Mail: J.W.POSEY@LARC.NASA.GOV

Dr. Clemans A. Powell
Mail Stop 462
NASA Langley Research Center
Hampton, VA 23681-0001
Ph.: 804-864-3640
FAX: 804-864-7687
E-Mail: C.A.POWELL@LARC.NASA.GOV

Mr. Robert G. Rackl
Mail Stop 6H-FR
Boeing Commercial Airplane Group
P.O. Box 3707
Seattle, WA 98124-2207
Ph.: 206-965-1207
FAX: 206-237-3808
E-Mail: RGR4320@MU.CA.BOEING.COM

Dr. Richard Rasket
Dept. of Physics and Astronomy
National Center for Physical Acoustics
University of Mississippi
University, MS 38677
Ph.: 601-232-5888
FAX: 601-232-7494
E-Mail: RASPET@NSXT1.NCPA.OLEMISS.EDU

Dr. Leick D. Robinson
Science Applications International Corporation
Suite 100
13091 Pond Springs Road
Austin, TX 78729
Ph.: 512-219-5511
FAX: 512-219-5519
E-Mail: LEICK@BGA.COM

Dr. Zvi Rusak
Dept. of Mechanical Engineering, Aeronautical
Engineering & Mechanics
JEC 4009
Rensselaer Polytechnic Institute
Troy, NY 12180-3590
Ph.: 518-276-3036
FAX: 518-276-2623
E-Mail: USERGLMB@MTS.RPI.EDU

Dr. Kevin P. Shepherd
Mail Stop 463
NASA Langley Research Center
Hampton, VA 23681-0001
Ph.: 804-864-3575
FAX: 804-864-8823
E-Mail: K.P.SHEPHERD@LARC.NASA.GOV

Mr. Michael J. Siclari
Mail Stop A08-35
Grumman Corporation
1111 Stewart Avenue
Bethpage, NY 11746
Ph.: 516-575-8067
FAX: 516-575-7716
E-Mail: N/A

Mr. Norbert F. Smith
Suite 120
McDonnell Douglas Aerospace
22 Enterprise Parkway
Hampton, VA 23666-5844
Ph.: 804-825-3350/838-2551
FAX: 804-838-8176
E-Mail: TBD

Dr. Victor W. Sparrow
Graduate Program in Acoustics
157 Hammond Building
The Pennsylvania State University
University Park, PA 16802
Ph.: 814-865-3162
FAX: 814-863-7222
E-Mail: SPARROW@HELMHOLTZ.PSU.EDU

Mr. David G. Stephens
Mail Stop 462
NASA Langley Research Center
Hampton, VA 23681-0001
Ph.: 804-864-3640
FAX: 804-864-7687
E-Mail: D.G.STEPHENS@LARC.NASA.GOV

Ms. Brenda M. Sullivan
Lockheed Engineering & Sciences Co.
Mail Stop 463
NASA Langley Research Center
Hampton, VA 23681-0001
Ph.: 804-864-3585
FAX: 804-864-8823
E-Mail: B.M.SULLIVAN@LARC.NASA.GOV

Mr. Louis C. Sutherland
Consultant in Acoustics
27803 Longhill Drive
Rancho Palos Verdes, CA 90274
Ph.: 310-541-1655
FAX: 310-322-9799
E-Mail: TBD

Dr. Leonard M. Weinstein
Mail Stop 170
NASA Langley Research Center
Hampton, VA 23681-0001
Ph.: 804-864-5543
FAX: 804-864-8348
E-Mail: L.M.WEINSTEIN@LARC.NASA.GOV

Mr. Alan R. Wenzel
Virginia Polytechnic Inst. & State Univ.
Mail Stop 460
NASA Langley Research Center
Hampton, VA 23681-0001
Ph.: 804-864-5267
FAX: 804-864-8290
E-Mail: N/A

Dr. Alan W. Wilhite
Mail Stop 119
NASA Langley Research Center
Hampton, VA 23681-0001
Ph.: 804-864-2982
FAX: 804-864-8852
E-Mail: A.W.WILHITE@LARC.NASA.GOV

REPORT DOCUMENTATION PAGE			Form Approved OMB No. 0704-0188	
Public reporting burden for this collection of information is estimated to average 1 hour per response, including the time for reviewing instructions, searching existing data sources, gathering and maintaining the data needed, and completing and reviewing the collection of information. Send comments regarding this burden estimate or any other aspect of this collection of information, including suggestions for reducing this burden, to Washington Headquarters Services, Directorate for Information Operations and Reports, 1215 Jefferson Davis Highway, Suite 1204, Arlington, VA 22202-4302, and to the Office of Management and Budget, Paperwork Reduction Project (0704-0188), Washington, DC 20503.				
1. AGENCY USE ONLY (Leave blank)	2. REPORT DATE December 1999	3. REPORT TYPE AND DATES COVERED Conference Publication		
4. TITLE AND SUBTITLE High-Speed Research: 1994 Sonic Boom Workshop <i>Configuration Design, Analysis, and Testing</i>			5. FUNDING NUMBERS WU 537-03-21-03	
6. AUTHOR(S) David A. McCurdy, Editor				
7. PERFORMING ORGANIZATION NAME(S) AND ADDRESS(ES) NASA Langley Research Center Hampton, VA 23681-2199			8. PERFORMING ORGANIZATION REPORT NUMBER L-17435	
9. SPONSORING/MONITORING AGENCY NAME(S) AND ADDRESS(ES) National Aeronautics and Space Administration Washington, DC 20546-0001			10. SPONSORING/MONITORING AGENCY REPORT NUMBER NASA/CP-1999-209699	
11. SUPPLEMENTARY NOTES				
12a. DISTRIBUTION/AVAILABILITY STATEMENT Unclassified-Unlimited Subject Category 02 Distribution: Nonstandard Availability: NASA CASI (301) 621-0390			12b. DISTRIBUTION CODE	
13. ABSTRACT (Maximum 200 words) The third High-Speed Research Sonic Boom Workshop was held at NASA Langley Research Center on June 1-3, 1994. The purpose of this workshop was to provide a forum for Government, industry, and university participants to present and discuss progress in their research. The workshop was organized into sessions dealing with atmospheric propagation; acceptability studies; and configuration design, and testing. Attendance at the workshop was by invitation only. The workshop proceedings include papers on design, analysis, and testing of low-boom high-speed civil transport configurations and experimental techniques for measuring sonic booms. Significant progress is noted in these areas in the time since the previous workshop a year earlier. The papers include preliminary results of sonic boom wind tunnel tests conducted during 1993 and 1994 on several low-boom designs. Results of a mission performance analysis of all low-boom designs are also included. Two experimental methods for measuring near-field signatures of airplanes in flight are reported.				
14. SUBJECT TERMS Sonic boom extrapolation; Sonic boom acceptability; Sonic boom minimization; Low-boom configurations			15. NUMBER OF PAGES 304	
			16. PRICE CODE A14	
17. SECURITY CLASSIFICATION OF REPORT Unclassified	18. SECURITY CLASSIFICATION OF THIS PAGE Unclassified	19. SECURITY CLASSIFICATION OF ABSTRACT Unclassified	20. LIMITATION OF ABSTRACT UL	